UNIVERSIDADE TÉCNICA DE LISBOA
INSTITUTO SUPERIOR DE AGRONOMIA

# CARACTERIZAÇÃO DA ÁREA QUEIMADA À ESCALA GLOBAL (1982-1999) E ANÁLISE DE ALGUNS DOS SEUS IMPACTOS CLIMÁTICOS E ECOLÓGICOS

**Bernardo Wildung Cantante Mota**

**ORIENTADOR:** Doutor José Miguel Oliveira Cardoso Pereira
**CO-ORIENTADOR:** Doutor Ricardo Machado Trigo

**JÚRI**

Presidente: Reitor da Universidade Técnica de Lisboa

Vogais: Doutor José Miguel Oliveira Cardoso Pereira, professor catedrático do Instituto Superior de Agronomia da Universidade Técnica de Lisboa;

Doutor Carlos do Carmo de Portugal e Castro da Câmara, professor associado da Faculdade de Ciências da Universidade de Lisboa;

Doutor Manuel Lameiras de Figueiredo Campagnolo, professor associado do Instituto Superior de Agronomia da Universidade Técnica de Lisboa;

Doutora Adélia Maria Oliveira Sousa, professora auxiliar da Escola de Ciências e Tecnologia da Universidade de Évora;

Doutor Ricardo Machado Trigo, investigador auxiliar do Laboratório Associado Infante D. Luiz da Universidade de Lisboa, na qualidade de especialista.

**¨Tese apresentada neste Instituto para obtenção do grau de doutor¨**

DOUTORAMENTO EM ENGENHARIA FLORESTAL

LISBOA
2010

Às mulheres da minha vida...
Paula, Libra e Bimba.

# Agradecimentos

O desenvolvimento, elaboração e conclusão desta tese não teria sido possivel sem o contributo de um grande número de pessoas, actividades e instituições. Entre estas estarei sempre grato:

Ao Professor José Miguel Oliveira Cardoso Pereira, orientador desta tese, pelos conhecimentos transmitidos, condições e oportunidades concedidas, e pelo incentivo dado.

Ao Doutor Ricardo Trigo, pelo apoio, pelas ideias, pelos exemplo e pelo incentivo que me deu, principalmente durante os anos críticos quando tudo parecia perdido.

À minha mulher, Paula, por todo o apoio e carinho que me deu e principalmente por ter a paciência de aturar as minhas 'birras' durante estes últimos 5 anos.

Aos meus pais, pelo amor incondicional, pelos princípios que incutiram e pela educação que me providenciaram.

Aos meus colegas , Ana Sá, Adélia Sousa e Yannick Lepage pelo exemplo, pela companhia e boa disposição com que me aturaram ao longo destes anos.

Agradeco também ao restantes colegas do Laboraório de Detecção Remota e Análise Geografia (LDRAG) do Instituto Superior de Agronomia (ISA) pelo seu apoio e companheirismo.

Ao Doutor Jorge Pinzon, pela experiência, apoio e condições que facilitou, durante a minha estadia no *Goddard Space Flight Center* (GSFC) da NASA, em Greenbelt, Maryland, EUA.

A fundação para a ciência e a Tecnologia (FCT) pela bolsa de doutoramento que concedeu (SFRH-/BD/25119/2005).

A Jim Drake e Hoyle Schweitzer por, em 1968 terem inventado o maravilhoso desporto de *Windsurf*, fundamental para meditar e sair dos 'becos sem saída' onde tantas vezes me deparei no decorrer deste trabalho.

Aos processadores da *Intel*, sem os quais não era possível processar o volume de dados.

# Abreviaturas

**ATSR** Along Track Scanning Radiometer

**AVHRR** Advanced Very High Resolution Radiometer

**BA** Burned Area

**BF** Burned frequency

**BRDF** bidirectional reflectance distribution function

**BRIC** Brasil, Russia, India e China

**CCA** Canonical correlation Analysis

**EMD** Empirical Mode Decomposition

**ENSO** El Niño/La Niña-Southern Oscillation

**ENVISAT** Environment Satellite

**ERS** European Remote Sensing

**FCT** Fundaçã para a Ciência e a Tecnologia

**FSD** Fire Size distribution

**GAC** Global Area Coverage

**GBA2000** Global VGT Burnt Area Product 2000

**GCM** Modelos de Circulação Global

**GEMI** Non-linear Vegetation Index

**GOES** Geostationary Satellites

**GSFC** Goddard Space Flight Center

**HRPT** High Resolution Picture Transmission Format

**IPCC** Intergovernmental Panel on Climate Change

**LAC** Local Area Coverage

**LBAP-PAL** Large Burnt Area Product based on PAL

**LTDR** Land Long Term Data Record

**L3JRC** Global VGT burnt area product 2000 -2007

**MCD45** MODIS Burned Area Product

**METEOSAT** Meteorological Satellites

**MNDVI** Maximum NDVI value multi-temporal compositing algorithm

**MODIS** Moderate Resolution Imaging Spectroradiometer

**NASA** National Aeronautics and Space Administration

**NDVI** Normalized Difference Vegetation Index

**NOAA** National Oceanic and Atmospheric Administration

**PAL** AVHRR Pathfinder Land (8km) Dataset

**PSF** Point Spread Function

**SPOT** Satellite Pour lObservation de la Terre

**TM** Thematic Mapper

**TR** Segmentation Threshold

**SZA** Solar Zenith Angle

**VIIRS** Visible/Infrared Imager Radiometer Suite

**WFA** World Fire Atlas

# Resumo

A actual preocupação de quais possam ser as consequências das alterações climáticas, nomeadamente no que diz respeito às mudanças que se observam nos regimes de fogo, tornam urgente estudos piro-climáticos. A ausência de um registo histórico, tanto da extensão como da variabilidade da área afectada, que complemente produtos recentes, apresenta-se como sendo um dos obstáculos à observação de mudanças significativas. Neste sentido, e tendo em conta a falta de informação para o período anterior ao ano 2000, elaborou-se uma cartografia global de áreas queimadas mensais para o período compreendido entre 1981 e 1999, usando o produto *NOAA Pathfinder AVHRR land (8km) dataset*. Em complemento, definiu-se como referência independente o produto *World Fire Atlas*, ao qual foram removidos todas as fontes de calor alternativas ao fogo de vegetação; e realizou-se um estudo de sensibilidade à capacidade de detecção de áreas queimadas usando sensores de baixa resolução espacial. O pré-processamento centrou-se na remoção de tendências espúrias, originadas pela deriva orbital dos satélites, com recurso à decomposição de modo empírico (EMD) das séries temporais, às quais foi desenvolvido e aplicado um classificador *random forest*, para determinar as áreas queimadas. Os resultados mostraram que, apesar da flexibilidade das metodologias desenvolvidas em lidar com os sucessivos problemas técnicos e com a complexidade das várias situações de ocorrência de fogo, a elevada subestimação explica-se pelo método de re-amostragem usado na elaboração do produto PAL e pela incapacidade dos sensores de baixa resolução de detecção de certos padrões de fogo.

Palavras-chave: área queimada, padrões espaciais, AVHRR, deriva orbital, EMD, *Random Forest*

# Abstract

The recent awareness to what would be the climate change consequences, namely in the observed changes in the fire regimes, highlight the urgency for piro-climatic studies. The lack of an historical burnt area dataset to complement recent products, covering the global extent and its full variability, makes it difficult to detect significant trends. Due to the lack of global information before year-2000, a burned area product based on the NOAA Pathfinder AVHRR land (8km) dataset was developed covering the period from 1981 to 1999. As reference we screened the World Fire Atlas dataset, by removing all the non wildfires and false alarm information and we addressed the expected detectable area made by the coarser sensor. Data pre-processing was prefomed by removing the satellite orbital drift trends with empirical mode decomposition and a burned area classification was done based on the Random Forest classification algorithm. Although the developed methodologies allowed to overcome many of the technical difficulties and the results showed high flexibility to cover the full extent of possible fire occurrences, burned areas were characterised by large underestimation. This is mainly explained by the PAL re-sampling procedure and by the limitations of the coarser sensor to detect certain burned scar spatial patterns.

Keywords: burnt area, spatial patterns, AVHRR, orbital drift, EMD, Random Forest

# Conteúdo

# Capítulo 1

# Introdução

## Sustentabilidade

A conferência de Copenhaga, realizada entre 7 e 18 de Dezembro de 2009 contou com a presença de 193 países e tinha como objectivo chegar a acordo sobre um tratado que desse seguimento ao Protocolo de Quioto no âmbito da Convenção-Quadro das Alterações Climáticas da ONU. O compromisso das Partes focar-se-ia sobre a redução das emissões de gases de efeito de estufa, sobre modos de minimizar as alterações climáticas e suas consequências, bem como em formas de financiar países em desenvolvimento a adaptarem-se à nova realidade das Alterações Climáticas. A inconscistência, por vezes até a ausência, de evidencias específicas nos sucessivos relatórios do IPCC (Parry 2007) e do *Millenium Ecosystem Assessment* (Assessment 2005), a pressão económica resultante de uma crise à escala global, a imposição do direito a uma taxa de desenvolvimento alta por parte das novas potencias regionais, os BRIC e, por fim, os requisitos do consumo de recursos cada vez mais elevado para uma população mundial de 6 biliões em crescente, conduziram o processo negocial a um rotundo fracasso.

Os relatórios supracitados são esclarecedores ao concluírem que, nos últimos 50 anos, a acção do Homem promoveu mudanças significativas e, em alguns casos, irreversíveis nos ecossistemas, sendo que a sua influência na superfície terrestre tornou-se globalmente, não só mais extensiva, como também mais intensiva (Turner 1990, Foley et al. 2005, Assessment 2005). Directamente, esta acção pode ser caracterizada pela alteração da paisagem. Estima-se que actualmente 40% da superfície terrestre está a ser explorada com fins agrícolas (Foley et al. 2005), a desflorestação atinge 8.5% das restantes florestas, especialmente na Amazónia e no Sudoeste Asiático (Lepers et al. 2005) e 10% das zonas áridas e semi-áridas estão consideradas degradadas. Neste sentido, calcula-se que 60% dos recursos dos ecossistemas estão desvalorizados (Assessment 2005). Indirectamente, a actividade humana faz-se sentir nos efeitos que a poluição atmosférica potencializou, como sejam o crescimento de gases de efeito de estufa e aerossóis, levando ao aquecimento da atmosfera em $0.6^oC$ no espaço de 100 anos, a uma mudança, no espaço e no tempo, dos padrões da precipitação e à subida do nível médio do mar entre 0.1 a 0.2 metros.

Estas mudanças, rapidas e de larga escala, motivadas em satisfazer as exigências de alimento, água, madeira e combustível (Assessment 2005), conduziram à degeneração dos recursos de água, à poluição, à fragmentação de habitats, extinção de espécies e perda de biodiversidade (Foley et al. 2005). Se o estado das coisas não é animador, as previsões ainda o são menos. Calcula-se aumentos de temperatura na ordem de 1.4 a $5.8^oC$, acompanhados por mais ondas de calor, frequentes mudanças nos padrões da precipitação, zonas áridas e semi-áridas mais se-

cas e elevação do nível do mar (Assessment 2005); tudo isto em combinação com uma população global, que segundo se estima, deverá atingir 9 biliões em 2050.

Tais perturbações, devido à longa escala temporal da dinâmica dos ecossistemas, irão afectar os ecossistemas mas também o clima durante séculos (Assessment 2005). Para termos uma ideia prática, mesmo que no presente fosse interrompida a emissão de $CO_2$, com os dados disponíveis, sabe-se que o arrefecimento da atmosfera de apenas umas décimas de grau levaria 1000 anos a ser atingido (Solomon et al. 2009).

Tendo em conta os múltiplos problemas ambientais, impõe-se a necessidade global de reavaliar as actividades humanas, os recursos existentes e a forma como estes se relacionam com os requisitos de uma população mundial crescente. Neste contexto, o fogo, na versão natural, de vegetação é hoje reconhecido como um dos processos que mais influenciam a atmosfera e a biosfera (Bowman et al. 2009). Tem impactos significativos directos nos reservatórios de carbono, nas mudanças de coberto vegetal e nas emissões atmosféricas; e indirectos através de interacções, efeitos de *feedback* e reacção em cadeia.

A significativa contribuição em emissões faz da biomassa queimada uma das fontes primárias de gases de efeito de estufa (Crutzen 1979, Crutzen and Andreae 1990). Em termos comparativos estima-se que equivalem a 50%, 16% e 43% do total de emissões antropogénicas de dióxido carbono ($CO_2$), metano($CH_4$) e monóxido de carbono ($CO$) (Houghton 1995, der Werf et al. 2006, Bowman et al. 2009). salientando-se como o processo que mais poderá aumentar no próximo século (Parry 2007).

Crê-se que foi há cerca de 500.000 anos, no Paleolítico, que o Homem aprendeu a utilizar o fogo para se aquecer, para se defender, cozinhar e, mais tarde, como ferramenta de gestão da paisagem. Hoje, num mundo que é uma 'aldeia global', e no qual assistimos a uma crescente demografia conjugada com uma decrescente disponibilidade de recursos, temos de ter normas de gestão, de sustentabilidade. Neste sentido, a forma como gerimos o fogo é crucial; e porque tem sido imperfeita, essa gestão poderá vir a ser dificultada por mudanças nos regimes do fogo, induzidas através das alterações climáticas (Bowman et al. 2009, Krawchuk et al. 2009). Assim, embora exista um esforço de incutir a componente fogo nos modelos dinâmicos de vegetação, o risco por eles representado continua a ser difícil de determinar. A extensão e dimensão dos seus impactos tornam urgente uma detecção mais precisa, uma redução das incertezas associadas às emissões e, um conhecimento mais profundo da relação fogo-clima.

## *Wildfires*, fogo de vegetação

Entendido como um processo físico de combustão cuja consequência directa é o consumo de matéria orgânica, o fogo de vegetação apresenta-se, naturalmente, interdependente da existência e história evolutiva da vegetação ou biomassa. Esta combustão, também denominada biomassa queimada, significa o consumo parcial ou total de, por exemplo, componentes de uma planta ou árvore (viva ou morta) com impactos directos e/ou indirectos muito variados na natureza.

Trata-se de um processo importante no funcionamento dos ecossistemas, pois promove a regeneração, recicla nutrientes e promove a biodiversidade. Após a passagem do fogo, por exemplo, o solo adquire nutrientes que estariam alocados na vegetação ardida. Sem este, também não haveria savanas tal como as conhecemos, pois estas evoluiriam em florestas (Bond and Keeley 2005). Considere-se ainda que muitas plantas evoluíram e adaptaram-se ao fogo criando mecanismos de sobrevivência, coabitando com o regime de fogo em que estão inseridas e para o qual contribuem. Há espécies cuja propagação depende do fogo, como é o conhecido caso das sequóias gigantes, nas quais as altas temperaturas são exigidas para que as suas sementes germinem.

O fogo de vegetação tem impactos na distribuição e composição da vegetação. O calor gerado modifica as propriedades do solo, como é o caso da porosidade e da fauna, podendo conduzir à erosão quando a frequência de eventos é elevada.

Quer resultem de causas naturais ou da actividade humana, os fogos libertam para a atmosfera quantidades consideráveis de gases e aerossóis (Andreae and Merlet 2001). O tipo e a quantidade de gás libertado dependem da vegetação ardida, do seu conteúdo de humidade, da oxigenação e do próprio tipo de fogo (com ou sem chama).

A maioria dos fogos ocorre nos trópicos, nas savanas de África, América do Sul e Austrália, e nas florestas tropicais da América do Sul e Sudoeste Asiático. As suas causas são maioritariamente humanas (90%) havendo uma pequena parte atribuída a causas naturais (Andreae and Merlet 2001). Estudos recentes (Schultz et al. 2008) mostram que a área média global afectada, todos os anos, pelos fogos é de $383 \times 10^6$ ha, o que corresponde a 42 vezes a área de Portugal continental.

Dependendo da metodologia adoptada, estima-se que anualmente as emissões atingiam valores entre 1428 e 2771 $TgC$ por ano (Galanter et al. 2000, Ito and Penner 2004, Schultz et al. 2008) podendo atingir valores máximos acima de 3000 $TgC$ durante os anos do *El Niño* (1992 e 1997). Para além do dióxido de carbono ($CO_2$), os principais gases libertados pela biomassa queimada são o metano ($CH_4$) e o monóxido de carbono ($CO$), também estes gases de efeito de estufa; e os $NO_x$, que são importantes precursores à formação de ozono ($O_3$), em particular sobre a forma de $N_2O$, cuja capacidade de absorver radiação é 300 vezes superior ao dióxido de carbono. Por sua vez os aerossóis elevam-se pela troposfera, podendo atingir, em eventos de fogo intenso, a baixa estratosfera. Através da circulação atmosférica e devido ao seu elevado tempo de residência, estes particulados dispersam-se, afectando o balanço global da transferência radiativa da atmosfera através da dispersão e absorção da radiação solar e alteram as propriedade microfísicas das nuvens e os mecanismos de convecção (Randerson et al. 2006, Andreae et al. 2004, Koren et al. 2004). Em conjunto e através de sistemas complexos de reacção em cadeia, a libertação de gases e aerossóis promove uma alteração significativa da composição química e das propriedades físicas da atmosfera (Crutzen and Andreae 1990, Laat et al. 2006).

O fogo pode ainda implicar um elevado custo económico (Williams 2004), quer seja pela perda de culturas e bens, por desgaste de equipamento em combate, ou por despesas de saúde (Butry et al. 2001). Por último, e mais importante, implica muitas vezes a própria vida humana, quer seja em acções de combate ou relacionado com doenças cardio-respiratórias.

**Determinantes do fogo**

Os regimes do fogo são descritos através das características associadas à ocorrência e propagação do fogo. Entre elas encontram-se o tipo de combustível consumido, o tamanho, a intensidade, a severidade, a frequência e a sazonalidade do fogo. Assim, a sua ocorrência é regulada pela disponibilidade do combustível, pelas condições climáticas que promovem a combustão e por eventos de ignição. Esta combinação de factores, globalmente variável, denominada triângulo do fogo (fig.1.1), é responsável por uma distribuição heterogénea dos regimes do fogo. O papel de cada factor e correspondentes interacções entre factores determinam o tipo de regime, entre os quais se destacam: fogos em savanas tropicais, florestas tropicais, florestas boreais e de agricultura.

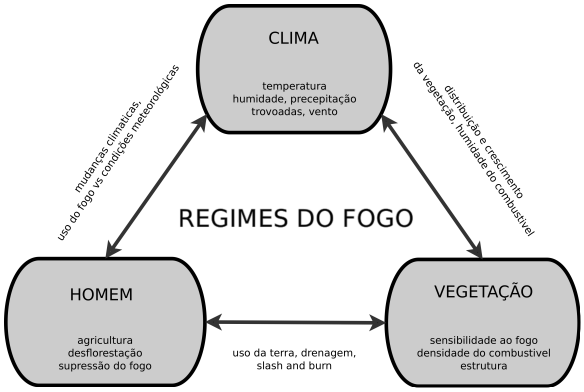


**Figure 1.1**: *Triângulo do fogo*

Para cada regime, há uma conjugação de factores e interacções que o determinam. A variação de um determinado factor irá reflectir-se nas interacções com os outros factores, resultando em eventos de fogo de maior ou menor dimensão, intensidade e severidade. Nas últimas décadas, observaram-se mudanças de regime do fogo em certas regiões. DE entre as causas, podemos destacar: a implementação de políticas de gestão do fogo, afectando maioritariamente as regiões temperadas (Houghton et al. 2000, Pyne 2001), a expansão de áreas agrícolas, preponderante nas regiões tropicais (Cochrane et al. 1999, DeFries et al. 2002) e o aquecimento global (Running 2006, Westerling et al. 2006) que, apesar do seu efeito ser global, parece afectar maioritariamente as zonas boreais (Stocks et al. 2002, Kasischke and Turetsky 2006).

De entre todos os factores, o clima é o que apresenta a maior variabilidade. À escala glo-

bal, o papel do clima, como determinante do fogo, mudou ao longo do tempo sendo que, até à Revolução Industrial (meados do século XVIII), a sua ocorrência era predominantemente determinada pela precipitação (Pechony and Shindell 2010). De uma forma directa ou indirecta, a precipitação rege os vários regimes do fogo. A disponibilidade de combustível, nomeadamente para as savanas, era determinada pela quantidade de precipitação ocorrida na época das chuvas. A precipitação teria também um efeito supressor, aumentando a humidade durante a época seca sendo, em geral, o fogo iniciado por ignições provocadas por trovoadas secas. A partir da colonização dos novos mundos no século XVIII, depois com a Revolução Industrial e consequente crescimento das populações, um dos resultados directos foi a alteração das paisagens: as florestas e as savanas foram gradualmente substituídas por pastagens e campos agrícolas. A ignição passou a ser prevalentemente antropogénica tendo como objectivo a limpeza de campos, do restolho de culturas prévias, de mata para dar lugar a novas culturas, de pragas de insectos ou répteis.
A acção humana não só contribui para o aumento de ignições como também se apresenta como efeito supressor do fogo através do combate que, no passado, ocorria por falta de combustível ou devido a condições meteorológicas propícias.

À escala regional, o papel do clima determina a sazonalidade, possibilitando a sobrevivência de um determinado nicho de espécies vegetais que, dependendo da variação do tipo de combustível, tipo de coberto e estrutura da vegetação, implicam uma determinada reacção do comportamento do fogo. A variabilidade do clima, seja provocada por eventos de larga escala como o *El Niño-Southern Oscillation* (ENSO) ou por eventos de escala menor como sistemas de bloqueio (Skinner et al. 1999), pode determinar indirectamente a quantidade e directamente as condições a que se encontra o combustível.
À escala local, as condições climáticas são um determinante fundamental para a propagação do fogo. Temperaturas elevadas e humidade baixa, por exemplo, são características propícias à ocorrência e propagação de fogos e, se associadas a vento forte, podem resultar em eventos extremos de dimensão considerável.

Nas últimas décadas verificou-se, um pouco por todo o mundo, o aumento de eventos extremos de fogos, não obstante o esforço humano de supressão (Stocks et al. 2002, Trigo et al. 2005, Pereira et al. 2005, Running 2006, Trigo et al. 2006, Boschetti et al. 2008, Pechony and Shindell 2010), afectando directamente a sociedade e influenciando o próprio clima (Gillett et al. 2004). Observou-se um aumento da área afectada, nomeadamente na América do Norte, como também um acréscimo na ocorrência de fogos em locais de baixa probabilidade de ocorrência e extremamente raros, como na Islândia em 2007. Como consequência desta tendência, estima-se que em 40 anos o aumento de emissões provenientes da biomassa queimada seja de 50% para o $CO_2$ e que haja uma duplicação da quantidade de $CO$ (Schultz et al. 2008).

Este crescimento deve-se, em boa parte, às políticas de desflorestação das florestas tropicais, mas também ao aumento do número de ocorrências e correspondente área de fogos em zonas boreais e temperadas (Kasischke and Turetsky 2006, der Werf et al. 2006, Schultz et al. 2008). Acredita-se que a tendência observada se deva ao aquecimento global (Gillett et al. 2004) e a períodos de

seca mais frequentes (Xiao and Zhuang 2007). Várias projecções resultantes de modelos apoiados em cenários climáticos, obtidos por modelos de circulação da atmosfera (GCM) (Krawchuk et al. 2009, Liu et al. 2010), mostram que o potencial de ocorrência de fogo a nível global irá aumentar. Haverá um balanço delicado entre as tendências da precipitação e da temperatura (Xiao and Zhuang 2007, Krawchuk et al. 2009) recolocando o clima no papel de determinante principal dos regimes do fogo à escala global (Pechony and Shindell 2010).

As interacções entre fogo e clima são complexas (Taylor et al. 2008) e na actualidade, apesar da influência antropogénica exercida nos regimes do fogo, o peso e o papel do clima tornam-se evidentes em eventos anómalos, quer em dimensão quer no período em que ocorrem. Tais eventos constituem uma oportunidade para aprofundar a análise e compreender como é que o clima modela os vários regimes. Torna-se, assim, necessário um conhecimento mais detalhado desta relação, quer no espaço quer no tempo, para se poder estimar futuras variações dos regimes do fogo em resposta à subida da temperatura associada a uma mudança global do clima (Taylor et al. 2008). Neste contexto, é fundamental para a compreensão dos processos e correspondentes impactos ecológicos, atmosféricos e climáticos, uma quantificação histórica, à escala global, da área afectada pela biomassa queimada.

## Importância da detecção remota

A utilização da detecção remota por sensores a bordo de satélites revolucionou a investigação do estudo da Terra, não só possibilitando a observação de zonas remotas de difícil acesso, mas também pondo ênfase na dinâmica a diferentes resoluções espaciais e temporais. Tendo tido o seu início na década de 70, a detecção remota, limitada à meteorologia, possibilitou a observação dos processos atmosféricos de 10% para 100% da superfície terrestre, melhorando significativamente o grau de confiança das previsões do tempo. O seu desenvolvimento e alargamento a outros campos da ciência proporcionou também novas descobertas e uma compreensão mais profunda dos processos terrestres e atmosféricos. De entre alguns destacam-se a capacidade de observar o buraco do ozono e entender a química associada, compreender as correntes oceânicas e o campo da temperatura da superfície do mar associadas ao fenómeno do *El Niño* bem como a perturbação climática associada à libertação de aerossóis provocada pela erupção do vulcão Pinatubo (15 de Junho 1991).

Nas últimas quatro décadas observou-se um desenvolvimento impressionante nas características espectrais dos sensores, nas plataformas de observação, na velocidade de transmissão e processamento de dados, possibilitando a caracterização da superfície terrestre e as mudanças de paisagem. Estas capacidades de observação são consideradas fundamentais pela comunidade científica e têm um papel importante em ajudar a sociedade a gerir os recursos planetários e também a lidar com os desafios ambientais.

#### Detecção de áreas queimadas

A área queimada é considerada como um dos parâmetros mais incertos para a quantifi-

cação das emissões atmosféricas. Pode ser medida *in situ* por bombeiros ou agentes da protecção civil, obtendo-se a máxima resolução espacial possível (+1m) mas, em contrapartida, uma menor resolução temporal (por evento); pode também ser obtida por sensores remotos, quer a bordo de aviões ou de satélites artificiais que, dependendo da órbita e características do sensor, variam entre 30m e 16 em 16 dias (*Thematic Mapper*) a 500m diário (MODIS). Por último, através da dendrocronologia, a informação de eventos pode ser obtida através da análise dos anéis das árvores (Arno and Sneck 1977) que apresentam uma resolução espacial pontual muito dispersa mas, em compensação, uma extensão temporal de séculos.
Ainda assim, a detecção remota, feita com recurso a imagens de satélite, é o único meio para analisar os regimes do fogo à escala global, obtendo-se dados comparáveis no espaço e no tempo.

Consoante o número de bandas espectrais e a sua localização no espectro electromagnético, é possível obter dois tipos de informação, áreas queimadas e fontes de calor, também denominados fogos activos. As áreas queimadas são maioritariamente obtidas pela informação adquirida nas bandas do visível e os focos de calor obtidos pelas bandas térmicas. Através do cálculo de índices que potenciem a informação do estado da superfície, seja ao nível da vegetação, do albedo ou das temperaturas do solo, e aplicando técnicas de agregação temporal, de forma a remover a contaminação atmosférica, em conjugação com regras em forma de classificador, é possível obter cartografias de áreas queimadas e respectivas estimativas de cargas de combustível (Sa et al. 2007).

Como em todos os campos da ciência, a evolução da detecção remota de áreas queimadas foi determinada por um balanço entre o interesse científico e o progresso tecnológico. Até ao fim da década de 90 foram efectuados muitos estudos locais, relacionados (directa ou indirectamente) com fogo de vegetação, abrindo o caminho ao desenvolvimento de técnicas de agregação temporal (Cabral et al. 2003, Sousa et al. 2003) e à criação de índices de vegetação (Pinty and Verstraete 1992, Flasse and Verstraete 1994, Pereira 1999), albedo (Saunders 1990, Csiszar and Gutman 1999, Pinty et al. 2000) e temperaturas superficiais (Price 1984, Sobrino et al. 1994). Como resultado, salienta-se a primeira estimativa da área queimada e de emissões libertadas pela biomassa à escala regional para África (Barbosa et al. 1999) e o estudo global de focos de calor onde, pela primeira vez, se estabeleceu a sazonalidade e distribuição espacial da ocorrência de fogos (Dwyer et al. 2000).
Na corrente década, devido à importância do tema, esforços por parte da comunidade científica foram canalizados para a elaboração de cartografias globais de áreas queimadas, onde se destaca o produto *Global Burnt Area 2000* (GBA2000) (Tansey, Grégoire, Stroppiana, Sousa, Silva, Pereira, Boschetti, Maggi, Brivio and Fraser 2004), elaborado com recurso a imagens do sensor *VEGETATION* a bordo do satélite *Satellite Pour lObservation de la Terre* (SPOT), durante o ano 2000. A importância do GBA2000, para além da quantificação da área global afecta ao fogo, é a de ter permitido elaborar uma estimativa global das emissões provenientes da biomassa queimada (Ito and Penner 2004).
Complementar ao GBA2000, o *World Fire Atlas* (WFA) baseado no sensor *Along Track Scanning Radiometer* (ATSR), a bordo dos satélites *European Remote Sensing* (ERS) e ENVISAT, consiste no inventário global de fogos activos desde 1995 (Arino and J.M. Rosaz 1999), o que permitiu re-

gistar e realçar a variabilidade inter-anual, fortemente influenciada por fenómenos climáticos de larga escala como o *El Niño*.

Na actualidade, os avanços qualitativos obtidos através das distribuições globais, tanto de focos de calor como da área ardida, obtidas pelos diversos produtos (Roy et al. 2002, Tansey, Grégoire, Binaghi, Boschetti, Brivio, Ershov, Flasse, Fraser, Graetz and Maggi 2004, Simon et al. 2004, Roy et al. 2005, Roy et al. 2008) possibilitaram estudos da variabilidade espacial e temporal a diferentes escalas (Kajii et al. 2002, Generoso et al. 2003, Hoelzemann et al. 2004, Ito and Penner 2004, der Werf et al. 2006).

No contexto das alterações climáticas, a resposta do comportamento do fogo à variabilidade climática, observada em certas regiões, realça a importância de uma continuidade em programas de cartografia global das áreas queimadas como, o produto MCD45, obtido através do sensor *Moderate Resolution Imaging Spectroradiometer* (MODIS) a bordo dos satélites Aqua e Terra e, o L3JRC baseado no produto GBA2000. Apesar das suas qualidades, ambos os produtos pecam pela falta de extensão, cobrindo apenas 9 e 7 anos, respectivamente. Esta amplitude revela-se insuficiente para se poder estudar, com um nível de significância satisfatório, o efeito e tendências do clima nos regimes do fogo. Surge, assim a necessidade da elaboração de uma cartografia complementar que cubra um período mais extenso (Schultz et al. 2008), onde o sensor AVHRR, suportando um longo e único registo histórico de imagens, pode desempenhar um papel fundamental.

***Advanced Very High Resolution Radiometer (AVHRR)***

O sensor AVHRR voa a bordo da série de satélites de órbita polar da *National Oceanic and Atmospheric Administration* (NOAA) a uma altitude de 830 km. Tem uma largura de varrimento da superfície de 2.800 km e uma resolução espacial de 1,1 km no *nadir*. A órbita do satélite permite duas passagens diárias, uma diurna e outra nocturna, sobre o mesmo local resultando em quatro coberturas diárias no equador e nas latitudes médias e oito passagens nas latitudes altas. A versão AVHRR/2, em funcionamento desde Junho de 1981, possui 5 bandas (Tabela 1.1). As bandas 1 e 2 são usadas na detecção de nuvens, medições do estado da vegetação e na detecção de áreas ardidas. A banda 3 é usada na detecção de fontes de calor, vindo a ser substituída na versão AVHRR/3 por duas bandas devido à sensibilidade de saturação durante as passagens diurnas. As bandas 4 e 5 fornecem informação térmica, sendo aplicadas para a determinação da temperatura da superfície do mar, do solo e das nuvens e, se combinadas, podem ser usadas para corrigir os efeitos atmosféricos.

O sensor AVHRR possui apenas calibração a bordo para as bandas térmicas o que torna difícil a utilização de longas séries de bandas do visível sem recorrer a re-calibrações. Devido à trajectória orbital e ao atrito espacial, o satélite deriva na sua órbita provocando um atraso na hora de passagem, estando a superfície sujeita a um ângulo de iluminação solar diferente.

A imagens capturadas pelo AVHRR são registadas em dois formatos, o *Local Area Coverage* (LAC)

**Table 1.1**: *Caracteristicas e aplicações do sensor AVHRR (Cracknell 1997)*

| **Banda** | **c.d.o.($\mu$m)** | **Tipo** | **Aplicações** |
|---|---|---|---|
| 1 | 0.58-0.68 | visível | superfície, nuvens, vegetação, albedo |
| 2 | 0.73-1.10 | infravermelho próximo | vegetação, áreas queimadas, albedo |
| 3 | 3.55-3.93 | térmico | fogo e vulcões |
| 4 | 10.5-11.3 | térmico | mar, terra, temperatura de nuvens e evapotranspiração |
| 5 | 11.5-12.5 | térmico | mar, terra, temperatura de nuvens e evapotranspiração |
| **Largura** | 2,800 km | **Ângulo de varrimento** | $\pm$ 55.4, Resolução no *nadir* 1.1 km |
| **Frequência** | 12 horas | **Repetição de ciclo** | 9.2 dias |

e o *Global Area Coverage* (GAC). O formato LAC, com a resolução máxima de 1.1 km, é gravado a bordo para posteriormente ser transmitido a estações de recepção colocadas estrategicamente sobre a superfície da terra ou/e, transmitido a qualquer estação dentro do seu campo de visão, tomando as imagens o nome de *High Resolution Picture Transmission Format* (HRPT). Como consequência de limitações de memória, através de um processo de reamostragem, também são gravadas imagens com uma resolução de 4 km, denominadas imagens GAC.

Embora tenha sido concebido como um satélite meteorológico para observação da atmosfera, a cobertura diária global por um conjunto de 5 bandas espectrais, escolhidas nas janelas atmosféricas, associado a um registo histórico longo, fez do sensor AVHRR um instrumento valioso para a observação da superfície terrestre. A sua utilização permitiu, entre outros estudos, a identificação de tendências na produtividade primária (Ricotta et al. 1999), da cobertura dos gelos (Bindschadler and Vornberger 1990), e da temperatura da superfície do mar (Walton 1988), propriedades ópticas da atmosfera (Holben et al. 2002), mudanças do coberto vegetal (Potter et al. 2005) e a detecção de áreas queimadas e fogos activos. O sucesso da adopção deste sensor ao estudo do fogos, tanto para detecção das áreas queimadas como de fogos activos, explica-se pelo potencial das características espectrais (Li and Giglio 1999, Harris 1996) e pelo vasto número de artigos científicos (Tabela 1.2).

A banda 1, na banda espectral do vermelho (RED), é muito sensível à verdura da vegetação. Este facto torna a diferença de reflectância durante a passagem do fogo dependente do tipo de coberto, do solo e do tipo de fogo. Por sua vez, a banda 2, no infravermelho próximo (NIR), é sensível aos diferentes tipos de coberto e ao elevado contraste entre vegetação e solo, o que resulta sempre num decréscimo de reflectância. Seja só ou em combinação com o vermelho, na forma de índice de vegetação ou albedo, é a banda mais utilizada para detecção de cicatrizes do fogo. A banda 3, no infravermelho médio, é muito sensível a fontes de temperatura. A sua utilização revelou-se muito útil na detecção de fogos activos em fogos florestais (Cahoon et al. 1994) e na detecção de manchas quentes escondidas debaixo da fumaça através da parte reflectida da banda. Infelizmente, esta banda apresenta a desvantagem de o sensor não precisar de temperaturas muito elevadas para saturar e a parte reflectida apenas responde até 10% da radiação emitida. As bandas térmicas 4 e 5 apresentam um baixo contraste, mas proporcio-

nam a distinção entre superfícies queimadas e água líquida, determinada por uma redução na evapotranspiração e pelo aumento da absorção de radiação pela superfície (Cahoon et al. 1994).

A tabela 1.2 apresenta algumas das características dos principais estudos de áreas queimadas e fogos activos efectuados com recurso a imagens AVHRR. Da amostra, pode concluir-se que o pico de actividade decorreu durante a década de 90, mas que as imagens continuam a ser utilizadas, em particular para estudos multi-anuais. A utilização de imagens AVHRR, nos seus vários formatos, não se restringiu no espaço nem no tempo. Existem estudos efectuados em todos os continentes, a diferentes escalas espaciais, nos diferentes períodos dos satélites e aplicando um leque variado de algoritmos de classificação. Destacam-se dois estudos pioneiros, a primeira análise continental multi-anual das áreas queimadas (1981-1991) para África (Barbosa et al. 1999) e o primeiro estudo global de fogos activos que possibilitou determinar a sazonalidade e extensão dos fogos de vegetação (Dwyer et al. 2000). Como resultado do esforço realizado por parte da comunidade científica, não restrito ao estudo dos fogos, foi possível estabelecer as fundações a partir das quais se desenvolveram os algoritmos aplicados a imagens dos sensores da geração seguinte, como é o caso do EOS-MODIS e do NPOESS-VIIRS.

**Table 1.2**: *Características de alguns estudos com aplicação de imagens AVHRR aos fogos.*

| **Área** | **Período** | **Data** | **Algoritmo** | **Referência** |
|---|---|---|---|---|
| Floresta Boreal | 1990 | AVHRR | máximo NDVI | (Kasischke et al. 1993) |
| África Ocidental | 1991-1992 | AVHRR | dinâmico | (Kennedy et al. 1994) |
| África | 1981-1990 | AVHRR-GAC | limiar múltiplo | (Koffi et al. 1996) |
| Floresta Boreal | 1990-1992 | AVHRR | máximo NDVI | (Kasischke and French 1995) |
| | | AVHRR-LAC | contextual | (Flasse and Ceccato 1996) |
| Espanha | 1993-1994 | AVHRR | Máximo NDVI | (Fernndez et al. 1997) |
| | | | analise de índices | (Pereira 1999) |
| África | 1981-1990 | AVHRR GAC | limiar múltiplo | (Barbosa et al. 1999) |
| Global | 1992-1993 | GAC | detecção fogos activos | (Dwyer et al. 2000) |
| América do Norte | 1995-1996 | HRPT | híbrido | (Fraser et al. 2000) |
| Senegal | 1996 | HRPT | estatístico | (Nielsen et al. 2002) |
| América do Norte | 1999 | AVHRR-HRPT | dinâmico | (Pu et al. 2004) |
| Rússia | 1995-2002 | HRPT | | (Sukhinin et al. 2004) |
| América do Norte | 1989-2000 | AVHRR-HRPT | detecção fogos activos | (Pu et al. 2007) |
| Canada | 1984-2006 | LAC-HRPT | dinâmico | (Chuvieco et al. 2008) |

## Objectivos

A tese aqui apresentada teve como objectivo principal a elaboração de uma base de dados de cartografia global de áreas queimadas e consequente análise dos seus impactos ecológicos e climáticos. Para atingir tal objectivo, dividiu-se o trabalho em duas fases com objectivos distintos. A primeira fase consiste na agregação de condições necessárias à produção de um *dataset* desta dimensão, bem como estabelecer metas e produzir dados complementares. A segunda fase, consistiu na produção da cartografia global das áreas ardidas, entre os anos de 1981 a 1999, com recurso à base de dados de imagens diárias AVHRR *Pathfinder*. Devido aos requisitos definidos em cada fase, foi necessário estabelecer objectivos intermédios, apresentados em anexo sob forma de artigos, publicados ou propostos a publicação. Os objectivos intermédios foram:

1. Fase:

   - Estabelecer uma fonte, independente e segura, através da qual se pudesse determinar uma climatologia da incidência dos fogos de vegetação. Para tal foi efectuado uma filtragem aos dados WFA com o objectivo de remoção da informação dos fogos não-vegetativos e dos falsos alarmes.

   - Quantificar e avaliar os possíveis erros de comissão e omissão, e seus determinantes, associados à classificação de imagens de satélite de menor resolução.

2. Fase:

   - Procedeu-se ao pré-tratamento da base de dados AVHRR *Pathfinder*, recorrendo não só a técnicas de agregação temporal para remoção de nuvens e correspondentes sombras e conservação de áreas ardidas como também à identificação e posterior remoção da informação espectral responsável pela deriva orbital do satélite.

   - Realizou-se a elaboração e classificação das imagens AVHRR *Pathfinder* tratadas, o que resultou na cartografia de áreas queimadas entre os anos 1981-1999.

## Estrutura

A presente tese fundamenta-se num conjunto de quatro estudos, publicados ou propostos a publicação em revistas com revisão cientifica e é constituída por quatro capítulos, onde se inclui esta introdução contextualizante. No segundo capítulo procura-se fazer uma síntese de cada um dos artigos, dos quais o primeiro encontra-se já publicado, estando os restantes em fase de revisão. No capítulo 3 apresentam-se as conclusões deste trabalho e expõem-se algumas perspectivas. As referências aparecem no capítulo 4; por fim, em anexo, surgem os artigos que integram esta tese .

Os artigos apresentam-se não só seguindo uma ordem cronológica, como também, uma lógica de

precedência, na qual cada estudo depende do trabalho e resultados do artigo anterior.

Os dois primeiros artigos são estudos preparatórios que tentam, em primeiro lugar, estabelecer uma fonte de dados independente, exclusivamente de fogos de vegetação e, em segundo lugar, gerir expectativas e balizar os possíveis erros associados ao uso de sensores de baixa resolução espacial. Este estudo não se restringe a um único sensor.

Os dois artigos seguintes, apresentam o trabalho de pré-processamento e produção do produto LPAL-PAL.

## Lista de artigos

Esta tese fundamenta-se nos seguintes estudos, desenvolvidos no âmbito dos objectivos propostos:

**artigo 1:** Mota, B., J.M.C. Pereira, D. Oom, M.J.P. Vasconcelos, and M. Schultz (2006). Screening the ESA ATSR-2 World Fire Atlas (1997-2001). Atmospheric Chemistry and Physics, 6: 116.

**artigo 2:** Mota, B.,, J.M.C. Pereira, A. Sousa (....) Burned area mapping accuracy limits: a global, multi-sensor assessment using the Pareto boundary approach. Remote Sensing of Environment.

**artigo 3:** Mota, B., J.M.C. Pereira, J. Pinzon (...) The Large Burned Area Product (LBAP-PAL): A global monthly series (1981-1999) based on the AVHRR Pathfinder land Data. Part I Compositing and Detrending.

**artigo 4:** Mota, B., J.M.C. Pereira, R. Trigo (...) The Large Burned Area Product (LBAP-PAL): A global monthly series (1981-1999) based on the AVHRR Pathfinder land Data. Part II Burned area classification.

No decorrer do período em que se desenvolveu o presente doutoramento, foram ainda publicados os seguintes trabalhos que não foram incluídos na tese, mas para os quais houve uma contribuição significativa ao nível do conhecimento:

Trigo, R.M., J.M.C. Pereira, M.G. Pereira, B. Mota, M.T. Calado, C.C. Da Camara, F.E. Santo e (2006) Atmospheric conditions associated with the exceptional fire season of 2003 in Portugal. International Journal of Climatology, 26: 17411757.

Le Page, Y., Pereira, J. M. C., Trigo, R., da Camara, C., Oom, D., and Mota, B. (2008): Global fire activity patterns (19962006) and climatic influence: an analysis using the World Fire Atlas, Atmospheric Chemistry and Physics, 8, 19111924.

Ana C.L. Sá, José M.C. Pereira, Bernardo Mota, Paulo M. Barbosa, Martin E. Charlton, Alexander S. Fotheringham. (2011) The pyrogeography of sub-Saharan Africa: a study of the spatial non-stationarity of fireenvironment relationships using GWR. Journal of Geographical Systems, Volume 13, Number 3, 227-248.

# Capítulo 2

# Resumos dos artigos

## Artigo 1: *Screening the ESA ATSR-2 World Fire Atlas (1997-2001)*

Mota, B., J.M.C. Pereira, D. Oom, M.J.P. Vasconcelos, and M. Schultz

O estudo aqui apresentado resultou da necessidade de se obter um conjunto de dados independente que pudesse servir de referência. Para tal foram filtrados os dados do *World Fire Atlas* (WFA), algoritmo 2 (com limiar em 308 K), para o período compreendido entre 1997-2002, recorrendo a um conjunto variado de bases de dados como o tipo de coberto vegetal, luzes nocturnas e actividade vulcânica. Foram também utilizadas técnicas de detecção de agregados espaço-temporais para identificar as ocorrências anómalas de fogo activo.

O produto WFA baseia-se em dados nocturnos do sensor *Along Track Scanning Radiometer* (ATSR) transportado a bordo do satelite *Second European Remote-Sensing Satellite* (ERS-2). O sensor tem uma resolução espacial de 1 km e uma frequência de observação de 3 dias sobre o equador. Como produto pioneiro que é, o WFA contém o registo de detecções de fogos activos de temporalidade mais extensa, tendo já sido utilizado em inúmeros estudos de biomassa queimada. Algumas das limitações do WFA consistem na inclusão de superfícies muito quentes, chamas de refinarias de gás e petrolíferas, luzes nocturnas e uma subestimação da actividade global do fogo devido à hora de passagem.

Contudo, pressupunha-se que só uma parte relativamente pequena do produto WFA é que não correspondia a fogos vegetativos. Os nossos resultados não corroboram tal pressuposto; mostram que anualmente a percentagem de falsos alarmes e fogos não vegetativos varia entre 20.6% em 1997 e 27.9% em 1998, sendo que os falsos alarmes, fogos não vegetativos, superfícies quentes e as chamas de refinarias de gás e petróleo representam a maior parte.

## Artigo 2: *Burned area mapping accuracy limits: a global, multi-sensor assessment using the Pareto boundary approach*

Mota, B.,, J.M.C. Pereira, A. Sousa

Este estudo teve como objectivo determinar as características da detecção de áreas queimadas para um conjunto de sensores com resoluções espaciais distintas. Para tal, procedeu-se a uma degradação espacial de 72 mapas de áreas queimadas, correspondendo a classificações de imagens *Landsat* (30m) globalmente distribuídas por vários tipos de coberto vegetal. A simulação da degradação foi obtida com recurso a uma distribuição gaussiana adaptada às características ópticas de cada sensor considerado no estudo, nomeadamente os sensores MODIS e AVHRR, e reamostrada para os sub-produtos GAC e PAL.

Utilizando o conceito da fronteira de *Pareto* aplicado à detecção remota, foi efectuada uma análise de sensibilidade de maximização da área detectável, aplicando três critérios de classificação a cada mapa e para cada sensor. A análise mostrou que a aplicação do limiar compensatório entre erros de comissão e erros de omissão conduz a melhores resultados de área detectável. O limiar varia com a resolução do sensor e com o tipo de padrão espacial das cicatrizes do fogo. Após a aplicação do critério de compensação a totalidade dos mapas, procedeu-se à análise da distribuição espacial das áreas detectáveis e à agregação dos resultados por tipo de coberto.

Os resultados mostram que, na maioria dos casos, ambas as resoluções do sensor MODIS apresentam erros de área detectável abaixo de 5% e que o sensor AVHRR, na versão 1.1km, revela algumas limitações de detecção nas florestas tropicais da América do Sul e nas paisagens das latitudes médias. Os sub-produtos, GAC e PAL, apresentam erros de subestimação que vão até 50% na América do Sul, mostrando incapacidade de detecção de áreas pequenas. As áreas ardidas do Noroeste Australiano, devido ao seu tamanho e padrão, são as que apresentam erros menores, sendo detectadas por todos os produtos.

## **Artigo 3:** *Large Burned Area Product (LBAP-PAL): A global monthly series (1981-1999) based on the Pathfinder AVHRR land Data. Part I - Compositing and Detrending*

Mota, B., J.M.C. Pereira, J. Pinzon

Este artigo, parte 1 de 2, teve como objectivo, proceder a uma pré-análise de critérios de agregação temporal e ao pré-processamento para eliminar a componente de deriva do satélite da base de dados de imagens *Advanced Very High-Resolution Radiometer* (AVHRR) segundo o produto *Pathfinder Land dataset* (PAL).

Na pré-análise, o produto de dados diários foi utilizado para produzir compósitos mensais para o ano de 1998, mediante a aplicação de 5 tipos de algoritmos de agregação temporal a partir dos quais se analisou a sensibilidade espacial e temporal da perturbação do sinal do fogo de vegetação, as características de iluminação e a eficiência de limpeza das nuvens e sombras. Os resultados confirmam que o algoritmo M4mALB, baseado na pela escolha do píxel com a temperatura de brilho da banda 4 máxima, de entre os 5 píxeis com o menor albedo, retém melhor a informação de pixéis pós-fogo, produz imagens mais limpas de nuvens e sombras e resulta numa menor variabilidade de ângulos de iluminação.

Após a aplicação do algoritmo à totalidade do produto PAL, procedeu-se ao cálculo de um conjunto de índices, nomeadamente a temperatura de superfície, o albedo e o GEMI. A metodologia adoptada para a remoção da componente de deriva orbital teve como base a elaboração de uma tabela de referência de áreas, provenientes do cruzamentos entre os produtos GLC2000 e *Eco-regions of the World*, a partir das quais as séries temporais foram decompostas com recurso à decomposição em modo empírico (EMD) e identificada a correspondente significância, através de uma análise de correspondência canónica.

Os resultados mostram que existem três categorias de áreas onde se faz sentir a deriva orbital, as quais vão desde as zonas tropicais de elevada sensibilidade até às latitudes médias onde a significância se esgota. O albedo e o GEMI são mais sensíveis, decaíndo rapidamente e a temperatura de superfície é menos sensível mas cobre uma área maior do globo.

## Artigo 4: *Large Burned Area Product (LBAP-PAL): A global monthly series (1981-1999) based on the Pathfinder AVHRR land Data. Part II - Burned area classification*

Mota, B., J.M.C. Pereira, R.M. Trigo

Este artigo, parte 2 de 2, tem por objectivo a elaboração de uma cartografia global de áreas queimadas para o período compreendido entre 1981-1999.
Para tal, foi desenvolvido um classificador supervisionado, *Random Forest*, através da recolha de áreas de treino.

Com o intuito de remover falsos alarmes, foram desenvolvidas máscaras mensais da climatologia do fogo baseadas nos fogos activos WFA. Através da combinação de probabilidades, das máscaras e do classificador, foi possível eliminar não só falsos alarmes como também potenciar a sazonalidade do fogo. Através da comparação, no tempo com estatísticas anuais de alguns países, no espaço com alguns mapas de área queimada continental e globalmente com estimativas de períodos recentes, conclui-se que o produto LBAP-APL é caracterizado por uma elevada subestimação. Os resultados anuais mostram uma crescimento significativo de área queimada para o período de estudo no Sul da Ásia e salientam a influência do factor humano nos regimes de fogo através da sua incidência por tipo de coberto. A razão da elevada subestimação é, em parte, atribuída ao procedimento de reamostragem PAL e ao padrão espacial dos fogos.

# Capítulo 3

# Conclusões

O objectivo principal, assim como os objectivos intercalares, da presente tese foram atingidos. Como resultado final, obteve-se o produto das grandes áreas ardidas mensais, à escala global, para o período compreendido entre 1981-1999 com a resolução espacial de 8km (LBAP-PAL). Apesar da elevada subestimação global e da incapacidade de detectar correctamente o efeito de eventos ENSO, foi possível detectar uma tendência crescente significativa de área queimada no sul da Ásia, bem como identificar a influência da acção do Homem nos vários regimes do fogo, em particular a prática de fogos agrícolas nos trópicos, e a desflorestação no Hemisfério Sul de África e no Sudoeste Asiático.

O produto é caracterizado por uma subestimação elevada da área queimada. Em comparação com produtos recentes, o LBAP-PAL estima valores médios globais de 1.4 $Mkm^2$, o que pode representar uma subestimação media de 60%. Esta elevada subestimação resulta de uma combinação de factores das quais se destacam:

- O processo de reamostragem do PAL é limitador, sendo-lhe atribuída uma parte significativa da subestimação global e sobrestimação em alguns casos. O valor de cada píxel (8km PAL) é determinado por uma média de 7% dos pixéis AVHRR de 1.1km, o que atribui uma probabilidade baixa a um fogo de dimensão inferior a 100ha (1 píxel AVHRR) ser seleccionado no processo de reamostragem para futura detecção.
- De igual modo, devido ao critério de maximização do NDVI do processo de reamostragem do formato GAC para PAL, é dada a preferência a pixeis não queimados em relação a pixéis queimados, diminuindo a probabilidade de detecção. A junção destes dois factores, implica que o cálculo das diferenças mensais dos pixeis possa não corresponder à mesma localização, levando assim, a um grau de incerteza tendencialmente negativo na classificação de pixéis queimados.
- A fragmentação da área característica de cada fogo pode induzir uma dificuldade adicional. Este factor, realçado no artigo 2, é limitador podendo conduzir facilmente à subestimação elevada ou total nas latitudes médias, onde os fogos têm uma área pequena e a uma subestimação elevada nas florestas tropicais onde a elevada fragmentação está associada a áreas pequenas. Por outro lado, os fogos grandes e fragmentados, localizados nas savanas africanas e australianas, podem conduzir a uma área detectável mais precisa.

Além das limitações encontradas no decorrer desta tese, e apesar de não se pretender contemplar qualquer solução, há que ter em conta as limitações de uma ineficiente calibração compen-

satória, da degradação dos sensores, da contaminação atmosférica provocada pelas duas grandes erupções vulcânicas e pelo efeito de *global dimming* (Stanhill and Cohen 2001, Wild et al. 2007).

Apesar da limitação dos resultados, o pré-processamento de remoção das tendências espúrias, devido ao efeito de deriva orbital, baseado numa decomposição de modo empírico (EMD), mostrou-se eficiente, recolocando os dados numa gama de valores comparáveis, quer entre satélites quer intra-satélites. A desvantagem deste procedimento pode advir de, juntamente com a tendência identificada e removida, estarem contidas tendências com outras origens como, a degradação do sensor, o *global dimming* e a evolução da vegetação.

A selecção dos índices GEMI, albedo e temperatura de supreficie, embora em formato analítico simples, revelou-se útil e explícita na recolha de áreas de treino para compreender e destacar diferenças após a passagem do fogo. Da mesma forma, a aplicação do algoritmo *Random Forest* para produzir um classificador global de áreas queimadas, mostrou-se muito eficaz em absorver a complexidade de situações possíveis de ocorrência de fogo, traduzidas por um conjunto variado de valores e diferenças de valores dos índices.

Embora constituídos por diferentes tipos de informação, ambos os produtos LBAP-PAL de áreas queimadas e o WFA de fogos activos beneficiaram de se utilizar informação complementar. No caso do WFA, como o artigo 1 mostrou, existe a desvantagem de se ter utilizado o algoritmo baseado apenas num limiar aplicado à banda térmica. A elevada percentagem de focos de calor e falsos alarmes não oriundos de fogo de vegetação salienta a multiplicidade de situações que podem dar origem a uma classificação de fogo errada.
A complementaridade com outros produtos, através do desenvolvimento de máscaras ou probabilidades, quando utilizada com cuidado, revela grande utilidade podendo resultar em informação mais precisa.
Neste sentido, a tese aqui apresentada estudou e desenvolveu metodologias para filtragem de falsos alarmes em fogos activos como, a de criar, com base nesta informação, mapas de probabilidade climatológica de ocorrência de fogo para serem combinados com a própria classificação de áreas ardidas, potenciando o fogo e atenuando as falsas detecções.

Desenvolver mapas de áreas queimadas com sensores de baixa resolução nunca será tarefa fácil; a possível área detectável está associada à área e à fragmentação de cada fogo. Como mostra o estudo 2, a optimização da área detectável implica que um classificador tenha uma flexibilidade na escolha de diferentes limiares consoante o tipo de fragmentação.

O recente produto *Long Term Data Record* (LTDR), actualmente na sua versão 3, apresenta inquestionáveis melhoramentos em relação ao PAL. De entre alguns destaca-se a geolocalização mais precisa, a revisão dos coeficientes de calibração, a correcção atmosférica ao nível do contedo de vapor de água, ozono e aerossóis, a correcção BRDF e os novos algoritmos de classificação de nuvens e de qualidade. Embora em fase experimental, o referido produto também contém informação da reflectância da banda 3 (no infravermelho médio), cuja utilidade é reconhecida para a observação de superfície através do fumo.

Apesar das referidas vantagens, o produto continua a não assegurar a continuidade dos dados após o ano 2000, como também não colmata a falha de dados observada no último trimestre de 1994. Qualquer futura aplicação, desta versão ou de versões posteriores, ao estudo das áreas queimadas terá de ter em conta que as imagens, continuarão a registar o efeito da deriva orbital e, em parte, a derivarem de dados GAC que, como se demonstra neste trabalho, tende a conduzir a uma subestimação global (Belward et al. 1994, Eva and Lambin 1998).
Neste contexto, a tese aqui exposta, apresenta um conjunto de metodologias facilmente adoptadas ao produto LTDR.

Como resultado, obtiveram-se dois conjuntos de dados cujo valor é inegável. A filtragem efectuada aos dados WFA, entretanto estendida até 2006 (10 anos), representa uma valiosa fonte de informação, já utilizada, em estudos de variabilidade do fogo (Page et al. 2008), caracterização da piro-geografia (Krawchuk et al. 2009) e como complemento na estimativa de emissões (Schultz et al. 2008, Mieville et al. 2010).

Esta base de dados apresenta três grandes vantagens. Primeiro, consiste no *dataset* de fogos activos mais longo. Segundo, é actualmente a única base de dados temporal que cobre um evento severo de ENSO. Terceiro, cobre tanto um período significativo anterior como posterior ao ano 2000. Tal característica, poderá ser útil para estabelecer factores de conversão entre um produto de áreas ardidas proveniente do LTDR e os recentes produtos globais de áreas ardidas, como MCD45 e L3JRC.

O produto LBAP-PAL, apesar da elevada subestimação e das limitações apresentadas, não deixa ainda de representar o historial de 19 anos de grandes áreas queimadas. Embora a sua aplicação seja limitada em termos de área efectiva, a sua relativização através do cálculo de anomalias sazonais poderá servir para quantificar a influência do clima em eventos de fogo extremo. Os mesmos dados poderão, no futuro, servir como termo de comparação com produtos de áreas queimadas provenientes de imagens do sensor AVHRR, METEOSAT ou GOES.

O acesso aos dados é livre e poderá ser solicitado ao autor através de *bmota@isa.utl.pt*.

# Bibliografia


Andreae, M. O. and Merlet, P.: 2001, Emission of trace gases and aerosols from biomass burning, *Global Biogeochemical Cycles* **15**(4), 955–966.

Andreae, M. O., Rosenfeld, D., Artaxo, P., Costa, A. A., Frank, G. P., Longo, K. M. and Silva-Dias, M. A. F.: 2004, Smoking rain clouds over the amazon, *Science* **303**(5662), 1337.

Arno, S. F. and Sneck, K. M.: 1977, *A method for determining fire history in coniferous forests of the mountain west*, Intermountain Forest and Range Experiment Station, Forest Service, US Dept. of Agriculture.

Assessment, M. E.: 2005, *Ecosystems and human well-being*, Vol. 5, Island Press.

Barbosa, P. M., Stroppiana, D., Grgoire, J. M. and Pereira, J. M. C.: 1999, An assessment of vegetation fire in africa (19811991): Burned areas, burned biomass, and atmospheric emissions, *Global Biogeochemical Cycles* **13**(4), 933–950.

Belward, A. S., Kennedy, P. J. and Gregoire, J. M.: 1994, The limitations and potential of AVHRR GAC data for continental scale fire studies, *International journal of remote sensing* **15**(11), 2215–2234.

Bindschadler, R. A. and Vornberger, P. L.: 1990, AVHRR imagery reveals antarctic ice dynamics, *EOS Transactions* **71**, 741.

Bond, W. J. and Keeley, J. E.: 2005, Fire as a global [] herbivore': the ecology and evolution of flammable ecosystems, *Trends in Ecology & Evolution* **20**(7), 387–394.

Boschetti, L., Roy, D., Barbosa, P., Boca, R. and Justice, C.: 2008, A MODIS assessment of the summer 2007 extent burned in greece, *International Journal of Remote Sensing* **29**(8), 2433–2436.

Bowman, D., Balch, J. K., Artaxo, P., Bond, W. J., Carlson, J. M., Cochrane, M. A., D'Antonio, C. M., DeFries, R. S., Doyle, J. C. and Harrison, S. P.: 2009, Fire in the earth system, *science* **324**(5926), 481.

Butry, D. T., Mercer, E. D., Prestemon, J. P., Pye, J. M. and Holmes, T. P.: 2001, What is the price of catastrophic wildfire?, *Journal of Forestry* **99**(11), 9–17.

Cabral, A., Vasconcelos, M., Pereira, J. M. C., Bartholome, E. and Mayaux, P.: 2003, Multi-temporal compositing approaches for SPOT-4 VEGETATION, *International Journal of Remote Sensing* **24**(16), 3343–3350.

Cahoon, D. R., Stocks, B. J., Levine, J. S., Cofer, W. R. and Pierson, J. M.: 1994, Satellite analysis of the severe 1987 forest fires in northern china and southeastern siberia, *Journal of Geophysical Research* **99**(D9), 18627–18638.

Chuvieco, E., Englefield, P., Trishchenko, A. P. and Luo, Y.: 2008, Generation of long time series of burn area maps of the boreal forest from NOAA-AVHRR composite data, *Remote Sensing of Environment* **112**(5), 2381–2396.

Cochrane, M. A., Alencar, A., Schulze, M. D., Jr, C. M. S., Nepstad, D. C., Lefebvre, P. and Davidson, E. A.: 1999, Positive feedbacks in the fire dynamic of closed canopy tropical forests, *Science* **284**(5421), 1832.

Cracknell, A. P.: 1997, *The advanced very high resolution radiometer (AVHRR)*, CRC.

Crutzen, P. J.: 1979, The role of NO and NO2 in the chemistry of the troposphere and stratosphere, *Annual Review of Earth and Planetary Sciences* **7**(1), 443–472.

Crutzen, P. J. and Andreae, M. O.: 1990, Biomass burning in the tropics: Impact on atmospheric chemistry and biogeochemical cycles, *Science* **250**(4988), 1669.

Csiszar, I. and Gutman, G.: 1999, Mapping global land surface albedo from NOAA AVHRR, *Journal of Geophysical Research* **104**, 6215–6228.

DeFries, R. S., Houghton, R. A., Hansen, M. C., Field, C. B., Skole, D. and Townshend, J.: 2002, Carbon emissions from tropical deforestation and regrowth based on satellite observations for the 1980s and 1990s, *Proceedings of the National Academy of Sciences of the United States of America* **99**(22), 14256.

der Werf, G. R. V., Randerson, J. T., Giglio, L., Collatz, G. J., Kasibhatla, P. S. and Jr, A. F. A.: 2006, Interannual variability of global biomass burning emissions from 1997 to 2004, *Atmospheric Chemistry and Physics Discussions* **6**(2), 3175–3226.

Dwyer, E., Pinnock, S., Grgoire, J. M. and Pereira, J. M. C.: 2000, Global spatial and temporal distribution of vegetation fire as determined from satellite observations, *International Journal of Remote Sensing* **21**(6), 1289–1302.

Eva, H. and Lambin, E. F.: 1998, Remote sensing of biomass burning in tropical regions: sampling issues and multisensor approach, *Remote Sensing of Environment* **64**(3), 292315.

Fernndez, A., Illera, P. and Casanova, J. L.: 1997, Automatic mapping of surfaces affected by forest fires in spain using AVHRR NDVI composite image data* 1, *Remote Sensing of Environment* **60**(2), 153–162.

Flasse, S. P. and Ceccato, P.: 1996, A contextual algorithm for AVHRR fire detection, *International Journal of Remote Sensing* **17**(2), 419–424.

Flasse, S. and Verstraete, M. M.: 1994, Monitoring the environment with vegetation indices: comparison of NDVI and GEMI using AVHRR data over africa, *Vegetation, Modelling and Climatic Change Effects* p. 107135.

Foley, J. A., DeFries, R., Asner, G. P., Barford, C., Bonan, G., Carpenter, S. R., Chapin, F. S., Coe, M. T., Daily, G. C. and Gibbs, H. K.: 2005, Global consequences of land use, *science* **309**(5734), 570.

Fraser, R. H., Li, Z. and Cihlar, J.: 2000, Hotspot and NDVI differencing synergy (HANDS):: a new technique for burned area mapping over boreal forest, *Remote Sensing of Environment* **74**(3), 362–376.

Galanter, M., Levy, I. I. H. and Carmichael, G. R.: 2000, Impacts of biomass burning on tropospheric CO, NO x, and o3, *Journal of Geophysical Research* **105**(D5), 6633–6653.

Generoso, S., Bron, F. M., Balkanski, Y., Boucher, O. and Schulz, M.: 2003, Improving the seasonal cycle and interannual variations of biomass burning aerosol sources, *Atmospheric Chemistry and Physics* **3**(4), 1222.

Gillett, N. P., Weaver, A. J., Zwiers, F. W. and Flannigan, M. D.: 2004, Detecting the effect of climate change on canadian forest fires, *Geophysical Research Letters* **31**(18), L18211.

Harris, A. J. L.: 1996, Towards automated fire monitoring from space: semi-automated mapping of the january 1994 new south wales wildfires using AVHRR data, *Int. J. Wildland Fire* **6**(3), 107–116.

Hoelzemann, J. J., Schultz, M. G., Brasseur, G. P., Granier, C. and Simon, M.: 2004, Global wildland fire emission model (GWEM): evaluating the use of global area burnt satellite data, *Journal of Geophysical Research* **109**(D14), D14S04.

Holben, B., Vermote, E., Kaufman, Y. J., Tanr, D. and Kalb, V.: 2002, Aerosol retrieval over land from AVHRR data-application for atmospheric correction, *Geoscience and Remote Sensing, IEEE Transactions on* **30**(2), 212–222.

Houghton, J. T.: 1995, *Climate change, 1994: Radiative forcing of climate change and an evaluation of the IPCC IS92 emission scenarios*, Cambridge Univ Pr.

Houghton, R. A., Hackler, J. L. and Lawrence, K. T.: 2000, Changes in terrestrial carbon storage in the united states. 2: The role of fire and fire management, *Global Ecology and Biogeography* **9**(2), 145–170.

Ito, A. and Penner, J. E.: 2004, Global estimates of biomass burning emissions based on satellite imagery for the year 2000, *Journal of Geophysical Research* **109**(D14), D14S05.

Kajii, Y., Kato, S., Streets, D. G., Tsai, N. Y., Shvidenko, A., Nilsson, S., McCallum, I., Minko, N. P., Abushenko, N. and Altyntsev, D.: 2002, Boreal forest fires in siberia in 1998: Estimation of area burned and emissions of pollutants by advanced very high resolution radiometer satellite data, *Journal of Geophysical Research* **107**(D24), 4745.

Kasischke, E. S. and French, N. H. F.: 1995, Locating and estimating the areal extent of wildfires in alaskan boreal forests using multiple-season AVHRR NDVI composite data, *Remote Sensing of Environment* **51**(2), 263–275.

Kasischke, E. S., French, N. H. F., Harrell, P., Jr, N. L. C., Ustin, S. L. and Barry, D.: 1993, Monitoring of wildfires in boreal forests using large area AVHRR NDVI composite image data, *Remote Sensing of Environment* **45**(1), 61–71.

Kasischke, E. S. and Turetsky, M. R.: 2006, Recent changes in the fire regime across the north american boreal regionspatial and temporal patterns of burning across canada and alaska, *Geophysical Research Letters* **33**(9), L09703.

Kennedy, P. J., Belward, A. S. and Gregoire, J. M.: 1994, An improved approach to fire monitoring in west africa usingAVHRR data, *International Journal of Remote Sensing* **15**(11), 2235–2255.

Koffi, B., Gregoire, J. M. and Eva, H. D.: 1996, Satellite monitoring of vegetation fires on a multiannual basis at continental scale in africa, *Remote sensing, modeling and inventory development, and biomass burning in Africa* p. 225.

Koren, I., Kaufman, Y. J., Remer, L. A. and Martins, J. V.: 2004, Measurement of the effect of amazon smoke on inhibition of cloud formation, *Science* **303**(5662), 1342.

Krawchuk, M. A., Moritz, M. A., Parisien, M. A., Dorn, J. V. and Hayhoe, K.: 2009, Global pyrogeography: the current and future distribution of wildfire, *PloS One* **4**(4), 5102.

Laat, A. T. J. D., Gloudemans, A. M. S., Schrijver, H., den Broek, M. M. P. V., Meirink, J. F., Aben, I. and Krol, M.: 2006, Quantitative analysis of SCIAMACHY carbon monoxide total column measurements, *Geophysical Research Letters* **33**(7), L07807.

Lepers, E., Lambin, E. F., Janetos, A. C., DeFRIES, R., Achard, F., Ramankutty, N. and Scholes, R. J.: 2005, A synthesis of information on rapid land-cover change for the period 19812000, *BioScience* **55**(2), 115–124.

Li, Z. and Giglio, L.: 1999, A review of AVHRR-based fire detection algorithms, *Forest fire monitoring and mapping: a component of global observation of forest cover. Report of a workshop*, p. 35.

Liu, Y., Stanturf, J. and Goodrick, S.: 2010, Trends in global wildfire potential in a changing climate, *Forest ecology and management* **259**(4), 685–697.

Mieville, A., Granier, C., Liousse, C., Guillaume, B., Mouillot, F., Lamarque, J.-F., Grégoire, J.-M. and Pétron, G.: 2010, Emissions of gases and particles from biomass burning during the 20th century using satellite data and an historical reconstruction, *Atmospheric Environment* **44**, 1469–1477.

Nielsen, T. T., Mbow, C. and Kane, R.: 2002, A statistical methodology for burned area estimation using multitemporal AVHRR data, *International Journal of Remote Sensing* **23**(6), 1181–1196.

Page, Y. L., Pereira, J. M. C., Trigo, R., Camara, C. D., Oom, D. and Mota, B.: 2008, Global fire activity patterns (19962006) and climatic influence: an analysis using the world fire atlas, *Atmos. Chem. Phys* **8**, 19111924.

Parry, M. L.: 2007, *Climate Change 2007: impacts, adaptation and vulnerability: contribution of Working Group II to the fourth assessment report of the Intergovernmental Panel on Climate Change*, Cambridge Univ Pr.

Pechony, O. and Shindell, D. T.: 2010, Driving forces of global wildfires over the past millennium and the forthcoming century, *Proceedings of the National Academy of Sciences* **107**(45), 19167.

Pereira, J. M. C.: 1999, A comparative evaluation of NOAA/AVHRR vegetation indexes forburned surface detection and mapping, *IEEE Transactions on Geoscience and Remote Sensing* **37**(1 Part 1), 217–226.

Pereira, M. G., Trigo, R. M., da Camara, C. C., Pereira, J. and Leite, S. M.: 2005, Synoptic patterns associated with large summer forest fires in portugal, *Agricultural and Forest Meteorology* **129**(1-2), 11–25.

Pinty, B., Roveda, F., Verstraete, M. M., Gobron, N., Govaerts, Y., Martonchik, J. V., Diner, D. J. and Kahn, R. A.: 2000, Surface albedo retrieval from meteosat 2. applications, *Journal of Geophysical Research* **105**(D14), 18113.

Pinty, B. and Verstraete, M. M.: 1992, GEMI: a non-linear index to monitor global vegetation from satellites, *Plant Ecology* **101**(1), 15–20.

Potter, C., Tan, P. N., Kumar, V., Kucharik, C., Klooster, S., Genovese, V., Cohen, W. and Healey, S.: 2005, Recent history of large-scale ecosystem disturbances in north america derived from the AVHRR satellite record, *Ecosystems* **8**(7), 808–824.

Price, J. C.: 1984, Land surface temperature measurements from the split window channels of the NOAA 7 advanced very high resolution radiometer, *Journal of Geophysical research* **89**(D5), 7231–7237.

Pu, R., Gong, P., Li, Z. and Scarborough, J.: 2004, A dynamic algorithm for wildfire mapping with NOAA/AVHRR data, *International Journal of Wildland Fire* **13**(3), 275–285.

Pu, R., Li, Z., Gong, P., Csiszar, I., Fraser, R., Hao, W. M., Kondragunta, S. and Weng, F.: 2007, Development and analysis of a 12-year daily 1-km forest fire dataset across north america from NOAA/AVHRR data, *Remote Sensing of Environment* **108**(2), 198–208.

Pyne, S. J.: 2001, *Fire: a brief history*, Jeremy Mills Publishing.

Randerson, J. T., Liu, H., Flanner, M. G., Chambers, S. D., Jin, Y., Hess, P. G., Pfister, G., Mack, M. C., Treseder, K. K. and Welp, L. R.: 2006, The impact of boreal forest fire on climate warming, *Science* **314**(5802), 1130.

Ricotta, C., Avena, G. and Palma, A. D.: 1999, Mapping and monitoring net primary productivity with AVHRR NDVI time-series: statistical equivalence of cumulative vegetation indices, *ISPRS Journal of Photogrammetry and Remote Sensing* **54**(5-6), 325–331.

Roy, D. P., Boschetti, L., Justice, C. O. and Ju, J.: 2008, The collection 5 MODIS burned area product–Global evaluation by comparison with the MODIS active fire product, *Remote Sensing of Environment* **112**(9), 3690–3707.

Roy, D. P., Jin, Y., Lewis, P. E. and Justice, C. O.: 2005, Prototyping a global algorithm for systematic fire-affected area mapping using MODIS time series data, *Remote Sensing of Environment* **97**(2), 137–162.

Roy, D. P., Lewis, P. E. and Justice, C. O.: 2002, Burned area mapping using multi-temporal moderate spatial resolution data–a bi-directional reflectance model-based expectation approach, *Remote Sensing of Environment* **83**(1-2), 263–286.

Running, S. W.: 2006, Is global warming causing more, larger wildfires?, *Science(Washington)* **313**(5789), 927–928.

Sa, A. C. L., Pereira, J. M. C. and Gardner, R. H.: 2007, Analysis of the relationship between spatial pattern and spectral detectability of areas burned in southern africa using satellite data, *International Journal of Remote Sensing* **28**(16), 3583–3601.

Saunders, R. W.: 1990, The determination of broad band surface albedo from AVHRR visible and near-infrared radiances, *International Journal of Remote Sensing* **11**(1), 49–67.

Schultz, M. G., Heil, A., Hoelzemann, J. J., Spessa, A., Thonicke, K., Goldammer, J. G., Held, A. C., Pereira, J. M. C. and van het Bolscher, M.: 2008, Global wildland fire emissions from 1960 to 2000, *Global Biogeochemical Cycles* **22**(2).

Simon, M., Plummer, S., Fierens, F., Hoelzemann, J. J. and Arino, O.: 2004, Burnt area detection at global scale using ATSR-2: the GLOBSCAR products and their qualification, *Journal of Geophysical Research* **109**(D14).

Skinner, W. R., Stocks, B. J., Martell, D. L., Bonsal, B. and Shabbar, A.: 1999, The association between circulation anomaliesin the Mid-Troposphere and area burnedby wildland fire in canada, *Theoretical and Applied Climatology* **63**(1), 89–105.

Sobrino, J. A., Li, Z. L., Stoll, M. P. and Becker, F.: 1994, Improvements in the split-window technique for land surfacetemperature determination, *IEEE Transactions on Geoscience and Remote Sensing* **32**(2), 243–253.

Solomon, S., Plattner, G. K., Knutti, R. and Friedlingstein, P.: 2009, Irreversible climate change due to carbon dioxide emissions, *Proceedings of the National Academy of Sciences* **106**(6), 1704.

Sousa, A. M. O., Pereira, J. M. C. and Silva, J. M. N.: 2003, Evaluating the performance of multitemporal image compositing algorithms for burned area analysis, *International Journal of Remote Sensing* **24**(6), 1219–1236.

Stanhill, G. and Cohen, S.: 2001, Global dimming: a review of the evidence for a widespread and significant reduction in global radiation with discussion of its probable causes and possible agricultural consequences, *Agricultural and Forest Meteorology* **107**(4), 255–278.

Stocks, B. J., Mason, J. A., Todd, J. B., Bosch, E. M., Wotton, B. M., Amiro, B. D., Flannigan, M. D., Hirsch, K. G., Logan, K. A. and Martell, D. L.: 2002, Large forest fires in canada, 19591997, *Journal of Geophysical Research* **107**(D1), 8149.

Sukhinin, A. I., French, N. H. F., Kasischke, E. S., Hewson, J. H., Soja, A. J., Csiszar, I. A., Hyer, E. J., Loboda, T., Conrad, S. G. and Romasko, V. I.: 2004, AVHRR-based mapping of fires in russia: New products for fire management and carbon cycle studies, *Remote Sensing of Environment* **93**(4), 546–564.

Tansey, K., Grégoire, J. M., Binaghi, E., Boschetti, L., Brivio, P. A., Ershov, D., Flasse, S., Fraser, R., Graetz, D. and Maggi, M.: 2004, A global inventory of burned areas at 1 km resolution for the year 2000 derived from SPOT VEGETATION data, *Climatic Change* **67**(2), 345–377.

Tansey, K., Grégoire, J. M., Stroppiana, D., Sousa, A., Silva, J., Pereira, J. M. C., Boschetti, L., Maggi, M., Brivio, P. A. and Fraser, R.: 2004, Vegetation burning in the year 2000: Global burned area estimates from SPOT VEGETATION data, *Journal of Geophysical Research* **109**(D14), D14S03.

Taylor, A. H., Trouet, V. and Skinner, C. N.: 2008, Climatic influences on fire regimes in montane forests of the southern cascades, california, USA, *International Journal of Wildland Fire* **17**(1), 60–71.

Trigo, R. M., Garca-Herrera, R., Daz, J., Trigo, I. F. and Valente, M. A.: 2005, How exceptional was the early august 2003 heatwave in france, *Geophys. Res. Lett* **32**(10).

Trigo, R. M., Pereira, J., Pereira, M. R. G., Mota, B., Calado, T. J., Dacamara, C. C. and Santo, F. E.: 2006, Atmospheric conditions associated with the exceptional fire season of 2003 in portugal, *International Journal of Climatology* **26**(13), 1741–1757.

Turner, M. G.: 1990, Spatial and temporal analysis of landscape patterns, *Landscape ecology* **4**(1), 21–30.

Walton, C. C.: 1988, Nonlinear multichannel algorithms for estimating sea surface temperature with AVHRR satellite data., *Journal of Applied Meteorology* **27**, 115–124.

Westerling, A. L., Hidalgo, H. G., Cayan, D. R. and Swetnam, T. W.: 2006, Warming and earlier spring increase western US forest wildfire activity, *Science* **313**(5789), 940.

Wild, M., Ohmura, A. and Makowski, K.: 2007, Impact of global dimming and brightening on global warming, *Geophysical Research Letters* **34**(4), L04702.

Williams, J.: 2004, Managing fire-dependent ecosystems: We need a public lands policy debate, *Fire Management Today* **64**(2), 6–11.

Xiao, J. and Zhuang, Q.: 2007, Drought effects on large fire activity in canadian and alaskan forests, *Environmental Research Letters* **2**, 044003.

# Anexos

Neste anexo, apresentam-se os artigos que integram esta tese de doutoramento.

# Artigo 1

## Screening the ESA ATSR-2 World Fire Atlas (1997-2001)

**Mota, B., J.M.C. Pereira** - Department of Forestry, Instituto Superior de Agronomia, 1349-017 Lisboa, Portugal.
**D. Oom, M.J.P. Vasconcelos** - Remote Sensing Centre, Tropical Research Institute, Tv. Conde da Ribeira 9 1300-142 Lisboa, Portugal.
**M. Schultz** - Max Planck Institute for Meteorology, Bundesstr. 53, 20146 Hamburg, Germany.

Atmos. Chem. Phys., 6, 1409–1424, 2006
www.atmos-chem-phys.net/6/1409/2006/


Atmospheric Chemistry and Physics

# Screening the ESA ATSR-2 World Fire Atlas (1997–2002)

**B. W. Mota[1], J. M. C. Pereira[1], D. Oom[2], M. J. P. Vasconcelos[2], and M. Schultz[3]**

[1]Department of Forestry, Instituto Superior de Agronomia, Tapada da Ajuda 1349-017 Lisboa, Portugal
[2]Remote Sensing Centre, Tropical Research Institute, Tv. Conde da Ribeira 9, 1300-142 Lisboa, Portugal
[3]Max Planck Institute for Meteorology, Bundesstr. 53, 20146 Hamburg, Germany

Received: 22 March 2005 – Published in Atmos. Chem. Phys. Discuss.: 12 July 2005
Revised: 16 January 2006 – Accepted: 1 February 2006 – Published: 4 May 2006

**Abstract.** We screened the algorithm 2 (308 K threshold) European Space Agency (ESA) World Fire Atlas (WFA), for the period 1997–2002, using ancillary land cover, night-lights and volcanic activity datasets, combined with statistical techniques to detect the occurrence of space-time clusters of anomalous observations. The WFA is built using night time data from the Along Track Scanning Radiometer (ATSR) onboard the Second European Remote-Sensing Satellite (ERS-2). The spatial resolution of the data is 1 km and the satellite revisiting period is 3 days at the equator. The WFA is the first and longest archive of global fire observations and has been used in numerous biomass burning studies. Known limitations of the WFA are the inclusion of warm surfaces, gas flares, and city lights, and an underestimation of actual global fire activity, due to the time of satellite overpass. Nevertheless, it has been considered that the WFA contains a relatively small proportion of observations that do not correspond to vegetation fires, which is not corroborated by our findings. During the study period, the annual percentage of false alarms and non-vegetation fires varied from a minimum value of 20.6% in 1997 to a maximum of 27.9% in 1998. Gas flares and hot bare soils are the major sources of false alarms and non-vegetation fires.

## 1 Introduction

Vegetation fires play an important environmental role over large areas of the Earth surface, influencing ecosystem productivity (Houghton, 2003; Potter et al., 2003), vegetation distributions patterns (Bachelet et al., 2001), and climate (Oglesby et al., 1999; Menon et al., 2002). Fires also represent a significant source of aerosols and trace gas emissions (Bey et al., 2001; Kinne et al., 2003; Langenfelds et al., 2002). Recent analyses based on data from the Global Burned Area 2000 (GBA2000) project (Grégoire et al., 2003) estimate that 3.5 million km$^2$ burned globally during the year 2000 (Tansey et al., 2003), corresponding to 2580 teragrams (Tg, dry matter) of burnt biomass (Ito and Penner, 2003).

Multi-annual, very broad geographical scale analyses of fire occurrence are scarce, and rely primarily on active fires data. Dwyer et al. (2000) and Stroppiana et al. (2000) analysed 21 months of global, daily daytime imagery from the Advanced Very High Resolution Radiometer (AVHRR) at 1 km spatial resolution, from April 1992 to December 1993. Arino and Rosaz (1999) and Arino and Plummer (2001) described the European Space Agency (ESA) World Fire Atlas (WFA), which is being produced using global daily night time data from the Along Track Scanning Radiometer (ATSR-2) at 1 km spatial resolution. Giglio et al. (2003) used data from the Tropical Rainfall Measuring Mission (TRMM) Visible and Infrared Scanner (VIRS), to map pan-tropical (40° N to 40° S) fire activity between January 1998 and August 2004. Other studies have analysed fire activity over smaller areas and shorter time periods, for example in support of field research campaigns (Olson et al., 1999; Pereira et al., 1999; Anyamba et al., 2003) or to document exceptional fire events (Malingreau et al., 1985; Gutman et al., 2000; Wooster and Strub, 2002).

Active fires detected by satellite provide a good indication of the spatio-temporal patterns of global fire incidence, but are inadequate to estimate biomass burning, due to areal and temporal sampling problems (Pereira et al., 1999a; Dwyer et al., 2000). Nevertheless, active fire data sets have been found useful by atmospheric chemistry researchers, to improve characterisation of the interannual variability and seasonality of emissions, and to assess the effects of biomass burning on the distribution dynamics of aerosols and trace gases. The ESA WFA has been extensively used for these

*Correspondence to:* J. Pereira
(jmcpereira@isa.utl.pt)

Published by Copernicus GmbH on behalf of the European Geosciences Union.

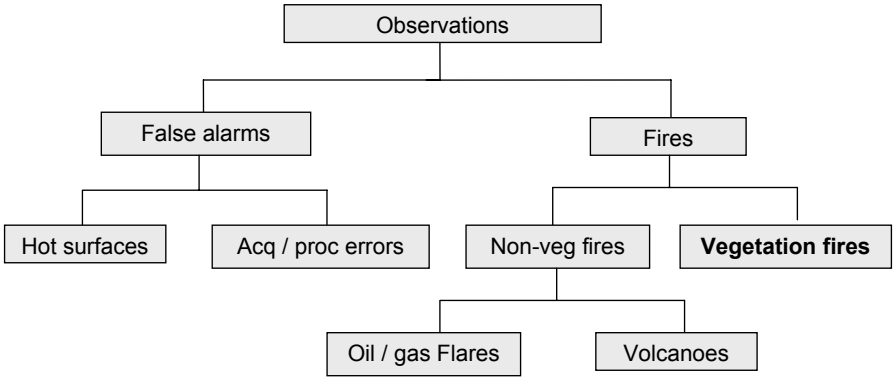


**Fig. 1.** Hierarchical arrangement of the WFA data classes used in the study.

purposes, in spite of the limitations described by Arino and Plummer (2001). Table 1 lists articles that used ESA's WFA data, mentioning the study area, the analysis time frame, and the main topic of the research.

A careful and thorough visual analysis of the WFA product in various regions of the world, namely in deserts and sparsely vegetated areas, suggested that the product contained a relatively large number of observations that did not correspond to vegetation fires. The purpose of the present work was to remove those observations from the WFA and provide the global change research community with an improved multi-annual, global fire activity dataset. Some of authors listed in Table 1 attempted screening of the WFA to remove non-vegetation fire data (for example, Generoso et al., 2003; Hoelzemann et al., 2003; Pereira, 2003; Pereira et al., 2004; Schultz, 2002), but less thoroughly than in the present study, and for shorter periods of time.

Throughout the paper we use the following terminology (Fig. 1): observation or count is the more generic designation and refers to each and every WFA element. False alarm designates observations that do not correspond to fires. They can be data acquisition/processing errors or hot ground surfaces. Fires are observations that display a high temperature resulting from energy generated by a combustion process. They include vegetation fires, gas flares and volcanic eruptions. The latter two are jointly designated non-vegetation fires. Our goal is to classify and remove from the WFA dataset all observations other than vegetation fires.

## 2 Data and methods

### 2.1 The World Fire Atlas

The ATSR-2 is a low spatial resolution sensor for environmental monitoring, carried onboard the Second European Remote Sensing Satellite (ERS-2). It has four visible and mid-infrared channels centred at 0.55 $\mu$m, 0.67 $\mu$m, 0.87 $\mu$m and 1.6 $\mu$m, and three thermal-infrared channels centred at 3.7 $\mu$m, 11.0 $\mu$m and 12.0 $\mu$m. The spatial resolution of the ATSR-2 is 1 km at nadir. A swath width of 512 km allows a revisiting period of 3 days at the equator. (Arino and Plummer, 2001). Additional information about the ATSR can be found at http://www.atsr.rl.ac.uk/documentation/docs/userguide/index.shtml.

The WFA (http://dup.esrin.esa.int/ionia/wfa/index.asp) is built using data acquired at night by the ATSR-2 nadir view camera. WFA data are available from November 1995 to July 2005, with a gap between January and June 1996. We restricted our analysis to the six full years of ATSR-2 data, from January 1997 to December 2002. After this period WFA data are obtained with the Advanced Along-Track Scanning Radiometer (AATSR), onboard the Environment Satellite (ENVISAT). We do not analyse AATSR data in this study.

Interannual variability of vegetation fires at the global scale is large (Duncan et al., 2003a), and is strongly influenced by climatic conditions (Holmgren et al., 2001; Hashimoto et al., 2004). Our six-year analysis encompasses a strong warm phase of the El Niño Southern Oscillation (ENSO) during 1997–1998, a cold phase from late 1998 through 2001, and another warm phase during the second half of 2002, according to the National Oceanic and Atmospheric Administration (NOAA) National Weather Service/Climate Prediction Center (http://www.cpc.ncep.noaa.gov/products/analysis_monitoring/ensostuff/ensoyears.shtml). Thus, it ought to adequately characterise fire interannual variability, at least to the extent that it is affected by this global scale climatic phenomenon.

The detection of observations for the WFA is based only on the 3.7 $\mu$m channel, which is highly sensitive to radiation emitted at temperatures from 500 K to 1000 K. Use of nighttime data is meant to minimise false alarms due to sun-glint, reflection off cloud edges, and bright soil surfaces. It is also expected to reduce false alarms caused by hot ground surfaces. The detection capability of the 3.7 $\mu$m channel ranges

**Table 1.** Articles that used World Fire Atlas data.

| Article | Study area | Time frame | Topic |
|---|---|---|---|
| Balis et al. (2003) | Northern Greece | Summer 2001 | Aerosols |
| Beirle et al. (2004) | Central Australia | 1999–2001 | $NO_x$ |
| Brooks and Legrand (2000) | Northern hemisphere Africa | 1984–1993 | Aerosols |
| Bruzzone et al. (2003) | Africa, Australia, Mexico, and Brazil | 1996–1999 | $NO_2$ |
| Chandra et al. (2002) | Africa, Brazil, and Indonesia | 1979–2000 | $O_3$ |
| Chin et al. (2002) | Global | 1990, 1996, 1997 | Aerosols |
| Clerbaux et al. (2001) | Global | June 1997 | CO |
| Davison et al. (2004) | Indonesia | Aug–Nov 1997 | Aerosols |
| Duncan et al. (2003a) | Global | 1979–2000 | CO |
| Duncan et al. (2003b) | SE Asia | Sep–Nov 1997 | CO, $O_3$ |
| Edwards et al. (2003) | Africa, Atlantic Ocean | Jan 2001 | $O_3$ |
| Formenti et al. (2002) | South Africa | 1998–1999 | Aerosols |
| Generoso et al. (2003) | Global | 1997–2001 | Aerosols |
| Goloub and Arino (2000) | Africa, America, Asia | 1996–1997 | Aerosols |
| Gumbricht et al. (2002) | Botswana | 1999–2000 | Peat fire detection |
| Hoelzemann et al. (2004) | Global | 2000 | 40+ chemical species, and aerosols |
| Jenkins et al. (1997) | Africa, Atlantic and Indian Oceans | Not provided | $O_3$ |
| Jenkins and Ryu (2003) | Atlantic ocean, W. Africa, S. America | 1979–2000 | $O_3$ |
| Jenkins and Ryu (2004) | Tropical Atlantic, Africa, S. America | 1998–2001 | $O_3$ |
| Kasischke et al. (2003) | Alaska, Canada, Russia | 1997–2002 | Fire counts |
| Kelha et al. (2003) | Scandinavia, W. Russia | 1999–2000 | Fire counts |
| Kim et al. (2001) | Pantropical | 1998–1999 | $O_3$ |
| Ladstätter-Weißenmayer et al. (2004) | Tropical Pacific ocean | Sep 1999 | $O_3$ |
| Langmann and Heil (2004) | Indonesia | 1997–1998 | Aerosols |
| Legg and Laumonier (1999) | Indonesia | Aug–Sep 1997 | Burned area |
| Martin et al. (2002a) | Global | July 1996 | $NO_2$ |
| Martin et al. (2002b) | Global | 1996–1997 | $O_3$ |
| Newchurch et al. (2001) | Global | 1978–1999 | $O_3$ |
| Pereira (2003) | Tropical savannas | – | Burned area |
| Pereira et al. (2004) | Southern Africa | – | Burned area |
| Pinty et al. (2000) | Africa | 1996 | Albedo change |
| Pochanart et al. (2003) | Thailand | 1997–2000 | CO |
| Richter and Burrows (2002) | Africa | 1997 | $NO_2$ |
| Rödenbeck et al. (2003) | Global | 1982–2000 | $CO_2$ |
| Sauvage et al. (2004) | Equatorial Africa | 1997–2003 | $O_3$ |
| Schultz (2002) | Global | 1996–2000 | CO |
| Silva et al. (2003) | Southern Africa | 2000 | Burned area |
| Spichtinger et al. (2004) | Panboreal | 1997–1998 | CO |
| Staudt et al. (2001) | Pacific Ocean | March–April 1999 | CO |
| Sudo et al. (2002) | Global | 1988–1999 | Multiple chemical species |
| van der Werf et al. (2003) | Global | 1998–2001 | C |
| van der Werf et al. (2004) | Global | 1997–2001 | $CO_2$, CO, $CH_4$ |
| Wooster and Strub (2002) | Indonesia | 1997 | Burned area |
| Yurganov et al. (2004) | Northern Hemisphere | 1996–2001 | CO |
| Zhao et al. (2000) | Northern Japan | 1995–1997 | HCN |
| Zhao et al. (2002) | Northern Japan | 1995–2000 | CO, $C_2H_6$, $C_2H_2$, HCN |

from a burning area of 0.1 ha at 600 K to 0.01 ha at 800 K (http://dup.esrin.esa.int/ionia/wfa/algorithm.asp). Wooster and Rothery (2002) calculated a sensor saturation envelope for observations of sub-pixel sized hotspots at 3.7 $\mu$m, as a function of hotspot temperature (°C) and hotspot size ($m^2$).

Two versions of the WFA are provided by ESA. The first includes all pixels with brightness temperature at 3.7 $\mu$m larger than 312 K (saturation temperature), and the second sets the threshold at 308 K. In this study we used only the dataset created with the 308° K threshold, designated algorithm 2. Underestimation of fire activity, considered the main limitation of the product (Kasischke et al., 2003), is expected to be less severe with this threshold. The trade off is a higher number of false alarms (Arino and Plummer, 2001).

**Table 2.** Annual results of WFA screening.

| Year | Original | Screened | %Screened | Vegetation Fires | %Vegetation Fires |
|---|---|---|---|---|---|
| 1997 | 164 221 | 33 878 | 20.63 | 130 343 | 79.37 |
| 1998 | 238 137 | 66 397 | 27.88 | 171 740 | 72.12 |
| 1999 | 155 718 | 39 461 | 25.34 | 16 257 | 74.66 |
| 2000 | 150 416 | 39 790 | 26.45 | 110 626 | 73.55 |
| 2001 | 141 215 | 35 460 | 25.11 | 105 755 | 74.89 |
| 2002 | 176 909 | 38 868 | 21.97 | 138 041 | 78.03 |
| Mean | 171 103 | 42 309 | 24.56 | 128 794 | 75.44 |

Single-channel (with the AVHRR channel 3, at 3.75 $\mu$m) algorithms for active fire detection were used before, namely by Muirhead and Cracknell (1985), Malingreau and Tucker (1988), Setzer and Pereira (1991), and Pereira and Setzer (1993). Martín et al. (1999) and Li et al. (2001) reviewed limitations of this approach and discussed alternative algorithms.

Between January 1997 and December 2002 there are some periods with missing (not a single 512 km by 512 km data frame available) or incomplete data (a variable number of 512 km by 512 km data frames not available). The year 2000 has 14 days with missing data. In 2001 there are 16 days of incomplete data and 25 days with missing data. In 2002 there are 15 days of incomplete data and 12 days with missing data. Above 60 degrees latitude north, data are missing from February to August 1997, due to processing problems. The various modes of operation of ERS-2 in 2001 affected significantly the geo-location accuracy of the ATSR data, mainly due to yaw mispointing in the satellite gyro-less mode (http://dup.esrin.esa.int/ionia/wfa/2001-ESA02-index.asp). The average magnitude of the location accuracy errors varied from 10 km between February and May 2001, down to 2–3 km from June 2001 onwards. Arino and Plummer (2001) discussed WFA limitations, identified during an extensive international product assessment. The main limitation of the WFA, for both temperature thresholds in channel 3, is underestimation of actual fire activity. This problem is less severe for algorithm 2. Omission errors are attributed mainly to the timing of image acquisition, the instrument revisit time, the spatial resolution of the ATSR, and the thermal thresholds selected. Fire activity tends to peak during the afternoon, both for wildfires and for prescribed burns. Thus, the night time ATSR overpass samples a moment of reduced activity in the diurnal fire cycle. The revisit time of the ATSR at the equator is three days, meaning that many short duration fires are not observed. Biome specific differences in fire persistence are likely to introduce a bias in favour of the detection of forest fires, to the detriment of shorter duration savanna fires (Giglio et al., 2006). The spatial resolution of 1 km also limits the ability of the ATSR to detect many small fires, to an extent that is dependent on fire intensity. This limitation is shared by other sensors, such as the AVHRR and MODerate resolution Imaging Spectrometer (MODIS), and is more severe in coarser resolution instruments, such as the Geostationary Operational Environmental Satellite (GOES). The thermal thresholds of algorithms 1 and 2 were designed to achieve an acceptable trade off between omission and commission errors. They may be too restrictive to capture active fires that affect only a small fraction of the area of a pixel. Underestimation of fire activity at high latitudes during the boreal summer was first described by Arino and Plummer (2001) and confirmed by Kasischke et al. (2003). Arino and Plummer (2001) considered commission errors to be less of a problem in the WFA than omission errors. They were attributed primarily to urban lights and oil and gas flares. Commission errors due to hot ground surfaces in deserts and sparsely vegetated areas were mentioned only for the algorithm 2 product. Overall, Arino and Plummer (2001) considered the main advantages of the WFA to be the low level of commission errors, and the adequate spatial distribution and location accuracy of the hotspots.

### 2.2 Screening procedure

The screening, or filtering, of false alarms and non-vegetation fires from among the set of observations included in the WFA was implemented in two stages. In the first stage, a series of spatial masks were used to classify false alarms and non-vegetation fires generated by specific types of land cover, gas flares, and volcanic activity. In the second stage, the WFA data were visually analysed, to classify erroneous observations not detected in the first stage. This two-stage classification of WFA observations is exhaustive, i.e. it addresses each and every count in WFA, but it is not mutually exclusive, i.e., a given observation may be captured by more than one filter. This may not be the ideal classification structure, but it was impossible to construct a priori a strict partition of the data. With the procedure followed, the number of observations allocated to each filter is independent from the order in which the filters were actually applied to the data. The screening procedure required the use of ancillary

datasets, namely a land cover map, a stable lights map, and volcanic activity location data.

### 2.3 Screening based on land cover

Two global land cover products are contemporary with the WFA data, and thus are potentially appropriate for screening non-vegetation fire counts. These products are the Global Land Cover (GLC) 2000 map (Fritz et al., 2003), and the MODIS MOD12 Land Cover map (Strahler et al., 1999; Friedl et al., 2002). The accuracy of the MODIS land cover map is 71.6±0.25%. Accuracy assessment for the GLC 2000 map is still in progress, but preliminary results indicate an accuracy level comparable to that of the MODIS product. Giri et al. (2005) provide a detailed comparison of these two land cover maps. The GLC2000 map (www-gvm.jrc.it/glc2000) is based on SPOT-VEGETATION satellite imagery acquired during the year 2000, at a spatial resolution of 1km. The map distinguishes 22 land cover classes. The MOD12 Land Cover map also has a spatial resolution of 1 km, and is based on 12 months of data acquired between 15 October 2000 and 15 October 2001. It uses the International Geosphere-Biosphere Programme (IGBP) 17-class global vegetation classification scheme. The legend of the GLC 2000 map was considered more adequate for the purposes of the present study. It separates bare (incombustible) land from sparsely vegetated (potentially combustible) land, while the MOD12 IGBP legend has a "barren and sparsely vegetated class", which is ambiguous from the standpoint of potential combustibility. The GLC 2000 land cover classes bare areas (24 629 888 $km^2$), natural and artificial water bodies (471 061 857 $km^2$), snow and ice (10 660 085 $km^2$), and artificial surfaces and associated areas (3 217 319 $km^2$) were considered incapable of supporting vegetation fires. Therefore, all WFA observations falling on these land cover classes were classified as false alarms or non-vegetation fires. Visual inspection of the data also revealed the presence of numerous counts in peri-urban industrial areas, primarily in Europe, North America, and Asia. Screening of these observations, not eliminated by the GLC 2000 artificial surfaces and associated areas, was accomplished with a spatial mask including all areas that were lighted in over 25% of the cloud-free observations in the Elvidge et al. (2001) human settlements layer.

### 2.4 Screening non-vegetation fires

The screening of observations corresponding to gas flares relied on data from the Defense Meteorological Satellite Program (DMSP) Operational Linescan System (OLS) Night time Lights of the World data product http://www.ngdc.noaa.gov/dmsp/download_world_change_pair.html. This product includes a gas flares layer for the year 2000, which contains mean OLS visible band digital numbers, from cloud-free observations. Gas flares are a subset of stable lights, defined as those lights visible in at least 10% of cloud-free observations. Gas flares are identified in the stable lights dataset based on their large circular appearance and lack of coincidence with populated places (Elvidge et al., 2001). The gas flares mask covers an area of 887 007 $km^2$. The WFA also contains counts generated by volcanoes. Elimination of these observations was based on volcanic activity timing and location data from the Global Volcanism Program (GVP) of the Smithsonian Institution http://www.volcano.si.edu/, from Volcano World http://volcano.und.edu/ and from the Hawaii Institute of Geophysics and Planetology (HIGP) MODVOLC WWW page http://modis.higp.hawaii.edu/.

Detailed reports available from these sources describing aspects of eruptions relevant for determining the nature of WFA observations, such as the extent and direction of lava flows, were used when deemed necessary. According to the GVP, 119 volcanoes were active globally between 1997 and 2002. The geographical coordinates of all 119 volcanoes were plotted together with the WFA data, and the dates of all WFA counts within a 10 km radius buffer around the volcano location were compared against dates of reported volcanic activity. The GLC2000 land cover map and Landsat scene bands 5-4-3 color composite quick-looks, with a nominal spatial resolution of 240 m–480 m (United States Geological Survey (USGS) Global Visualization Viewer, http://glovis.usgs.gov/) were often used, to determine if the counts might be vegetation fires, possibly ignited as a result of volcanic eruptions. Observations that coincided with periods of volcanic activity, and did not appear to occur over vegetated areas were classified as non-vegetation fires.

### 2.5 Additional data screening

Preliminary visual inspection of the WFA data revealed the presence of large clusters of observations unlikely to correspond to vegetation fires. Some of the clusters exhibited regular geometric shapes, such as triangles and lines. These very conspicuous geometric clusters of observations were visually identified and labeled false alarms caused by image acquisition/processing errors. Other clusters contained very large numbers of observations, concentrated in very short periods of time, over sparsely vegetated areas that typically exhibited almost no fire activity. Identification of anomalous space-time data clusters was accomplished with exploratory spatial and temporal data analysis. The difference between daily observation counts and five-day moving means helped identify exceptional temporal clusters in a time-series of the full study period. Global counts maps were then generated for the periods of anomalous time clustering. The location of spatial clusters occurring during these periods was highlighted using kernel density estimation, a spatial interpolation technique appropriate for individual point locations (Bailey and Gatrell, 1995). The likelihood of each space-time cluster of observations actually representing vegetation fires was assessed via visual inspection of contemporary Advanced Very High Resolution Radiometer (AVHRR)

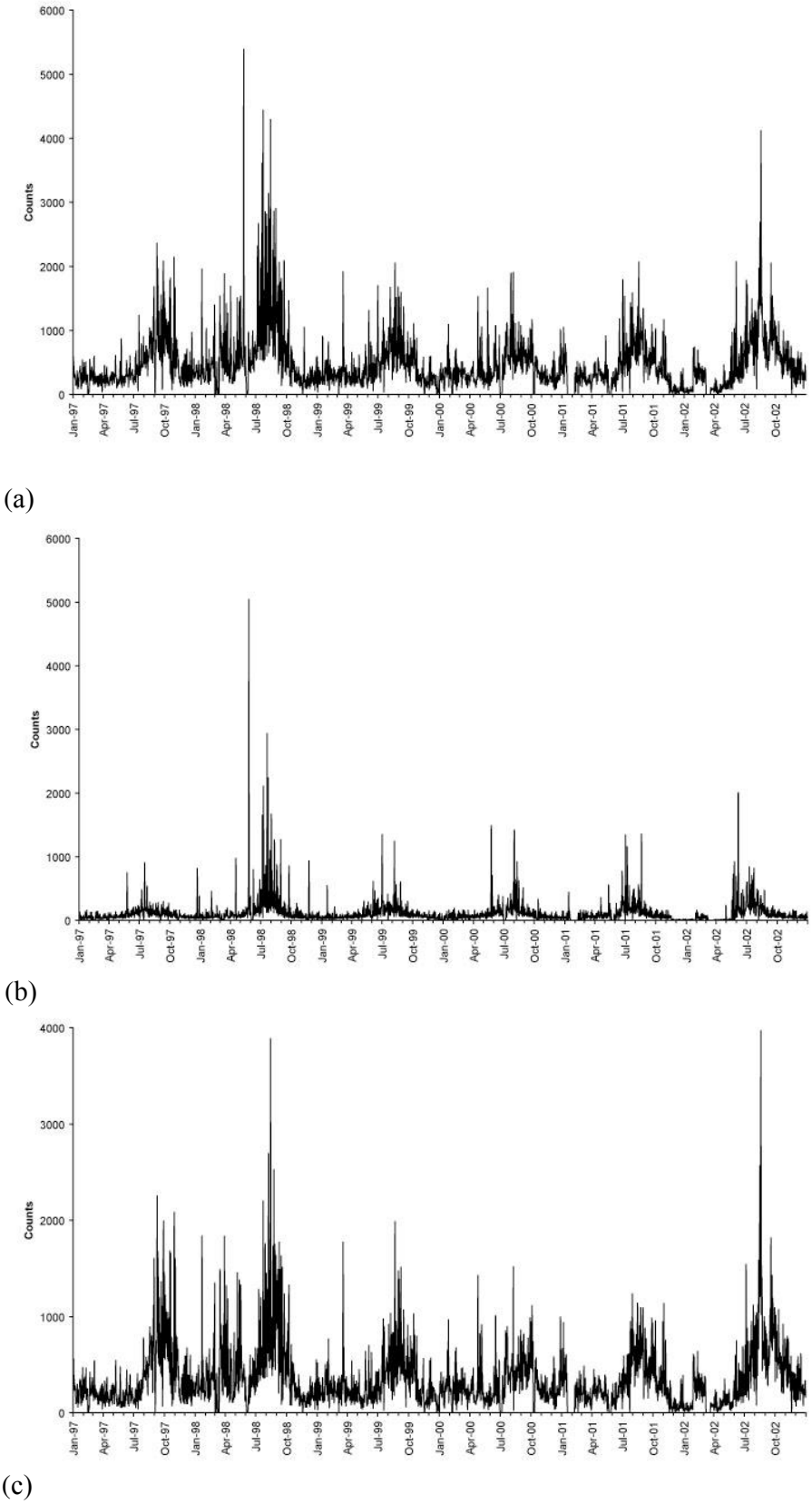


**Fig. 2.** Daily time-series of original WFA observations **(a)**, data removed from the WFA **(b)**, and screened data set **(c)**.

**Table 3.** Number of observations captured by each filter. An observation may have been captured by more than one filter.

| | Land cover | | | | Gas flares | Volcanoes | Acq/proc[1] | S-T clusters[2] | Total |
|---|---|---|---|---|---|---|---|---|---|
| Year | Bare | Water | Artificial | Snow & Ice | | | | | |
| 1997 | 11 334 | 10 305 | 5721 | 119 | 17 258 | 868 | 1293 | 2816 | 49 714 |
| 1998 | 25 605 | 12 146 | 6883 | 139 | 21 384 | 1205 | 1685 | 22 973 | 92 020 |
| 1999 | 14 686 | 10 173 | 6195 | 3 | 19 250 | 846 | 184 | 5752 | 57 089 |
| 2000 | 11 306 | 9220 | 5882 | 11 | 20 079 | 1350 | 1227 | 8163 | 57 238 |
| 2001 | 11 754 | 8723 | 4094 | 80 | 15 639 | 1181 | 378 | 7757 | 49 606 |
| 2002 | 16 190 | 8595 | 4635 | 56 | 13 153 | 1297 | 1166 | 13 622 | 58 714 |
| Total | 90 875 | 59 162 | 33 410 | 408 | 106 763 | 6747 | 5933 | 61 083 | 364 381 |

[1] Data acquisition and processing errors.
[2] Space-time clusters.
[3] The grand total exceeds the number of screened observations due to counting by more than one filter.

satellite imagery, at 1 km$^2$ spatial resolution, and/or Landsat scene quick-looks. The AVHRR imagery was obtained from the National Oceanic and Atmospheric Administration/National Environmental Satellite, Data and Information Service (NOAA/NESDIS) Comprehensive Large Array-data Stewardship System (CLASS), (http://www.class.noaa.gov/nsaa/products/welcome).

## 3 Results

### 3.1 Temporal analysis

The original WFA dataset contained 1 026 616 observations, of which 772 762 (75.27%) were considered to actually represent vegetation fires, while 253 854 (24.73%) correspond to false alarms and non-vegetation fires. The annual proportion of screened observations varied between 21% and 28%. Table 2 summarizes the results of the WFA screening process, with results displayed per year. Figure 2 shows the daily resolution time-series of the original WFA data set (Fig. 2a), the time series of false alarms and non-vegetation fires removed from the WFA (Fig. 2b), and the time series of the screened dataset, containing only vegetation fires (Fig. 2c). The time-series in Fig. 2a reveals markedly seasonal patterns, with larger numbers of observations detected during the boreal summer, approximately between July and October, and peaking in August–September. In 1997 the peak fire activity occurred later, during the month of October. The year with the most counts was 1998, when very high numbers were detected between April and October. The time-series of non-vegetation fires and false alarms removed from the WFA (Fig. 2b) also exhibits a seasonal pattern, similar to that of the original data set. Most of the days with very large ($>$1000) number of counts screened occur between June and September 1998. Smaller data spikes in other years also occur during the boreal summer. The screened WFA time-series (Fig. 2c) has fewer spikes and relatively to the original data set, the seasonal component displays lower amplitude, while the phase does not appear to have shifted. The anomalously low numbers of observations recorded in January, February and December 2001, and in February and March 2002 correspond to periods of missing or incomplete data, as indicated in the WFA World Wide Web (WWW) page. Figures 3a–e disaggregate the time-series of false alarms and non-vegetation fires into those of the various filters applied to the data. Note the scale variations in the different figures. The observations screened with the land cover filter and with the gas flares filter (Figs. 3a–b) show a continuous distribution and a clearly seasonal trend, with more observations during the boreal summer. In the case of the land cover filter, this seasonality is induced by hot land surfaces in the larger land expanses of the northern hemisphere. The seasonality in the counts screened with the gas flares filter results from an overlap with the land cover filter and with space-time clusters, as shown in Table 3. The seasonal trend is believed to be induced mostly by hot land surfaces, and ought not be inherent in the gas flares activity. Since our purpose is not to engage in a detailed analysis of the various types of observations included in the WFA, but only to eliminate those that do not correspond to vegetation fires, we did not attempt to remove the overlap between observations captured with the land cover and gas flares filters. Observations screened with the volcanoes filter (Fig. 3c) also occur continuously but with a very low background level, and exhibit sporadic spikes corresponding to large eruptions. The acquisition/processing false alarms (Fig. 3d) occur sporadically. Finally, the space-time hot surfaces clusters (Fig. 3e) display a discontinuous but markedly seasonal pattern, occurring only during the boreal summer.

### 3.2 Geographical and quantitative analysis

Figure 4 shows the location of space-time clusters of observations, acquisition/processing errors, and counts due to volcanic activity. All acquisition/processing errors are

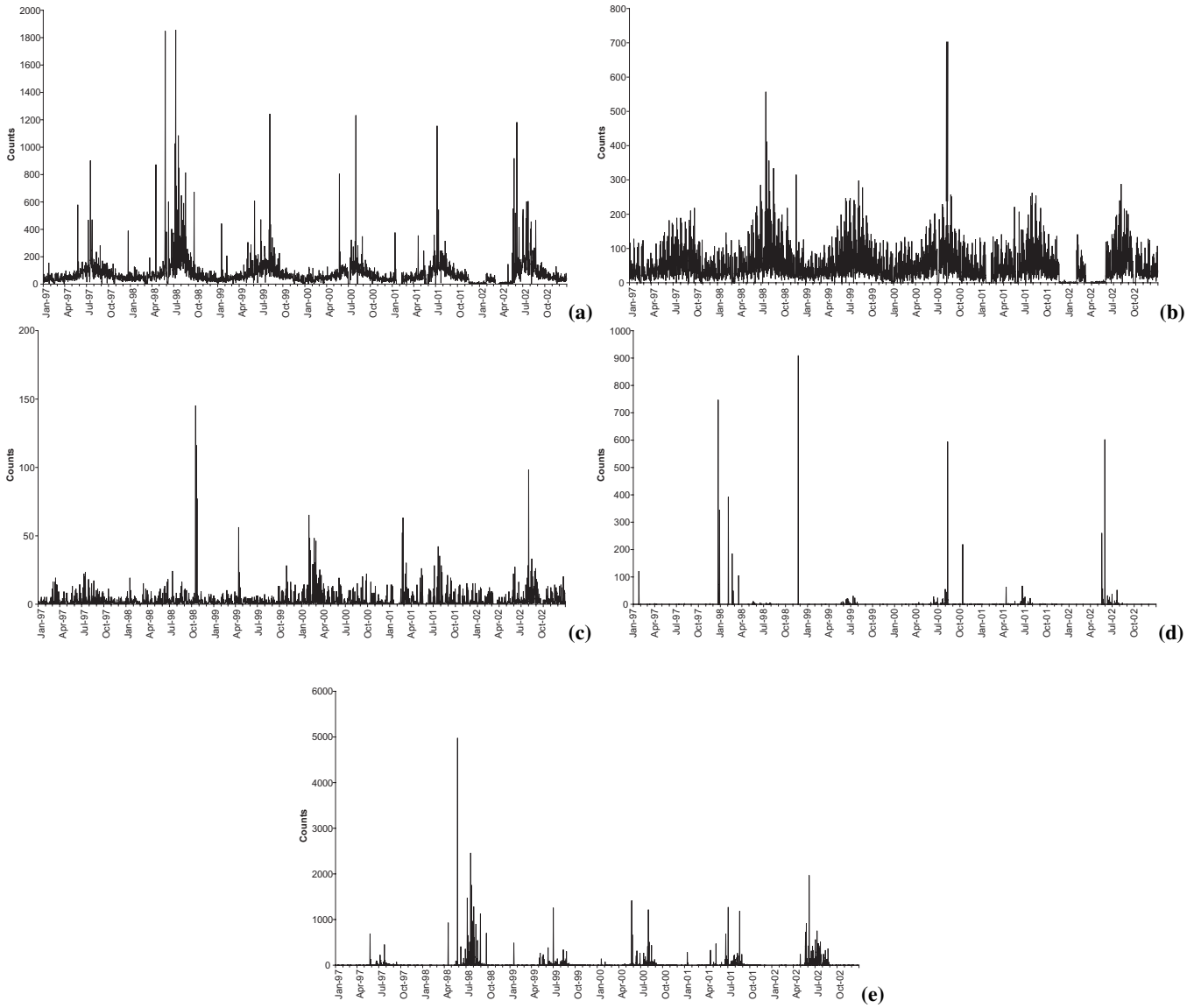


**Fig. 3.** Daily time series of observations removed from the WFA using various filters: land cover (**a**), oil and gas flares (**b**), volcanoes (**c**), data acquisition/processing errors (**d**), and anomalous space-time clusters (**e**).

**Table 4.** Number of observations captured by various filter intersections.

| Year | LC[1] ∩ Fl | LC ∩ Vol | Fl ∩ Vol | LC ∩ Fl ∩ Vol | Clu ∩ LC | Clu ∩ Fl | LC ∩ A/P |
|---|---|---|---|---|---|---|---|
| 1997 | 11 808 | 525 | 0 | 0 | 1829 | 84 | 524 |
| 1998 | 13 739 | 457 | 281 | 77 | 8558 | 836 | 15 |
| 1999 | 12 659 | 433 | 0 | 0 | 2851 | 441 | 16 |
| 2000 | 12 299 | 374 | 192 | 19 | 2880 | 443 | 60 |
| 2001 | 9724 | 539 | 125 | 19 | 2624 | 463 | 83 |
| 2002 | 8534 | 541 | 218 | 57 | 8690 | 101 | 704 |
| Total | 68 763 | 2869 | 816 | 172 | 27 432 | 2368 | 1402 |

[1] LC: land cover; Fl: gas flares; Vol: volcanoes; Clu: space-time clusters; A/P: acquisition/processing; ∩ is the set intersection symbol.

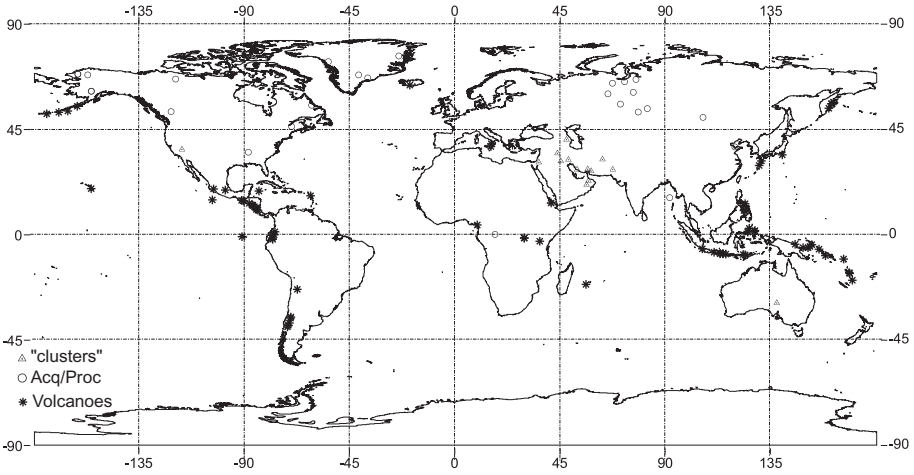


**Fig. 4.** Location of the major anomalous space-time clusters of observations, of data acquisition/processing errors, and of observations resulting from volcanic activity.

located in the northern hemisphere, at relatively high latitudes. The space-time clusters of observations occur at lower latitudes, mostly in tropical and sub-tropical areas. No acquisition/processing errors, or space-time clusters are found in Africa or South America. Most counts of these three kinds occur in North America and Eurasia. Figures 5a–c display maps of the original WFA data set, the screened false alarms and non-vegetation fires, and the vegetation fires data set, respectively. At the scale used, Figs. 5a and c are very similar, due to the strong spatial clustering of the screened data (Fig. 4b). Figure 5c displays the clusters of genuine fire activity, in southern Mexico, the cerrado savannas of Brazil, the savannas of the northern hemisphere of Africa, Indonesia, and the Siberian Far East. The 1997–1998 El Niño event strongly contributed to all of these concentrations of fire activity, with the possible exception of the African cluster (Nepstad et al., 1999; Siegert and Hoffmann, 2000; Page et al., 2002; Wooster and Strub, 2002; Haugaasen et al., 2003; van der Werf et al., 2004; Soja et al., 2004; Roman-Cuesta et al., 2004).

Figure 6 shows the histogram of counts screened per 0.5° cell, revealing the heavy positive skew of the distribution. In order to emphasize the location of the major observation clusters, the data displayed in Fig. 5b were smoothed to a 0.5° grid cell (Fig. 7), using kernel density estimation (Bailey and Gatrell, 1995) with an adaptive Gaussian kernel encompassing 250 observations. This figure clearly shows the locations of the major clusters of screened observations, in the Death Valley, California, USA, in Algeria and in coastal Nigeria, in the Persian Gulf region, extending east to Pakistan, and in north-central Siberia. Table 3 shows the annual number of observations captured by each filter. The year with the largest number of counts is 1998, mostly due to false alarms. This is to be expected, since those counts are generated by hot ground surfaces and 1998 was the hottest year on record at the global scale, according to the NASA Goddard Institute for Space Studies (http://data.giss.nasa.gov/gistemp/). The year 2001 has the lowest number of observations, probably because it is the year with the most days of missing or incomplete data.

The land cover filter captured a total of 183 855 observations, corresponding to 17.91% of the original WFA data. The bare areas class captures the most observations (8.85%), followed by water bodies (5.76%). Observations located over artificial surfaces and associated areas represent 3.3%, while only 0.04% of counts are found in the snow and ice class. Gas flares, volcanoes, acquisition/processing errors, and space-time clusters respectively represent 10.4%, 0.6%, 0.58% and 5.95% of the original number of WFA observations. One-hundred and nineteen volcanoes contained a total of 7145 observations within the 10-km radius buffer. Some of the observations located within the buffer of these volcanoes were considered actual vegetation fires, thus reducing to 6747 the number of observations screened out. In four cases, lava flows expanded beyond the buffer. Those observations were manually screened. The Kilauea, in Hawaii, USA, the Nyamuragira, in the Democratic Republic of Congo, and the Etna, in Italy, generated the most counts (2307, 1004 and 658, respectively). Data acquisition/processing errors were found in northern Alaska, the Bohai Bay in China, central Congo, western Siberia, Greenland, the Russia-Mongolia border area, the Bay of Bengal in the Indian Ocean, the Northwestern Territories, British Columbia and Quebec (Canada), and in the state of Tennessee (USA). The most important ones were those located in western Siberia (2193 counts) and in northern Alaska (917 counts). Corrupted satellite telemetry is a possible explanation for this kind of WFA counts. Figure 8 displays examples of data acquisition/processing errors.

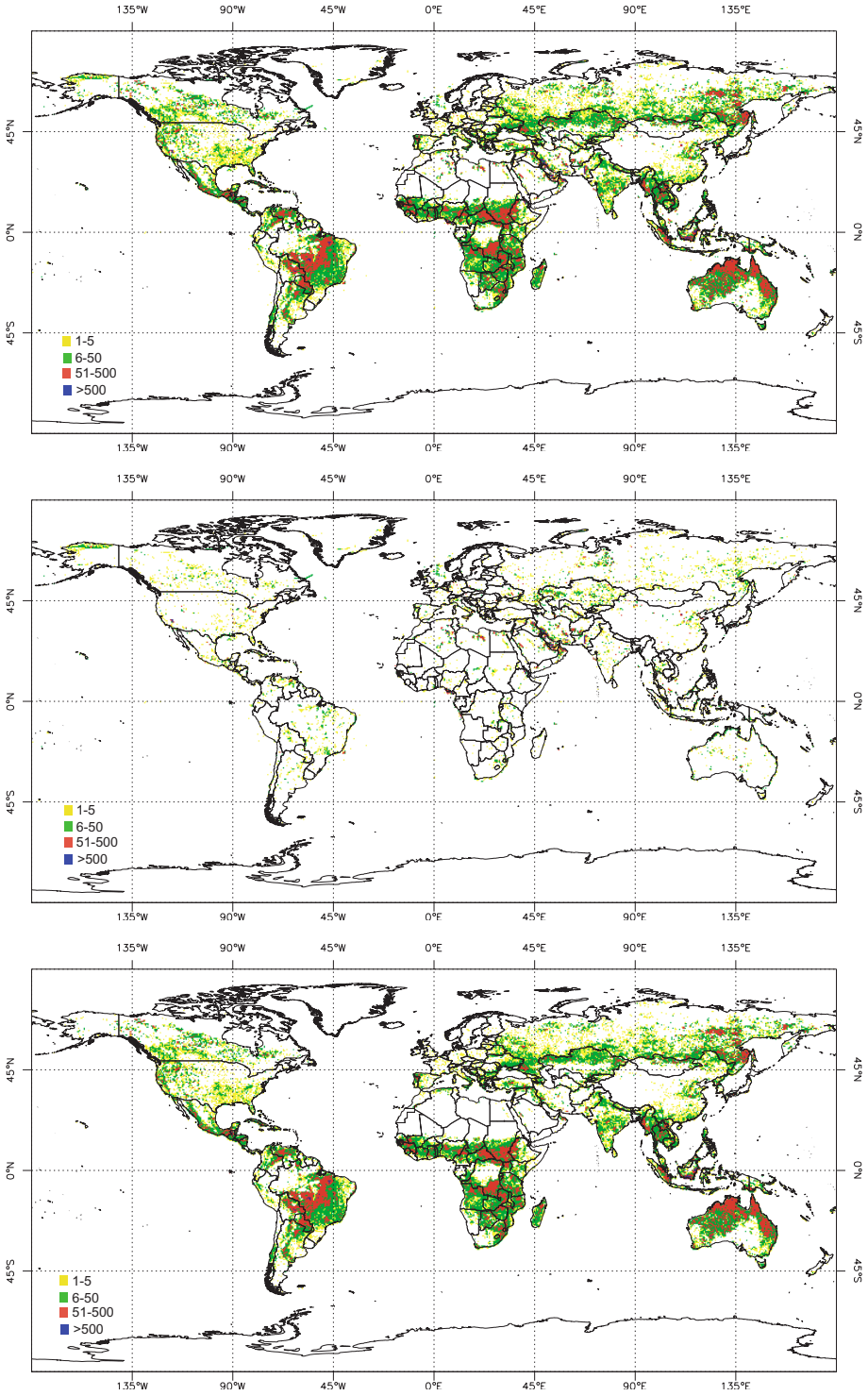


**Fig. 5.** Global maps (1997–2002) of original WFA fire counts (**a**), data removed from the WFA (**b**), and screened data set (**c**).

Space-time observation clusters were all located in bare or sparsely vegetated surfaces of hot, arid regions, namely: Lake Eyre (Southern Australia), the Denakil depression (Ethiopia/Eritrea), the Zagros mountains foothills (Iran), the Dead Sea (Israel), Death Valley (California, USA), the Kirthar range foothills (Pakistan), and southern Afghanistan. The most important ones are those in the Zagros foothills (12 898 counts) and the Kirthar foothills (9854 counts).

Table 4 displays the number of counts for the major filter intersections, i.e. numbers of observations that were captured by more than one filter. The filter intersections that capture the most observations are the one between land cover and gas flares, and the one between land cover and space-time clusters. The majority of gas and oil exploration sites are located either offshore or in desert areas. Thus, they intersect extensively with the water bodies and bare areas classes of the land cover mask. Space-time clusters typically occur on hot ground surfaces, and therefore predominate over the bare areas land cover class. Again, the year 1998 displays the largest and 2001 the lowest number of screened observations, for the reasons already mentioned.

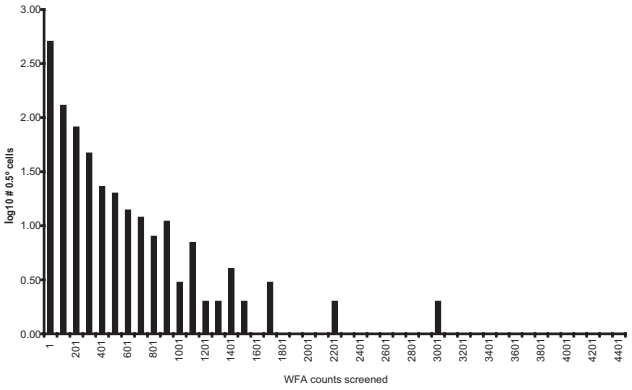


**Fig. 6.** Statistical distribution of the number of WFA counts removed in each 0.5° grid cell.

## 4 Discussion and conclusions

The WFA algorithm 2 data set contains a large number of observations that are not vegetation fires, in spite of having been built using only night time data. Commission errors, generated by a variety of causes, including hot ground surfaces, gas flares, volcanoes, and image acquisition/processing problems, represent almost one-quarter of all observations. We used a combination of geographical masks and visual data inspection to classify and subsequently remove these non-vegetation fires and false alarms from the dataset. The most time consuming step of the screening procedure was the identification of anomalous space-time clusters of observations in areas that can carry fire, but where it is unlikely to occur massively in very short periods of time. WFA screening based only on geographical masks would eliminate most of the unwanted data and is relatively easy to implement. However, non-negligible errors would remain, located mostly in the Middle East and occurring during the boreal summer. Commission errors found are not randomly distributed but, on the contrary, are highly clustered in space and in time. Such clustering reflects, to some extent, the screening procedures employed. By design, the gas flare screening, the night time lights screening, the volcano screening, and the visual/statistical cluster screening identify commission errors that are clustered in space an time. Any practical data screening procedure for a dataset of this size can only be expected to remove the relatively more obvious false alarms and non-vegetation fires. Scattered, individual erroneous observations are very likely to escape the screening procedures employed, except for those eliminated by the land cover mask. Nevertheless, we believe that the clustered, relatively obvious false alarms and non-vegetation fires represent the majority of errors, especially the more persistent ones, and thus the filtered data set is considered a substantial improvement over the original, unfiltered WFA. Accuracy of the screening procedure is expected to be lower during the periods of more imprecise data location, especially during the first semester of 2001, and mostly near the edges of the various spatial masks used. Screening based on visual and statistical cluster detection procedures ought to remain essentially unaffected.

The temporal structure of errors may affect the characterization of vegetation fire seasonality, but appears to have a larger impact upon estimates of inter-annual variability. The spatial pattern of errors may affect estimates of the magnitude and geographical distribution of emissions sources, especially in studies that included areas where large clusters of errors were found, and possibly also in the case of global analyses. These effects may have influenced results of research papers that used the original WFA data. The screened dataset provides a better characterisation of global fire geography, seasonality and inter-annual variability. It may contribute to improving the accuracy of emissions inventories based on statistics scaled with fire activity data (Schultz, 2002; Generoso et al., 2003), and also of burned area products derived by combining the spectral signal of fire scars and that of active fires (Fraser et al., 2000; Giglio et al., 2006). Analyses of the relationships between fire and vegetation or land cover will also be more accurate, due to the removal of very large numbers of false alarms located in deserts and sparsely vegetated areas.

As additional WFA data become available, detection of exceptional events may be automated using statistical methods for space-time cluster analysis (Baker, 1996; Kulldorff et al., 1998). In future near-real time active fire monitoring systems, detection of space-time clusters may be implemented on-line, based on surveillance procedures such as those developed by Rogerson (1997, 2001) and Kulldorff (2001).

The screened WFA dataset developed in this study will be available at the REanalysis of the TROpospheric chemical composition over the past 40 years (RETRO) project WWW page (http://retro.enes.org/datasets.html). Additional data screening, up to July 2005 is in progress.

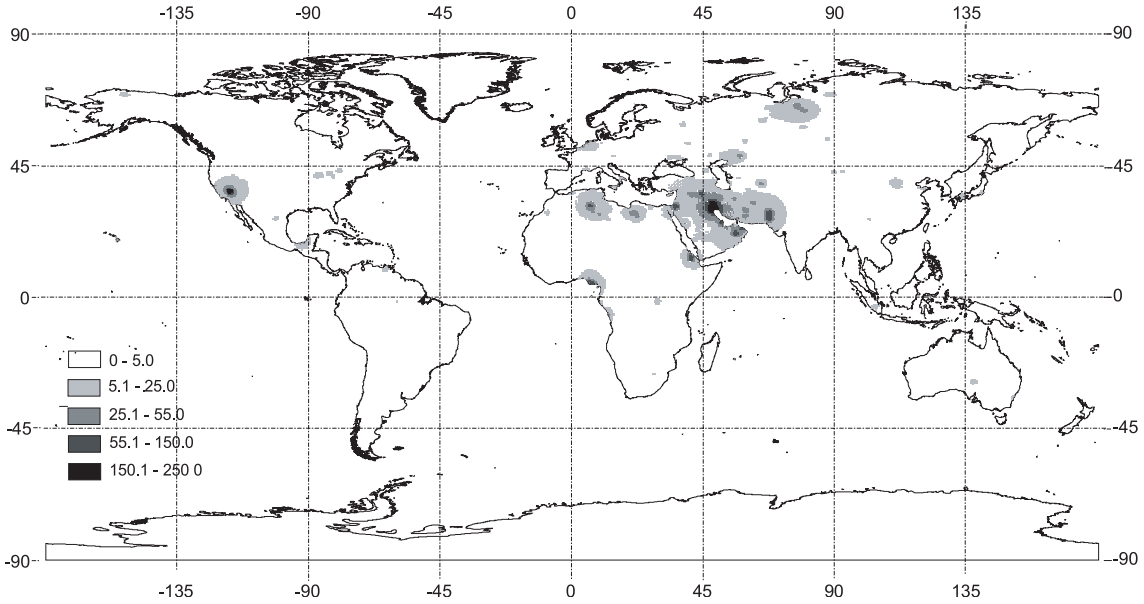


**Fig. 7.** Kernel density estimation maps of data removed from the WFA.

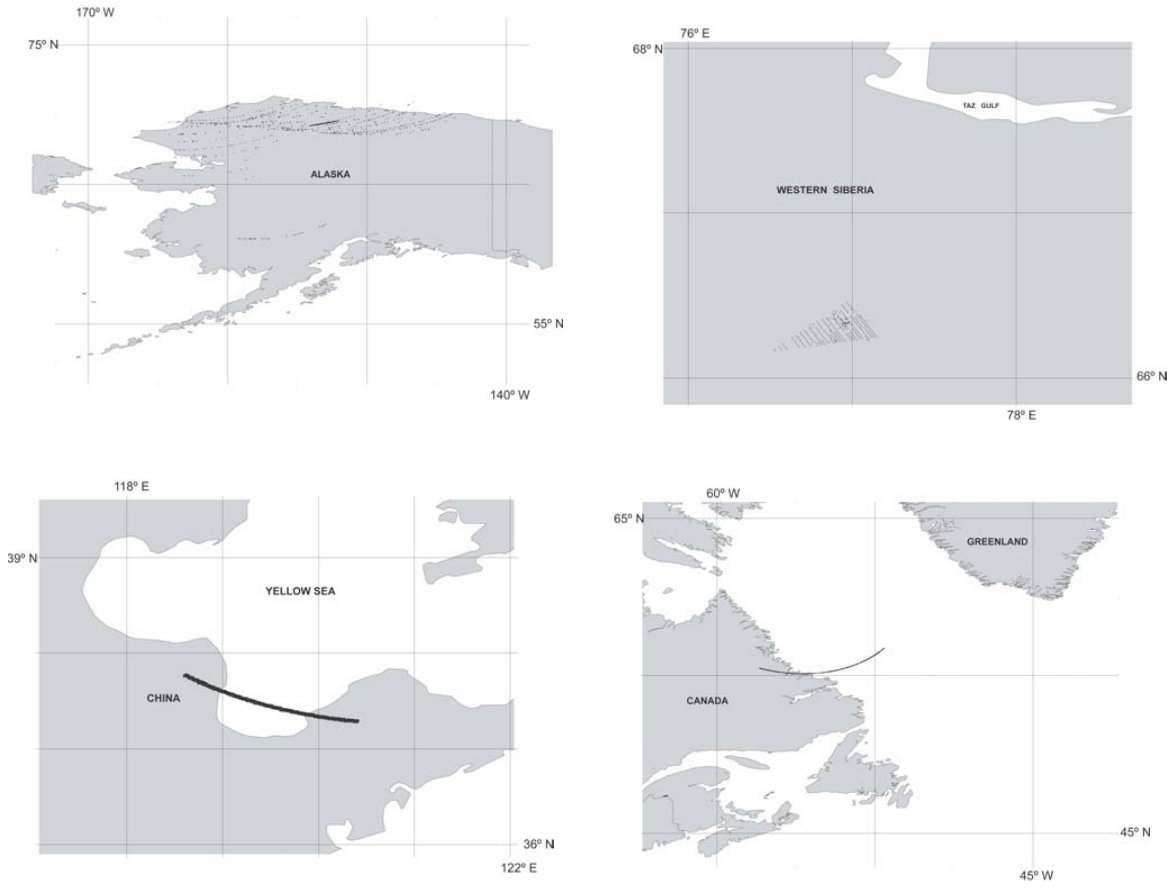


**Fig. 8.** Examples of data acquisition/processing errors, located in northern Alaska, western Siberia, northeastern China, and northeastern Canada.

*Acknowledgements.* The data used in this study are from the ATSR World Fire Atlas, European Space Agency-ESA/ESRIN, via Galileo Galilei, CP 64, 00044 Frascati, Italy. This research was funded by the European Union Fifth Framework Programme research project REanalysis of the TROpospheric chemical composition over the past 40 years (RETRO) (EVK2_CT-2002-00170).

Edited by: A. B. Guenther

## References

Anonymous: Validation of the consistent-year V003 MODIS land cover product, (http://www-modis.bu.edu/landcover/userguidelc/), 2004.

Anyamba, A., Justice, C. O., Tucker, C. J., and Mahoney, R.: Seasonal to interannual variability of vegetation and fires at SAFARI 2000 sites inferred from Advanced Very High Resolution Radiometer time series data, J. Geophys. Res.-Atmos., 108(D13), 8507, doi:10.1029/2002JD002464, 2003.

Arino, O. and Rosaz, J.-M.: 1997 and 1998 World ATSR Fire Atlas using ERS-2 ATSR-2 data, Proceedings of the Joint Fire Science Conference (Boise, Idaho: University of Idaho and the International Association of Wildland Fire), 177–182, 1999.

Arino, O. and Plummer, S.: The Along Track Scanning Radiometer World Fire Altas – Detection of night-time fire activity, IGBP-DIS Working Paper #23, Potsdam, Germany, 2001.

Bachelet, D., Neilson, R. P., Lenihan, J. M., and Drapek, R. J.: Climate change effects on vegetation distribution and carbon budget in the United States. Ecosystems, 4, 164–185, 2001.

Bailey, T. C. and Gatrell, A. C.: Interactive Spatial Data Analysis, Burnt Mill, Essex, England: Longman Scientific & Technical, 1995.

Baker, R. D.: Testing for space-time clusters of unknown size, J. Appl. Stat., 23, 543–554, 1996.

Balis, D. S., Amiridis, V., Zerefos, C., Gerasopoulos, E., Andreae, M., Zanis, P., Kazantzidis, A., Kazadzis, S., and Papayannis, A.: Raman lidar and sunphotometric measurements of aerosol optical properties over Thessaloniki, Greece during a biomass burning episode, Atmos. Environ., 37, 4529–4538, 2003.

Beirle, S., Platt, U., Wenig, M., and Wagner, T.: NOx production by lightning estimated with GOME, Adv. Space Res., 34, 793–797, 2004.

Bey, I., Jacob, D. J., Yantosca, R. M., Logan, J. A., Field, B., Fiore, A. M., Li, Q., Liu, H., Mickley, L. J., and Schultz, M.: Global modeling of tropospheric chemistry with assimilated meteorology: Model description and evaluation, J. Geophys. Res.-Atmos., 106, 23 073–23 096, 2001.

Brooks, N. and Legrand, M.: Dust variability over northern Africa and rainfall in the Sahel, in: Linking Climate Change to Land Surface Change, edited by: McLaren, S. and Kniveton, D., Dordrecht: Kluwer Academic Publishers, 1–25, 2000.

Brown, J. F., Loveland, T. R., Ohlen, D. O., and Zhu, Z.: The Global Land-Cover Characteristics Database: The Users' Perspective, Photogrammetric Engineering and Remote Sensing, 65(9), 1069–1074, 1999.

Bruzzone, L., Casadio, S., Cossu, R., Sini, F., and Zehner, C.: A system for monitoring $NO_2$ emissions from biomass burning by using GOME and ATSR-2 data, Int. J. Remote Sens., 24(8), 1709–1721, 2003.

Chandra, S., Ziemke, J. R., Bhartia, P. K., and Martin, R. V.: Tropical tropospheric ozone: Implications for dynamics and biomass burning, J. Geophys. Res.-Atmos., 107(D14), 4188, doi:10.1029/2001JD000447, 2002.

Chin, M., Ginoux, P., Kinne, S., Torres, O., Holben, B. N., Duncan, B. N., Martin, R. V., Logan, J. A., Higurashi, A., and Nakajima, T.: Tropospheric aerosol optical thickness from the GOCART model and comparisons with satellite and Sun photometer measurements, J. Atmos. Sci., 59(3), 461–483, 2002.

Clerbaux, C., Hadji-Lazaro, J., Hauglustaine, D., and Megie, G.: Assimilation of carbon monoxide measured from satellite in a three-dimensional chemistry-transport model, J. Geophys. Res.-Atmos., 106(D14), 15 385–15 394, 2001.

Danko, D. M.: The Digital Chart of the World, Photogrammetric Engineering and Remote Sensing, 58(8), 1125–1128, 1992.

Davison, P. S., Roberts, D. L., Arnold, R. T., and Colvile, R. N.: Estimating the direct radiative forcing due to haze from the 1997 forest fires in Indonesia, J. Geophys. Res.-Atmos., 109, D10207, doi:10.1029/2003JD004264, 2004.

Duncan, B. N., Bey, I., Chin, M., Mickley, L. J., Fairlie, T. D., Martin, R. V., and Matsueda, H.: Indonesian wildfires of 1997: Impact on tropospheric chemistry, J. Geophys. Res.-Atmos., 108(D15), 4458, doi:10.1029/2002JD003195, 2003b.

Duncan, B. N., Martin, R. V., Staudt, A. C., Yevich, R., and Logan, J. A.: Interannual and seasonal variability of biomass burning emissions constrained by satellite observations, J. Geophys. Res.-Atmos., 108(D2), 4100, doi:10.1029/2002JD002378, 2003a.

Dwyer, E., Pinnock, S., Grégoire, J.-M., and Pereira, J. M. C.: Global spatial and temporal distribution of vegetation fire as determined from satellite observations, Int. J. Remote Sensing, 21, 1289–1302, 2000.

Edwards, D. P., Lamarque, J.-F., Attié, J.-L., Emmons, L. K., Richter, A., Cammas, J.-P., Gille, J. C., Francis, G. L., Deeter, M. N., Warner, J., Ziskin, D. C., Lyjak, L. V., Drummond J. R., and Burrows, J. P.: Tropospheric ozone over the tropical Atlantic: a satellite perspective, J. Geophys. Res.-Atmos., 108(D8), 4237, doi:10.1029/2002JD002927, 2003.

Elvidge, C. D., Baugh, K. E., Kihn, E. A., Kroehl, H. W., and Davis, E. R.: Mapping of city lights using DMSP Operational Linescan System data, Photogrammetric Engineering and Remote Sensing, 63(6), 727–734, 1997.

Elvidge, C. D., Imhoff, M. L., Baugh, K. E., Hobson, V. R., Nelson, I., Safran, J., Dietz, J. B., and Tuttle, B. T.: Night-time lights of the world: 1994–1995 ISPRS, J. Photogrammetry and Remote Sensing, 56, 81–99, 2001.

Formenti, P., Winkler, H., Fourie, P., Piketh, S., Makgopa, B., Helas, G., and Andreae, M. O.: Aerosol optical depth over a remote semi-arid region of South Africa from spectral measurements of the daytime solar extinction and the night time stellar extinction, Atmos. Res., 62(1–2), 11–32, 2002.

Fraser, R. H., Li, Z., and Cihlar, J.: Hotspot and NDVI Differencing Synergy (HANDS) A New Technique for Burned Area Mapping over Boreal Forest, Remote Sens. Environ., 74(3), 362–376, 2000.

Friedl, M. A., McIver, D. K., Hodges, J. C. F., Zhang, X. Y., Muchoney, D., Strahler, A. H., Woodcock, C. E., Gopal, S., Schnei-

der, A., Cooper, A., Baccini, A., Gao, F., and Schaaf, C.: Global land cover mapping from MODIS: algorithms and early results, Remote Sens. Environ., 83(1–2), 287–302, 2002.

Fritz, S., Bartholomé, E., Belward, A., Hartley, A., Stibig, H.-J., Eva, H., Mayaux, P., Bartalev, S., Latifovic, R., Kolmert, S., Roy, P. S., Agrawal, S., Bingfang, W., Wenting, X., Ledwith, M., Pekel, J.-F., Giri, C., Mücher, S., de Badts, E., Tateishi, R., Champeaux, J.-L., and Defourny, P.: Harmonisation, mosaicing and production of the Global Land Cover 2000 database (Beta Version), European Commission, DG-JRC, EUR 20849 EN, 2003.

Generoso, S., Breon, F.-M., Balkanski, Y., Boucher, O., and Schultz, M.: Improving the seasonal cycle and interannual variations of biomass burning aerosol sources, Atmos. Chem. Phys., 3, 1211–1222, 2003.

Giglio, L., Kendall, J. D., and Mack, R.: A multi-year fire data set for the tropics derived from the TRMM VIRS, Int. J. Remote Sens., 24(22), 4505–4525, 2002.

Giglio, L., van der Werf, G. R., Randerson, J. T., Collatz, G. J., and Kasibhatla, P.: Global estimation of burned area using MODIS active fire observations, Atmos. Chem. Phys., 6, 957–974, 2006.

Giri, C., Zhu, Z., and Reed, B.: A comparative analysis of the Global Land Cover 2000 and MODIS land cover data sets, Remote Sens. Environ., 94(1), 123–132, 2005.

Goloub, P. and Arino, O.: Verification of the consistency of Polder Aerosol Index over land with ATSR-2/ERS-2 fire product, Geophys. Res. Lett., 27(6), 899–902, 2000.

Grégoire, J.-M., Tansey, K., and Silva, J. M. N.:, The GBA2000 initiative: developing a global burnt area database from SPOT-VEGETATION imagery, Int. J. Remote Sens., 24(6), 1369–1376, 2003.

Gumbricht, T., McCarthy, T. S., McCarthy, J., Roy, D., Frost, P. E., and Wessels, K.: Remote sensing to detect sub-surface peat fires and peat fire scars in the Okavango Delta, Botswana, South African J. Sci., 98(7–8), 351–358, 2002.

Gutman, G., Csiszar, I., and Romanov, P.: Using NOAA/AVHRR products to monitor El Nino impacts: Focus on Indonesia in 1997–98, Bull. Am. Meteorol. Soc., 81(6), 1189–1205, 2000.

Hashimoto, H., Nemani, R. R., White, M. A., Jolly, W. M., Piper, S. C., Keeling, C. D., Myneni, R. B., and Running, S. W.: El Niño–Southern Oscillation–induced variability in terrestrial carbon cycling, J. Geophys. Res., 109, D23110, doi:10.1029/2004JD004959, 2004.

Haugaasen, T., Barlow, J., and Peres, C. A.: Surface wildfires in central Amazonia: short-term impact on forest structure and carbon loss, Forest Ecology and Management, 179(1–3), 321–331, 2003.

Hoelzemann, J. J., Schultz, M. G., Brasseur, G. P., and Granier, C.: Global Wildland Fire Emission Model (GWEM): Evaluating the use of global area burnt satellite data, J. Geophys. Res., 109, D14S04, doi:10.1029/2003JD003666, 2004.

Holmgren, M., Scheffer, M., Ezcurra, E., Gutiérrez, J. R., and Mohren, G. M. J.: El Niño effects on the dynamics of terrestrial ecosystems, Trends in Ecology & Evolution, 16(2), 89–94, 2001.

Houghton, R. A.: Revised estimates of the annual net flux of carbon to the atmosphere from changes in land use and land management 1850–2000, Tellus, 55B, 378–390, 2003.

Ito, A. and Penner, J. E.: Global estimates of biomass burning emissions based on satellite imagery for the year 2000, J. Geophys. Res.-Atmos., 109, D14S05, doi:10.1029/2003JD004423, 2004.

Jenkins, G. S. and Ryu, J.-H.: Linking horizontal and vertical transports of biomass fire emissions to the Tropical Atlantic Ozone Paradox during the Northern Hemisphere winter season: climatology, Atmos. Chem. Phys., 4, 449–469, 2004.

Jenkins, G. S., Mohr, K., Morris, V. R., and Arino, O.: The role of convective process over the Zaire-Congo Basin to the southern hemispheric ozone maximum, J. Geophys. Res.-Atmos., 102(D15), 18 963–18 980, 1997.

Jenkins, G. S. and Ryu, J.-H.: Space-borne observations link the tropical atlantic ozone maximum and paradox to lightning, Atmos. Chem. Phys., 4, 361–375, 2004.

Kasischke, E. S., Hewson, J. H., Stocks, B., van der Werf, G., and Randerson, J.: The use of ATSR active fire counts for estimating relative patterns of biomass burning – a study from the boreal forest region, Geophys. Res. Lett., 30(18), 1969, doi:10.1029/2003GL017859, 2003.

Kelha, V., Rauste, Y., Hame, T., Sephton, T., Buongiorno, A., Frauenberger, O., Soini, K., Venalainen, A., San Miguel-Ayanz, J., and Vainio, T.: Combining AVHRR and ATSR satellite sensor data for operational boreal forest fire detection, Int. J. Remote Sens., 24(8), 1691–1708, 2003.

Kim, J. H., Newchurch, M. J., and Han, K.: distribution of tropical tropospheric ozone determined by the scan-angle method applied to TOMS measurements, J. Atmos. Sci., 58(18), 2699–2708, 2001.

Kinne, S., Lohmann, U., Feichter, J., Schulz, M., Timmreck, C., Ghan, S., Easter, R., Chin, M., Ginoux, P., Takemura, T., Tegen, I., Koch, D., Herzog, M., Penner, J., Pitari, G., Holben, B., Eck, T., Smirnov, A., Dubovik, O., Slutsker, I., Tanré, D., Torres, O., Mishchenko, M., Geogdzhayev, I., Chu, D. A., and Kaufman, Y.: Monthly averages of aerosol properties: A global comparison among models, satellite data, and AERONET ground data, J. Geophys. Res.-Atmos., 108(D20), 4634, doi:10.1029/2001JD001253, 2003.

Kulldorff, M., Athas, W., Feuer, E., Miller, B., and Key, C.: Evaluating cluster alarms: A space-time scan statistic and brain cancer in Los Alamos, American Journal of Public Health, 88, 1377–1380, 1998.

Kulldorff, M.: Prospective time-periodic geographical disease surveillance using a scan statistic, J. Roy. Stat. Soc., Series A, 164, 61–72, 2001.

Ladstätter-Weißenmayer, A., Meyer-Arnek, J., Schlemm, A., and Burrows, J. P.: Influence of stratospheric airmasses on tropospheric vertical O3 columns based on GOME (Global Ozone Monitoring Experiment) measurements and backtrajectory calculation over the Pacific, Atmos. Chem. Phys., 4, 903–909, 2004.

Langenfelds,, R. L., Francey, R. J., Pak, B. C., Steele, L. P., Lloyd, J., Trudinger, C. M., and Allison, C. E.: Interannual growth rate variations of atmospheric CO2 and its D13C, H2, CH4, and CO between 1992 and 1999 linked to biomass burning, Global Biogeochemical Cycles, 16(3), 1048, doi:10.1029/2001GB001466, 2002.

Langmann, B. and Heil, A.: Release and dispersion of vegetation and peat fire emissions in the atmosphere over Indonesia 1997/1998, Atmos. Chem. Phys., 4, 2145–2160, 2004.

Legg, C. A. and Laumonier, Y.: Fires in Indonesia, 1997: A remote sensing perspective, Ambio, 28, 479–485, 1999.

Li, Z., Kaufman, Y. J., Ichoku, C., Fraser, R., Trishchenko, A., Giglio, L., Jin, J.-Z., and Yu, X.: A review of AVHRR-based active fire detection algorithms: principles, limitations, and recommendations, in: Global and Regional Vegetation Fire Monitoring from Space: Planning a Coordinated International Effort, edited by: Ahern, F. J., Goldammer, J. G., and Justice, C. O., The Hague, The Netherlands: SPB Academic Publishing, 199–225, 2001.

Lobert, J. M., Keene, W. C., Logan, J. A., and Yevich, R.: Global chlorine emissions from biomass burning: Reactive Chlorine Emissions Inventory, J. Geophys. Res.-Atmos., 104(D7), 8373–8389, 1999.

Malingreau, J.-P., Stephens, G., and Fellows, L.: Remote-sensing of forest-fires – Kalimantan and North-Borneo in 1982–83, Ambio, 14(6), 314–321, 1985.

Martín, M. P., Cecatto, P., Flasse, S., and Downey, I.: Fire detection and fire growth monitoring using satellite data, in: Remote Sensing of Large Wildfires in the European Mediterranean Basin, edited by: Chuvieco, E., Berlin: Springer-Verlag, 101–122, 1999.

Martin, R. V., Chance, K., Jacob, D. J., Kurosu, T. P., Spurr, R. J. D., Bucsela, E., Gleason, J. F., Palmer, P. I., Bey, I., Fiore, A. M., Li, Q., Yantosca, R. M., and Koelemeijer, R. B. A.: An improved retrieval of tropospheric nitrogen dioxide from GOME, J. Geophys. Res.-Atmos., 107(D20), 4437, doi:10.1029/2001JD001027, 2002.

Martin, R. V., Jacob, D. J., Logan, J. A., Bey, I., Yantosca, R. M., Staudt, A. C., Li, Q., Fiore, A. M., Duncan, B. N., Liu, H., and Ginoux, P.: Interpretation of TOMS observations of tropical tropospheric ozone with a global model and in-situ observations, J. Geophys. Res.-Atmos., 107(D18), 4351, doi:10.1029/2001JD001480, 2002.

Menon, S., Hansen, J., Nazarenko, L., and Luo, Y.: Climate effects of black carbon aerosols in China and India, Science, 297, 2250–2253, 2002.

Nepstad, D. C., Veríssimo, A., Alencar, A., Nobre, C., Lima, E., Lefebvre, P., Schlesinger, P., Potter, C., Moutinho, P., Mendoza, E., Cochrane, M., and Brooks, V.: Large-scale impoverishment of Amazonian forests by logging and fire, Nature, 398, 505–508, 1999.

Newchurch, M. J., Liu, X., and Kim, J. H.: Lower tropospheric ozone (LTO) derived from TOMS near mountainous regions, J. Geophys. Res.-Atmos., 106(D17), 20 403–20 412, 2001.

Oglesby, R. J., Marshall , S., and Taylor, J. A.: The climatic effects of biomass burning: investigations with a global climate model, Environmental Modelling & Software, 14, 253–259, 1999.

Olson, J. R., Baum, B. A., Cahoon, D. R., and Crawford, J.: Frequency and distribution of forest, savanna, and crop fires over tropical regions during PEM-Tropics A, J. Geophys. Res.-Atmos., 104(D5), 5865–5876, 1999.

Page, S. E., Siegert, F., Rieley, J. O., Boehm, H.-D. V., Jaya, A., and Limin, S.: The amount of carbon released from peat and forest fires in Indonesia during 1997, Nature, 420(6911), 61–65, 2002.

Pereira, J. M. C.: Remote sensing of burned areas in tropical savannas, Int. J. Wildland Fire, 12, 259–270, 2003.

Pereira, J. M. C., Mota, B. W., Privette, J. L., Caylor, K. K., Silva, J. M. N., Sá, A. C. L., and Ni-Meister, W.: A simulation analysis of the detectability of understory burns in miombo woodlands, Remote Sens. Environ., 93, 296–310, 2004.

Pereira, J. M. C., Pereira, B. S., Barbosa, P. M., Stroppiana, D., Vasconcelos, M. J. P., and Grégoire, J.-M.: Satellite monitoring of the overall fire activity in the EXPRESSO study area during the dry season experiment: active fires, burnt areas, and atmospheric emissions, J. Geophys. Res.-Atmos., 104, 30 701–30 712, 1999a.

Pinty, B., Verstraete, M. M., and Gobron, N.: Do man-made fires affect Earth's surface reflectance at continental scales? EOS,Transactions, American Geophysical Union, 81(34), 381 and 388–389, 2000.

Pochanart, P., Akimoto, H., Kajii, Y., and Sukasem, P.: Carbon monoxide, regional-scale transport, and biomass burning in tropical continental Southeast Asia: Observations in rural Thailand, J. Geophys. Res.-Atmos., 108(D17), 4552, doi:10.1029/2002JD003360, 2003.

Potter, C., Tan, P.-N., Steinbach, M., Klooster, S., Kumar, V., Myneni, R., and Genovese, V.: Major disturbance events in terrestrial ecosystems detected using global satellite data sets, Global Change Biology, 9(7), 1005–1021, 2003.

Prins, E. M. and Menzel, W. P.: Geostationary satellite detection of biomass burning in South America, Int. J. Remote Sens., 13, 2783–2799, 1992.

Prins, E. M. and Menzel, W. P.: Trends in South American biomass burning detected with the GOES VAS from 1983–1991, J. Geophys. Res.-Atmos., 99(D8), 16 719–16 735, 1994.

Richter, A. and Burrows, J. P.: Retrieval of tropospheric NO2 from GOME measurements, Adv. Space Res., 29, 1673–1683, 2002.

Rödenbeck, C., Houwelling, S., Gloor, M., and Heimann, M.: $CO_2$ flux history 1982–2001 inferred from atmospheric data using a global inversion of atmospheric transport, Atmos. Chem. Phys., 3, 1919–1964, 2003.

Rogerson, P.: Surveillance systems for monitoring the development of spatial patterns, Statistics in Medicine, 16, 2081–2093, 1997.

Rogerson, P.: Monitoring point patterns for the development of space-time clusters, Journal of the Royal Statistical Society, Series A, 164, 87–96, 2001.

Roman-Cuesta, R. M., Retana, J., and Gracia, M.: Fire trends in tropical Mexico-A case study of Chiapas, J. Forestry, 102(1), 26–32, 2004.

Sauvage, B., Thouret, V., Cammas, J.-P., Gheusi, F., Athier, G., and Nédélec, P.: Tropospheric ozone over Equatorial Africa: regional aspects from the MOZAIC data, Atmos. Chem. Phys., 5, 311–335, 2005.

Schultz, M. G.: On the use of ATSR fire count data to estimate the seasonal and interannual variability of vegetation fire emissions, Atmos. Chem. Phys., 2, 387–395, 2002.

Setzer, A. W. and Pereira, M. C.: Amazonia biomass burnings in 1987 and an estimate of their tropospheric emissions, Ambio, 20(1), 19–22, 1991.

Siegert, F. and Hoffmann, A. A.: The 1998 forest fires in East Kalimantan (Indonesia): a quantitative evaluation using high resolution, multitemporal ERS-2 SAR images and NOAA-AVHRR hotspot data, Remote Sens. Environ., 72, 64–77, 2000.

Silva, J. M. N., Pereira, J. M. C., Cabral, A. I., Sá, A. C. L., Vasconcelos, M. J. P., Mota, B., and Grégoire, J.-M.: An estimate of the area burned in southern Africa during the 2000 dry season using SPOT-VEGETATION satellite data, J. Geophys. Res.-Atmos., 108(D13), 8498, doi:10.1029/2002JD002320, 2003.

Soja, A. J., Sukhinin, I., Cahoon Jr., D. R., Shugart, H. H., and Stackhouse Jr., P. W.: AVHRR-derived fire frequency, distribu-

tion and area burned in Siberia, Int. J. Remote Sens., 25(10), 1939–1960, 2004.

Spichtinger, N., Damoah, R., Eckhardt, S., Forster, C., James, P., Beirle, S., Marbach, T., Wagner, T., Novelli, P. C., and Stohl, A.: Boreal forest fires in 1997 and 1998: a seasonal comparison using transport model simulations and measurement data, Atmos. Chem. Phys., 4, 1857–1868, 2004 .

Staudt, A. C., Jacob, D. J., Ravetta, F., Logan, J. A., Bachiochi, D., Krishnamurti, T. N., Sandholm, S., Ridley, B., Singh, H. B., and Talbot, B.: Sources and chemistry of nitrogen oxides over the tropical Pacific, J. Geophys. Res.-Atmos., 108(D2), 8239, doi:10.1029/2002JD002139, 2003.

Staudt, A. C., Jacob, D. J, Logan, J. A., Bachiochi, D., Krishnamurti, T. N., and Sachse, G. W.: Continental sources, transoceanic transport, and interhemispheric exchange of carbon monoxide over the Pacific, J. Geophys. Res.-Atmos., 106(D23), 32 571–32 590, 2001.

Strahler, A., Muchoney, D., Borak, J., Friedl, M., Gopal, S., Lambin, E., and Moody, A.: MODIS land cover product algorithm theoretical basis document (ATBD) version 5.0–MODIS land cover and land cover change. (http://modis.gsfc.nasa.gov/data/atbd/atbd_mod12.pdf), 1999.

Stroppiana, D., Pinnock, S., and Grégoire, J.-M.: The Global Fire Product: daily fire occurrence from April 1992 to December 1993 derived from NOAA AVHRR data, Int. J. Remote Sens., 21(6–7), 1279–1288, 2000.

Sudo, K., Takahashi, M., and Akimoto, H.: CHASER: A global chemical model of the troposphere 2, Model results and evaluation, J. Geophys. Res.-Atmos., 107, doi:10.1029/2001JD001114, 2002.

Tansey, K., Grégoire, J.-M., Stroppiana, D., Sousa, A., Silva, J., Pereira, J. M. C., Boschetti, L., Maggi, M., Brivio, P. A., Fraser, R., Flasse, S., Ershov, D., Binaghi, E., Graetz, D., and Peduzzi, P.: Vegetation burning in the year 2000: Global burned area estimates from SPOT VEGETATION data, J. Geophys. Res.-Atmos., 109(D14), D14S03, doi:10.1029/2003JD003598, 2004.

van der Werf, G., Randerson, J. T., Collatz, G. J., and Giglio, L.: Carbon emissions from fires in tropical and subtropical ecosystems, Global Change Biology, 9, 1–16, 2003.

van der Werf, G. R., Randerson, J. T., Collatz, G. J., Giglio, L., Kasibhatla, P. S., Arellano Jr., A. F., Olsen, S. C., and Kasischke, E. S.: Continental-scale partitioning of fire emissions during the 1997 to 2001 El Nino/La Nina period, Science, 303(5654), 73–76, 2004.

Wooster, M. J. and Strub, N.: Study of the 1997 Borneo fires: Quantitative analysis using global area coverage (GAC) satellite data, Global Biochemical Cycles, 16(1), doi:10.1029/2000GB001357, 2002.

Wooster, M. J. and Rothery, D. A.: A review of volcano surveillance applications using the ATSR instrument series, Adv. Environ. Monitoring and Modelling, 1(1), 97–123, 2002.

Yurganov, L. N., Blumenstock, T., Grechko, E. I., Hase, F., Hyer, E. J., Kasischke, E. S., Koike, M., Kondo, Y., Kramer, I., Leung, F.-Y., Mahieu, E., Mellqvist, J., Notholt, J., Novelli, P. C., Rinsland, C. P., Scheel, H. E., Schulz, A., Strandberg, A., Sussmann, R., Tanimoto, H.,Velazco, V., Zander, R., and Zhao, Y.: A quantitative assessment of the 1998 carbon monoxide emission anomaly in the northern hemisphere based on total column and surface concentration measurements, J. Geophys. Res.-Atmos., 109(D15), D15305, doi:10.1029/2004JD004559, 2004.

Zhao, Y., Kondo, Y., Liu, X., Koike, M., Irie, H., Suzuki, K., Sera, M., and Ikegami, Y.: Seasonal variations of HCN over northern Japan measured by ground-based infrared solar spectroscopy, Geophys. Res. Lett., 27(14), 2085–2088, 2000.

Zhao, Y., Strong, K., Kondo, Y., Koike, M., Matsumi, Y., Irie, H., Rinsland, C. P., Jones, N. B., Suzuki, K., Nakajima, H., Nakane, H., and Murata, I.: Spectroscopic measurements of tropospheric CO, $C_2H_6$, $C_2H_2$, and HCN in northern Japan, J. Geophys. Res.-Atmos., 107, 4343, doi:10.1029/2001JD000748, 2002.

# Artigo 2

## Burned area mapping accuracy limits: a global, multi-sensor assessment using the Pareto boundary approach

**Mota, B., J.M.C. Pereira** - Department of Forestry, Instituto Superior de Agronomia, 1349-017 Lisboa, Portugal.
**A. Sousa** - Department of Rural Engineering, University of Évora, Apartado 94, 7002-554 Evora, Portugal.

# Classification accuracy limits induced by burned area spatial patterns: a global, multi-sensor analysis

Bernardo Mota[a], José M.C.Perreira[a], Adélia Sousa[b]

[a]*Department of Forestry, Instituto Superior de Agronomia, 1349-017 Lisboa, Portugal.*
[b]*Department of Rural Engineering, University of vora, Apartado 94, 7002-554 Evora, Portugal.*

**Abstract**

Degradation analysis was performed on 72 Landsat burned area maps simulating three types of sensor optical characteristics (MODIS and AVHRR) and two re-sampled products (GAC and PAL). Pareto boundary approach was applied using three threshold criteria to each degraded map and a sensitivity analysis was preformed to determine areal accuracy and scar patterns variations. Results show that the compensating effect between commission and omission errors provided the highest accuracy for burned area estimation and that fragmentation and land-cover type also play a role. The results show that MODIS sensors can provide accuracies to global burned areal estimates, with errors lower than 5% and that AVHRR sensor reveals limitations for the South American forests and the mid-latitudes. The GAC and PAL products provide the larger errors, of up to 50% underestimation in South America, and low burned area scar scenarios can be undetected. The Northern Australian and the African savannas burned areas due to their size and pattern can be accurately detected by all the covered resolutions.

*Keywords:*
Spatial Degradation, PSF, Pareto Boudary, Scar Fragmentation, Area overestimate

## 1. Introduction

The drastic increase in greenhouse gases and pollutant species emissions over the past century has influenced the Earths climate and the welfare of its population (Houghton et al., 2001). One of the major source of many trace gases and particles released into the atmosphere each year is biomass burning (Andreae, 1991, Ito and Penner, 2004). Uncertainties in emission estimates provided by the amount of biomass burnt are still high (Crutzen and Andreae, 1990, Schultz, 2002), and result from uncertainties associated with burned area and fuel load estimates and combustion factors (Ito and Penner, 2004).

Burned area mapping using satellite imagery has proven to be highly valuable for investigating the impact of biomass burning on the climate system and on vegetation. In the past decade, many application have been carried out using different sensors at different scales. Burned area maps, can now cover larger areas, from local to regional and global scales. Fine resolution images (up to 60m spatial resolution) are limited in both temporal sampling and spatial coverage but are widely used by many forest services to measure their annual burned areal extent because they are considered as the *ground truth* representation (Bourgeau-Chavez et al., 1997, Chuvieco and Congalton, 1988, Pereira, 1999, Roy et al., 2005, Russell-Smith et al., 1997). Burned area maps derived from fine resolution have also been largely accepted by the scientific community as the operational satellite images used for validation purposes and accuracy assessment. Most of the coarser resolution burned area products were validated and its accuracy assessed by applying double sampling with a regression estimator approach (Sá et al., 2007, Silva et al., 2003, Stroppiana et al., 2003). The moderate and coarse spatial resolution sensors (up to 1km and higher, respectively) have proven to be an effective tool for mapping regional (Chuvieco et al., 2008a), continental (Barbosa et al., 1999b, Pu et al., 2007, Sukhinin et al., 2004) and global (Roy et al., 2005, Tansey et al., 2004a) burned areas. Although their detail and accuracy are not sufficient for local resource management applications, they can complement existing conventional burned area surveys (Justice and Korontzi, 2001). At this resolution, images are used to provide inexpensive annual burned maps that can easily be converted into compatible large-scale formats for spatial modelling of carbon budget and fire emissions (Barbosa et al., 1999a, Hoelzemann et al., 2004, Schultz et al., 2008, van der Werf et al., 2010a). For example, Ito and Penner (2004) based on the Global Burned Area 2000 (GBA2000) product (Grégoire et al., 2003, Tansey et al., 2004b) estimated for year 2000 that 2580 $TgDMyr^{-1}$ and 4054 $TgCO_2yr^{-1}$ were released into the atmosphere by the $3.5x10^6km^2$ of global burned area. Also, the GFED product (van der Werf et al., 2010b), in its 3rd version, provides emission estimates from 1996 until 2009 based on burned area maps derived from MODIS imagery (Giglio et al., 2009).

Although large improvements have been made in the development of annual global burned area products (Roy et al., 2008, Tansey et al., 2007), there are still large uncertainties associated with areal estimates. Boschetti et al. (2004b) have shown through an inter-comparison of two global 1km spatial resolution burned area datasets that, while there can be good spatial agreement, areal estimates can largely disagree. In the same study, the authors have shown that the larger discrepancies were

found in north America and in Sub-Saharan Africa, where the GLObal Burn SCARs (Simon et al., 2004) product detected twice and less than half the area the GBA2000 (Grégoire et al., 2003, Tansey et al., 2004b) product, respectively. Burned area product validation is very important (Kaufman et al., 2002, Morisette et al., 2002) and preferably should be done with an independent data source. For coarser and moderate resolution burned area maps, the accepted validation procedure is based on comparison with finer resolution burned area maps, where the error matrix between the two datasets provides the means for classification accuracy (Congalton, 2001, Stehman, 1997). This procedure is the basis for the guidelines developed by the CEOS Land Product Validation Subgroup (LPVS) for validation of global burned area products with long time-series.

Burned scar detection at coarser resolutions highly depend on the degree of spectral contrast with the background landscape, which in turn depends on landcover (vegetation and soils), time since fire, weather conditions, and vegetation recovery rate (Pereira and Santos, 2003). Additionally, fragmentation (either natural or due to human activity) and size of the objects mapped strongly influences the accuracy at coarse resolutions (Eva and Lambin, 1998, Laris, 2005, Sá et al., 2007, Silva et al., 2005). The presence of area patches smaller than the spatial resolution can remain undetected. Each spatial resolution is therefore limited by best possible accuracy when commission and omission errors are minimised (Boschetti et al., 2004c).

In contrast to other remote sensing products such as ocean color, sea or land surface temperature, burned area maps are not continuous fields of data graduated into pixel values but binary maps of burned/unburned. These traditionally result from threshold optimisation in the algorithm output probabilities, or by other ranking systems, that represent the burned proportion of the courser resolution pixels. The fraction of burned biomass for a pixel to be considered burned varies with ecosystem, spectral response within different bands (Eva and Lambin, 1998) and with energy emitted by the surrounding pixels (Cahoon et al., 2000). In Eva and Lambin (1998), the authors labelled coarse resolution cells as burnt if 40% or 50% of their area in the corresponding fine resolution cell was affected by fire. These thresholds were based on an empirical analysis of the relationship between Landsat MSS and AVHRR data. The same study showed that high fragmentation burned area patterns are strongly eroded with the 50% threshold resulting in high underestimation. And that, in landscapes composed by large compact fire scars, burned area is dilated, leading to overestimation of the area actually burnt. In this case, both thresholds produced minor differences. Barbosa et al. (1998), based on Razafimpanilo et al. (1995) also selected a low threshold value of 20% for burned signature for a 5km GAC AVHRR pixel because it was only expected to detect large burned areas. Sousa (2005), for South America, and Sousa (1999) for Portugal, spatially degraded Landsat fine resolution burned area maps to VGT and AVHRR pixels sizes, and found that optimal threshold values ranged from 10% to 40% and 65%, respectively and that thresholds were highly related to the mean fire scar size. Hlavka and Dungan (2002) also found that applying thresholds of 30% to 40% to AVHRR data resulted in estimates close to the fine resolution maps, 20% to 30% overestimate and 50% underestimate.

Until now, these studies only covered local or regional extents, focusing on a particular fire-regime. For some vegetation types, burnt scars can be smaller than the pixel size, and determining the area burnt within a pixel is still the subject of ongoing research. From the emission modellers point of view, fire-regimes where scars are highly fragmented or small can be associated with large biomass loads. Failure to detect these small areas can result in large pyrogenic emission errors.

Since year 2000, efforts have been made in the development of operational burned area products based on the continuous satellite programs with coarse-resolution sensors on board. Among these are: the MCD45A1 (Roy et al., 2008) based on MODIS images (500m); the L3JRC (Tansey et al., 2007, 2008) based on VGT images (1km) and recently the ESA Fire CCI program, which will develop combined burned area maps based on VGT (1km), AATSR/ATSR2 (1km) and MERIS full resolution (300m) images. Their importance for model emission estimates is fundamental but they are limited in time. The large historical AVHHR sensor record, extending further back in time, can provide imagery for burned area mapping covering the 80s and 90s. With this in mind, assessment of the accuracy limits, for the coarser resolution and re-sampled products is essential for the Burned Area (BA) algorithm developers to tune classification algorithms performance. Additionally, it can also provide areal errors estimates for the emission modellers.

The main objective of this study is to assess classification limits on burned area mapping imposed by the spatial characteristics (extent, fragmentation) for three different sensors and derived products. In order to attain this objective, we: (a) analysed burnt scars fragmentation, fire size distribution and affected land cover type from a large dataset of fine spatial resolution BA maps; (b) we then degraded these fine spatial resolution BA maps using spatial filters to emulate three moderate and coarser spatial resolution sensors followed by re-sampling methods to derived standard BA products; (c) we then applied different threshold criteria (based on commission and omission errors) of pixel burned fraction to the spatial degraded burned area maps to evaluate accuracy and two contrasting BA maps were analysed in detail; (d) finally, we evaluated the spatial distribution of each sensor accuracy limits and stratified the results by land cover type.

## 2. Data and Methods

### *2.1. Landsat burned area maps*

The use of Landsat (LS) derived imagery can help estimate the total burnt area at a regional scale throughout a burning season. Among others the Portuguese forest service, the Catalonia Forest service and the US forest service have been providing annual assessment of burned area extent based on Landsat imagery. These fine resolution images are used for validation and accuracy assessment of the coarser resolution BA products. In this study, we used a total of 72 Landsat derived burned area maps. The maps were obtained from multiple sources with different projections (Table 1) and were re-formatted into

lat/long coordinates with approximate 30-meter spatial resolution, coded with a binary coding for burned, unburned and not observed. Each image had been classified and validated using different approaches depending on the source. Most of the maps were previously used for coarser resolution burned area map validation and accuracy assessment.

The spatial distribution did not follow a formal statistical sampling scheme but their selection tried to cover most of the Tropical Savannas, Boreal Forests and the temperate regions: 16 images is Africa; 14 images in South America; 11 in Asia; 15 in Australia; 12 in North America and four images plus one single composite in Europe (Fig.1). Their acquisition dates were all from the year 2000, except for Portugal where the 1990 six-frame spatial composite was added because it was considered to have been an average burning season.

### *2.2. Emulating coarse resolution burned area maps*

#### *2.2.1. Moderate resolutions*

The spatial resolution of any remote sensing satellite imagery is determined by the sensor optical specifications and the satellite orbit altitude. For simulation purposes, the spatial degradation of raster grids is commonly performed with a mean filter (a.k.a. majority filter) due to its simplicity (Benson and MacKenzie, 1995, Boschetti et al., 2004a, Saura, 2004). However, assuming that all pixels within the filter footprint (corresponding to the instrument field of view) are to be weighted equally does not reflect the actual image formation process (Huang et al., 2002, Saura, 2004). A point spread function (PSF) is best used to simulate how each individual satellite sensor would capture the same image because it describes the response of the imaging system to the point source or point object. Accurate modeling of the in-flight PSF of any sensor is very difficult, due to difficulties in quantifying contributions of the atmospheric and view angle effects, deviations from preflight optical characteristics, and along-track asymmetry (Moreno and Melia, 1994, Oleson et al., 1995). Nevertheless, the sensors spatial response can be modeled as an extended Gaussian filter, where pixel weights decrease non-linearly with distance from the kernel center (Benson and MacKenzie, 1995). It is also considered that nearby signals beyond the output grid can also contribute to the current pixel value. For this study we used (Oleson et al., 1995) optical point spread functions and applied it to each binary map image (Hlavka and Dungan, 2002, Hlavka and Spanner, 1995, Huang et al., 2002, Oleson et al., 1995)). The function is given by:

$$G(X,Y) = \frac{1}{2\pi\sigma^2} e^{-\frac{x^2+y^2}{2\sigma^2}}, \quad (1)$$

where $\sigma$ is the half width of the sensor ground instantaneous field of view (IFOV) and x and y are the pixel locations within the lower resolution grid (Schowengerdt, 2007).

We emulated moderate and coarse resolution burned area maps based on the spatial characteristics of various sensors and data products: the Moderate Resolution Imaging Spectroradiometer (MODIS) (250m and 500m) and the Advanced Very High Resolution Radiometer (AVHRR) (1.1km) Imagery sensors. Each of these sensors fly aboard the AQUA or TERRA and National Oceanic and Atmospheric Administration (NOAA) satellites, respectively. By considering the effect of the nearby surrounding pixels, each sensor imagery pixel was emulated by degrading the fine resolution maps using eq.1 where $\sigma$ was set to 8, 16 and 22 Landsat pixels for the MODIS 250m, MODIS 500m and AVHRR 1.1km, respectively. These instruments were selected due to their wide use in burned area mapping studies, including Roy et al. (2002) and Chuvieco et al. (2008b) for MODIS, and Barbosa et al. (1999b), Cahoon (1991), Cahoon et al. (1994), Eva and Lambin (1998), Fernandez et al. (1997), Fraser et al. (2000), Justice et al. (1996), Kasischke and French (1995), Langaas (1992), Li et al. (2000), Pereira (1999), Stroppiana et al. (2000) and Sukhinin et al. (2004) for AVHRR.

#### *2.2.2. Re-sampled coarse resolutions*

The development of relatively long time series of satellite imagery, useful for carbon cycle and climate change studies, have relied on remotely sensed data sets based on reduced spatial resolution AVHRR imagery. These time series of archived data under the form of Global Area Coverage (GAC) and Pathfinder AVHRR Land (PAL) formats have been used to derive multi-year, continental or global burned area extents (Barbosa et al., 1999b, Carmona-Moreno et al., 2005, Koffi et al., 1995, Riano et al., 2007). The operational re-sampling procedure for the GAC data is an inverse binning mapping method based on a re-sampling procedure that uses a 3 lines by 5 columns AVHRR pixel blocks, on which the mean value of the first 4 pixels of the first line is assigned the geo-location given by a 4km grid point closest to the same averaged pixels mean geo-location (Eva and Lambin, 1998). For PAL case, the re-sampling procedure relies on selecting the highest NDVI pixel, within every two by two GAC pixel blocks. Since we could not calculate NDVI values, one GAC pixel was selected randomly from among the four possible choices to represent the PAL pixel.

### *2.3. Burned scar patterns and land-cover characterisation*

In order to quantify the burned area pattern of each Landsat BA map and derived BA degraded maps, we used the Matheron Fragmentation Index (MFI) defined by Klein et al. (1993) as:

$$MFI = 10 \times \frac{Br}{\sqrt{B_p} \times \sqrt{T_p}}, \quad (2)$$

where $Br$ is the extent of the boundary between burned and unburned pixels, $B_p$ is the total number of burned pixels and $T_p$ is the total number of burned and unburned pixels. A high MFI value corresponds to highly fragmented burned areas, while low values represent large, compact fire scar shapes or total low burned area extent. Accordingly to Saura (2004) fragmentation indexes can be consistent when area size is conserved. Each LS map contains a significant number of fragments that enables a statistical characterisation of size distribution. For each scene, we computed the fire size distribution (FSD) by counting the number of scars in each size class and the corresponding fraction of total area burned. The adopted class size scale was defined by a $log_{10}$ scale.

Table 1: Landsat burned area map properties

| Path/Row | Satellite | location | Associated project | Reference |
|---|---|---|---|---|
| 175/77 | Landsat 7 ETM+ | Botswana, Africa | SAFARI/GLCF/EOS/ISA | (Silva et al., 2005) |
| 165/70 | Landsat 7 ETM+ | Mozambique, Africa | SAFARI/GLCF/EOS/ISA | ” |
| 168/77 | Landsat 7 ETM+ | Mozambique, Africa | SAFARI/GLCF/EOS/ISA | ” |
| 180/54 | Landsat 7 ETM+ | CAR, Africa | SAFARI/GLCF/EOS/ISA | ” |
| 171/77 | Landsat 7 ETM+ | South Africa, Africa | SAFARI/GLCF/EOS/ISA | ” |
| 171/51 | Landsat 7 ETM+ | Sudan, Africa | SAFARI/GLCF/EOS/ISA | ” |
| 175/70 | Landsat 7 ETM+ | Zambia, Africa | SAFARI/GLCF/EOS/ISA | ” |
| 196/53 | Landsat 7 ETM+ | Burkina Faso, Africa | SAFARI/GLCF/EOS/ISA | ” |
| 175/74 | Landsat 7 ETM+ | Botswana, Africa | SAFARI/GLCF/EOS/ISA | ” |
| 174/65 | Landsat 7 ETM+ | DRC, Africa | SAFARI/GLCF/EOS/ISA | ” |
| 173/55 | Landsat 7 ETM+ | Sudan , Africa | SAFARI/GLCF/EOS/ISA | ” |
| 172/73 | Landsat 7 ETM+ | Zimbabwe, Africa | SAFARI/GLCF/EOS/ISA | ” |
| 171/56 | Landsat 7 ETM+ | Sudan, Africa | SAFARI/GLCF/EOS/ISA | ” |
| 197/35 | Landsat 7 ETM+ | Angelia, Africa | ESA/Globcarbon | (Simon et al., 2004) |
| 199/52 | Landsat 7 ETM+ | Mali, Africa | CSU/Paul Laris | (Laris, 2005) |
| 199/52 | Landsat 7 ETM+ | Mali, Africa | CSU/Paul Laris | ” |
| 220/66 | Landsat 7 ETM+ | Paraguay, South America | INPE | (Sousa, 2005) |
| 221/66 | Landsat 7 ETM+ | Brazil, South America | INPE | ” |
| 02/01/67 | Landsat 7 ETM+ | Brazil, South America | INPE | ” |
| 231/68 | Landsat 7 ETM+ | Brazil, South America | INPE | ” |
| 227/68 | Landsat 7 ETM+ | Brazil, South America | INPE | ” |
| 224/67 | Landsat 7 ETM+ | Brazil, South America | INPE | ” |
| 224/68 | Landsat 7 ETM+ | Brazil, South America | INPE | ” |
| 223/66 | Landsat 7 ETM+ | Brazil, South America | INPE | ” |
| 222/66 | Landsat 7 ETM+ | Brazil, South America | INPE | ” |
| 222/73 | Landsat 7 ETM+ | Brazil, South America | INPE | ” |
| 225/78 | Landsat 7 ETM+ | Brazil, South America | GLCF/ISA | (Tansey et al., 2004a) |
| 05/01/56 | Landsat 7 ETM+ | Venezuela, South America | GLCF/ISA | ” |
| 06/01/55 | Landsat 7 ETM+ | Colombia, South America | GLCF/ISA | ” |
| 06/01/57 | Landsat 7 ETM+ | Colombia, South America | GLCF/ISA | ” |
| 160//15 | Landsat 7 ETM+ | Russia, Asia | ESA/Globcarbon | (Simon et al., 2004) |
| 162/16 | Landsat 7 ETM+ | Russia, Asia | ESA/Globcarbon | ” |
| 121/44 | Landsat 7 ETM+ | Russia, Asia | ESA/Globcarbon | ” |
| 118/42 | Landsat 7 ETM+ | China, Asia | ESA/Globcarbon | ” |
| 180/34 | Landsat 7 ETM+ | China, Asia | ESA/Globcarbon | ” |
| 181/32 | Landsat 7 ETM+ | Turkey, Asia | ESA/Globcarbon | ” |
| 124/22 | Landsat 7 ETM+ | Turkey, Asia | JRC/ ISA | (Tansey et al., 2004a) |
| 118/23 | Landsat 7 ETM+ | Russia, Asia | JRC/ ISA | ” |
| 162/14 | Landsat 7 ETM+ | Russia, Asia | IKI/ Serguey Bartalev/ ISA | - |
| 127/26 | Landsat 7 ETM+ | Mongolia, Asia | JRC/GLCF/ISA | (Tansey et al., 2004a) |
| 127/27 | Landsat 7 ETM+ | Mongolia, Asia | JRC/GLCF/ISA | ” |
| 107/72 | Landsat 7 ETM+ | Australia, Oceania | ESA/Globcarbon | (Simon et al., 2004) |
| 101/74 | Landsat 7 ETM+ | Australia, Oceania | ESA/Globcarbon | ” |
| 102/73 | Landsat 7 ETM+ | Australia, Oceania | ESA/Globcarbon | ” |
| 112/76 | Landsat 7 ETM+ | Australia, Oceania | ESA/Globcarbon | ” |
| 112/77 | Landsat 7 ETM+ | Australia, Oceania | ESA/Globcarbon | ” |
| 110/72 | Landsat 7 ETM+ | Australia, Oceania | JRC | (Stroppiana et al., 2003) |
| 113/75 | Landsat 7 ETM+ | Australia, Oceania | JRC | ” |
| 105/70 | Landsat 7 ETM+ | Australia, Oceania | JRC | ” |
| 105/70 | Landsat 7 ETM+ | Australia, Oceania | JRC | ” |
| 105/74 | Landsat 7 ETM+ | Australia, Oceania | BNT | (Yates and Russell-Smith, 2002) |
| Composites | Landsat 7 ETM+ | Australia, Oceania | BNT | ” |
| Composites | Landsat 7 ETM+ | Australia, Oceania | BNT | ” |
| Composites | Landsat 7 ETM+ | Australia, Oceania | BNT | ” |
| 42/29 | Landsat 7 ETM+ | Oregon, North America | ESA/Globcarbon | (Simon et al., 2004) |
| 42/31 | Landsat 7 ETM+ | USA, North America | ESA/Globcarbon | ” |
| 40/31 | Landsat 7 ETM+ | USA, North America | ESA/Globcarbon | ” |
| 39/31 | Landsat 7 ETM+ | USA, North America | ESA/Globcarbon | ” |
| 39/33 | Landsat 7 ETM+ | USA, North America | ESA/Globcarbon | ” |
| 27/39 | Landsat 7 ETM+ | USA, North America | ESA/Globcarbon | ” |
| 25/39 | Landsat 7 ETM+ | USA, North America | ESA/Globcarbon | ” |
| 60/14 | Landsat 7 ETM+ | Canada, North America | ESA/Globcarbon | ” |
| 54/15 | Landsat 7 ETM+ | Canada, North America | ESA/Globcarbon | ” |
| 16/33 | Landsat 7 ETM+ | USA, North America | USFS/National Park Service | - |
| 62/47 | Landsat 7 ETM+ | USA, North America | USFS/National Park Service | - |
| 37/35 | Landsat 7 ETM+ | USA, North America | USFS/National Park Service | - |
| 197/31 | Landsat 7 ETM+, Landsat 5 TM | Spain, Europe | ESA/Globcarbon | (Simon et al., 2004) |
| 193/31 | Landsat 7 ETM+, Landsat 5 TM | France, Europe | ESA/Globcarbon | ” |
| 184/34 | Landsat 7 ETM+, Landsat 5 TM | Greece, Europe | ESA/Globcarbon | ” |
| 182/31 | Landsat 7 ETM+, Landsat 5 TM | Bulgaria, Europe | ESA/Globcarbon | ” |
| Composites | Landsat 7 ETM+ | Portugal, Europe | DGRF/ ISA | (Pereira and Santos, 2003) |

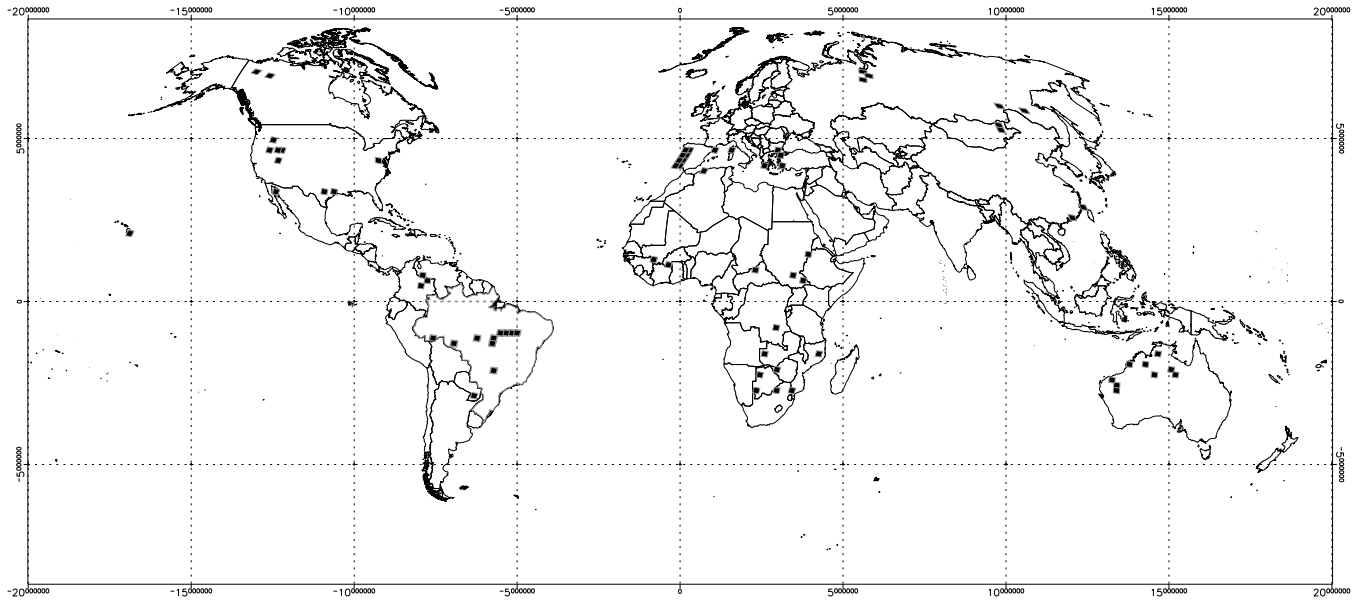

Figure 1: Spatial distribution of Landsat frame burned area maps

Land cover can effect the detectability of burns in spatially degraded Landsat imagery Eva and Lambin (1998) Silva et al. (2005) and Sá et al. (2007) found that bright surfaces, such as dry grasslands, enhance the contrast between burned and unburned areas and, therefore, yield better classification results on the degraded images. To analyse the use of land cover as a proxy for differentiating burned area patterns we used the Global Landcover Classification product (GLC2000) (Bartholome and Belward, 2005) developed by the JRC/IES Global Vegetation Monitoring Unit (GVM). The dataset is available at `http://www-gem.jrc.it/glc2000/` in a geographic lat/long grid with 1km spatial resolution and uses the FAO Land Cover Classification System (LCCS) legend. In order to reduce the number of land cover classes, we grouped all the unvegetated classes (Bare Areas, Water Bodies, Snow and Ice and Artificial surfaces) and all land cover classes that occupied less than 1% of the global surface area into a single class *other* (Table 2). For each Landsat frame, the land cover pixels were flagged as burned or unburned and each class percentage within each scene was calculated. Each Landsat scene was flagged with the dominant land cover class for the fire affected Landsat areas.

Table 2: Regrouped GLC2000 classes

| Class | Description |
|---|---|
| TBE | Tree Cover - Broadleaved evergreen |
| TBDC | Tree Cover Close broadleaved deciduous |
| TBDO | Tree Cover Open broadleaved deciduous |
| TNE | Tree Cover Needle-leaved evergreen |
| TND | Tree Cover Needle-leaved deciduous |
| TM | Tree Cover Mixed leaf type |
| MTN | Mosaic Tree cover and natural vegetation |
| SE | Shrub cover - evergreen |
| SD | Shrub cover deciduous |
| HRB | Herbaceous cover |
| SHSS | Sparse herbaceous and sparse shrub cover |
| CMA | Cultivated and managed areas |
| MCTO | Mosaic Cropland, tree cover and natural vegetation |
| MCSG | Mosaic Cropland, shrub and grass cover |
| O | Others |

### *2.4. Pareto boundary analysis*

Degrading the spatial resolution of burned area maps leads to changes in size and shape of fire patches, and to disappearance of small objects at critical resolution thresholds (Mayaux and Lambin, 1995). In this study, we used the Pareto boundary methodology applied to remote sensing (Boschetti et al., 2004c) to identify segmentation thresholds representing the best possible compromise between omission and commission errors. The Pareto boundary concept is a methodology originally developed in econometrics. Its application to remote sensing is based on statistical indexes extracted from the classical error matrix to evaluate the influence of spatial resolution on the accuracy of the final mapped product, obtained with hard classification methods. It can reveal the extent to which classification accuracy of a low spatial resolution dichotomous map depends on imperfections of the classification procedure and on spatial information loss induced by low resolution. The methodology developed by Boschetti et al. (2004c), involves overlaying a low-resolution grid over the high-resolution map and assigning to each new grid cell its corresponding burned area proportion. The new degraded resolution map is then composed by pixels with burned proportions, on a continuous scale, ranging from 0 (totally unburned) to 1 (totally burned). Defining increasingly larger thresholds of proportions present within the low-resolution map, above which each cell is considered totally burned, creates a series of virtual binary classifications. For each new low-resolution map it is possible to determine the

commission and omission errors provided solely by the presence of mixed cells. The line connecting each threshold point in the commission-omission error plane is a discrete approximation of the Pareto boundary curve. Lower segmentation thresholds lead to large commission errors while higher segmentation thresholds favour larger omission errors (fig.2 in Boschetti et al. (2004c)). Although all points on the Pareto curve represent the best error compromise due only to spatial degradation, they provide different areal estimates. A point dominated by commission (omission) errors will lead to area overestimation (underestimation), meaning that area estimates are directly related to the selected segmentation threshold. From the user point of view, the intent is to obtain a product with the lowest possible area error estimates. In theory, the point on the Pareto boundary closest to the origin of the Omission/Commission error plane determines the minimal error accumulation (a.k.a high accuracy map). In practice, due to the shape of the curves, this is translated by preference of lower commission than omission error (Boschetti et al., 2004c). On the other hand, the best compromise between commission/omission error could be determined by a threshold that favours compensation between overestimation and underestimation. This option may be preferred if one is concerned with grid based areal estimates rather than individual scar area accuracy, i.e., extent over geographical detail. This criterion can be important in areas with high load of biomass for small fires. In this study we applied a continuous-scaled threshold (TR) to the degraded resolution burned area maps at 0.05 pixel burned fraction intervals. This provided a good piecewise linear approximation to the Pareto curves and helped determine segmentation threshold according to the following three criteria:

1. A minimum distance criterion, defined by the minimum distance between the origin of the commission/omission plane and the Pareto curve. This criterion minimises the sum of omission and commission errors;
2. An optimum criterion, defined by the point on the curve closest to the plane bisection line, representing the compensating effect between commission and omission errors;
3. A fixed 0.5 burned pixel threshold criterion (unbiased majority rule).

It order to represent areal accuracy, we calculated the Percent of Detectable Area (PDA) by dividing the estimated sensor-degraded burned area by the original burned area, as estimated from the Landsat data, and multiplied by 100. Values under 100% correspond to area underestimation, limited by zero representing a complete miss. Values above 100% have no upper limit and correspond to burned area overestimation. To simplify, for the remaining of this study, areal accuracy based on PDA is simply refered as accuracy.

### *2.5. Accuracy analysis*

For all LS scenes, threshold values for the three criteria were calculated and a detailed analysis was performed in two scenes, with the highest contrast in fragmentation. For both scenes and for the three criteria, variations in TR, MFI, PDA and FSD caused by the different sensor resolutions were compared and spatial patterns were visually analysed. The criteria that scored the highest accuracy was selected for analysis of PDA global distribution for each sensor and derived products. To understand accuracy limits, land-cover was used as a proxy for stratification of BA and MFI values for the high resolution maps, and TR and PDA values for each sensor and for the resampled products. Land-cover stratification was preformed by averaging BA, MFI, TR and PDA values for the scenes where the dominant land-cover type occupied, at least, 40% of the area burned. Analysis was restricted to land-covers flagged with more than 3 scenes.

## 3. Results

### *3.1. Fine resolution burned area map characterisation*

BA and MFI values calculated individually for the full set of Landsat maps revealed similar distributions, both being positively skewed (Fig.2a-b). This indicated that most of the scenes contained compact burned areas, covering a small fraction of the total area. Exceptions were only noted on a few African and Australian frames with very high MFI and BA values representing extensive highly fragmented burning. The FSD revealed that over 80.6% of scars have sizes up to 100ha, corresponding only to 1.6% of the total burned area (Fig.2c). A small number of scars (1.2%) in the two larger size classes (above 10000ha) represent over 83.0% of the total burned area mapped.

Regarding land-cover occupation, Shrub Cover Deciduous (SD), Herbaceous Cover (HRB), Sparse Herbaceous or Sparse Shrub (SHSS) and Cultivated and Managed Areas (CMA) were the most represented land-cover classes in the Landsat scenes (Fig.3). Together, not only did they cover 51% of the total area but were also the most frequently observed classes present on the full set of scenes. The least represented classes were the Tree Cover Needle leaved Deciduous (TND), Tree Cover Mixed Leaf type (TM), Mosaic Tree Cover and Natural Vegetation (MTN), Sparse Cover Evergreen (SE) and Mosaic Cropland, tree cover and Natural Vegetation (MTCO). The class distribution, for the scenes extents and for only the burned fraction, are quite representative of global distribution coverage. With the exception of the SD class that is over-represented and the TBE that is under-represented, all land-cover classes have similar global representations, in both the scenes and burned area sets. The results also show differences in distribution between the scenes total extent and just the burned fraction area. Fire incidence is higher on Tree Cover Needle leaved Evergreen (TNE) and SD classes and lower in the TND and Other (O) class.

### *3.2. Pareto Analysis of reduced resolution burned area maps*

Pareto boundary analysis was applied to every LS scene using the simulated reduced resolution burned area maps. The Pareto curves obtained reveal that, on average, commission and omission errors increase and burned/unburned segmentation thresholds decrease with decreasing spatial resolution. In order to help interpret the observed shape variability of the

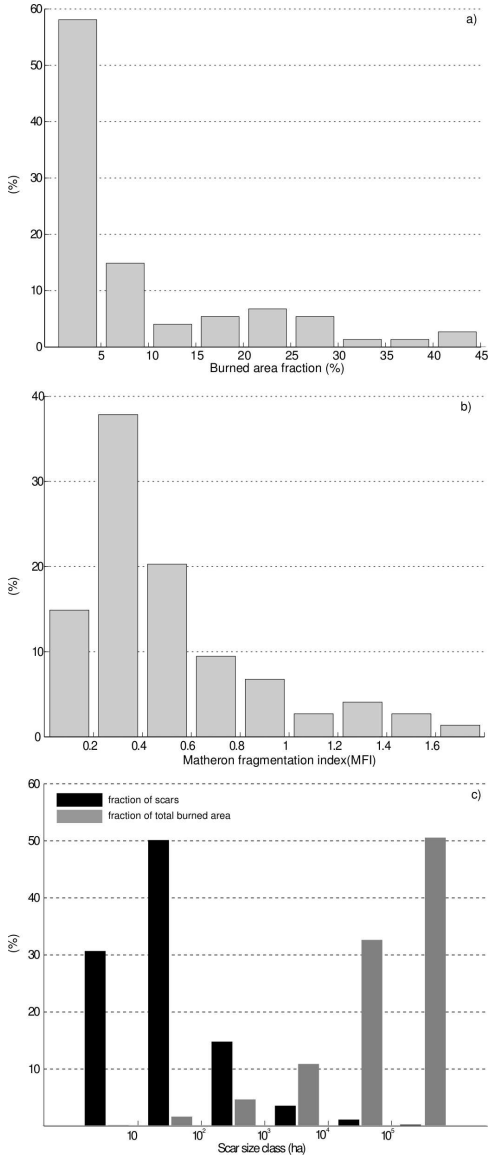


Figure 2: Distribuition of the Landsat a) scenes burned area fraction (BA), b) scenes fragmentation index (MFI) and, c) Fire Size Distribution (FSD) in logarithmic scale of the number of fires (grey) and corresponding fractions of burned area (black).

Pareto curves, two frames with contrasting fragmentation patterns where analysed in detail. The Mali scene has 6261 individual fire scars with a MFI value of 1.64, representing 10% of its area. At the opposite extreme, the Mongolia scene has an MFI of 0.08 with 49 fire scars covering 16% of scene area. In the highly fragmented Mali scene (Fig.4a), the Pareto curve for each sensor shows very gradual transitions between the regions dominated by commission errors to regions dominated by omission errors. For all curves, both errors are always high and individual sensor curves appear distinct, clearly spaced apart, with the higher resolution sensors characterised by lower commission/omission errors. For the Mongolian scene (Fig.4b), the curves have steeper transitions between commission and omission dominating errors; they are more closely spaced. For this scene, the AVHRR and re-sampled products appear as a distinctive group of curves, with higher commission and omission errors.

For each curve, the threshold points representing the different criteria were identified and the application of these thresholds to all the sensors resulted in different outputs in shape and area of scars. For the Mali frame, the minimum distance threshold criterion is always characterised by producing higher commission than omission errors, whereas the 0.5 threshold tends to have larger omission than commission errors, resulting in area overestimation and underestimation, respectively. Located between both these criterion, the optimal threshold criterion compensates between both types of error. For the lower resolution sensors these contrasts are more evident, resulting in higher error pair differences. For the Mongolian scene, these characteristics are less evident. Not only do all threshold criteria have identical commission and omission errors, but they are also closely spaced.

Independently of the non-fixed criteria criteria, both high and low fragmentation maps, show that thresholds always decreases for the coarser resolution sensors (Fig.5). PDA and MFI variations for the two scenes are also different. For the Mali scene, the 0.5 threshold results in MFI decrease and continuous area underestimation down to 10% for PAL product (Fig.5a). The minimum distance criterion, always showing the lower thresholds, results in MFI increase and area overestimation of up to 300% for PAL product (Fig.5b). Regarding the spatial patterns, the lower thresholds results in the detection of a higher number of burned scars (Fig.6). The optimal threshold criterion lowers the TR value enough to achieve the compensating effect; providing the minimum area estimation error. It also tends to conserve MFI values, maintaining an approximately constant spatial pattern, even for the 8km resolution PAL data.

For the low fragmentation Mongolian scene, PDA and MFI values tend to be juxtaposed and less variable, where only small increase exceptions are observed for the GAC and PAL products (Fig.5b). This scene is less sensitive to TR value changes, as shown by the small PDA and MFI differences amongst the three threshold criteria; the main patches are conserved (Fig.7).

The mean results of the full burned area maps are consistent with the results analysed for the two scenes (Table 3). The 0.5 threshold criterion overestimates and the minimum distance segmentation criterion underestimates burned area. Underestimation but with the highest accuracy is obtained with the optimal segmentation threshold criterion. We selected the optimum criterion to be applied to rest of this study, not only because it always yields higher areal accuracy but also because it preserves the scar spatial patterns by minimal MFI variations.

Table 3: Mean areal accuracy for the three sensors and resampled products as obtained by the application of the three threshold criteria.

| | Modis(250m) | Modis(500m) | AVHRR(1.1km) | GAC(4km) | PAL(8km) |
|---|---|---|---|---|---|
| Min.dist | 104.46 | 110.01 | 119.52 | 120.24 | 121.58 |
| 0.5 | 97.28 | 89.16 | 80.6 | 52.05 | 55.49 |
| Optimum | 97.75 | 98.64 | 98.39 | 86.33 | 85.74 |

The optimal criterion FSD for the two sensor-degraded burned area maps (Mali and Mongolia) shows distinctive distributions. For the Mali scene, the number of fires per size class

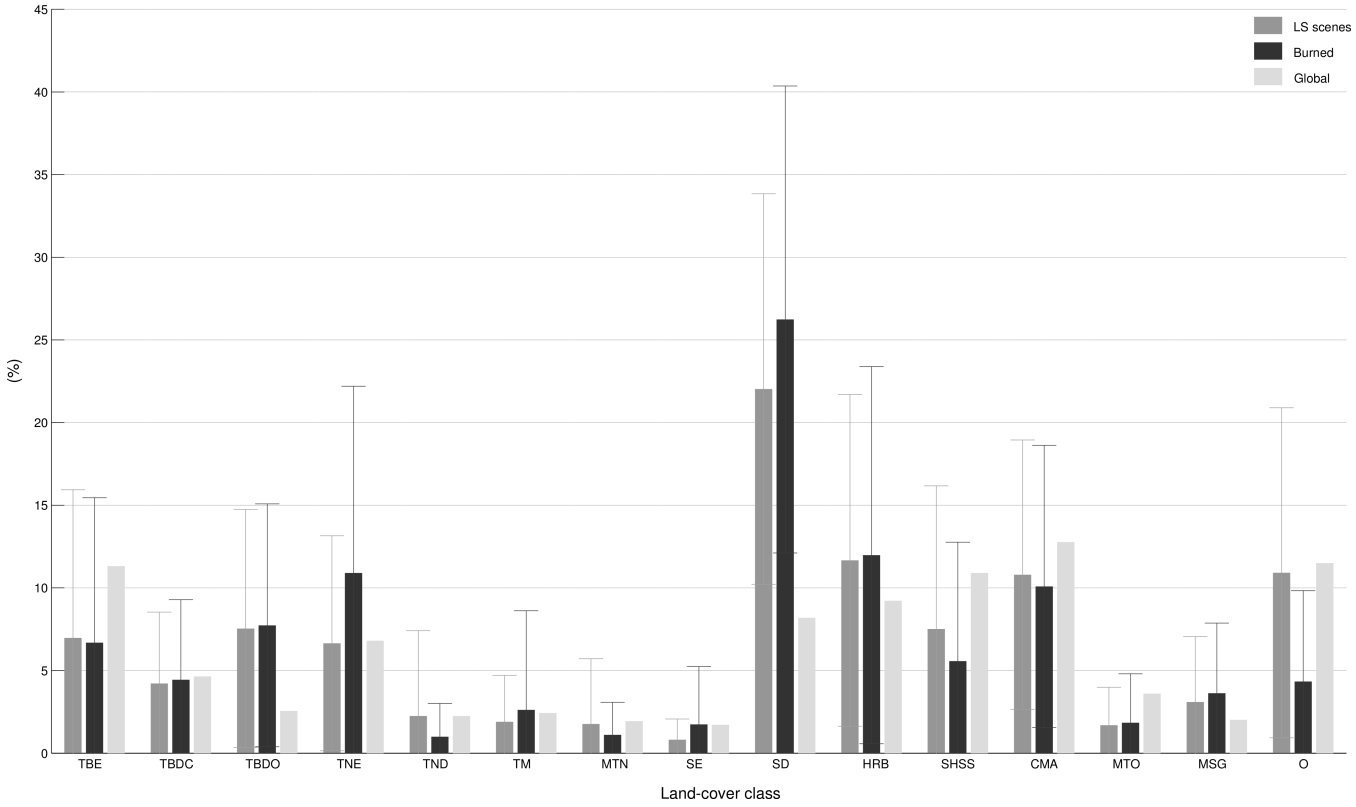


Figure 3: Global grouped GLC2000 Class percentage (light grey), covered only by the Landsat scenes (grey) and, mean burned class percentage (black) for the landsat burned area maps, and corresponding standard deviations.

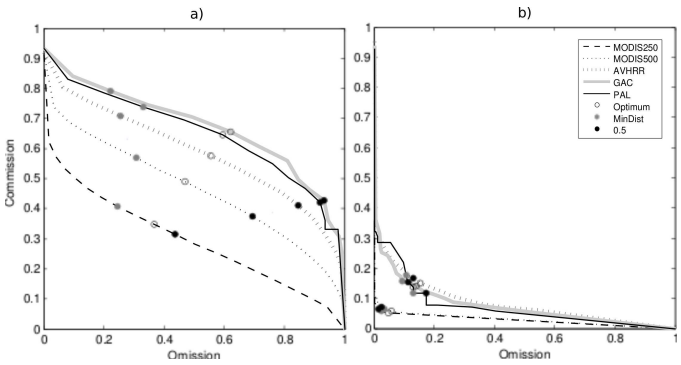


Figure 4: Sensor derived Pareto curves for the a) Mali Landsat scene and b) the Mongolia Landsat scene burned area maps.

and corresponding burned area fractions, shift their peaks to higher size classes as the pixel size increases (Fig.8a). Lower resolution sensors increasingly fail to detect the smaller scars. Threshold value is determined by the larger scars that tend to increase in size and in number. This feature indicates that, for the coarser resolutions, fire scars can be of sub-pixel size achieved at the cost of very low thresholds, changing the spatial pattern from many small scars to a few larger scars. For the Mongolia scene, there is also a shift in size class peak for the number of fires, but the corresponding burned area fractions remain almost constant (Fig.8b). The major contribution to the total area burned is always made by the larger scars. In this scene, sub-pixel scar detection is never an issue resulting in an unchanged spatial pattern.

### *3.3. Accuracy global distribution*

The mean PDA value for all Landsat scenes is smaller for lower spatial resolutions (Table 3). This highlights the tendency for the coarser resolution sensors to underestimate burned area. As indicated by the two scenes, the PDA results for the full LS burned area maps are not uniform throughout the globe. Different scenes have different TR decreasing rates, that result in underestimation or overestimation. PDA spatial differences are also not constant and depend on the spatial resolution. In order to easily identify the degree of underestimation or overestimation, PDA values for each scene were colour coled (Fig.9). A colour ramp was defined accordingly to highlight the smaller and larger estimation errors. Both MODIS sensors provide the lower area estimation errors (Fig.9a-b). For the 250m sensor, this value does not exceed 5% overestimation or underestimation, in any scene. For the 500m sensor most scenes have errors smaller than 5%, with some exceptions. Overestimation can reach 10% for the Senegal and Texas scenes and 10% underestimation for the Venezuela and Hawaii scenes, one scene in Brazil and one in Russia. Errors for the AVHRR sensor are above 5% for most of south American scenes with the Paraguay scene and one Brazil scene exceeding 10% overestimation and underestimation, respectively (Fig.9c). As for the MODIS 500m sensor, area burned in the Hawaii and Texas scene is un-

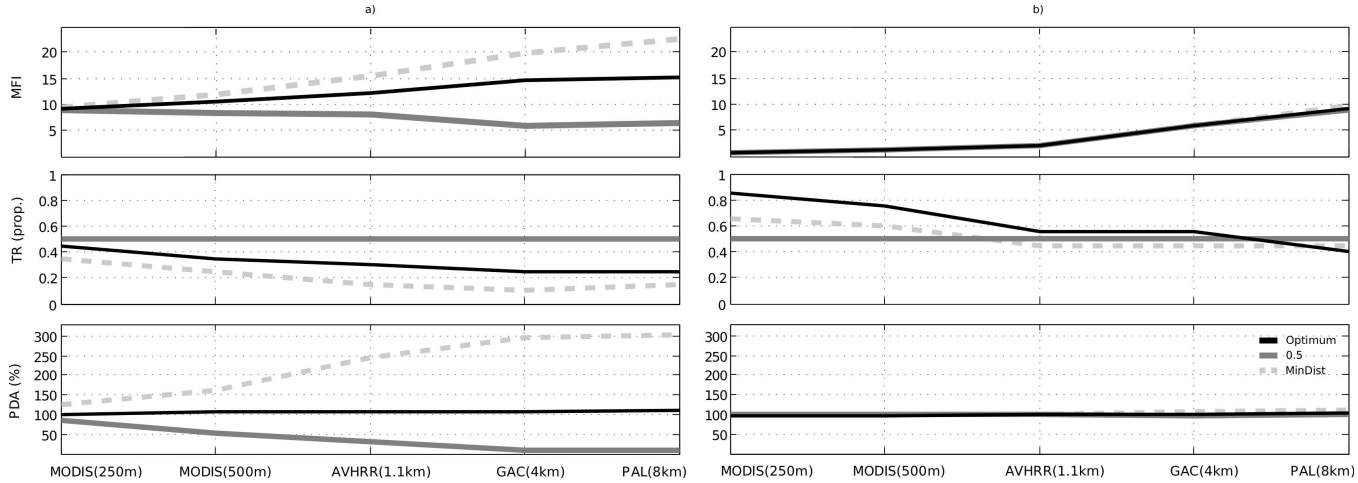


Figure 5: Matheron Fragmentation Index (upper panel), Proportion of Detected Area (central panel) and segmentation threshold (lower panel) for the optimal (black), minimum distance (dashed gray) and 0.5 (gray) threshold criteria applied to a) Maly scene b) Mongolia scene.

derestimated and overestimated, respectively, by values exceeding 10%. In Africa, underestimation in the Sudan and Mozambique scenes reaches 10% and in Senegal burned area overestimation remains below 10%. In Europe, both Turkey scenes have underestimation errors below 5%. The GAC and PAL products yield the larger errors and, in some scenes, burned areas are completely undetected . For the GAC product (Fig.9d), all South America frames show underestimation reaching up to 50%. Many European, Californian and an Australian scene, show underestimation values larger than 5%. For the Hawaii and Texas frames burned area goes completely undetected. Exceptions to underestimation are the Ivory Coast, China, and one of the California scenes, which show overestimation values of up to 50%. As expected, the PAL sensor shows the larger errors, reaching in some cases more than 50% overestimation and underestimation (Fig.9e). In addition to Hawaii and Texas, burned areas are totally missed in some scenes in California, Siberia, one in China, one in Europe and one in Australia. The only scenes with overestimation or underestimation bellow 5% are half the Australian, some African scenes and that from Mongolia.

### *3.4. Accuracy limit stratified by Land cover class*

In the previous section we showed that PDA values vary throughout the globe suggesting that land cover, prior to burn, can serve as a proxy to determine limitations in accuracy by the sensors. Aggregation of PDA and threshold values into burned land-cover types resulted in the exclusion of the TND, TM, MTM, SE, MCTO, MCSG and O dominated land cover classes due to the minimum number scenes criterion. Together, they represented less than 7% of the total burned area covered by this study. Aggregation by land-cover class showed that mean TR and PDA values decrease for the lower spatial resolutions, varies with land-cover.

TBE, TBDC and TNE land-cover classes are characterised by low mean BA values and low variability. Fragmentation is similarly behaved but higher for the TBE land-cover scenes (Fig.10). By comparison, the remaining classes (TBDO, SD, HRD, SHSS and CMA) show higher burned areas, higher fragmentation and associated variabilities. Exception is only noted for the CMA land-cover with lower MFI variability, yielding that burned area can appear with different extents but have similar fragmentation patterns.

As observed for the two scenes in section 3.2, TR values decrease for the lower spatial resolution for all land-cover types. When compared with the AVHRR re-sampled products, resolutions finer than AVHRR are characterised by low threshold variability and inter-class differences tend to be maintained. For the re-sampled products threshold severely decreases and its associated variability increases. TBE land-covers located on South America and Hawaii, and TNE land-covers located at the mid latitudes of the northern hemisphere are characterised by the lowest threshold values for all resolutions (Fig.11). In contrast, for the two MODIS resolutions, the SD, HRD, SHSS, CMA land-covers show mean threshold values above 0.5. For all resolutions, the TBDC and TCDO land-covers, located in South America and in southern hemisphere Africa, are characterised by similar thresholds and associated variabilities. The SD class is the most represented in our analysis; the scenes are located in the African Sahel and in Northern Australia. Along with the SHSS located on Mongolia and Australia, both land-covers show the highest TR values in the set.

As a resulted of the selected TR, PDA values were only lower than 95% for the AVHRR and derived products, where the TBE, HRD and CMA reveal the larger underestimations. The least underestimating classes are the TBDC, TBDO and SD land covers with mean PDA values above 75%, for all the spatial resolutions. TNE tends to produce results with high variability and mean overestimation can easily occur for the PAL product. The SHSS land-cover shows high accuracy but overestimation can occur for the PAL product. Complete miss-detections occur for some scenes characterised by TBE, TNE, SD and HRB land-covers only for the re-sampled AVHRR products resolutions.

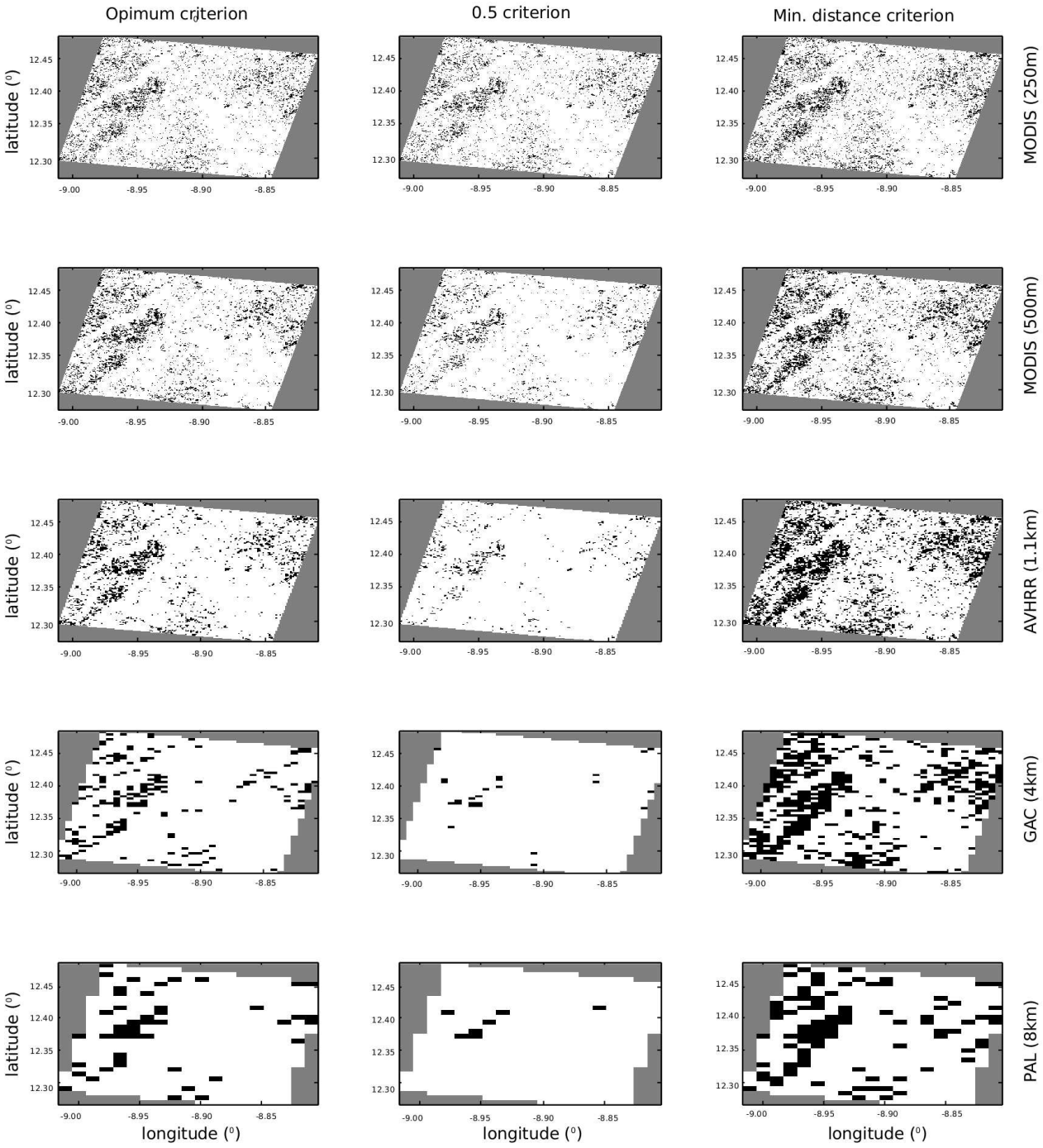


Figure 6: Mali scene spatial degradation, emulated for the three different sensors and derive products, applying three different threshold criteria.

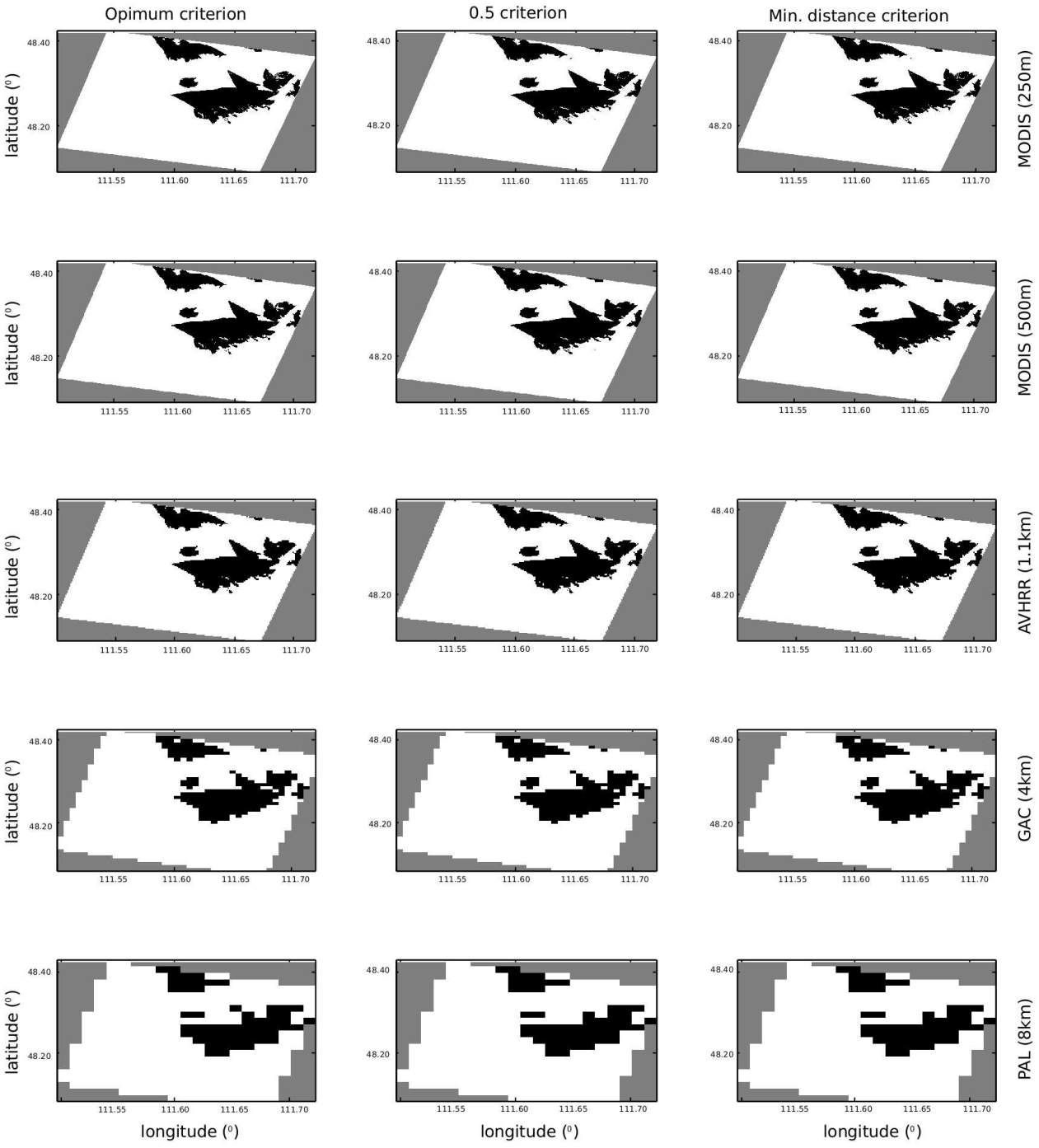


Figure 7: As in Figure 6 but for the Mongolia scene.

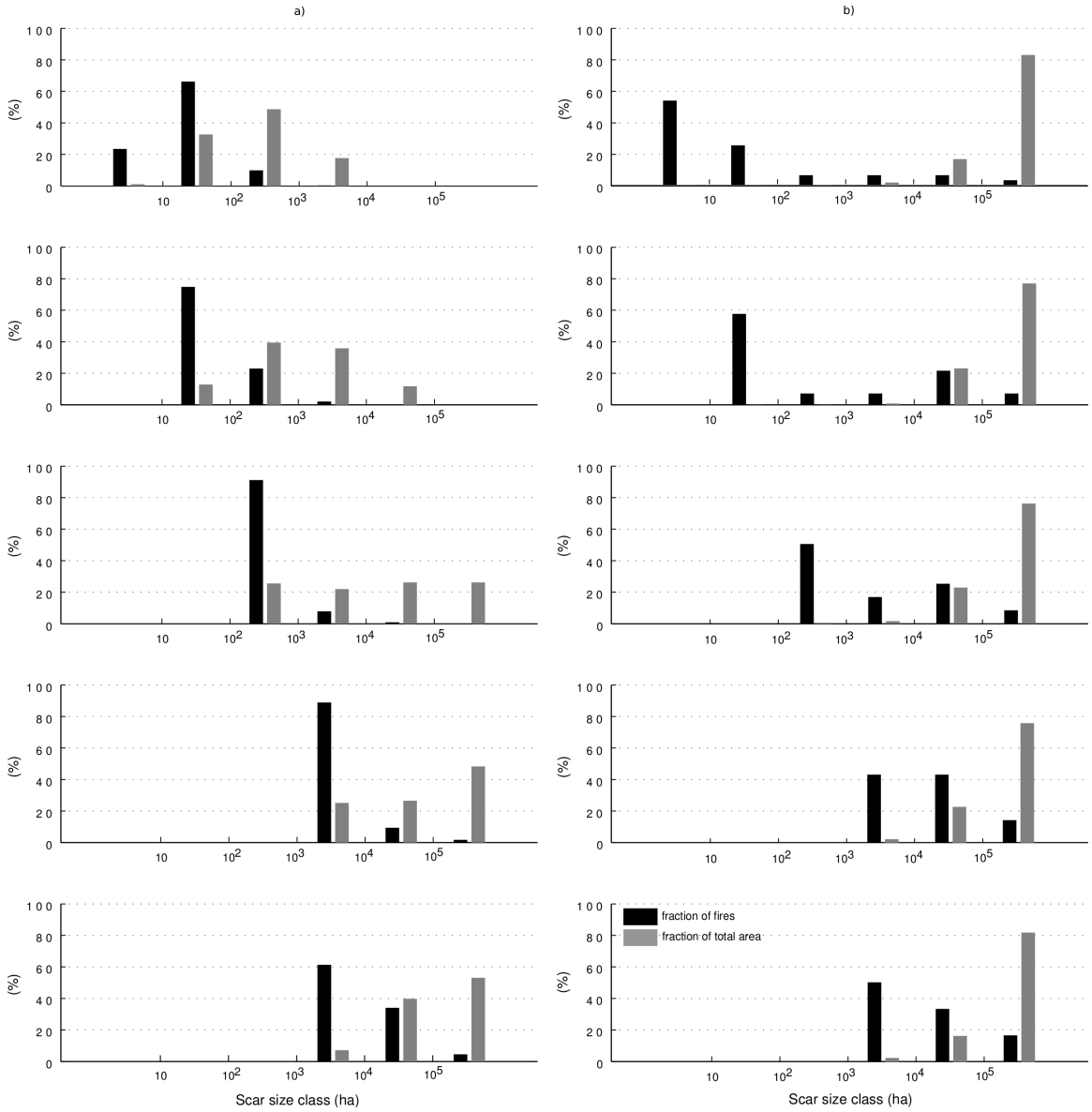


Figure 8: Number of fire scars (black) and corresonding area fractions (grey), by fire size class, for the Mali (a) and Mongolia (b) scenes for the three sensor and derived products, based on the optimal threshold criterion.

## 4. Discussion and conclusions

In this study, our objective was to assess the classification limits on burned area mapping imposed by the spatial characteristics (extent, fragmentation). To attain this objective we used a large dataset of burned area maps derived from the classification of Landsat fine resolution images. Most of these Landsat scenes were characterized by low burned area fraction and low fragmentation. Exceptions were noted on some SD and HRB land-cover scenes where scars covered a large area with a highly fragmented pattern. Although no formal spatial statistical sampling was used for scene selection, the fine resolution land-cover class distribution showed good agreement with global surface distribution. Fire incidence is disproportionally high in the SD and the TNE classes, disproportionally low in the O and TND classes. Median burn scar size is less then 100ha, but its corresponding area proportion was small. Big fires (above 1000ha) are responsible for a very large fraction of total burned area. These results were in conformity with other studies. Strauss et al. (1989) for western United States, found that the proportion of area burned by the 1% of largest fires ranges from 80%-96%. Korontzi et al. (2003) found for Africa that in semi arid areas a few very large fires (above 10000ha) accounted for about 60% of the total area burned and in humid areas approximately 60% of the fire scars had and area below 1000ha. Díaz-Delgado and Pons (2001) found that 7% of fires that occurred from 1975 to 1995 in the Catalonia province were large fires (>2000ha) corresponding to 60% of the total burned area. Although dominated by the large fires, total burned area is always characterised by a proportion of smaller scars that represent a detection challenge for coarser resolution sensors.

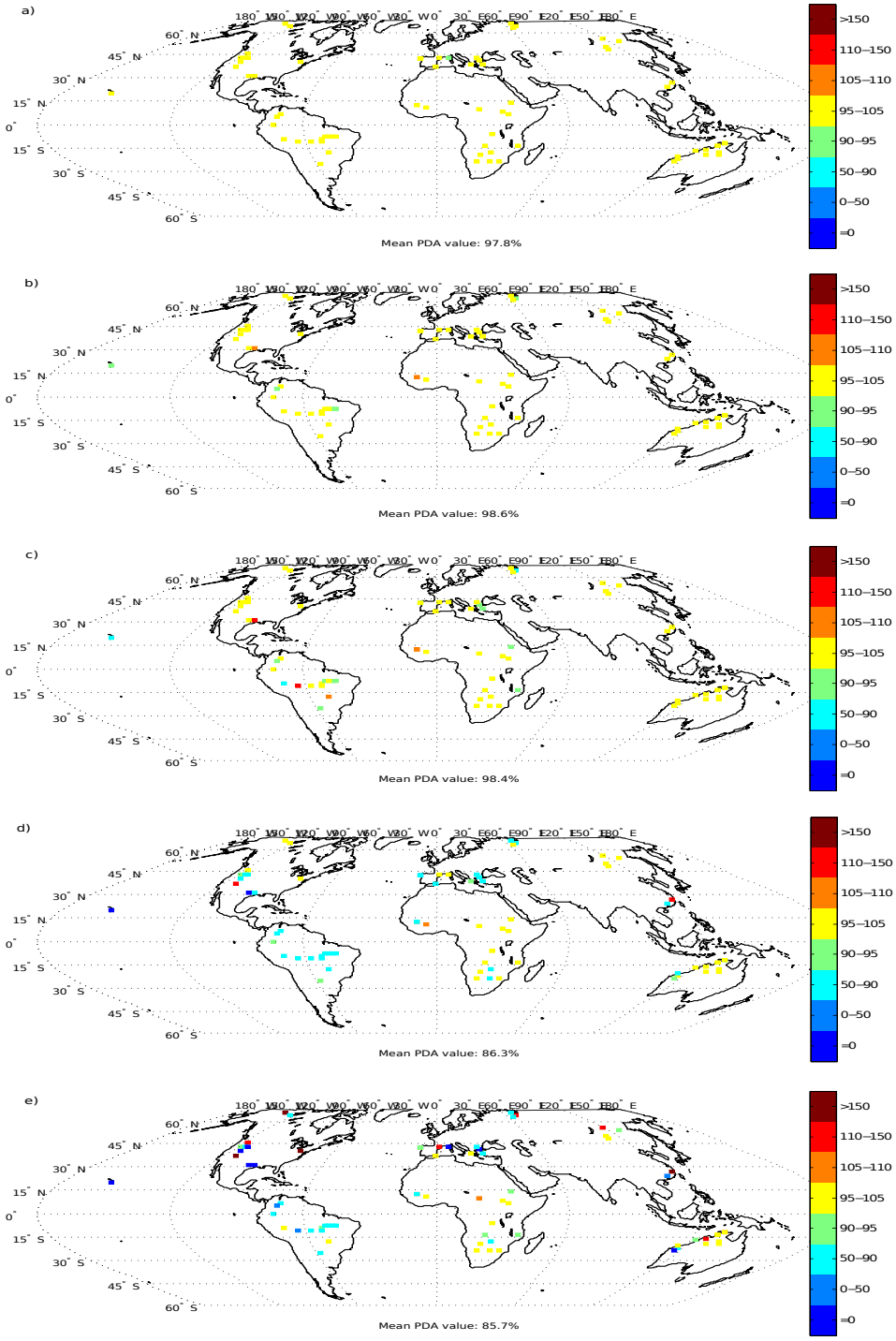


Figure 9: Spatial distribution of the LS scenes Percentage of Detected Area as a results of spatial degradation based on the optimum threshold criterion for the a)MODIS 250m, b)MODIS 500m, c)AVHRR 1.1Km, d)GAC 4Km and e) PAL 8Km sensors.

The obtained PDA values, compared with other studies where accuracy assessment of coarse resolution burned area map was made by comparison with fine resolution maps, show similar and different results. Most of the work that used LS frames to validate Modis (500m) burned area products revealed that omission prevails over commission errors; Giglio et al. (2006) and Loboda and Csiszar (2007) reported 15% underestimation in area burned in Asia; and Chuvieco et al. (2008b) reported underestimation values of 40% to 60% in South America. Predominance of commission errors was found in AVHRR derived sensor imagery classifications; Sukhinin et al. (2004) and Loboda and Csiszar (2007), both for Asia; Yates and Russell-Smith (2002) in five out of six LS scenes for Australia; Eva and Lambin (1998) for Senegal. The VEGETA-

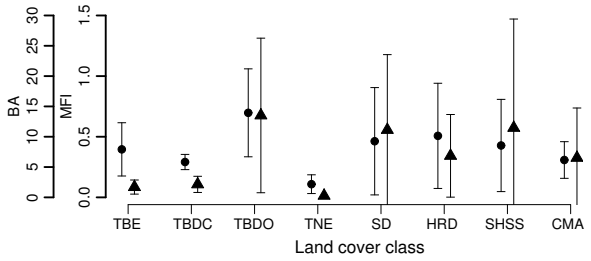


Figure 10: Landsat scenes burned area fraction (circles) and Matheron fragmentation index (triangles) aggregated by land-cover class.

TION (VGT) sensor aboard the SPOT satellite has a spatial resolution identical to the AVHRR sensor. Burned area classification derived from this imagery, when compared with fine resolution burned area maps, revealed a wide range of underestimation values for Africa (Laris, 2005, Silva et al., 2004), Asia (Zhang et al., 2003) and overestimation for North America (Fraser et al., 2004), Australia (Stroppiana et al., 2003) and South America (Sousa, 2005).

The reported studies reflect some inadequacies of the burned area classification algorithms and data limitations relatively to what would be theoretically achievable. In reality, different classifications relied on different algorithms; the VGT sensor shows spectral detectability limitations due to lack of a thermal channel and for coarser resolutions small unburned islands can be mapped as burned (Fraser et al., 2004). On the other hand, Sá et al. (2007), using MODIS imagery for Africa, showed that spectral detectability of burned area increases for threshold values above 50% due to the decrease of mixed pixels. Underestimation or overestimation can also be a byproduct of supervised classifications when collecting spectral signatures of pixels that appear burned. The degree of burned completeness of the collected pixels will determine the classifier flexibility. For a restrictive selection, fire-affected pixels containing considerable amounts of unburnt vegetation may remain unidentified resulting in underestimation and a less conservative selection will allow unburned vegetation to be classified as burned. The accuracy results presented in this study are due to the spatial patterns degradation alone. They are a simulation of what a perfect classification algorithm could achieve.

Our analysis has identified several FSD scenarios which result in underestimation or overestimation. For the large compact fire scar scenarios, like the Mongolia scene map, the proportion of area burned in mixed pixels is lower. Burned area estimation is less sensitive to threshold selection because the overall area contribution of the mixed pixels is much lower. As a result, burned area is always determined by the completely burned pixels yielding lower area estimation errors. For a single, or dispersed, small fire scar scenario, in order for the optimum criteria to compensate between commission and omission errors it needs to adjust the threshold to yield the highest accuracy. When scar size is below the sensor spatial resolution, subpixel detection is only managed by forcing the threshold to drop to very low values. This decrease is only possible up to a certain level, beyond which PDA values become very high, yielding large overestimation. This scenario was observed in some mid latitude scenes. For intermediate mixed scar size scenarios (i.e. large and small fires), the class containing the highest percentage of total area burned will bias the threshold selection to be applied. If scars are low fragmented, the completely burned pixels will dominate over mixed pixels; high accuracy is achieved at the expense of the completely burned scars and accuracy will be insensitive to threshold selection. In contract, when scars are highly fragmented, mixed pixels will dominate

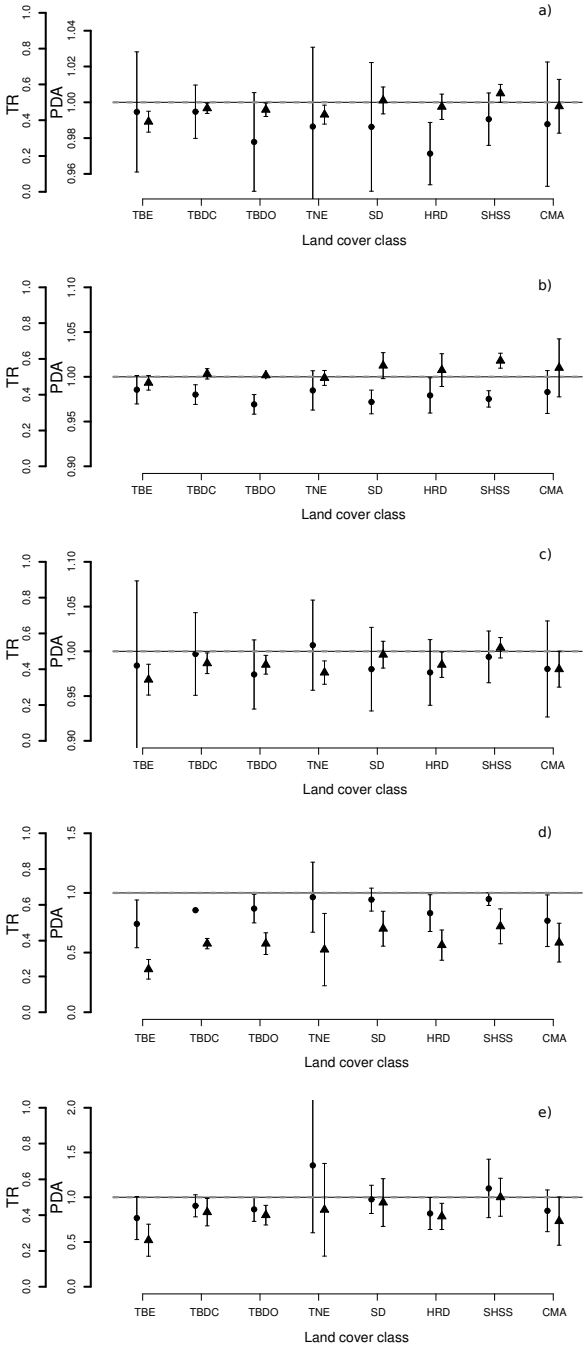


Figure 11: Emulated sensor burned area map optimum thresholds (triangles) and precentage of detectable area (circles) aggregated by land-cover class, for a)MODIS 250m, b)MODIS 500m, c)AVHRR 1.1Km, d)GAC 4Km and e) PAL 8Km sensors.

over the completely burned pixels and the dominating scar size class (high number of fires) will bias threshold selection. For example, in a scene dominated by two fire size classes, one of small compact fires and the other of few large fragmented fires, both with similar burned area amounts, the optimal threshold criterion will be decided between two different threshold levels. Any decision will results in errors; the lowest overall error can easily be biased by the larger fire size class in terms of area fraction. As the highly fragmented large scars tend select lower thresholds, the smaller less fragmented size scars will appear over-sized in the final burned area map. This overestimation commonly occurs in South America and West Africa highly fragmented scenes for the coarser resolutions.

The described scenarios can change with spatial resolution. A totally burned pixel can become part of a new mixed coarser resolution pixel and a small scar can easily become of sub-pixel size. The FSD dictates the burned area fraction of each fire size class according to each segmentation threshold. High accuracy requires a particular threshold to balance all the fire size class area contributions. The information provided by the global FSD shows that, on average, a leverage point is found between fires with 100ha and 1000ha. This suggests why the AVHRR sensor, with its 121ha spatial resolution, starts to reveal detection limitations, representing the turning point upon which detection can easily be made at the sub-pixel scale. At this spatial resolution higher commission and omission errors can occur, especially for the low fragmentation and low burned area maps.

The Pareto boundary position and shape, acting as a limiting factor for map accuracy, showed sensitiveness to spatial resolution. Coarser spatial resolutions will have Pareto curves characterised by higher commission and omissions values, implying that small variations in segmentation thresholds can easily lead to overestimation or underestimation. As reported by Eva and Lambin (1998) and Silva et al. (2003), landscapes dominated by very fragmented burned scars, most coarse resolution pixels tend to be dominated by the unburned class, leading to an underestimation of true burned area. If large and compact burned scars patches dominate, the spatial scaling of this pattern results in overestimation. Our results show that threshold values need to change with spatial resolution in order to maintain accuracy. The minimum distance criterion, representing minimal omission errors, leads to large overestimation errors and the 0.5 threshold leads to large underestimation errors. The optimal threshold criterion was selected for application because it guarantees the highest accuracy and the lowest MFI increase. Threshold selection based on the compromise between commission and omission errors is the best approach to achieve areal accuracy.

Aggregation by land-cover allowed to distinguish burned extents and fragmentation differences and identify some limitations. The TBDO, TBDC, SD, HRD and SHSS classes, due to the complexity and the multitude of scenarios, are less limited and produce higher accuracies for all resolutions. Due to the small scar sizes, burned areas in TBE, TNE and CMA land-cover classes result in overestimation, they are of sub-pixel size. For these, detection is only achievable for the higher resolution sensors, namely the two MODIS and the AVHRR sensor. In conclusion, different land-cover types can be characterised by their own fire size distribution that depending of the spatial resolution will have a optimal segmentation threshold, representing the pixel fraction of area burned, that provides the best areal accuracy (Eq. **??**). This threshold will be lower for increased fragmentation patterns and for the coarser resolution sensors.

From the point of view of the burned area product developer, when tunning a classification algorithm, one must be more flexible in the high fragmented or small burned areas and more restrictive for the low fragmentation burned areas. This presents a challenge because the user does no have a prior knowledge of the burned pattern. Nevertheless, our result shows that the TBDO, TBDC, TNE, SD, HRD and SHSS classes allow setting a single mean threshold for each sensor and the TNE, TBE and CMA, will require the a variable threshold. The SD land-cover class low variability suggest consistency and criterion robustness throughout a wide range of thresholds.

In terms of area estimations, one must be aware that both MODIS sensors are able to provide global to local accurate area estimations with errors around 5%. The 1.1 km resolution sensor (AVHRR) can also provide good global results, but the South American broadleaf forests and the temperate regions highlight the sensor limitations and provide larger estimate errors. The GAC and PAL imagery generally underestimate the burned area. South America and the temperate regions have the higher errors reaching 50%. The least affected regions are located in Northern Australian and African savannas.

From the point of view of the modeller, the existence of areal error is very important. For example, burned areas associated to TBE land-cover, on average represent only 75% of the actual area for the GAC and PAL products. This implies that coarser resolution based on these products have an associated error of 33%. These values associated with land-covers where biomass load is high, can results in significant severe underestimation of biomass burning emissions.

The limited number of scenes, covering some land cover types, needs to be improved. Future studies would benefit from a larger spatial distribution of the Landsat frames including scenes from Southeast Asia, Central America and eastern Australia, unrepresented here. Fires regimes in these unsampled regions are less known, but may have continental or global relevance. The use of Landsat derived burned area maps can also be misleading. Not only are they also limited by a 30m spatial resolution, but they are a snapshot of the burned activity. In fire regimes, like those in the African savannas, the high fragmentation pattern is not caused by few large fragmentation fires, but can represent the union effect (mathematical operation) of several small fires that occurred during the long fire season. Monthly or weekly burned maps will result in different patterns and should also be considered. This study used theoretical PSF which can differ from on-board PSF. Application of these improved functions on the spectral images, and not to the burned area maps, can provide a better understanding of the up-scalling effect in mixture of spectral signatures with burned surfaces. We also have assumed that there is a perfect co-registration between the types of satellite data and geometric errors should also be considered. Output results are due to

the degradation spatial patterns alone. They are a simulation of a perfect classification algorithm and undoubtedly there will be additional errors.

The methodology developed in this study was applied to a limited number of sensors, from moderate to low spatial resolutions. The same simulations can be done to the MERIS, VGT, ATSR sensors by applying the corresponding spatial filter. The same can also be done to the LTDR product, by applying the corresponding AVHRR re-sample procedure.

## 5. Acknowledgements

The authors would like to thank the Portuguese Science Foundation for the financial sponsorship of Bernardo Mota through PhD grant (SFRH/BD/25119/2005) and to all scientists who contributed with the Landsat burned area maps. These were: Ana Sá and Ana Barros from the Forest Research Center, Portugal; Allan Grant from Bushfires, Australia; Serguey Bartalev from the Space Research Institute of Russian Academy of Sciences, Russia; Andrew Edwards from the Tropical Savannas Management Cooperative Research Center, Australia; Carl Keys from the Northern Rocky Mountain Science Center, USA; Paul Laris from the Department of Geography, California State University, USA; and Daniela Stroppiana from the Consiglio Nazionale della Ricerca (CNR), Italy.

## 6. References

Andreae, M. O., 1991. Biomass burning - Its history, use, and distribution and its impact on environmental-quality and global climate. Global Biomass Burning, 321.

Barbosa, P., Stroppiana, D., Grégoire, J., Pereira, J., 1999a. An assessment of vegetation fire in africa (1981–1991): Burned areas, burned biomass, and atmospheric emissions. Global Biogeochemical Cycles 13 (4), 933–950.

Barbosa, P. M., Gregoire, J. M., Pereira, J. M. C., 1999b. An algorithm for extracting burned areas from time series of AVHRR GAC data applied at a continental scale. Remote Sens. Environ. 69 (3), 253263.

Barbosa, P. M., Pereira, J. M. C., Gregoire, J. M., 1998. Compositing criteria for burned area assessment using multitemporal low resolution satellite data-a non-linear index to monitor global vegetation from satellites. Remote Sensing of Environment 65 (1), 38–49.

Bartholome, E., Belward, A. S., 2005. GLC2000: a new approach to global land cover mapping from earth observation data. International Journal of Remote Sensing 26 (9), 19591977.

Benson, B., MacKenzie, M., 1995. Effects of sensor spatial resolution on landscape structure parameters. Landscape Ecology 10 (2), 113–120.

Boschetti, L., Brivio, P. A., Flasse, S., 2004a. Pareto boundary: a useful tool in the accuracy assessment of low spatial resolution thematic products. In: 2004 IEEE International Geoscience and Remote Sensing Symposium, 2004. IGARSS'04. Proceedings. Vol. 6.

Boschetti, L., Eva, H. D., Brivio, P. A., Gregoire, J. M., 2004b. Lessons to be learned from the comparison of three satellite-derived biomass burning products. Geophys. Res. Lett. 31 (21), 4.

Boschetti, L., Flasse, S. P., Brivio, P. A., 2004c. Analysis of the conflict between omission and commission in low spatial resolution dichotomic thematic products: The pareto boundary. Remote Sensing of Environment 91 (3-4), 280292.

Bourgeau-Chavez, L. L., Harrell, P. A., Kasischke, E. S., French, N. H. F., 1997. The detection and mapping of alaskan wildfires using a spaceborne imaging radar system. International Journal of Remote Sensing 18 (2), 355373.

Cahoon, D., 1991. The great chinese fire of 1987- a view from space. Global biomass burning- Atmospheric, climatic, and biospheric implications(A 92-37626 15-42). Cambridge, MA, MIT Press, 1991,, 61–66.

Cahoon, D., Stocks, B., Alexander, M., Baum, B., Goldammer, J., 2000. Wildland fire detection from space: Theory and application. Biomass burning and its inter-relationships with the climate system, 151–169.

Cahoon, D. R., Stocks, B. J., Levine, J. S., Cofer, W. R., Pierson, J. M., 1994. Satellite analysis of the severe 1987 forest fires in northern china and southeastern siberia. Journal of Geophysical Research 99 (D9), 1862718638.

Carmona-Moreno, C., Belward, A., Malingreau, J. P., Hartley, A., Garcia-Alegre, M., Antonovskiy, M., Buchshtaber, V., Pivovarov, V., 2005. Characterizing interannual variations in global fire calendar using data from earth observing satellites. Glob. Change Biol. 11 (9), 15371555.

Chuvieco, E., Congalton, R. G., 1988. Using cluster analysis to improve the selection of training statistics in classifying remotely sensed data. Photogrammetric engineering and remote sensing (USA).

Chuvieco, E., Englefield, P., Trishchenko, A., Luo, Y., 2008a. Generation of long time series of burn area maps of the boreal forest from noaa–avhrr composite data. Remote Sensing of Environment 112 (5), 2381–2396.

Chuvieco, E., Opazo, S., Sione, W., Valle, H., Anaya, J., Bella, C. D., Cruz, I., Manzo, L., Lopez, G., Mari, N., 2008b. Global burned-land estimation in latin america using MODIS composite data. Ecological Applications 18 (1), 64–79.

Congalton, R. G., 2001. Accuracy assessment and validation of remotely sensed and other spatial information. International Journal of Wildland Fire 10 (3/4), 321328.

Crutzen, P. J., Andreae, M. O., 1990. Biomass burning in the tropics: Impact on atmospheric chemistry and biogeochemical cycles. Science 250 (4988), 16691678.

Díaz-Delgado, R., Pons, X., 2001. Spatial patterns of forest fires in catalonia (ne of spain) along the period 1975-1995:: Analysis of vegetation recovery after fire. Forest Ecology and Management 147 (1), 67–74.

Eva, H., Lambin, E. F., 1998. Remote sensing of biomass burning in tropical regions: sampling issues and multisensor approach. Remote Sensing of Environment 64 (3), 292315.

Fernandez, A., Illera, P., Casanova, J. L., 1997. Automatic mapping of surfaces affected by forest fires in spain using AVHRR NDVI composite image data. Remote Sensing of Environment 60 (2), 153–162.

Fraser, R. H., Hall, R. J., Landry, R., Lynham, T., Raymond, D., Lee, B., Li, Z., 2004. Validation and calibration of canada-wide coarse-resolution satellite burned-area maps. Photogrammetric engineering and remote sensing 70 (4), 451–460.

Fraser, R. H., Li, Z., Landry, R., 2000. SPOT VEGETATION for characterizing boreal forest fires. International Journal of Remote Sensing 21 (18), 35253532.

Giglio, L., Loboda, T., Roy D, P., Quayle, B., Justice C, O., 2009. An active-fire based burned area mapping algorithm for the modis sensor. Remote Sensing of Environment 113, 408–420.

Giglio, L., Werf, G. R. V. D., Randerson, J. T., Collatz, G. J., Kasibhatla, P., 2006. Global estimation of burned area using MODIS active fire observations. Atmospheric Chemistry and Physics 6 (4), 957–974.

Grégoire, J., Tansey, K., Silva, J., 2003. The gba2000 initiative: developing a global burnt area database from spot-vegetation imagery. International Journal of Remote Sensing 24 (6), 1369–1376.

Hlavka, C., Dungan, J., 2002. Areal estimates of fragmented land cover: effects of pixel size and model-based corrections. International Journal of Remote Sensing 23 (4), 711–724.

Hlavka, C. A., Spanner, M. A., 1995. Unmixing AVHRR imagery to assess clearcuts and forest regrowth inOregon. IEEE Transactions on Geoscience and Remote Sensing 33 (3), 788–795.

Hoelzemann, J., Schultz, M., Brasseur, G., Granier, C., Simon, M., 2004. Global wildland fire emission model (gwem): Evaluating the use of global area burnt satellite data. J. Geophys. Res 109 (D14S04), 2004.

Houghton, J. T., Ding, Y., Griggs, D. J., Noguer, M., van der Linden, P. J., Dai, X., Maskell, K., Johnson, C. A., 2001. Climate change 2001: the scientific basis. Cambridge University Press Cambridge.

Huang, C., Townshend, J. R. G., Liang, S., Kalluri, S. N. V., DeFries, R. S., 2002. Impact of sensor's point spread function on land cover characterization: assessment and deconvolution. Remote Sensing of Environment 80 (2), 203212.

Ito, A., Penner, J. E., 2004. Global estimates of biomass burning emissions based on satellite imagery for the year 2000. J. Geophys. Res.-Atmos. 109 (D14), 18.

Justice, C., Korontzi, S., 2001. A review of the status of satellite fire moni-

toring and the requirements for global environmental change research. SPB Academic Publishing bv, The Hague, The Netherlands.

Justice, C. O., Kendall, J. D., Dowty, P. R., Scholes, R. J., 1996. Satellite remote sensing of fires during the SAFARI campaign using NOAA advanced very high resolution radiometer data. Journal of Geophysical Research 101 (23), 85123.

Kasischke, E. S., French, N. H. F., 1995. Locating and estimating the areal extent of wildfires in alaskan boreal forests using multiple-season AVHRR NDVI composite data. Ann Arbor 1001, 48113–4001.

Kaufman, Y., Justice, C. O., Giglio, L., Korontzi, S., Owens, J., Morisette, J. T., Roy, D., Descloitres, J., Alleaume, S., Petitcolin, F., 2002. The MODIS fire products. Remote Sens. Environ. 83 (1-2), 244262.

Klein, C., Dees, M., Pelz, D. R., 1993. Sampling aspects in the TREES project: global inventory of tropical forests. Final Report to the Joint Research Center. Freiburg Universitt, Freiburg, Germany.

Koffi, B., Gregoire, J. M., Mahe, G., Lacaux, J. P., 1995. Remote sensing of bush fire dynamics in central africa from 1984 to 1988: analysis in relation to regional vegetation and pluviometric patterns. Atmospheric Research 39 (1-3), 179–200.

Korontzi, S., Justice, C. O., Scholes, R. J., 2003. Influence of timing and spatial extent of savanna fires in southern africa on atmospheric emissions. Journal of Arid Environments 54 (2), 395–404.

Langaas, S., 1992. Temporal and spatial distribution of savanna fires in senegal and the gambia, west africa, 1989-90, derived from multi-temporal AVHRR night images. Int. J. Wildl. Fire. 2 (1), 21–36.

Laris, P. S., 2005. Spatiotemporal problems with detecting and mapping mosaic fire regimes with coarse-resolution satellite data in savanna environments. Remote Sensing of Environment 99 (4), 412424.

Li, Z., Nadon, S., Cihlar, J., 2000. Satellite-based detection of canadian boreal forest res: development and application of the algorithm. International Journal of Remote Sensing 21, 30573069.

Loboda, T. V., Csiszar, I. A., 2007. Reconstruction of fire spread within wildland fire events in northern eurasia from the MODIS active fire product. Global and Planetary Change 56 (3-4), 258–273.

Mayaux, P., Lambin, E. F., 1995. Estimation of tropical forest area from coarse spatial resolution data: a two-step correction function for proportional errors due to spatial aggregation. Remote sensing of environment 53 (1), 115.

Moreno, J. F., Melia, J., 1994. An optimum interpolation method applied to the resampling of NOAAAVHRR data. IEEE Transactions on Geoscience and Remote Sensing 32 (1), 131151.

Morisette, J. T., Privette, J. L., Justice, C. O., 2002. A framework for the validation of MODIS land products. Remote Sensing of Environment 83 (1), 77–96.

Oleson, K. W., Sarlin, S., Garrison, J., Smith, S., Privette, J. L., Emery, W. J., 1995. Unmixing multiple land-cover type reflectances from coarse spatial resolution satellite data. Remote sensing of environment (USA).

Pereira, J., Santos, M., 2003. Fire risk and burned area mapping in portugal. Tech. rep., Ministério da Agricultura, Desenvolvimento Rural e Pescas.

Pereira, J. M. C., 1999. A comparative evaluation of NOAA/AVHRR vegetation indexes forburned surface detection and mapping. IEEE Transactions on Geoscience and Remote Sensing 37, 217–226.

Pu, R., Li, Z., Gong, P., Csiszar, I., Fraser, R., Hao, W., Kondragunta, S., Weng, F., 2007. Development and analysis of a 12-year daily 1-km forest fire dataset across north america from noaa/avhrr data. Remote Sensing of Environment 108 (2), 198–208.

Razafimpanilo, H., Frouin, R., Iacobellis, S., Somerville, R., 1995. Methodology for estimating burned area from avhrr reflectance data. Remote Sensing of Environment 54 (3), 273–289.

Riano, D., Ruiz, J. A. M., Isidoro, D., Ustin, S. L., 2007. Global spatial patterns and temporal trends of burned area between 1981 and 2000 using NOAA-NASA pathfinder. Glob. Change Biol. 13 (1), 4050.

Roy, D. P., Boschetti, L., Justice, C. O., Ju, J., 2008. The collection 5 MODIS burned area product–Global evaluation by comparison with the MODIS active fire product. Remote Sensing of Environment 112 (9), 3690–3707.

Roy, D. P., Jin, Y., Lewis, P. E., Justice, C. O., 2005. Prototyping a global algorithm for systematic fire-affected area mapping using MODIS time series data. Remote Sensing of Environment 97 (2), 137–162.

Roy, D. P., Lewis, P. E., Justice, C. O., 2002. Burned area mapping using multi-temporal moderate spatial resolution data-a bi-directional reflectance model-based expectation approach. Remote Sensing of Environment 83 (1-2), 263286.

Russell-Smith, J., Ryan, P. G., Durieu, R., 1997. A LANDSAT MSS-Derived fire history of kakadu national park, monsoonal northern australial, 1980-94: Seasonal extent, frequency and patchiness. Journal of Applied Ecology 34 (3), 748–766.

Sá, A. C. L., Pereira, J. M. C., Gardner, R. H., 2007. Analysis of the relationship between spatial pattern and spectral detectability of areas burned in southern africa using satellite data. International Journal of Remote Sensing 28 (16), 3583–3601.

Saura, S., 2004. Effects of remote sensor spatial resolution and data aggregation on selected fragmentation indices. Landscape Ecology 19 (2), 197–209.

Schowengerdt, R., 2007. Remote sensing: models and methods for image processing. Academic Pr.

Schultz, M., Heil, A., Hoelzemann, J., Spessa, A., Thonicke, K., Goldammer, J., Held, A., Pereira, J., van het Bolscher, M., 2008. Global wildland fire emissions from 1960 to 2000. Global Biogeochemical Cycles 22 (2), GB2002.

Schultz, M. G., 2002. On the use of ATSR fire count data to estimate the seasonal and interannual variability of vegetation fire emissions. Atmos. Chem. Phys 2 (5), 387395.

Silva, J. M. N., Cadima, J., Pereira, J. M. C., Grgoire, J. M., 2004. Assessing the feasibility of a global model for multi-temporal burned area mapping using SPOT-VEGETATION data. International Journal of Remote Sensing 25 (22), 4889–4913.

Silva, J. M. N., Pereira, J. M. C., Cabral, A. I., S, A. C. L., Vasconcelos, M. J. P., Mota, B., Grgoire, J. M., 2003. An estimate of the area burned in southern africa during the 2000 dry season using SPOT-VEGETATION satellite data. Journal of Geophysical Research-Atmospheres 108 (D13), 8498.

Silva, J. M. N., Sa, A. C. L., Pereira, J. M. C., 2005. Comparison of burned area estimates derived from SPOT-VEGETATION and landsat ETM plus data in africa: Influence of spatial pattern and vegetation type. Remote Sensing of Environment 96 (2), 188201.

Simon, M., Plummer, S., Fierens, F., Hoelzemann, J. J., Arino, O., 2004. Burnt area detection at global scale using ATSR-2: the GLOBSCAR products and their qualification. Journal of Geophysical Research 109 (D14).

Sousa, A. M. O., 1999. Desenvolvimento de uma metodologia para a cartografia de áreas ardidas superiores a 500ha para a penisula iberica com dados avhrr. Ph.D. thesis, Universidade Tecnica de lisboa.

Sousa, A. M. O., 2005. Cartografia das áreas queimadas e análise de padrões espaciais de ocurrência de fogos no brasil, usando dados de detecão remota. Ph.D. thesis, Universidade de Évora.

Stehman, S. V., 1997. Selecting and interpreting measures of thematic classification accuracy. Remote sensing of Environment 62 (1), 7789.

Strauss, D., Bednar, L., Mees, R., 1989. Do one percent of the forest fires cause ninety-nine percent of the damage? Forest Science 35 (2), 319–328.

Stroppiana, D., Grgoire, J. M., Pereira, J. M. C., 2003. The use of SPOT VEGETATION data in a classification tree approach for burnt area mapping in australian savanna. International journal of remote sensing 24 (10), 21312151.

Stroppiana, D., Pinnock, S., Gregoire, J. M., 2000. The global fire product: daily re occurrence from april 1992 to december 1993 derived from NOAA AVHRR data. International Journal of Remote Sensing 21, 12791288.

Sukhinin, A., French, N., Kasischke, E., Hewson, J., Soja, A., Csiszar, I., Hyer, E., Loboda, T., Conrad, S., Romasko, V., et al., 2004. Avhrr-based mapping of fires in russia: New products for fire management and carbon cycle studies. Remote Sensing of Environment 93 (4), 546–564.

Tansey, K., Gregoire, J. M., Pereira, J. M. C., Defourny, P., Leigh, R., Pekel, J. F., Barros, A., Silva, J., van Bogaert, E., Bartholome, E., 2007. L3JRC-A global, multi-year (2000-2007) burnt area product (1 km resolution and daily time steps). In: Remote Sensing and Photogrammetry Society Annual Conference. pp. 11–14.

Tansey, K., Grgoire, J. M., Binaghi, E., Boschetti, L., Brivio, P. A., Ershov, D., Flasse, S., Fraser, R., Graetz, D., Maggi, M., 2004a. A global inventory of burned areas at 1 km resolution for the year 2000 derived from SPOT VEGETATION data. Climatic Change 67 (2), 345–377.

Tansey, K., Grgoire, J. M., Defourny, P., Leigh, R., Pekel, J. F., van Bogaert, E., Bartholom, E., 2008. A new, global, multi-annual (2000-2007) burnt area product at 1 km resolution. Geophys. Res. Lett 35 (1).

Tansey, K., Grgoire, J. M., Stroppiana, D., Sousa, A., Silva, J., Pereira, J. M. C., Boschetti, L., Maggi, M., Brivio, P. A., Fraser, R., 2004b. Vegetation burning in the year 2000: Global burned area estimates from SPOT VEGETATION data. Journal of Geophysical Research 109 (D14), D14S03.

van der Werf, G., Randerson, J., Giglio, L., Collatz, G., Mu, M., Kasibhatla,

P., Morton, D., DeFries, R., Jin, Y., van Leeuwen, T., 2010a. Global fire emissions and the contribution of deforestation, savanna, forest, agricultural, and peat fires (1997–2009). Atmos. Chem. Phys 10 (23), 11707–11735.

van der Werf, G., Randerson, J., Giglio, L., Collatz, J., Kasibhatla, P., Morton, D., Defries, R., 2010b. The improved global fire emissions database (gfed) version 3: contribution of savanna, forest, deforestation, and peat fires to the global fire emissions budget. EGU General Assembly 2010, held 2-7 May, 2010 in Vienna, Austria, p. 13010 12, 13010.

Yates, C., Russell-Smith, J., 2002. An assessment of the accuracy of DOLAs northern australian NOAA-AVHRR fire affected area (FAA) map products. Australian fire regimes: Contemporary patterns (April 1998March 2000) and changes since European settlement.(Eds J Russell-Smith, R Craig, AM Gill, R Smith and JE Williams). Australia: State of the Environment Second Technical Paper Series 2.

Zhang, Y. H., Wooster, M. J., Tutubalina, O., Perry, G. L. W., 2003. Monthly burned area and forest fire carbon emission estimates for the russian federation from SPOT VGT. Remote Sensing of Environment 87 (1), 115.

# Artigo 3

## Large Burned Area Product (LBAP-PAL): A global monthly series (1981-1999) based on the Pathfinder AVHRR land Data. Part I - Compositing and Detrending

**Mota, B., J.M.C. Pereira** - Department of Forestry, Instituto Superior de Agronomia, 1349-017 Lisboa, Portugal.
**J. Pinzon** - Goddard Space Flight Center, Greebelt, Maryland, USA.

# The Large Burned Area Product (LBAP-PAL): A global monthly series (1981-1999) based on the Pathfinder AVHRR land Data. Part I - Compositing and Detrending.

Bernardo Mota, José M.C. Perreira, and Jorge Pinzón

***Abstract*—The Advanced Very High-Resolution Radiometer Pathfinder Land dataset was used to produce global monthly composites using five different algorithms. A series of tests was preformed to evaluate each algorithm sensitivity to fire perturbation and its global cloud screening effectiveness. The M4mALB algorithm provided the higher clear sky pixel coverage, high sensibility to fire activity perturbation, lower variability in illumination angles, offered the higher probability of after fire pixels selection and was applied to the remaining PAL dataset. Due to the satellite orbital drift a detrending procedure was developed and applied. The procedure was based on a Look up table of homogeneous areas from which temporal profiles of the Albedo, GEMI, Surface Temperature and Solar Zenith Angle were extracted. The profiles were decomposed using the Empirical Mode Decomposition method where the orbital drift trend was identified and filtered. The filtering results showed the existence of 3 categories of trend affected areas. Full variable set of significant trends severely affecting areas in the tropics and less severe closer to the mid-latitudes. Deserts, high altitudes and the mid-latitudes have revealed mix variable set significant trends. Surface temperature affected areas cover the widest area but the GEMI and albedo decay more rapidly over affected areas.**

## I. Introduction

THE Advance Very High-Resolution Radiometer (AVHRR) radiation-detection sensor aboard the US National Oceanic and Atmospheric Administration (NOAA) polar orbiting satellites is the longest running series of earth observation sensor imagery. The AVHRR/2, the first five-channel instrument, started with the NOAA-7 satellite launch in August 1981 and after 29 years it still runs on-board the NOAA-18 satellite in the form of a six-channel version (AVHRR/3). The AVHRR/2 spectral bands are in the red (RED), near-infrared (NIR), middle-infrared and thermal infrared and are acquired twice daily, in an ascending and ascending pass, with a spatial resolution of 1.1km. Although its development was intended as a meteorological sensor for global weather monitoring, it is widely used due to its potential for monitoring land surface variables at regional and global scales. The low data volume, spectral specifications and imagery inexpensive access makes it valuable instrument for the scientific community to conduct many studies on earth observation. The low spatial resolution but high temporal frequency, that constitutes the AVHRR data record makes it an invaluable archive of historical land information [1], [2] widely used in global change research [3], [4]. Because the 1.1km resolution data are too voluminous to be captured and stored daily, the data are subsampled and averaged onboard, by averaging four out of five pixels on every third scan line, and then transmitted to central receiving stations in the form of Global Area Coverage (GAC) data with a nominal resolution of 4km at *nadir* providing full global daily coverage. Based on these GAC data many studies have been produced like vegetation at continental scale [5], land-cover classifications [6] and change [7], climate and energy [8] and finally burned area detection [9] where the AVHRR Spectral bands offer considerable benefits to fire monitoring [10], [11]. Since burned area assessment is of major importance due to its trace gas emissions there is a need for high quality global multi-year burned area dataset from which global atmospheric emissions can be estimated [12], [13].

The long-term AVHRR data record and the daily global coverage provided by the GAC product format makes it suitable for climate monitoring from which two derived vegetation global products stand out. The Global Vegetation Index Products (GVI) produced by NOAA [14], [15] (http://www.osdpd.noaa.gov/ml/land/gvi.html) at 16km spatial resolution and the Global Inventory Modelling and Mapping Studies produced by the NASA's Goddard Space Flight Center [16], [17] http://gimms.gsfc.nasa.gov/ at a 8km spatial resolution. Both products are based on the Normalized Difference Vegetation Index (NDVI) [18] and constitute the first attempts to produce temporal series of vegetation imagery at a global scale. However, their success is limited to ecological studies like land cover classification, crop areal estimation, plant stress detection and vegetation dynamics. The NOAA-Pathfinder AVHRR Land (8km) dataset [19]–[21] constituted the first attempt to produce a consistent time series of the sensor imagery at a global scale and daily frequency. Its program was established by a Land Science Working Group (LSWG) that provided the algorithms and guidance to the operational team for production [20]. Its intent was to support global climate change research by providing the data made available by AVHRR calibrated individual bands, i.e., reflectances and radiometric temperatures.

Earth surface observations from satellites are affected by

J. Pinzon is with the Science Systems and Applications, Inc. at the NASA Goddard Space Flight Center.

B. Mota and J.M.C. Perreira are with the Departamento de Engenharia Florestal at the Universidade Técnica de Lisboa.

Manuscript in preparation December 20, 2010.

three main problems; i) instrument degradation and inefficient calibration, ii) atmospheric contamination and iii) satellite orbital drift. The AVHRR sensor aboard the NOAA satellites is no exception. The sensor lacks onboard calibration and degrades with age [22]. The broad spectral bands lead to contamination by the atmosphere and its limited number reduces, by contemporary standards, the accuracy retrieval of atmospheric parameters for correction. Water vapor and aerosols, namely of volcanic origin, contaminate the data [23]. The NOAA satellite series is also characterised by orbital drift trends attributed to the selection of a satellite orbit which was designed to avoid direct sunshine on the instruments [24]. Since the satellites lack orbiting adjusting systems they will tend to overpass the same location later in the day where each replacement satellite only restores the overpass time temporarily until itself starts to drift. This change of illumination conditions results in a cooling effect on the brightness temperature channels [24], [25] and different reflectance responses to land cover type [26], [27] which are more severe for the afternoon ascending satellites. These effects, characterised by changes in Solar Zenith Angle (SZA) vary with season, time since launch and latitude [28]. Because of the earths curvature, these effects, are lower for the higher latitudes than for the equator. These trends are also reflected in the PAL dataset where [29] found by observing the land surface temperature that the drift effect was greater for bare soil than for the vegetated land cover classes. Identical results were also recorded by [23], [30] and [31] found inconsistencies in zenith angles measured by the different instruments in the NOAA series. Several attempts have been made to remove orbital drift effect. [32]–[34] used NDVI measurements to correct the temperature channels and [29] made a simple empirical correction based on the solar zenith angle to correct brightness temperatures following [32] regression correction. [35] developed a look up table for representative land skin temperatures diurnal cycles which depended on vegetation type, season and latitude. Together they were combined to remove the cooling effect. [36] found that statistical NDVI values change with the increase of SZA and used a regression method to remove the increase in NDVI values. In the development of the GIMMS product [37] used the Empirical Mode Decomposition (EMD) method to identify the induced artifacts in the NDVI series and found it suitable to remove the orbital shifting. Hopefully, the future Long Term Data Record (LTDR) (http://ltdr.nascom.nasa.gov/cgi-bin/ltdr/ltdrPage.cgi) project which is intended to produce, validate and distribute a global land surface data record based on the AVHRR sensor imagery at 0.05 latitude/longitude spatial resolution will eliminate these trends. It will apply improved atmospheric correction based on the the Pathfinder II project [38] that proposed different algorithms for visible calibration, namely the water vapor atmospheric correction which provides better accuracy and less noisy time series [39]. It will also address the Orbital drift issue by preforming a BRDF correction to the data. The project will release intermediate data sets available for evaluators and its final product will undoubtedly be an invaluable asset for climate change research.

The objective of this study, part one of two, is to produce a time series of global monthly composites images of the earth surface, cloud and shadow screened, to be used for burned area classification based on the PAL dataset. In order to achieve this, we evaluated a set of five multi-temporal compositing criteria for clouds and shadow screening and burnt surface retention. Second, identify and filter out the orbital drift component present on the surface temperature, GEMI and albedo derived from the monthly composites. The burned area classification will be applied in second part of this study.

## II. Data

### A. The NOAA-AVHRR Pathfinder (8km) Land Dataset

The Pathfinder AVHRR Land (8km) land dataset [19] was produced from the original GAC 4km dataset. The adopted spatial re-sampling procedure to convert from GAC to PAL, consisted in a nearest neighbour re-projection of each two by two GAC pixel block followed by the maximum NDVI value criterion to untie chosen pixels. Pre-processing procedures consisted in calibration of the visible channels with coefficients incorporating vicarious calibration techniques and aircraft under-flight calibration [40]. The thermal channels were calibrated using methods to account for the nonlinear detector effect [41]. The Visible and near-infrared data were corrected for the effects of Rayleigh scattering and ozone absorption, but no correction was preformed for aerosol or water vapor. Navigation errors were corrected with the University of Colorado's orbital model [42] and the Goddard Space Flight Center/SeaWiFS geolocation system [43]. Cloud flags and quality control flags were also added to the dataset as information layers. The cloud flag was produced using the NOAA Clouds from AVHRR (CLAVR) algorithm [44] where each pixel is classified as clear, mixed, and cloudy. The quality control flag (QC) [44] included error and warning conditions identified during data processing. The final PAL dataset product was composed of 11 layers of information, i.e., five AVHRR radiometric channels, three satellite and sensor viewing and illumination angles (solar zenith angle, relative azimuth angle and scan angle), quality control flag, cloud flag and acquisition time. The dataset was supplied by the Earth Observing System Distributed Active Archive Center (DAAC), NASA Goddard Space Flight Center in Greenbelt, Maryland, USA in the form HDF daily files with global coverage. The images were acquired by four NOAA satellites (7, 8 11 and 14), covering the period from July 1981 to December 2001 with one interruption from 14 September 1994 to 5 January 1995, due to the NOAA13 satellite launch failure. The data were mapped onto a global 8 km equal area grid in Goodes Interrupted Homolosine projection, designed to reduce distortion of the major land masses, while maintaining equal area [45], [46].

Pre-analysis of the dataset revealed several limitations:

- Detailed visual inspection showed recurrent periods of incomplete coverage at high latitude during each hemisphere winter. This is due to the Earth's seasonal inclination that causes the observed solar illuminated surface to be lower during winter, preventing the daily ascending satellite pass to acquire a full global image [19].

- Seasonal saturation of channel 3 at the lower and mid latitudes, caused by the low thermal saturation threshold (Fig.1a).
- Anomalous reflectances in years 2000 and 2001, believed to be caused by changes in the calibration. This was not explained by the data suppliers and results in unusable data, limiting our study to the period July 1991 to December 1999 (Fig.1a).
- Finally, the satellite orbital drift effect already mentioned (Fig.1b), to be addressed in section III-C.

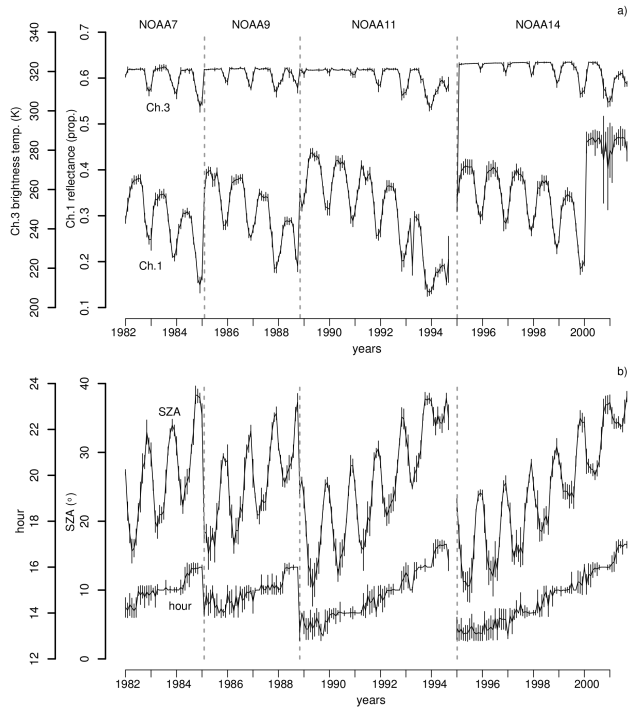


Fig. 1. Temporal profiles of average a) AVHRR channel 1 and 3, b) solar zenith angle and acquisition hour values over a five by five 8km pixel block located in the Sahel.

### B. Global Land Cover 2000

The Global Landcover Classification (GLC2000) [47] was developed by the Global Vegetation Monitoring Unit (GMV), of the Institute for Environment and Sustainability at the Joint Research Center (JRC/IES) for the year 2000 with the objective to provide a harmonised land cover database over the whole globe. This land-cover product was based on a 14-month dataset of pre-processed daily global data acquired by the VEGETATION instrument on board the SPOT 4 satellite and uses the Food and Agriculture Organisation (FAO) Land Cover Classification System (LCCS). The data are available at http://www-gem.jrc.it/glc2000/ in a geographic lat-long projection with 1km spatial resolution which, for this study, was re-sampled into Goodes Interrupted Homolosine in a 8km spatial resolution using a majority filter.

### C. Terrestrial Ecoregions of the World

The Terrestrial Ecoregions of the World [48] are large units of land containing distinct assemblages of natural communities and species, with boundaries that approximate the original extent of natural communities prior to major land-use change. These ecoregion delineations were based on hundreds of biogeographical studies, refined and synthesized informations from regional workshops over ten years. The ecoregions were nested within two higher-order classifications: 14 biomes within eight biogeographic realms. The dataset was supplied by the World Wildlife Fund (WWF) at www.worldwildlife.org in geographic vector format and each single ecoregion biome within each realm was rasterized into Goodes Interrupted Homolosine projection with 1km spatial resolution and later reprojected to 8km spatial resolution using a majority filter.

### D. Screened World Fire Atlas

The European Space Agency (ESA) World Fire Atlas (WFA) [49] was developed using night time data from the Along Track Scanning Radiometer (ATSR) onboard the Second European Remote-Sensing Satellite (ERS-2). The spatial resolution of the data is 1 km and the satellite revisiting period is three days at the equator. Known limitations of the WFA are the inclusion of warm surfaces, gas flares, and city lights, and an underestimation of actual global fire activity due to the time of satellite overpass. The screened version of its algorithm 2, threshold at 308 K, was screened by [50] using ancillary land cover, night-lights and volcanic activity datasets, combined with statistical techniques to detect the occurrence of space-time clusters of anomalous observations. The authors found that, depending on the year, false alarms range between 20% and 28% with the gas flares and hot bare soils are the major contributes. The data were aggregated into counts of active fires within each 8km pixel in Goodes Interrupted Homolosine projection.

## III. Methods

### A. Multi-temporal composing assesment

Remote sensing sensors aboard satellites look downwards to earth recording an image of the Top of the Atmosphere (TOA) which frequently contains clouds, shadows aerosol contamination, off-nadir viewing angles and sometimes random noise. Multi-temporal compositing is commonly used to produce cloud-free mosaics of land surfaces for studies of terrestrial vegetation structure and dynamics [5], [51]–[53] and wildfire regime characterisation and emissions, based on burned area mapping [54]–[56]. These compositing procedures are based on the selection, for each individual image pixel in a given time step, of the pixel that retains the desired information, which in our case is burned areas under clear sky conditions. By far the most applied method is the maximum value composite (MVC; [18]) computed by selecting the image values of the day when its pixel value is maximum. This set of rules, compiled in the form of an algorithm, is then applied to the imagery bands to enhance burnt scars and avoid clouds and shadows.

Our objective was to further evaluate and complement previous work [54]–[57] and determine which multi-temporal compositing algorithm best enhances the signal from areas affected by vegetation fires, to be applied to the PAL dataset. In order to achieve this, we analysed the performance of each

compositing algorithm, from a selection proposed by [56], [57] for the AVHRR and SPOT Vegetation sensor imagery. This set of algorithms differ from each other by their selection criterion and spectral channels. The algorithms are as follow:

1) NDVI maximum value (MNDVI);
2) Minimum NIR (ch.2) reflectance (m2);
3) Maximum ch.4 temperature (M4);
4) Maximum ch.4 temperature of five lowest albedo values (M4mAlb);
5) Maximum ch.4 temperature of five lowest NIR values (M4m2);

The MNDVI was proposed by [18] and is based on the pixel selection with the highest NDVI (i.e. the greenest) value. The main known disadvantage for burned area mapping is that it prefers unburned pixels over burned ones, since the former tend to have higher NDVI values [56]–[58] and burned scar retention can be seriously affected. In addition, clouds may display higher NDVI values than recent burns [58] and will be kept in composing images. This algorithm was included in our analysis in order to compare its results with other compositing techniques, since it is still the most used criterion worldwide. NDVI was computed from AVHRR channels 1 (RED) and 2 (NIR). The m2 criterion was proposed by [59] as an alternative to MNDVI and was applied by [9] for burned area mapping in Africa with AVHRR-GAC data. It tends to avoid clouds and green vegetation selecting burned surfaces, but it can retain cloud shadows, which appear dark in the NIR. There is also the issue of selecting atmospheric contaminated pixels because atmospheric effects tend to depress the NIR reflectance [60]. The M4 algorithm was developed for obvious physical reasons. Burned surfaces will have higher brightness temperatures than vegetation due to charcoal and ash higher solar radiation absorbency, which result in the selection of burned over unburned, surface over cloud and land over water pixels. It was also tested as an alternative to MNDVI by [54], [61], [62] and revealed higher number of nearest to nadir pixels and images with less speckle [61]. The M4mALB or M4m2 algorithms use two criteria in sequence [55], [56], [62], [63]. For both algorithms, the selection is based on the pixel with the highest channel 4 brightness temperature, from a pre-selection set of the five pixels with the lowest albedo or lowest channel 2 reflectance, depending on the algorithm. For the M4mALB algotithm, we calculated the albedo as the arithmetic mean of the AVHRR channel reflectances [64]. Using albedo instead of channel 2 reflectance is considered to be an advantage because it partly offsets the tendency to select atmospherically contaminated pixels. [54] found it to be the best single criterion algorithm for burned area mapping in Africa. The M4mALB algorithm was first introduced by [56], where the authors found that one known advantage is that it solves the problem of cloud shadow retention and reduces image speckle while maintaining a good discriminability of burned areas.

Each algorithm was applied to the pathfinder AVHRR daily data in monthly time periods for composing and algorithm comparison was preformed with a series of tests. Two of the tests used fire activity information, provided by WFA data, to assess burned area spectral and temporal discrimination. Year 1998 was selected because of the strong *El Nino* occurrence, ensuring a large fire perturbation event and also due to the short WFA-PAL period overlap. Five study regions from each continent were chosen, based on high WFA count density, to cover major fire regimes (fig.2). The selected areas were located over the Northern Territory of Australia (NTA), the Central African Republic in Africa (CAR), the Amazon forest in South America (AMO), Alaska in North America (ALK) and over Eastern Siberia (ESB). Region extent varies from 0.4 (AMO) to 1.8 (CAR) million $km^2$. For the same period and regions, the corresponding WFA annual percentages were determined to identify months where fire activity occurred and a threshold of 10% was applied to determine seasonal length, and which pixels were potentially affected by fire.

To evaluate the suitability of each multi-temporal composite algorithm, we applied two tests to assess temporal displacement and spectral discrimination. The former was performed by comparing the distributions of pixel dates, selected by each algorithm, and the corresponding active fire date distribution. The monthly differences in date distribution average for the season provided an identification of which algorithm is better at selecting post-fire pixels. An algorithm that, on average, selects pre-fire dates (negative values) in opposition to post-fire dates (positive values) is less able to capture fire scar signatures. For the latter, the Jeffries-Matussita index (JM) was calculated based on four AVHRR channels (1,2,4 and 5) for consecutive months over the selected fire-affected areas to highlight potential spectral separability dynamics. The J-M index is based on the Mahalanobis distance and serves as a measure of spectral distinctiveness where the maximum value of 1.4 represents full distinction and the minimum value of 0 perfect identity. The most adequate composite algorithm would produce the highest average JM value representing larger spectral variations that would lead to better scar identification.

To evaluate data quality and cloud contamination of the resulting monthly composites, three additional tests were applied. The third test was based on the inter-algorithm comparison of the sensor scanning angles. The closer to nadir an acquisition is, the lower the effect of atmospheric disturbances [65] and lower pixel spatial distortion, the highest geometrical accuracy. The composite with average lowest variation of sensor scanning angles would be the optimal. The fourth test is performed to detect the presence of artifacts in the compositing algorithm images. The quality layer information extracted over the full extent of each region can show if there are pixels with radiometric problems and, more important, if a particular algorithm is more sensitive to selecting those pixels. We have considered good quality pixels, those that do not fail the radiometric range-check test, revealing out of bound values, as described by the pathfinder AVHRR manual (Table 2-4, page 23 , [19]). The fifth test is performed to evaluate cloud screening effectiveness; clear and mixed sky pixel percentages, based on the Cloud Classification Algorithm for the Advanced Very High Resolution Radiometer (CLAVRD) flags (Table 2-3, page 22, [19]) were extracted from the pixels of each composites. The most adequate composite would be the one that retained the least atmospherically contaminated pixels indicated by a higher percentage of cloud free pixels.

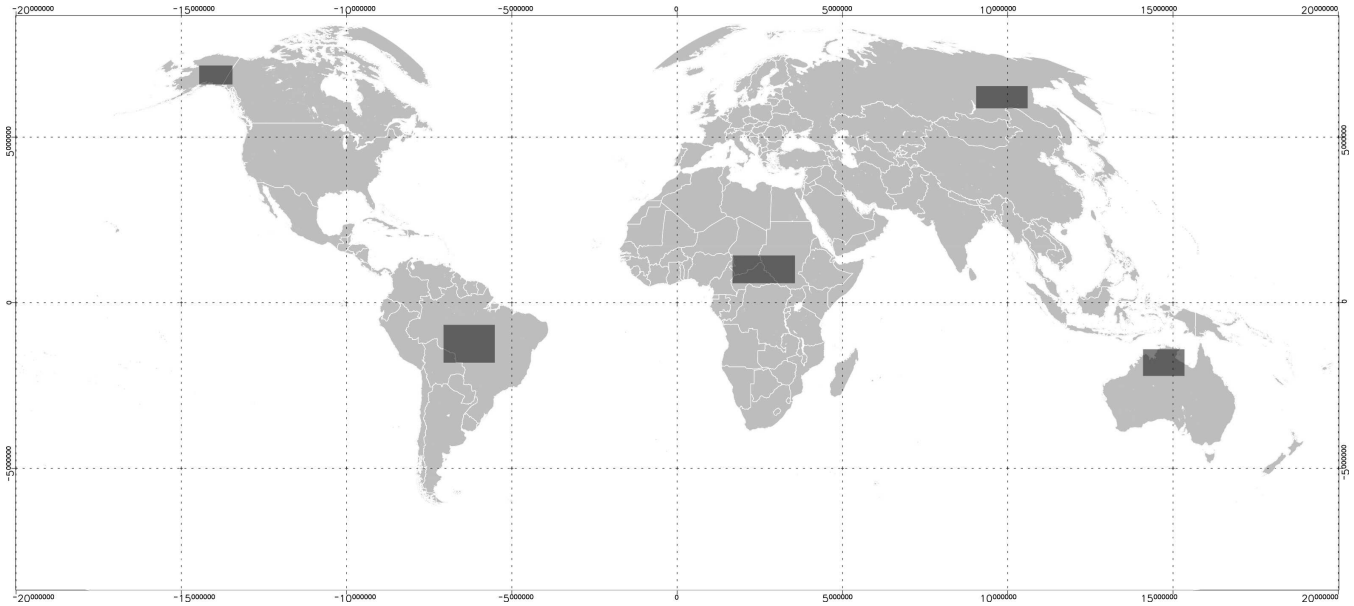

Fig. 2. Geographical regions used for multi-temporal compositing algorithm assessment. Region selection was based on WFA active count density for year 1998.

Finally, based on [55] and [54] studies, a single index to rank the performance of the different compositing criteria was performed. The original numerical scale of the test results was converted to a common 0 to 1 scale and values were weighted accordingly to its importance. The normalisation was based on a linear function, defined by the minimum and maximum value of each test results, and a single performance index was defined as follows:

$$F = 2 * (JM + TFD) + SAd + QA + CL,$$

where F is the algorithm performance value, JM is the normalised seasonal value for the average J-M distances between consecutive months for the fire activity months, TFD is the normalised seasonal mean time difference between WFA active fire dates and the algorithm mean day selection, SAd is the normalised seasonal average of the scanning angle standard deviation of the sensor, CL the normalised value of the seasonal percentage of cloud-free pixels in each composite and QA the normalised value of the seasonal percentage of free quality data errors. The first two tests were weighted double because they highlight each composite algorithm sensitivity to distinguish fire activity. The other three tests were included to assure the global radiometric (and to some extent geometric) quality of the final composite image.

### *B. Classification Variables*

Fire consumes vegetation, green or dry, by combustion leaving the surface darker by deposition of char residues. The new surface, partly or completely depraved of green vegetation surface depending on the severity of the fire, is characterised by lower humidity and higher surface temperatures due to the high solar radiation absorvance (lower albedo) and lower evapotranspiration [66], [67]. Considering the spectral changes induced by fire, our choice of variables was based on simplicity and adequacy for burned area mapping performed in part two of this study. They are as follows:

*1) Surface temperature:* Satellite-based land surface temperature (LST) is sometimes referred to as skin temperature [68] and accurate estimation requires correction for both the atmospheric and the surface emissivity effect [69]. Several studies have been carried out to develop and improve methodologies for retrieving LST from the AVHRR brightness temperatures channels [24], [70], [71] and to quantify uncertainties driven by emissivity errors. In semi-arid regions with high atmospheric water vapor content the atmospheric effect can account for 90% of the correction whereas the emissivity effect typically accounts for only 10% [30]. In this study we used the algorithm proposed by [24] due to its simplicity. Considering surface emissivities equal to one, the proposed formula simplifies to the form of:

$$T_s = T_4 + 2.79(T_4 - T_5),$$

where $T_4$ and $T_5$ are the AVHRR brightness temperature recorded by channel 4 and 5, respectably. This equation provides an approximate surface temperature able to reflect the required temporal variability.

*2) Albedo:* Land surface albedo represents the proportion of the incoming radiative flux reflected by the surface. In addition to natural albedo, changes driven by the seasons, other events due to anthropogenic activities like deforestation, reforestation agriculture and biomass burning also contribute to modification of the surface spectral proprieties [72]. In northern hemisphere Africa, during the dry season, albedo decrease is attributed to the extensive man made fires [73]. This change provides a powerful detection tool for burned area mapping in which algorithms based on albedo products have been developed, namely from the Meteosat Surface Albedo [74] and MODIS BRDF/albedo product [75], [76].

Other studies have also highlighted the AVHRR advantages for calculating surface albedo. When compared to other sensor satellites with only visible channels, the AVHRR channel 2) provides the capability of deriving broadband albedo within 10-15% of accuracy citeCsiszar1999. In this study, we used the average between avhrr channel 1 and 2 as a simple narrow band-to-broadband albedo conversion [64].

*3) Vegetation:* For a vegetation index we used the Global Vegetation Monitoring Index (GEMI), developed and introduced by [78]. This index is characterised by large dynamic range of surface vegetation cover, insensitivity to darker soil colour changes and includes a built-in atmospheric correction. When compared with the NDVI, on varying atmospheric and illumination conditions, it has a larger capability to detect partial vegetation covers. The GEMI also uses the same AVHRR channels as the NDVI but applying a non-linear transformation, making them functionally unrelated [79]. This non-linearity provides higher sensitivity and therefore better results to discriminate burned areas in several biomes [9], [80], [81]. NDVI can be used to produce accurate burned area maps in the Boreal Forests [82] but its application for the mid and low latitude land covers is limited, leading to large commission errors [81].

The GEMI vegetation index is defined as follows:

$$GEMI = \eta(1 - 0.25\eta) - \frac{c_2 - 0.125}{1 - c_2},$$

where

$$\eta = \frac{2(c_1^2 - c_2^2) + 1.5c_1 + 0.5c_2}{c_2 + c_1 + 0.5},$$

and where $c_1$ and $c_2$ are the AVHRR reflectances recorded by channel 1 and 2, respectavely.

### C. Detrending Procedure

Due to space friction and the chosen satellite orbit, daily satellite crossing time over the equator runs late. This effect causes the reflectance channels to record geometry shifts in pixel illumination and the thermal channels to record later solar radiation. This results in positive sun zenith angle trends and negative trends for each of the sensor channels. The Pathfinder AVHRR dataset is highly affected by satellite drift as past studies [23], [29], [30] have highlighted this problem, which caused biased results [30]. [37] developed a methodology to deal with this issue based on the application of the empirical mode decomposition (EMD) in the development of the GIMMS product. In this study we applied a similar methodology to our selected set of indexes. The detrending methodology is based on the following procedure:

1) Look up table of area temporal profiles;
2) Determination of variable and corresponding SZA trends;
3) Identification of trend significance followed by filtering.

*1) Look up table of area temporal profiles:* Each pixel spectral response and its inherent dynamics reflect the seasonal behaviour and perturbations suffered by the landscape soil and vegetation coverage. The GLC2000 land cover classification and the WWF Terrestrial Ecoregions of the World datasets were combined and used to developed a refined classification of homogeneous areas. The derived classification used the GLC2000 as the main classification overlaid by the higher hierarchy class biomes of the Ecoregions dataset to form subdivisions within each GLC2000 class. The resulted class mixing produced a large number (14,613) of areas with different shapes and sizes. This large number was mainly composed of small size areas that could lead to problems when preforming monthly averages due to insufficient cloud-free pixels. A sensitivity analysis was performed to reduce the number of areas using several global spatial coverage thresholds and yield that 0.1% of the global surface produced be best commitment in total percentage of discarded areas. This operation produced a look up table (LUT) by reducing the number of areas by 84% (to 2410) and still covered 91% of the global land surface. Within the discarded classes, the most affected GLC2000 class was the cultivated and managed areas, due of its highly fragmented pattern (Tabel I). Temporal profiles for each of the LUT areas were extracted by averaging index and SZA values from the monthly composites and using the CLAVRD layer to exclude remaining pixels classified as cloudy or mixed cloud. In cases where only one monthly interruption occurred an interpolation was performed to ensure a higher number of LUT areas with a continuity series.

TABLE I
GLC2000 LAND-COVER CALSS FRACTIONS EXCLUDED BY THE 0.1% GLOBAL AREA THRESHOLD FILTER

| Global Landcover Class | Missed (%) |
|---|---|
| Tree Cover, broadleaved, evergreen | 11.3 |
| Tree Cover, broadleaved, deciduous, closed | 9.4 |
| Tree Cover, broadleaved, deciduous, open | 6.1 |
| Tree Cover, needle-leaved, evergreen | 9.0 |
| Tree Cover, needle-leaved, deciduous | 3.6 |
| Tree Cover, mixed leaf type | 5.2 |
| Tree Cover, regularly flooded, fresh water | 4.2 |
| Tree Cover, regularly flooded, saline water | 3.6 |
| Mosaic: Tree Cover / Other natural vegetation | 4.0 |
| Tree Cover, burnt | 2.0 |
| Shrub Cover, closed-open, evergreen | 5.1 |
| Shrub Cover, closed-open, deciduous | 12.3 |
| Herbaceous Cover, closed-open | 12.7 |
| Sparse herbaceous or sparse shrub cover | 9.1 |
| Regularly flooded shrub and/or herbaceous cover | 7.0 |
| Cultivated and managed areas | 14.2 |
| Mosaic: Cropland / Tree Cover / Other natural vege | 10.5 |
| Mosaic: Cropland / Shrub and/or grass cover | 6.3 |
| Bare Areas | 5.0 |
| Water Bodies | 0.0 |
| Snow and Ice | 7.3 |
| Artificial surfaces and associated areas | 8.0 |

*2) Determination of index and corresponding SZA trends:* The EMD technique was first introduced by [83] as an alternative to standard decomposition techniques for nonlinear and non-stationary data. Unlike the Fourier decomposition [84], [85], the EMD is based on the signal from the data themselves. The EMD is empirical, intuitive, direct, a posteriori, and adaptive, with the decomposition functions based on and derived from the data [83], [86]. These functions, known as Intrinsic Mode Functions (IMF), are sufficient to describe the signal even though they are not necessarily orthogonal. They can be important because natural processes

often have multiple causes that may happen at specific time intervals. The decomposition uses the simple assumption that any signal consists of different intrinsic coexisting modes of oscillations. Each mode may not be linear, and will have the same number, or differ at most by one, of extrema and zero-crossings. Furthermore, the oscillation will also be symmetric with respect to the local mean. To extract each IMF, one has to derive the local means by computing the mean between the upper and lower envelopes and remove it from the original signal. To satisfy all its requirements a shifting process [83] is perform. This process is based on the repetition of the previous step, where the resulting signal takes the place of the original data, and repeated as many times as required. This process serves to eliminate riding waves and to turn wave profiles more symmetric. The shifting process can be stopped either when the component or the residue becomes so small that is less than the predetermined value or when residue becomes a monotonic function from which no more IMF can be extracted. Even for data with zero mean, the final residue can still be different from zero. In signals characterised by a trend, the final residue should contain it. Signal decomposition is expressed by:

$$x(t) = \sum_{i=1}^{n} imf_i(t) + r_s(t),$$

where $x(t)$ is the original signal, $imf_i(t)$ are the intrinsic mode functions and the $r_s(t)$ is the residual. The applied EDM methodology, developed by [83], was ported to R-code by [87] and providing the additional data overextension at the boundaries using a 'wave' function to reduce problems at the profile extremities. For each satellite, all the LUT area variables (GEMI, Surface temperature and Albedo) plus the SZA time profiles values were decomposed and its residue was determined.

*3) Identification of trend significance followed by filtering:* In order to quantify the degree of influence and spatial distribution of the satellite drift interference over each index a Canonical Correlation Analysis (CCA) was performed. The CCA is a multivariate statistical technique used to examine and describe the strength of a linear association between two sets of random variables. The resulted canonical factors contribute an optimal orthogonal basis between each index trend and the SZA trend component. The contribution of each 'loadings' from the first canonical factor, which explains the highest variability, will determine the interference strength. This procedure was independently applied for each variable and for the four satellite periods, and the Fisher-Jenks (natural-breaks) algorithm [88] was applied to divide between drift affected an unaffected. The filtering out process was applied for each LUT area, when classified as drift affected and when variables were highly negatively correlated ($< -0.9$) with the SZA trend, for at least one of the satellites periods. The applied filtering cannot be considered as a satellite drift correction because, along with it, other trends can also be removed.

## IV. Results

### A. Algorithms comparison

The five monthly compositing algorithms were applied to the daily Pathfinder data from December 1997 to December 1998. The time frame for the compositing criteria analysis was determined by the consecutive months where WFA activity was above 10% of annual fire activity. This obtained period, representing each region fire season, was characterised by different beginning and seasonal length of the fire season. The details presented in table II show that the CAR region is characterised by the longest period, of 5 months (November to February), and that NAT, AMO and ESB regions had a fire season of 3 months, all from July to September. The ALK region showed a season length of 4 months, starting in May and ending in August. These temporal results cannot be considered as each region normal season duration due to the fact that they were only calculated with 1998 data, where a strong *El Nino* year occurred severely affected the northern latitude regions.

TABLE II
SPATIAL AND TEMPORAL PROPERTIES OF THE STUDY REGIONS USED IN THE MULTI-TEMPORAL COMPOSING ALGORITHM ASSESMENT

| Region | Start | End | months | Area($Mkm^2$) | Fire activity(%) |
|---|---|---|---|---|---|
| Northern Australia (NTA) | July | September | 3 | 9.98 | 86.06 |
| Central Africa (CAR) | October | February | 5 | 15.49 | 100.00 |
| Amazon (AMO) | July | September | 3 | 17.54 | 100.00 |
| Alaska (ALK) | May | August | 4 | 3.53 | 98.67 |
| East Siberia (ESB) | July | September | 3 | 10.31 | 99.99 |

For each region and composite algorithm, quality and cloud flags and sensor scanning angles values were extracted for the determined fire season period. Additionally, for each composite the monthly mean day differences between the active fire and pixel dates calculated for the fire affected areas and the corresponding JM distances, were averaged into seasonal values. Also, for both the QA and CL test and SAd test, monthly percentages and standard deviations were calculated and averaged into a seasonal value. Results are presented in Table III. The SAd test results show that the M4 and the M4mALB algorithms always tend to chose pixels with the least variation in scan angles, highlighting consistency and near to nadir geometries. In contrast, the MNDVI algorithm preforms poorly by showing the widest variation in scan angles. Both the M4m2 and the m2 algorithms produce similar results to the M4mAlb but with wider distributions. As an example, we present in figure 3a for the NTA region in September the angle distribution that clearly highlights the SAd results; wide MNDVI scan angle dispersion can lead to speckle effects on the compositing images. Table III also shows that, on average, the higher latitude region reveal less angle variation than for the lower latitude regions, but for individual algorithm results can differ.

The QA and CL tests reveal similar results with less variations between algorithms. Exception is only noted for the MNDVI algorithm in the CL test, characterised by less than half the mean percentage than the other four algorithms. The data for the Africa region does not appear to have quality issues because all pixels (100%) are classified as *good quality* during the fire season and the CL test confirm that fire season is normally characterised by a dry season, with low cloud contamination. Common to all five algorithm is the higher cloudy days frequency fot the higher latitude regions (ALK

TABLE III
MULTI-TEMPORAL COMPOSITING ALGORITHM TEST RESULTS, BOLD VALUES REFER TO BEST PERFORMANCE

| | **M4mAlb** | **M4m2** | **MNDVI** | **M4** | **m2** |
|---|---|---|---|---|---|
| JM | | | | | |
| NTA | 0.55 | 0.53 | **0.56** | 0.54 | 0.39 |
| CAR | 0.56 | 0.56 | **0.62** | 0.55 | 0.52 |
| AMO | 0.55 | 0.53 | **0.56** | **0.56** | 0.37 |
| ALK | 0.87 | **0.89** | 0.67 | 0.87 | 0.79 |
| ESB | **0.61** | 0.59 | 0.50 | 0.51 | 0.41 |
| TFD(days) | | | | | |
| NTA | -0.17 | -0.04 | -3.45 | -3.15 | **1.35** |
| CAR | -0.62 | -0.87 | **2.12** | -4.11 | 2.22 |
| AMO | **1.69** | 1.59 | -0.84 | -1.49 | 1.13 |
| ALK | 1.95 | 0.54 | **4.90** | 4.55 | -0.53 |
| ESB | 2.12 | 0.78 | -3.31 | **5.86** | -3.77 |
| SAd | | | | | |
| NTA | **8.29** | 9.63 | 16.30 | 9.70 | 11.15 |
| CAR | **7.56** | 8.38 | 23.26 | 11.55 | 9.08 |
| AMO | **8.77** | 9.21 | 21.95 | 12.32 | 10.61 |
| ALK | **5.93** | 8.86 | 9.19 | 13.73 | 7.17 |
| ESB | **6.94** | 7.54 | 14.82 | 9.89 | 7.82 |
| QA(%) | | | | | |
| NTA | 98.03 | 97.67 | **99.61** | 99.25 | 98.81 |
| CAR | **100.00** | **100.00** | **100.00** | **100.00** | **100.00** |
| AMO | 99.88 | 99.89 | 99.85 | 99.88 | **99.90** |
| ALK | **99.80** | 99.60 | 99.16 | 98.45 | 99.39 |
| ESB | **99.98** | 99.97 | 99.95 | 99.74 | 99.93 |
| CL(%) | | | | | |
| NTA | 98.94 | 98.62 | 24.87 | **99.11** | 89.70 |
| CAR | **99.98** | 99.97 | 57.92 | 99.96 | 98.89 |
| AMO | 98.92 | 98.86 | 37.14 | **99.04** | 91.35 |
| ALK | **88.20** | 87.66 | 26.01 | 86.39 | 82.66 |
| ESB | **98.80** | 98.07 | 9.92 | 97.58 | 91.37 |
| Z-scores | | | | | |
| JM | **1.00** | 0.96 | 0.65 | 0.84 | 0.00 |
| TFD | **1.00** | 0.46 | 0.00 | 0.40 | 0.18 |
| SAd | **1.00** | 0.87 | 0.00 | 0.59 | 0.83 |
| QA | 0.39 | 0.00 | **1.00** | 0.13 | 0.63 |
| CL | **1.00** | 0.99 | 0.00 | 0.99 | 0.91 |
| F | **6.39** | 4.71 | 2.31 | 4.21 | 2.71 |

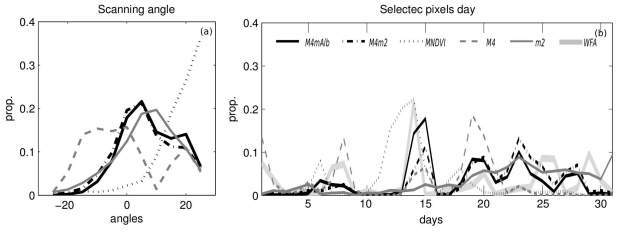


Fig. 3. Comparison of Multi-temporal algorithm composites for a) scan angle distribuition for NTA region during September b) selected pixel date for ESB during August.

and ESB) that can contaminate composite images. For the TFD test, the algorithms based on AVHRR Ch4 (M4mAlb, M4m2 and M4) revealed higher frequency of choosing pixels with post-fire dates, preforming better for the higher latitude regions and worst in the tropical regions. The MNDVI and m2 algorithms, based only on reflectance data (AVHRR channel 1 and 2) revealed the poorer results by choosing the majority of dates prior to fire events. As an example we present in Figure 3b, for the ESB region in August, pixel and WFA date distribution, where it can be seen the poor MNDVI results in the contrast with the ch.4 based algorithms. The seasonal JM distance shows that the MNDVI algorithm can discriminate slightly better the monthly spectral changes for the CAR and NTA regions and that M4mAlb and M4m2 algorithms perform better for the higher latitude regions. Common to all algorithms is the higher JM values for the ALK region, yielding higher spectral changes. The final score was obtained by applying eq.III-A to the normalised global averages. The result showed that the higher and lower scores belonged to the M4mALB and MNDVI algorithms, respectively. Because of its high performance, the M4mAlb compositing algorithm was selected to be applied to the rest of the full pathfinder AVHRR dataset.

*1) Detrending results:* For each of the 2140 mixed GLC-Ecoregions in the LUT, temporal profiles of the three variables (Albedo, GEMI, Surface temperature) and solar zenith angle values were extracted. The spatial averaging process, within each LUT area, was filtered by the quality control layers to avoid anomalous values to influence the signal behaviour. Additionally, the *clear* or *mixed* pixels, flagged by the CLAVRD layer, determined which pixels were considered for averaging. For each of the four satellite periods, the temporal profiles of the indexes were decomposed using the EMD methodology into *n*-implicit mode functions, plus a final residue representing the data trend. On average the GEMI and the Albedo index series were decomposed into four IMFs and the surface temperature series into five IMFs. The SZA, which is composed of a simpler signal with less noise, only required three IMFs to determine its trend. The results showed that for each of the satellite periods the extracted trends behave differently. Some had a more linear shape and others clearly a non-linear behaviour. The NOAA11 satellite representing the longest period, displays the stronger trends, while NOAA7 the shortest period, displays the smaller trends. The results show that the level of trend severity not only depends on the variable but also on the LUT area location. In order to illustrate these results we selected six different LUT areas representing the different types of variable behaviour and trend magnitude. The first area is located over the Amazon forest close to the equator (fig..4) where the albedo is considered low, GEMI is considered high and has moderately high surface temperature. Results show that all variable signals are characterised by very low seasonality and trend magnitude can be considered severe, exceeding for the NOAA11 period, 100%, 250% and 45% of the seasonality range for the Albedo, GEMI and surface temperature, respectively. The second area is located over South Africa (fig.5). Variable temporal profiles are marked by seasonal oscillations with a low albedo range and high GEMI and surface temperature values. The identified trends exceed the seasonal range by 88%, 100% and 58% for the albedo, GEMI and surface temperature, respectably. The third area located in the heart of the Sahara desert (fig.6), is clearly marked by high albedo and high surface temperature and very low GEMI values. The extracted trends show signal decrease to lower values up to 100% and 23% of the seasonal range for the albedo and the surface temperature but GEMI shows a positive trend up to 3% of the seasonal range with loss of seasonality. The Fourth analysed LUT area is located over

Europe (fig.7). Variable temporal profiles show clear seasonal oscillations with a wide range of values for the GEMI and low range over low mean albedo and surface temperature values. The trends are characterised by lower variations, almost unperceptible, with severity values reaching 1%, 20% and 12% for the albedo, GEMI and surface temperature, respectively. The next LUT area is located over Asia, on the Mongolian planes, is characterised by high surface temperature variations along the seasons, low albedo variations with minor perturbations and high GEMI variations over low values. Trends have low variations, representing only 3% of the albedo and GEMI seasonal variations. For the surface temperature trend, values are bigger representing 19% of its seasonal variation. The last LUT are is located over the Canadian boreal forest (Fig.9). The variable time series are characterised by low surface temperature and albedo with less clear seasonality and high GEMI values with noisier seasonal variations. The obtained trends are almost linear and its values do not reach 1% of each variable seasonal variation.

The CCA between the three individual variables and the SZA, supplied the loadings that reflect each LUT area trend significance and the Fisher-Jenks algorithm allowed to determine the threshold values, separating significant from insignificant trends (fig.10). For the four satellite periods and for each variable individually, the significant trend coverage map showed similarities with minor differences that were visually inspected. The global extent of the trend severeness can be summarised into three categories of variable sets, affected by orbital drift: 1- The first category is characterised by the full set (GEMI+albedo+surface temperature) tagged as significantly affected by orbital drift. It includes different levels of trend severity, decreasing from the tropics to the mid latitudes (fig.4,5). Areas like Australia, Southeast Asia, India, China (excluding deserts and the Tibetan plateau), Africa (except the Sahara desert) and from the mid-latitudes of mainland United States down to $35^o$ south in South America, fall into this category. 2- The second category is the mix variable set tagged as trend significance. It is restricted to the transition zones in the mid-latitudes, deserts and elevated areas. This category is characterised by one, or two, out of the three variables in which trend was considerate significant. The two out of three index set is divided into the areas located in the mid latitudes where the albedo trend is considerate insignificant (fig.6) and in the areas where GEMI trend is considerate insignificant, mainly located over the deserts and high-altitude areas (fig.7). The one out of three index set is characterised by only a significant trend for the surface temperature series located on the mid-latitudes (fig.8). 3-The last category is characterized by no significant trend for the three indexes (fig.9). This category is mainly located above $40^o$ north and in the southern hemisphere, in Tasmania and New Zealand.

For all the significant affected areas, each variable signal was filtered by removing its corresponding trend. For the first category, trend filtering allow to retrieve each variable time series to comparable seasonal values; even for lower latitude tropics where signal can be noisier and less seasonal. For the last category, each index time series appear totally untrended with clear seasonal oscillations for most of the satellite periods.

## V. Discussion and concluding remarks

We tried to evaluate a set of five multi-temporal compositing criteria. The developed and applied tests not only confirm results from other studies [54]–[57] but also add improvements for algorithm evaluation. The use of active fires revealed to be useful for spectral change evaluation. In areas with no fine resolution burned maps to compare or with large extents, active fire-affected areas can be an alternative from which spectral change can be evaluated. Assuming that, a sufficient large number of active fires can represent areas that suffered from burned activity - changing the spectral signatures and providing date information of when - temporal spectral-discrimination can be evaluated and assessed. Although an active fire can be detected for fires with lower sizes that the reference pixel, indicating that a pixel base analysis would be impractical, the average observed over a large area can capture the spectral perturbation along with other changes. The JM results show that, on average discrimination is higher for the northern latitudes. At these latitudes, due to the land-cover and long period of scar retention, it is known that there is no difficulties producing images that retain the burned scars independently of the applied compositing algorithm. For the lower latitude regions, spectral changes are less evident and can be undistinguished from the changes due to the drying of the season. This lower spectral changes detectability can be caused by two factors; lower sensitivity to thermal changes and inadequate composite time frame. These factors can severely affect burned scar detection at the tropics. On the one hand, the type of vegetation that burns in the tropical savannas is already dry with low evapotranspiration; detected thermal changes are then caused by fire itself that occurs quickly. As a consequence, the use of a thermal channel will not improve discrimination between burn and unburn at these latitudes. On the other hand, the applied temporal composite frame of one month can be large. Fires burns and moves quickly resulting in lower quantities of char and ash that quickly disperse, revealing the soil underneath. The MNDVI algorithm selects larger viewing angles which can lead radiometric speckle as identified by [54], [56], [57], [89]. It also prefers vegetated over burned pixels that lead to lower temperatures and higher reflectances. Both 2-step algorithm results are very similar because channel 1 is the least sensitive to algorithm rule changes. The high M4 algorithm final score, along with both the 2-step algorithms, highlight the importance of using a thermal information for compositing.

It is the opinion of the authors, that the developed and applied detrending procedure worked. The identification of the trend component and its associated significance revealed to be well adjustable to the multitude and magnitude of the different index conditions present on the Earth's surface. The lack of seasonality, high noise level, different land-covers reflecting different combinations of variable mean values, did not present an obstacle and trend was accurately determined. The areal coverage of the significant trends provided maps of LUT areas where each variable trend could be filtered. In general, these

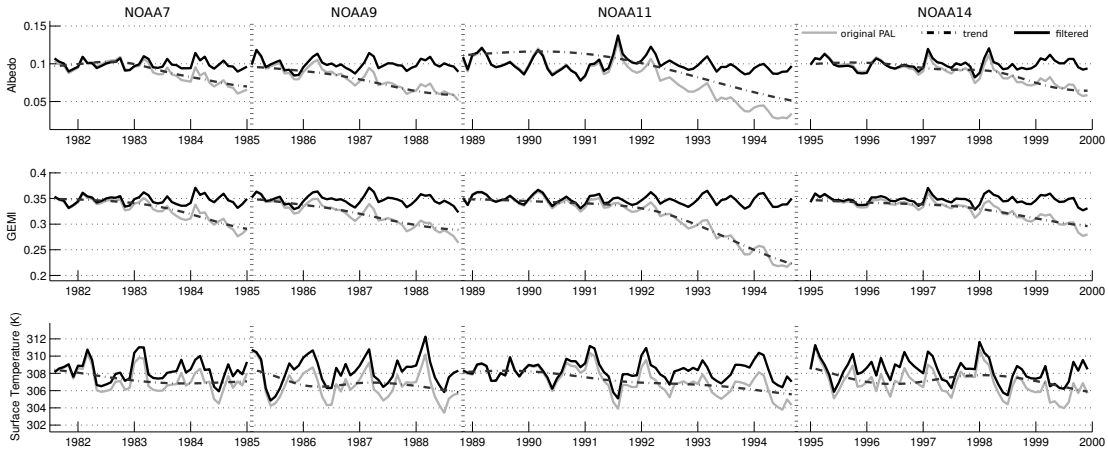


Fig. 4. Albedo, GEMI and Surface Temperature monthly temporal variations from July 1981 to December 1999 for the LUT area located over the Amazon (Point A in fig.10) characterized by severe trends

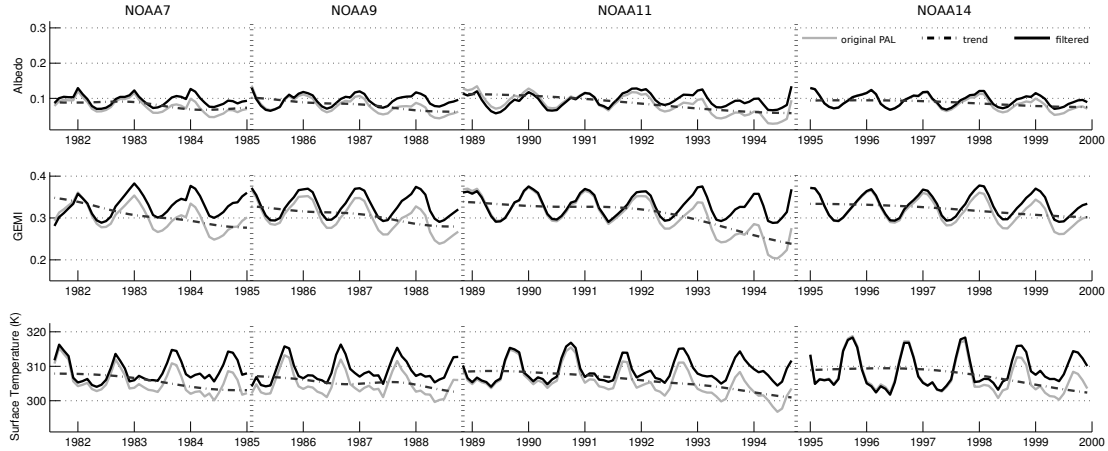


Fig. 5. As in Figure 4 but for the LUT area located over South Africa (Point B in fig.10) characterized by moderate trends

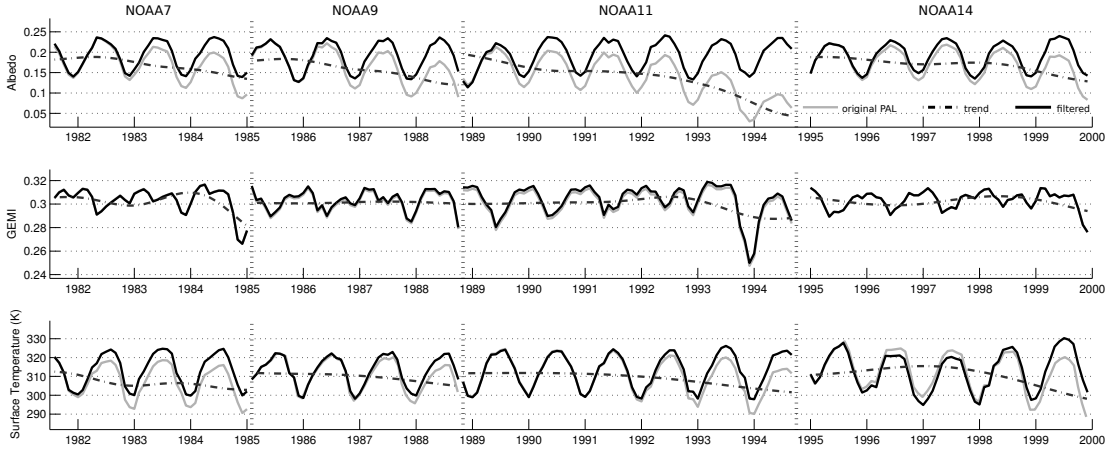


Fig. 6. As in Figure 4 but for the LUT area located over the Sahara desert (Point C in fig.10) characterized by albedo and surface temperature index significant trends

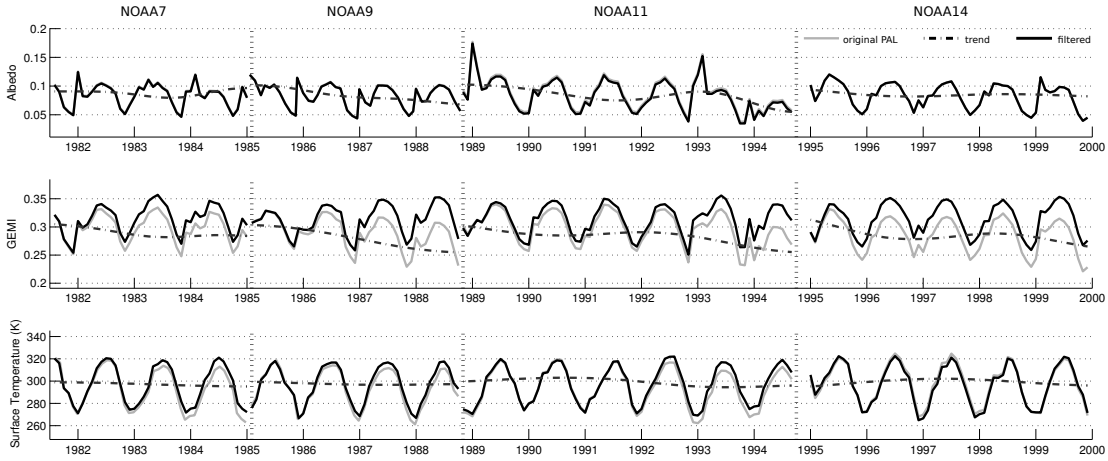


Fig. 7. As in Figure 4 but for the LUT area located over Europe (Point D in fig.10) characterized by GEMI and surface temperature significant trends

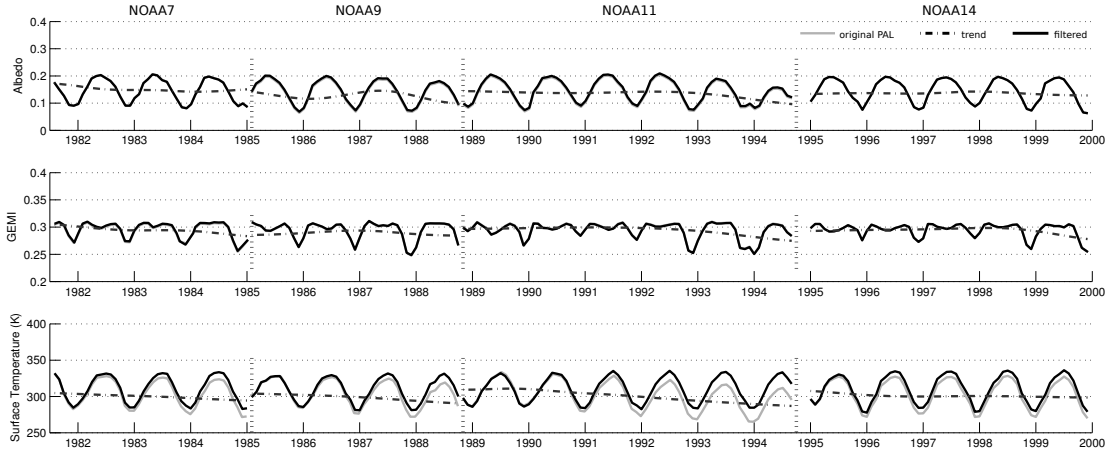


Fig. 8. As in Figure 4 but for the LUT area located Asia (Point E in fig.10) characterized by surface temperature significant trend

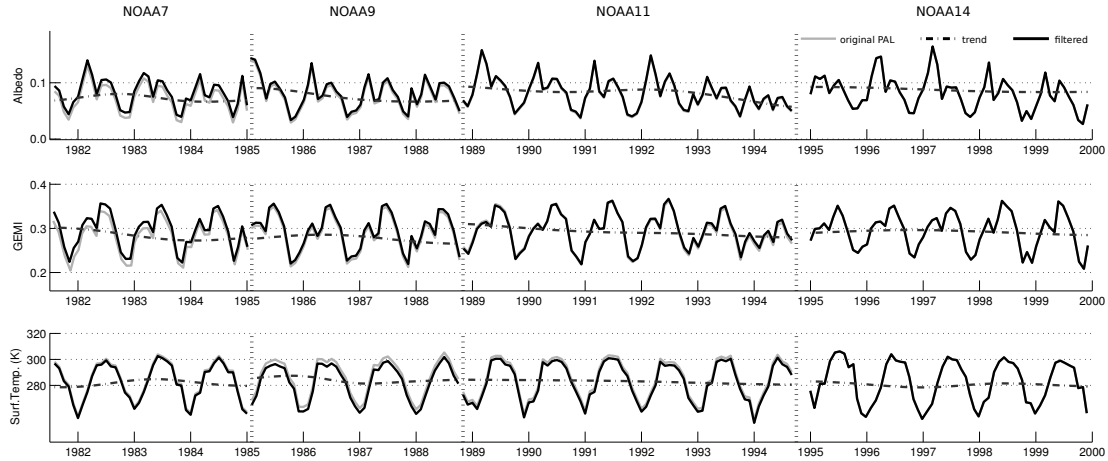


Fig. 9. As in Figure 4 but for the LUT area located over North America (Point F in fig.10) characterized by no significan trends

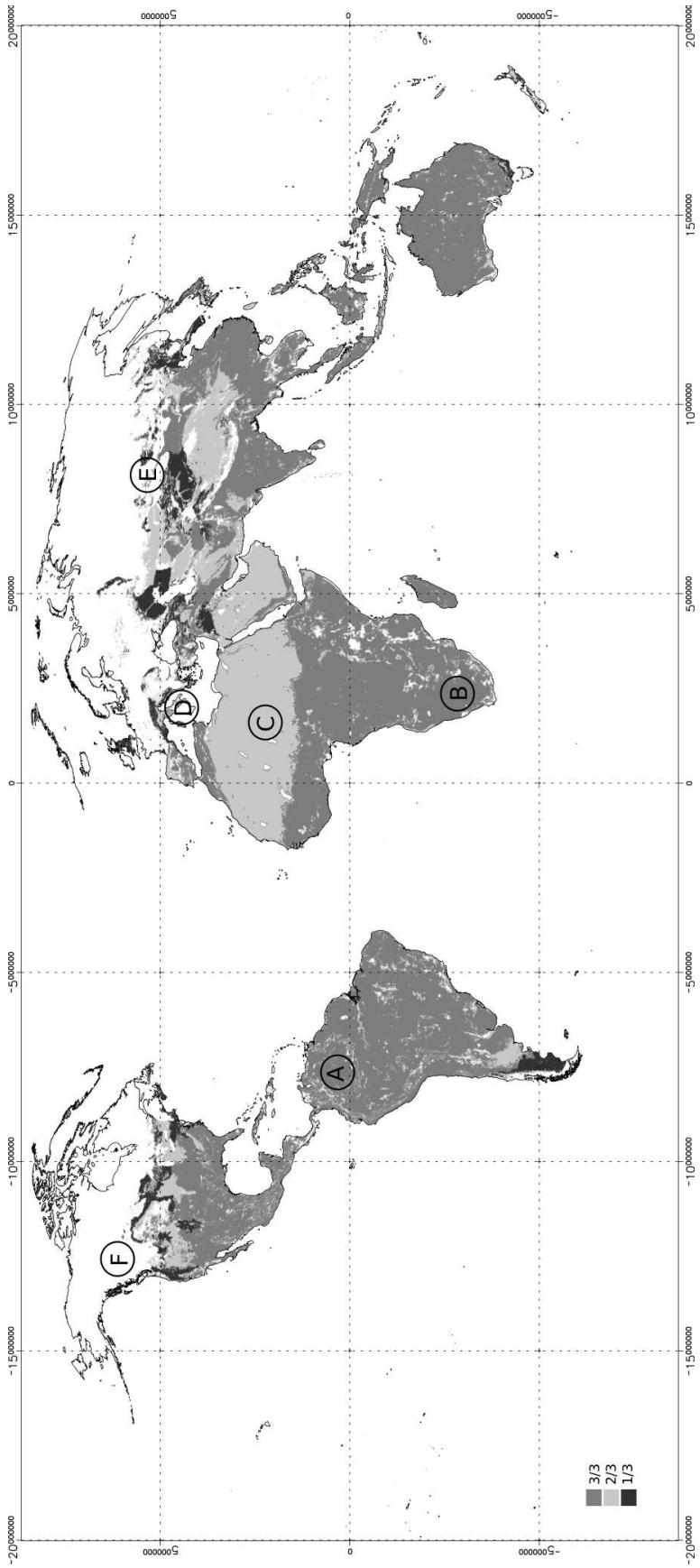


Fig. 10. Filtered trend proportion of the three indexes (GEMI, albedo and surface temperature) for the defined Look up table areas. Trends were determined by the EMD detrending procedure and considered significant by the loadings of each index CCA with the SZA.

areas correspond to trend severity values exceeding 10% of the seasonal variation. In addition, the required high negative correlation of each index with the SZA trend ($< -0.9$), ensured that trends could be attributed to the satellite orbital drift effect. The GEMI results are in agreement with the NDVI results obtained by [16], [37] for the development of the GIMMS product. In both cases the higher latitudes, deserts and elevated areas show the least orbital drift influence. But in this study, the GEMI non-linear relationship between the AVHRR reflectance channels, is responsible for a small increase trend observed over the deserts. This positive trend is in phase with the positive trend of the SZA, violating the filtering criterion of maximum out-of-phase correlation. The albedo provided similar significant areal extents, but included the deserts and elevated areas. As for the GEMI case, the albedo showed high trend severity in the tropics and low severity for the mid-latitudes. This sharp transition can be attributed to the reflectance channels sensitivity to mid day solar angle illumination changes. Although, revealing the smallest trends and severity, surface land temperature significant trends cover the largest area with the smother latitudinal transitions. These results, suggests that the satellite drift effect can be detected in a largest area by radiation emittance, but reflectance radiation is more sensitive to its effects, by causing the higher trends. The trend filtering re-established the temporal changes to levels where intra and inter satellite comparison is possible. It is accepted that the PAL product contains well documented problems, ranging from calibration to geo-processing, but the applied methodology allowed to overcome the orbital drift effect off the monthly composite images. Changes due to effects of systematic atmospheric or surface changes and sensor degradation fall out of the scope of this study. These should be considered in future developments of AVHRR imagery series, like the LTDR project. Orbital drift can not be considered corrected. Variables have been filtered by the removal of the signal component mostly affected by the orbital drift. It is possible for the data to still have trends in areas where the trend is insignificant in comparison with the SZA trend. Additionally, trend filtering could remove trends associated with other processes, like land-cover shifts, or simply induce additional artificial trends.

This study provides a dataset of monthly global maps of the Albedo, GEMI index and surface temperature based on the PAL product. The monthly composites are cloud and shadow screened with high burned scar retention and the satellite orbital drift component is filtered out. It is composed of 216 months covering July 1981 until December 1999 with the last 3 months of 1994 missing. Overall the data set represents a significant advance over the original PAL dataset and an advantage over the GIMMS product, due to the applied compositing algorithm and produced variable set. This dataset was used for burned area detection and its results will be presented in part two of this study.

## ACKNOWLEDGMENT

The authors would like to thank the Goddard Space Flight Center (GSFC) and the AVHRR Land Science team for producing and the DAAC server for supplying the PAL dataset. We would also like to thank Dr. Compton Tucker at the GSFC for his support and availability. PhD grant (SFRH/BD/25119/2005) and financial sponsorship of the Portuguese Science Foundation supported Bernardo Mota.

## REFERENCES

[1] A. P. Cracknell, *The advanced very high resolution radiometer (AVHRR)*. CRC, 1997.

[2] ——, "The exciting and totally unanticipated success of the AVHRR in applications for which it was never intended," *Advances in Space Research*, vol. 28, no. 1, pp. 233–240, 2001.

[3] D. Ehrlich, J. E. Estes, and A. Singh, "Applications of NOAA-AVHRR 1 km data for environmental monitoring," *International Journal of Remote Sensing*, vol. 15, no. 1, pp. 145–161, 1994.

[4] G. G. Gutman, "On the use of long-term global data of land reflectances and vegetation indices derived from the advanced very high resolution radiometer," *Journal of Geophysical Research*, vol. 104, no. 6, p. 62416255, 1999.

[5] C. O. Justice, J. R. G. Townshend, B. N. Holben, and C. J. Tucker, "Analysis of the phenology of global vegetation using meteorological satellite data," *International Journal of Remote Sensing*, vol. 6, no. 8, pp. 1271–1318, 1985.

[6] R. S. DeFries and J. R. G. Townshend, "NDVI-derived land cover classifications at a global scale," *International Journal of Remote Sensing*, vol. 15, no. 17, pp. 3567–3586, 1994.

[7] H. Saito, Y. Sawada, N. Furuya, and S. Preap, "Land cover change mapping of the mekong river basin using NOAA pathfinder AVHRR 8-km land dataset," *Forest Environments in the Mekong River Basin*, pp. 159–167, 2007.

[8] J. D. Tarpley, "Monthly evapotranspiration from satellite and conventional meteorological observations," *Journal of Climate*, vol. 7, no. 5, pp. 704–713, 1994.

[9] P. M. Barbosa, J. M. Gregoire, and J. M. C. Pereira, "An algorithm for extracting burned areas from time series of AVHRR GAC data applied at a continental scale," *Remote Sens. Environ.*, vol. 69, no. 3, p. 253263, 1999.

[10] A. J. L. Harris, "Towards automated fire monitoring from space: semi-automated mapping of the january 1994 new south wales wildfires using AVHRR data," *Int. J. Wildland Fire*, vol. 6, no. 3, pp. 107–116, 1996.

[11] Z. Li and L. Giglio, "A review of AVHRR-based fire detection algorithms," in *Forest fire monitoring and mapping: a component of global observation of forest cover. Report of a workshop*, 1999, p. 35.

[12] E. S. Kasischke and J. E. Penner, "Improving global estimates of atmospheric emissions from biomass burning," *J. Geophys. Res.-Atmos.*, vol. 109, no. D14, p. 9, 2004.

[13] M. Simon, S. Plummer, F. Fierens, J. J. Hoelzemann, and O. Arino, "Burnt area detection at global scale using ATSR-2: the GLOBSCAR products and their qualification," *Journal of Geophysical Research*, vol. 109, no. D14, 2004.

[14] K. B. Kidwell, "NOAA global vegetation index users guide," *US Department of Commerce, National Oceanic and Atmospheric Administration, National Environmental Satellite, Data, and Information Service, Washington DC http://www2ncdc. noaa. gov/docs*, 1997.

[15] J. D. Tarpley, "The NOAA global vegetation index product–A review," *Global and Planetary Change*, vol. 4, no. 1-3, pp. 189–194, 1991.

[16] J. Pinzon, M. E. Brown, and C. J. Tucker, "Satellite time series correction of orbital drift artifacts using empirical mode decomposition," *Hilbert-Huang Transform: Introduction and Applications*, p. 167186, 2004.

[17] C. J. Tucker, J. E. Pinzn, M. E. Brown, D. A. Slayback, E. W. Pak, R. Mahoney, E. F. Vermote, and N. E. Saleous, "An extended AVHRR 8-km NDVI dataset compatible with MODIS and SPOT vegetation NDVI data," *International Journal of Remote Sensing*, vol. 26, no. 20, pp. 4485–4498, 2005.

[18] B. N. Holben, "Characteristics of maximum-value composite images from temporal AVHRR data," *International Journal of Remote Sensing*, vol. 7, no. 11, pp. 1417–1434, 1986.

[19] P. A. Agbu and M. E. James, "The NOAA/NASA pathfinder AVHRR land data set users manual," *Goddard Distributed Active Archive Center, NASA, Goddard Space Flight Center, Greenbelt*, 1994.

[20] M. E. James and S. N. V. Kalluri, "The pathfinder AVHRR land data set: an improved coarse resolution data set for terrestrial monitoring," *International Journal of Remote Sensing*, vol. 15, no. 17, pp. 3347–3363, 1994.

[21] P. M. Smith, S. N. V. Kalluri, S. D. Prince, and R. DeFries, "The NOAA/NASA pathfinder AVHRR 8-km land data set," *PE & RS-Photogrammetric Engineering & Remote Sensing*, vol. 63, no. 1, p. 12, 1997.

[22] C. R. N. Rao and J. Chen, "Post-launch calibration of the visible and near-IR channels of AVHRR on NOAA-7,-9, and-11 spacecraft," *NOAA Technical Report NESDIS*, vol. 78, 1994.

[23] Y. Julien, J. A. Sobrino, and W. Verhoef, "Changes in land surface temperatures and NDVI values over europe between 1982 and 1999," *Remote Sensing of Environment*, vol. 103, no. 1, pp. 43–55, 2006.

[24] S. D. Prince, "Satellite remote sensing of primary production: comparison of results for sahelian grasslands 1981-1988," *International Journal of Remote Sensing*, vol. 12, no. 6, pp. 1301–1311, 1991.

[25] G. G. Gutman, "Normalization of multi-annual global AVHRR reflectance data over land surfaces to common sun-target-sensor geometry," *Advances in Space Research*, vol. 14, no. 1, pp. 121–124, 1994.

[26] F. N. Kogan and X. Zhu, "Evolution of long-term errors in NDVI time series: 1985-1999," *Advances in Space Research*, vol. 28, no. 1, pp. 149–153, 2001.

[27] L. Di and D. A. Hastings, "Temporal stability of some global NDVI products derived from NOAA/AVHRR GVI," *International Journal of Remote Sensing*, vol. 16, no. 18, pp. 3569–3583, 1995.

[28] J. L. Privette, C. Fowler, G. A. Wick, D. Baldwin, and W. J. Emery, "Effects of orbital drift on advanced very high resolution radiometer products: Normalized difference vegetation index and sea surface temperature," *Remote Sensing of Environment*, vol. 53, no. 3, pp. 164–171, 1995.

[29] A. C. R. Gleason, S. D. Prince, S. J. Goetz, and J. Small, "Effects of orbital drift on land surface temperature measured by AVHRR thermal sensors," *Remote Sensing of Environment*, vol. 79, no. 2-3, pp. 147–165, 2002.

[30] J. A. Sobrino, Y. Julien, and L. Morales, "Multitemporal analysis of PAL images for the study of land cover dynamics in south america," *Global and Planetary Change*, vol. 51, no. 3-4, pp. 172–180, 2006.

[31] A. Hartley, M. Garcia-Alegre, and M. Antonovkiy, "Characterizing interannual variations in global fire calendar using data from earth observing satellites," *Global Change Biology*, vol. 11, pp. 1537–1555, 2005.

[32] G. G. Gutman, "On the monitoring of land surface temperatures with the NOAA/AVHRR: removing the effect of satellite orbit drift," *International Journal of Remote Sensing*, vol. 20, no. 17, pp. 3407–3413, 1999.

[33] M. Jin and R. E. Dickinson, "Interpolation of surface radiative temperature measured from polar orbiting satellites to a diurnal cycle. i-without clouds," *Journal of Geophysical Research*, vol. 104, no. D2, pp. 2105–2116, 1999.

[34] S. O. Los, G. J. Collatz, P. J. Sellers, C. M. Malmstrm, N. H. Pollack, R. S. DeFries, L. Bounoua, M. T. Parris, C. J. Tucker, and D. A. Dazlich, "A global 9-yr biophysical land surface dataset from NOAA AVHRR data," *Journal of Hydrometeorology*, vol. 1, no. 2, pp. 183–199, 2000.

[35] M. Jin and R. E. Treadon, "Correcting the orbit drift effect on AVHRR land surface skin temperature measurements," *International Journal of Remote Sensing*, vol. 24, no. 22, pp. 4543–4558, 2003.

[36] M. Deng, L. Di, I. Raytheon, and M. D. Lanham, "Solar zenith angle correction of global NDVI time-series from AVHRR," in *IEEE 2001 International Geoscience and Remote Sensing Symposium, 2001. IGARSS'01*, vol. 4, 2001.

[37] J. Pinzon, M. E. Brown, and C. J. Tucker, "EMD correction of orbital drift artifacts in satellite data stream," *The HilbertHuang transform and its applications*, pp. 167–183, 2005.

[38] H. Ouaidrari, S. N. Goward, K. P. Czajkowski, J. A. Sobrino, and E. Vermote, "Land surface temperature estimation from AVHRR thermal infrared measurements-An assessment for the AVHRR land pathfinder II data set," *Remote Sensing of Environment*, vol. 81, no. 1, pp. 114–128, 2002.

[39] H. Ouaidrari, N. E. Saleous, E. F. Vermote, J. R. Townshend, and S. N. Goward, "AVHRR land pathfinder II (ALP II) data set: evaluation and inter-comparison with other data sets," *International Journal of Remote Sensing*, vol. 24, no. 1, pp. 135–142, 2003.

[40] C. R. N. Rao, *Non-linearity corrections for the thermal infrared channels of the Advanced High Resolution Radiometer: assessment and recommendations, NOAA technical Report NESDIS-69*. NOAA/NESDIS, 1993.

[41] C. R. N. Rao, J. Chen, F. W. Staylor, P. Abel, Y. J. Kaufman, E. Vermote, and W. R. Rossow, "Degradation of the visible and near-infrared channels of the advanced very high resolution radiometer on the NOAA-9 spacecraft: Assessment and recommendations for corrections," *NOAA Technical Report NESDIS*, vol. 70, 1993.

[42] D. G. Baldwin and W. J. Emery, "A systematized approach to AVHRR image navigation," *Annals of Glaciology*, vol. 17, pp. 414–414, 1993.

[43] F. S. Patt and W. W. Gregg, "Exact closed-form geolocation algorithm for earth survey sensors," *International journal of remote sensing(Print)*, vol. 15, no. 18, pp. 3719–3734, 1994.

[44] L. L. Stowe, E. P. McClain, R. Carey, P. Pellegrino, G. G. Gutman, P. Davis, C. Long, and S. Hart, "Global distribution of cloud cover derived from NOAA/AVHRR operational satellite data," *Advances in Space Research*, vol. 11, pp. 51–54, 1991.

[45] D. R. Steinwand, "Mapping raster imagery to the interrupted goode homolosine projection," *International journal of remote sensing(Print)*, vol. 15, no. 17, pp. 3463–3471, 1994.

[46] D. R. Steinwand, J. A. Hutchinson, and J. P. Snyder, "Map projections for global and continental data sets and an analysis of pixel distortion caused by reprojection," *Photogrammetric Engineering and Remote Sensing*, vol. 61, no. 12, pp. 1487–1497, 1995.

[47] E. Bartholome and A. S. Belward, "GLC2000: a new approach to global land cover mapping from earth observation data," *International Journal of Remote Sensing*, vol. 26, no. 9, p. 19591977, 2005.

[48] D. M. Olson, E. Dinerstein, E. D. Wikramanayake, N. D. Burgess, G. V. N. Powell, E. C. Underwood, J. A. D'amico, I. Itoua, H. E. Strand, and J. C. Morrison, "Terrestrial ecoregions of the world: a new map of life on earth," *BioScience*, vol. 51, no. 11, pp. 933–938, 2001.

[49] O. Arino and J. Rosaz, "1997 and 1998 world atsr fire atlas using ers-2 atsr-2 data," in *Proc. Joint Fire Sci. Conf.* Boise, ID, 1999, pp. 177–182.

[50] B. W. Mota, J. M. C. Pereira, D. Oom, M. J. P. Vasconcelos, and M. Schultz, "Screening the ESA ATSR-2 world fire atlas (1997-2002)," *Atmos. Chem. Phys.*, vol. 6, pp. 1409–1424, 2006.

[51] J. R. G. Townshend, T. E. Goff, and C. J. Tucker, "Multitemporal dimensionality of images of normalized difference vegetation index at continental scales," *IEEE Transactions on Geoscience and Remote Sensing*, pp. 888–895, 1985.

[52] J. P. Malingreau, "Global vegetation dynamics: satellite observations over asia," *International Journal of Remote Sensing*, vol. 7, no. 9, pp. 1121–1146, 1986.

[53] J. P. Malingreau, F. Achard, C. Estregubl, H. Stebig, and G. D'Souza, "NOAA-AVHRR Based Tropical ForestT Mapping for South-East Asia, validated and calibrated with higher spatial resolution imagery," *Advances in the use of NOAA AVHRR Data for Land Applications*, pp. 279–310, 1996.

[54] P. M. Barbosa, J. M. C. Pereira, and J. M. Gregoire, "Compositing criteria for burned area assessment using multitemporal low resolution satellite data-a non-linear index to monitor global vegetation from satellites," *Remote Sensing of Environment*, vol. 65, no. 1, pp. 38–49, 1998.

[55] E. Chuvieco, G. Ventura, M. Martín, and I. Gómez, "Assessment of multitemporal compositing techniques of modis and avhrr images for burned land mapping," *Remote Sensing of Environment*, vol. 94, no. 4, pp. 450–462, 2005.

[56] A. M. O. Sousa, J. M. C. Pereira, and J. M. N. Silva, "Evaluating the performance of multitemporal image compositing algorithms for burned area analysis," *International Journal of Remote Sensing*, vol. 24, no. 6, pp. 1219–1236, 2003.

[57] A. Cabral, M. Vasconcelos, J. M. C. Pereira, E. Bartholome, and P. Mayaux, "Multi-temporal compositing approaches for SPOT-4 VEGETATION," *International Journal of Remote Sensing*, vol. 24, no. 16, pp. 3343–3350, 2003.

[58] J. Pereira, A. Sousa, and A. Sá, "Regional-scale burnt area mapping in southern europe using noaa-avhrr 1 km data," 1999.

[59] D. R. Cahoon, B. J. Stocks, J. S. Levine, W. R. Cofer, and J. M. Pierson, "Satellite analysis of the severe 1987 forest fires in northern china and southeastern siberia," *Journal of Geophysical Research*, vol. 99, no. D9, p. 1862718638, 1994.

[60] Y. J. Kaufman, "The atmospheric effect on remote sensing and its correction," *Theory and applications of optical remote sensing*, pp. 336–428, 1989.

[61] J. Cihlar, D. Manak, and N. Voisin, "Avhrr bidirectional reflectance effects and compositing," *Remote Sensing of Environment*, vol. 48, no. 1, pp. 77–88, 1994.

[62] J. Qi, "Compositing multitemporal remote sensing data." 1993.

[63] G. Ventura, E. Chuvieco, and P. Martín, "Multitemporal compositing techniques for burned land mapping," in *Fourth international workshop on remote sensing and GIS applications to forest fire management. Innovative concepts and methods*, 2003, pp. 196–201.

[64] R. W. Saunders, "The determination of broad band surface albedo from AVHRR visible and near-infrared radiances," *International Journal of Remote Sensing*, vol. 11, no. 1, pp. 49–67, 1990.

[65] J. D. van Leeuwen W, R. Huete A, and W. Laing T, "Modis vegetation index compositing approach: A prototype with avhrr data," *Remote Sensing of Environment*, vol. 69, pp. 264–280, 1999.

[66] R. J. Whelan, *The ecology of fire*. Cambridge Univ Pr, 1995.

[67] M. Garcia and V. Caselles, "Mapping burns and natural reforestation using thematic mapper data," *Geocarto International*, vol. 6, no. 1, pp. 31–37, 1991.

[68] R. E. Dickinson, "Satellite systems and models for future climate change," *World Survey of Climatology*, pp. 245–279, 1995.

[69] R. K. Vincent, "The potential role of thermal infrared multispectral scanners in geological remote sensing," *Proceedings of the IEEE*, vol. 63, no. 1, pp. 137–147, 1975.

[70] J. A. Sobrino, Z. L. Li, M. P. Stoll, and F. Becker, "Improvements in the split-window technique for land surfacetemperature determination," *IEEE Transactions on Geoscience and Remote Sensing*, vol. 32, no. 2, pp. 243–253, 1994.

[71] H. Yang and Z. Yang, "A modified land surface temperature split window retrieval algorithm and its applications over china," *Global and Planetary Change*, vol. 52, no. 1-4, pp. 207–215, 2006.

[72] M. Andreae, "Biomass burning- its history, use, and distribution and its impact on environmental quality and global climate," *Global biomass burning- Atmospheric, climatic, and biospheric implications(A 92-37626 15-42). Cambridge, MA, MIT Press, 1991*, 1991.

[73] B. Pinty, M. M. Verstraete, N. Gobron, F. Roveda, and Y. Govaerts, "Do man-made fires affect earths surface reffectance at continental scales," *Eos Trans. AGU*, vol. 81, no. 381, p. 388389, 2000.

[74] Y. M. Govaerts, J. M. Pereira, B. Pinty, and B. Mota, "Impact of fires on surface albedo dynamics over the african continent," *Journal of Geophysical Research-Atmospheres*, vol. 107, no. D22, p. 4629, 2002.

[75] D. P. Roy, Y. Jin, P. E. Lewis, and C. O. Justice, "Prototyping a global algorithm for systematic fire-affected area mapping using MODIS time series data," *Remote Sensing of Environment*, vol. 97, no. 2, pp. 137–162, 2005.

[76] Y. Jin and D. P. Roy, "Fire-induced albedo change and its radiative forcing at the surface in northern australia," *Geophysical Research Letters*, vol. 32, no. 1, 2005.

[77] I. Csiszar and G. Gutman, "Mapping global land surface albedo from NOAA AVHRR," *Journal of Geophysical Research*, vol. 104, pp. 6215–6228, 1999.

[78] B. Pinty and M. M. Verstraete, "GEMI: a non-linear index to monitor global vegetation from satellites," *Plant Ecology*, vol. 101, no. 1, pp. 15–20, 1992.

[79] S. Flasse and M. M. Verstraete, "Monitoring the environment with vegetation indices: comparison of NDVI and GEMI using AVHRR data over africa," *Vegetation, Modelling and Climatic Change Effects*, p. 107135, 1994.

[80] E. Chuvieco, M. P. Martin, and A. Palacios, "Assessment of different spectral indices in the red-near-infrared spectral domain for burned land discrimination," *International Journal of Remote Sensing*, vol. 23, no. 23, pp. 5103–5110, 2002.

[81] J. M. C. Pereira, "A comparative evaluation of NOAA/AVHRR vegetation indexes forburned surface detection and mapping," *IEEE Transactions on Geoscience and Remote Sensing*, vol. 37, no. 1 Part 1, pp. 217–226, 1999.

[82] R. H. Fraser, Z. Li, and J. Cihlar, "Hotspot and NDVI differencing synergy (HANDS)-A new technique for burned area mapping over boreal forest," *Remote Sensing of Environment*, vol. 74, no. 3, pp. 362–376, 2000.

[83] N. E. Huang, Z. Shen, S. R. Long, M. C. Wu, H. H. Shih, Q. Zheng, N. C. Yen, C. C. Tung, and H. H. Liu, "The empirical mode decomposition and the hilbert spectrum for nonlinear and non-stationary time series analysis," *Proceedings: Mathematical, Physical and Engineering Sciences*, vol. 454, no. 1971, pp. 903–995, 1998.

[84] D. S. Wilks, *Statistical methods in the atmospheric sciences: an introduction*. Academic press San Diego, 1995.

[85] L. N. Trefethen and D. Bau, *Numerical linear algebra*. Society for Industrial Mathematics, 1997.

[86] N. E. Huang, Z. Shen, and S. R. Long, "A New View of Nonlinear Water Waves: the hilbert spectrum 1," *Annual Review of Fluid Mechanics*, vol. 31, no. 1, pp. 417–457, 1999.

[87] D. Kim and H. S. Oh, "EMD: a package for empirical mode decomposition and hilbert spectrum."

[88] G. F. Jenks and F. C. Caspall, "Error on choroplethic maps: definition, measurement, reduction," *Annals of the Association of American Geographers*, vol. 61, no. 2, pp. 217–244, 1971.

[89] J. Cihlar, D. Manak, and M. D'iorio, "Evaluation of compositing algorithms for AVHRR data over land," *IEEE Transactions on Geoscience and Remote Sensing*, vol. 32, no. 2, pp. 427–437, 1994.

**Bernardo Mota** received the undergraduate degree in geosciences-metreology and oceanography in 2000 from the Faculdade de Ciências at the Universidade de Lisboa, Portugal, and is presently finishing is Ph.D. Degree in forestry engineering at the Instituto Superior de Agronomia, Universidade Técnica de Lisboa, Lisbon, Portugal. He is a researcher with the Departmant of Forestry, Instituto Superior de Agronomia, Universidade Técnica de Lisboa, and his current research interests include the development of remote sensing algorithms for burned area mapping, climate and biomass burning relations, feedbacks and trends.

**Jorge Pinzón** received the B.Sc. degrees in mathematics and computer science, respectively, from the Universidad de los Andes, Bogot, Colombia, in 1985 and 1986, respectively, and the M.S. and Ph.D. degrees in applied mathematics from the University of California, Davis, in 1996 and 1998, respectively. He was a Postdoctoral Fellow with the University of Maryland, College Park, for two years, and is currently with Science Systems and Applications, Inc. (SSAI), Biospheric Sciences Branch, NASA/Goddard Space Flight Center, Greenbelt, MD, as a Senior Scientist. His research interests include data representation and pattern recognition in time series and remote sensing.

**José M.C. Pereira** received the undergraduate degree in forestry in 1983 from the Instituto Superior de Agronomia, Universidade Técnica de Lisboa, Lisbon, Portugal, and a Ph.D. Degree in renewable natural resources studies in 1989 from the University of Arizona, Tucson. He is an associate Professor with the Departmant of Forestry, Instituto Superior de Agronomia, Universidade Técnica de Lisboa, teaching courses in vegetation fires, forest ecology and remote sensing. His current research interests include the geographical ecology of wildfires in southern Europe and the development of remote sensing algorithms for burned area mapping at regional and global scales.

(this page is black on propose)

# Artigo 4

## Large Burned Area Product (LBAP-PAL): A global monthly series (1981-1999) based on the Pathfinder AVHRR land Data. Part II - Burned area classification

**Mota, B., J.M.C. Pereira** - Department of Forestry, Instituto Superior de Agronomia, 1349-017 Lisboa, Portugal.
**R.M. Trigo** - Faculty of Sciences, University of Lisbon, Lisboa, Portugal.

# The Large Burned Area Product (LBAP-PAL): A global monthly series (1981-1999) based on the AVHRR Pathfinder land Data. Part II - Burned area classification.

Bernardo Mota, José M.C. Perreira, and Ricardo M. Trigo

***Abstract*—An orbital drift detrended version of the Pathfinder AVHRR (8km) dataset was used to produce a global burnt area dataset covering the period between 1981 and 1999.**

**A Random Forest algorithm, based on training data collected for four individual years, plus some severe events, dictated surface temperature and GEMI combined with land-cover discrimination were important and that albedo was less important.**

**Active fires were used to produce a climatological fire season mask, which were combined with the burnt area classification to produce maps screened of false alarms. The comparison with annual statistics, with other continental burnt area maps derived from remote sensing and with global estimates from recent burned area products showed that the LBAP-PAL severely underestimates burned area extents. The results also show a significant increase in burnt area time series for the South Asia region plus evidence of human influence present in different land cover types. The large underestimation was, in part, attributed to the PAL re-sampling procedure.**

## I. Introduction

BIOMASS burning is a major source for many trace gases and particles released each year into the atmosphere on a regional and global scale [1], [2]. These emissions significantly influence the Earth's atmosphere and climate, highlighting the need for accurate estimates from global atmospheric chemistry models. One of the main source of uncertainties in emission estimates, at a global scale, is the areal extent covered by burned vegetation. Fire activity alters the land surface properties and its spectral response, allowing it to be detected by radiometric sensors onboard Earth observing satellites. Since the 1980s, remote sensing has been used to monitor the Earth surface and in particular it has been successfully used for burned area mapping. Early, studies covered limited areas and short time spams. Gradually, as the computational capabilities allowed and ecological interest grew, larger areas were mapped reaching the scale of countries [3], continents [4], [5], global [6], [7], [8], [9], [10] and finally, global mapping at continuous time intervals [11], [12], [13], [14], [15]. Up until the year 2000, most studies relied on AVHRR sensor imagery flying aboard the NOAA satellites, which proved to have good spectral capabilities for burned area mapping [16], [17]. In the last decade, efforts have been made for the development of near real-time global burned area mapping based on modern remote sensors. Two of these products are the L3JRC [15], [14] and the MCD45 [12], [11], [13] , that provide maps of burnt affected areas at regular time intervals covering several years. The L3JRC is based on imagery acquired by VEGETATION sensor onboard the SPOT satellite and the MCD45 is based on the MODIS imagery acquired aboard the Aqua and Terra satellites. Both have moderate spatial resolutions (500m and 1km, respectively) that enable lower uncertainties [39] but are limited by a short time series of maps reaching less than a decade (2001 to 2009 and 2000 to 2007, respectively). This achievement, although relevant, still fails to provide a sufficient long time series required for climatological studies.

Systematic and available land surface imagery before 2000 was only acquired by the AVHRR sensor. This sensor, in its five channel version, has been acquiring images since July 1981, onboard several NOAA satellites. This data archive is of valuable historical information to conduct climatic and land surface studies [18]. The sensor has a 1.1km spatial resolution at nadir that is subsampled and averaged on-broad into 4km spatial resolution pixels in the form of the Global Area Coverage (GAC) product before it is transmitted to the ground receiving stations. Due to the high volume of data, several projects were conducted to provide a global dataset workable on a daily scale. The Global Inventory Modelling and Mapping Studies (GIMMS) [19], [20] and Global Vegetation Index (GVI) [21] data products were developed based on the original GAC, in which the data were resampled and composited into the Normalised Difference Vegetation Index (NDVI) maps based on the MNDVI algorithm [22]. This revealed to be a disadvantage for burned area mapping, specially for the tropical savannas where burn scars are very short-lived [23], [24]. The Pathfinder AVHRR Land dataset (PAL) [25], [26], [27] was the only product that provided daily images of global coverage for each individual channel. Several attempts have been made to produce maps from these data. [28] applied a classification which revealed potential, [29], [30] produced the Global Burnt Area Product (GBA8299) of burned probabilities but [31] found that these maps were severely influenced by each satellite orbital drift trend that affects the dataset. To compensate for the orbital drift effect highlighted by several studies [32], [33], [34] various authors have approached the problem differently [18], [35], [36], [32], [37], [38], [39]. The recent Long Term Data Record (LTDR) project, when

B. Mota and J.M.C. Perreira are with the Departamento de Engenharia Florestal at the Universidade Técnica de Lisboa.

R. Trigo is with the Faculty of Science of the University of Lisbon.

Manuscript in preparation December 20, 2010.

completed, will provide the full AVHRR daily imagery at a global scale on a $0.05^\circ$ grid format. It is expected to solve many radiometric problems and allow the data to be compatible with recent sensor imagery, like VEGETATION and MODIS.

The objective of this study, part two of two, was to produce 19 years of monthly global burned area probability maps based on the PAL dataset (LBAP-PAL). To achieve this, we used monthly orbital detrended composites of albedo, GEMI and surface temperature produced in part one of this study with a 2-step classification algorithm based on a Random Forest [40] combined with climatological probability masks based on satellite active fire data. The burned areas maps were compared with other data from the same period, including remote sensing data, official statistics, and a continental-level comparison was made using recent global burned area products. The datasets used to produce the LBAP-PAL product are described in section II. Section III describes the data processing system, algorithms, and analysis methodology. In section IV results are presented and analyzed for their accuracy and in the last section V, a discussion followed by concluding remarks is given.

## II. Data

### A. Remote sensing imagery series

The imagery time-series used in this study is the detrended monthly multi-temporal composites of the Albedo [41], GEMI [42] and surface temperature [43], produced in part one of this study. The dataset was produced with a 2-step multi-temporal composite algorithm [44], [45], [5] to screen out cloud and cloud shadows and retain burned scars. Due to orbital satellite drift of the four NOAA (7, 8, 11 and 14) satellites, a filtering procedure based on the Empirical Mode Decomposition [46], [47] was used to filter out the signal component best related to the orbital drift from a set of defined areas combined by land cover and ecoregion classifications. Due to the non-uniform distribution of the trend effect, canonical correlation analysis was applied to determine the trend significance of each area. The results showed a trend of decreasing significance, from the tropics to the boreal latitudes, where the trend was considered insignificant. The dataset is composed of monthly variables images of the Albedo, GEMI and surface temperature, mapped on the original PAL projection and resolution of global 8 km equal area grid, in Goodes Interrupted Homolosine projection [48], [49]. It covers the period from July 1981 to December 1999 with exception of the last 6 months of 1994 due to missing imagery and data quality issues.

### B. Global Land Cover 2000

The Global Landcover Classification (GLC2000) [50] was developed by the Institute for Environment and Sustainability at the Joint Research Centre (JRC/IES) Global Vegetation Monitoring Unit (GVM) with the objective to provide a harmonized land cover database over the whole globe for the year 2000. This Landcover product was based on a 14-month dataset of pre-processed daily global data acquired by the VEGETATION instrument on board the SPOT 4 satellite and uses the FAO Land Cover Classification System (LCCS), where the combustible classes account for 83% of the global land coverage (Table I). The data are available at http://www-gem.jrc.it/glc2000/ in a geographic lat-long coordinates with 1km spatial resolution. For the present study, the map was re-sampled into Goodes Interrupted Homolosine projection [48], [49] at 8km spatial resolution, using an 8x8 pixel majority filter.

TABLE I
Extents of the Global Land Cover 2000 fuel classes

| Description | | global surface (%) |
|---|---|---|
| Tree Cover, broadleaved, evergreen | TBE | 10.31 |
| Tree Cover, broadleaved, deciduous, closed | TBDC | 5.20 |
| Tree Cover, broadleaved, deciduous, open | TBDO | 3.04 |
| Tree Cover, needle-leaved, evergreen | TNE | 7.96 |
| Tree Cover, needle-leaved, deciduous | TND | 0.43 |
| Tree Cover, mixed leaf type | TM | 2.31 |
| Tree Cover, regularly flooded, fresh water | TFF | 0.38 |
| Tree Cover, regularly flooded, saline water | TFS | 0.08 |
| Mosaic: Tree Cover, Other natural vegetation | M | 1.51 |
| Shrub Cover, closed-open, evergreen | SCE | 1.38 |
| Shrub Cover, closed-open, deciduous | SCD | 8.85 |
| Herbaceous Cover, closed-open | HRB | 10.33 |
| Sparse herbaceous or sparse shrub cover | SHSS | 10.84 |
| Regularly flooded shrub, herbaceous cover | FSHC | 1.01 |
| Cultivated and managed areas | CM | 15.02 |
| Mosaic: Cropland, Tree Cover, Other natural vege | MCTN | 2.44 |
| Mosaic: Cropland, Shrub, grass cover | MSG | 2.00 |
| **Total** | | **83.10** |

### C. Screened World Fire Atlas

The World Fire Atlas (WFA) developed by the European Space Agency (ESA) [51] was built using night time data from the Along Track Scanning Radiometer (ATSR), onboard the Second European Remote-Sensing Satellite (ERS-2). The spatial resolution of the data is 1 km and the satellite revisiting period is three days at the equator. Known limitations of the WFA are the inclusion of warm surfaces, gas flares, and city lights, and an underestimation of actual global fire activity, due to the time of satellite overpass. The screened version of its algorithm 2, thresholded at 308 K, was screened by [52] using ancillary land cover maps, night-lights and volcanic activity datasets, combined with statistical techniques to detect the occurrence of space-time clusters of anomalous observations. The authors found that, depending on the year, false alarms range between 20% and 28%, with gas flares and hot bare soils are the major contributors. The data cover a 10 year period, beginning in July 1996 until June 2006, and were aggregated into active fire counts within each 8km pixel, in Goodes Interrupted Homolosine projection [48], [49].

## III. Methods

### A. Burned area classification

Classification of burnt scars based on remote sensing images has become the standard in burned area map production used by researchers and government agencies. In this process, several classification techniques have been developed and applied to a wide range of imagery systems using different spatial and temporal resolutions. Since the 1990's, AVHRR imagery has been used in developing different types of classifications methods, from one phase algorithms, where burned pixels are discriminated individually in a processing chain [4], [53], [54], [55], [56], [57], and two phase algorithms where an

additional step is added by applying a contextual algorithm to refine the pixel discrimination from its surroundings [58], [59], [60], [61]. In this study, we introduce a different two phase algorithm where each pixel is classified and its burned probability is weighted with a seasonal probability determined by a fire mask. This classification differs from the classical two phase classifiers, because it uses independent climatological fire information to weight burn activity, instead of information from surrounding pixels.

Burnt areas result in surface change, yielding different land spectral responses in radiation reflectance and emittance. The lack of partial or total vegetation depends on fire severity and affected vegetation type, which leads to different levels of surface darkening by deposition of char residues or lightly burned vegetation. The loss of water content by lower evapotranspiration and the high solar radiation absorbance leads to low humidity and higher surface temperatures. Based on this, burned activity will result in lower values of vegetation index, albedo and higher values of surface temperature [62]. These spectral changes can persist over time, until vegetation recovers to its initial status. The period of scar detectability is longer in the boreal forest and shorter for the tropical savannas, which sets a time frame dependent on vegetation type and on the underlying soil colour. Seasonality can also yield different spectral changes between early and late season fires. In the tropical savannas the contrast between green and dry biomass, early and late dry season conditions, leads to different drops in reflectance according to the vegetation state [56]. Phenological changes can also mimic some of the spectral changes produced by fire, where the leaf falling in deciduous coniferous forests present a challenge [9]. Finally, other non-phenological spectral changes can also occur leading to miss-classification. For example, agricultural residue burns in central Asia are a tool to clear and fertilize the soils right after snow melts. This change, if not considered, can easily be missed due to the high pre-burn reflectance values. False detections corresponding to seasonal flooded areas, cropland harvest and forest clearcuts need also to be taken into account. Any global classifier has to consider multiple scenarios which results in a very complex algorithm. It will benefit from incorporating a land cover classification to help distinguish the different fire regimes, with their different unburned-burned vegetation, temperature and albedo variations occurring at different levels. Additionally, it would also benefit from a revison based on seasonal fire activity information, not only to avoid false detections but also to highlight potential detections. The complexity of temporal and spatial changes occurring at different levels, led to the selection of the Random Forest algorithm to develop a classification to be applied through out the full imagery series.

*1) Random Forest classification:* The Random Forest (RF) was developed by [40] and is derived from the classical regression trees algorithms, which have proved to be successful for burned area mapping [63]. In general terms, RF consists in a ensemble of tree-type classifiers, characterised by an additional randomness component to bagging, in which each tree is constructed using a bootstrap sample of the training data, and where each node is split using a subset of randomly chosen predictors. Since each tree is only using a portion of the input variables, the RF algorithm is considerably lighter than conventional bagging to tree-type classifiers, allowing it to handle high dimensional data and develop a large number of trees without becoming computationally intensive. Because a large number of trees can be grown, there is limited generalisation error avoiding over-fitting the data [40], [64], [65]. The final classification result is obtained by aggregating the number of predicted trees, grown to maximum size without pruning, in majority votes. Although appearing as a counter-intuitive strategy, [40], [64] proved to perform very well when compared to many other classifiers and has been successfully used in land cover classifications [65] and ecology studies [64], [66]. To estimate the accuracy, the out-of-bag samples of each tree (the remaining training set samples that are not in the bootstrap) are classified (cross-validation). RF also allows output results in membership probabilities of the different classes, these are estimated by the proportions of out-of-bag predictions in each class. Another advantage is that RF algorithms can evaluate the importance of variables by randomly permuting all the values of the variable in the out of bag samples. The resulted variation in out-of-bag errors estimates determines the importance of each variable. The RF classifier can be easily tuned by only parametrising the number of variables randomly selected at each node and the total number of trees in the forest, i.e., the number of sample subsets produced by bootstrapping. This feature allows the random forest classifier to be very user-friendly and at the same time be a powerful classification method for satellite imagery classification. In this study we used the Random Forest package [67] for the R language, available at www.r-project.org which provides an interface to the original Fortran code [40]. The selected input variables were the albedo, GEMI and surface temperature, and their corresponding monthly differences (current-previous month) and the GLC2000 land cover class (Table I). The training data were visually selected, representing not only burn and unburnt surfaces, but also different contrasting conditions within each land cover class. The main periods for this information extraction were concentrated in the years 1983, 1986, 1991 and 1997, representing the half-term of the four satellite periods. Additional training data were also selected covering major fire events recorded in the literature. The Random Forest classification algorithm developed with the training data was applied to each monthly set of global index maps to produce burn probability maps.

*2) Climatological fire probability mask:* In order to account for the seasonality effect, monthly probability maps were produced using the screened version of the WFA active fire counts [52]. The fire counts were aggregated and compiled into the 12 months of the year to represent the monthly climatological fire activity. For each month the cumulative global count distribution was determined after which each individual cell count was converted into its corresponding proportion distribution. The resulting maps are monthly probabilities, where the higher probabilities represent few cells with high number of counts and the lower probabilities represent a large number of cells with low number of fire counts. To enlarge the mask areal extent to neighbouring areas where no count was

recorded during the 10 year period of the WFA, a Gaussian filter with 80km radius was applied to each monthly map. This operation not only increased the covered area from 16% to 88% of the global burnable area (combustible land surface) but also smoothed the probability maps.

*3) Final probability maps:* The Random Forest classification probability maps and the corresponding climatological monthly probability maps were combined to produce the final burned event probability map for the full 19 year series. The adopted procedure, used a method to combine probability [68], [69] with the following formula:

$$P_{final} = \frac{1}{1 - e^{\left[log\left(\frac{1-P_{RF}}{P_{RF}}\right) - log\left(\frac{P_{month}}{1-P_{month}}\right)\right]}}$$

where $P_{RF}$ are the probabilities from the Random Forest classification maps and $P_{month}$ are the probabilities from the monthly climatological maps. The resulting probability maps were converted to binary burned and unburned maps by applying thresholds, determined by the monthly average of the smooth climatological probability maps. A temporal filter was also applied to avoid the same pixel being classified as burned twice within a six month period, in which only the first recorded event was considered. Results for the 216 months classified were analysed and characterised spatially and temporally at a global and continental scale. A set of eight geographical study regions covering hemispheric continents were defined, in order to highlight the different fire seasons and burned regimes (table II). Annual global estimates were tested for trends using the Mann-Kendall trend test [70] and for each study area, the monthly distribution, the burned land cover distribution and temporal series was also analysed. In order to help characterise the different fire regimes of each study area, the burn frequency (BF) and the burning season peak was calculated. The BF was defined as the number of times a pixel burned during the 19 year period and the seasonal peak was defined by the month with the highest burning activity for the same period. Burnt land cover preference was established by comparing the land cover areal proportions between each study region and its burned area.

TABLE II
AREAL EXTENTS OF THE STUDY AREAS FOR ANALYSIS

| Region | Latitude | Longitude | Land area($km^2$) |
|---|---|---|---|
| North America | 24.7N - 69.5N | 72.6W - 34.6W | 19,474,880 |
| South America | 70.6S - 12.5N | 88.2W - 18.1W | 18,062,336 |
| Europe | 31.7N - 70.5N | 4.0W - 939.8E | 9,025,152 |
| North Africa | 0N - 16.8N | 18.4W - 51.3E | 11,361,344 |
| Southern Africa | 38.5S - 0S | 6.1E - 54.3E | 9,959,552 |
| North Asia | 43.5N - 72.5N | 38.5E - 149.1E | 209,769,060 |
| South Asia | 8.3S - 40.6N | 66.1E - 134.9E | 16,124,416 |
| Australia | 44.3S - 11.2S | 110.1E - 155.6E | 7,797,824 |

## B. Accuracy assessment

Accuracy assessment, both temporal and spatial, of classification coarse resolution imagery is normally done by comparison with independent finer resolution imagery classifications of a sampled proportion of the study area. High resolution burned area mapping prior to year 1999 is almost non-existent and the development of a significant set of fine resolution maps covering the entire series and multiple fire regimes would be valuable, but falls outside the scope of this study. In this study, we relied on other independent information sources. Most information on burned areas is in the form of annual statistics or maps developed by national fire departments or forest management agencies [71]. Recently, several regional burned area maps were developed [72], [73] for ecological studies based on coarser spatial resolution remote-sensing imagery. Accuracy analysis was conducted using three different approaches: annual comparison of burned areal estimates with a set of documented statistics; comparison of burned area cell proportions with different burned area classification maps derived from remote sensing imagery; and comparison of global estimates with recent global burned area products covering different years derived with higher resolution imagery. All the data used in this analysis were produced and published in independent studies and their details are summarised in the following paragraphs.

*1) Annual comparison:* Burned area statistics by country, or region, are often reported by total affected area during each fire season. Additional information is sometimes provided, indicating individual fire size, location or occurrence. This information comes mainly from governmental forestry agencies or fire departments, and combine GPS measurements and fire fighter reports. This information is valuable for comparison in terms of season severity and inter-annual trend identification. Most of the documental information was obtained from the Global Forest Fire Assessment (FRA2000) report and the International Forest Fire News (IFFN) reports available at www.fire.uni-freiburg.de/iffn/iffn.htm. For Portugal the annual burned area estimates derived from fine resolution burned area maps [3]. For Canada, annual amounts were calculated from the Canadian Large fire database compiled by [74]. Detailed information for each area is given in Table III.

*2) Spatial comparison:* Overlaying coarse and fine spatial resolution data can be a problem due to spatial mismatch. To avoid generating additional errors due to geographical displacements, dataset comparison at two different resolution sources is usually based on burned area proportion in larger grid cells covering the entire target area [75]. A regression equation can then be fitted between the two maps, providing an assessment of underestimation or overestimation. For this study, we overlayed burned area proportions in 45 by 45 km cells, which represent a five by five 8km pixels block, between the LBAP-PAL classification and the finer-resolution burned area classifications. The selected independent burned area products used (Table IV) were also based on the original 1.1km AVHRR sensor, covering large areas and several years. As shown in part one of this study, the NOAA satellites suffer from orbital drift but, the effect is expected to be almost insignificant for the northern hemisphere products. In the case of the Australian burned area maps, the drift effect can be significant and caution be must be taken in the interpretation of the results. For each study region, a regression was fitted for the full period and proportion extremes of underestimation and overestimation were analysed.

*3) Global burned area products comparison:* The following analysis not only evaluates the LBAP-PAL classification accuracy at the continental level, but aims to verify if the

TABLE III
BURNED AREA ESTIMATES BASED ON COUNTRY STATISTICS AND OTHER REPORTS USED FOR ANNUAL BURNED AREA ESTIMATES COMPARISON TO THE LBAP-PAL PRODUCT.

| Continent | Countries | Area($km^2$) | Source | Time-frame | Website link |
|---|---|---|---|---|---|
| Europe | Portugal | 92,090 | National Forestry Authority, Ministry of Agriculture, Portugal | 1984-1999 | www.afn.min-agricultura.pt |
| | Spain | 505,992 | National Forest Fire Service, Ministry of Environment, Spain | 1990-1999 | http://www.unece.org/timber/ff-stats.html |
| | Southeasthern Europe (Greece, Turkey, Albania, Croatia and Italy) | 1302123 | Forest Resources Assessment Programme, Working Paper 55 | 1991-1999 | http://www.unece.org/timber/ff-stats.html |
| North America | USA | 9,372,610 | National Interagency Fire Center | 1981-1999 | http://www.nifc.gov/fire_info/fires_acres.htm |
| | Canada | 9,970,610 | Canadian Large Fire Database (LFDB) | 1981-1999 | http://cwfis.cfs.nrcan.gc.ca/en~CA/lfdb |
| South America | Chile | 756,096 | Fire Control Programme Statistical System, CONAF | 1981-1999 | http://www.conaf.cl |
| | Argentina | 2,780,092 | Forest Resources Assessment Programme, Working Paper 55 | 1993-1999 | http://www.unece.org/timber/ff-stats.html |
| Asia | Russia | 17,075,400 | Forest Resources Assessment Programme, Working Paper 55 | 1986-1999 | http://www.unece.org/timber/ff-stats.html |
| | Mongolia | 1,564,116 | Forest Resources Assessment Programme, Working Paper 55 | | |

TABLE IV
CONTINENTAL BURNED AREA PRODUCTS USED FOR SPATIAL BURNED PROPORTION COMPARISON WITH THE LBAP-PAL PRODUCT.

| Continent | Country | Area ($Mkm^2$) | Period (years) | Imagery | Spatial Resolution | Reference |
|---|---|---|---|---|---|---|
| North America | USA, Canada | 9.984 | 1989-1999 | AVHRR HRPT and LAC | 1.1km | [73] |
| Asia | Russia | 17.075 | 1996-1999 | AVHRR HRPT and LAC | 1.1km | [72] |
| Australia | Western Australia and Nothern Territory states | 4.067 | 1996-1997 | AVHRR | 1.1km | http://138.80.128.152/nafi2/ |

annual burned area estimates is in the range of values obtained by other recent products and, serves to check if no residual trend persists. In this approach, burned area averages are compared with averaged estimates derived from recent burned area products based on remotely sensed data acquired over the last decade. The three main products are; the Global VGT burnt area product 2000 (GBA2000) [9], [10], [6] assessment based on SPOT-VEGETATION imagery for the year 2000, the MODIS Burned Area Product (MCD45) collection 5 [12], [11], [13] based on MODIS imagery from 2001 until 2009; and the Global Fire Emissions Database version 2 (GFEDv2) [76], based on active fire information which is converted to burned cell proportions, covering the period from 1997 to 2006. Details for each product are given in table V and additional information can be found on each product website.

In order to establish a lower limit on the potential underestimation effect that results from resampling procedures [77], the MCD45 product was re-sampled into an 8km resolution. The applied resampling procedure was as follows: conversion to 1km was based on majority vote on each two by two 500m MODIS pixel block, followed by the GAC re-sampling procedure where four out of five pixels every three lines were subject to a majority vote, followed by a random selection of each two by two 4km GAC pixel block, to represent the potential PAL 8km product. The final classification maps (MCD45re) would represent a conservative scan approach indicating the highest possible underestimation solely based on the resampling effect.

## IV. RESULTS

### A. Classification algorithm

In total, 23702 training data pixels were selected, of which 23% represent burned pixels and 76% represent unburned pixels. The Random Forest classifier was developed based on the training data and tuned for 1000 trees and for two randomly selected variables at each split node. The out-of-bag (OOB) error rate was 4.52% (Table VI)

TABLE VI
CONFUSION MATRIX BASED ON THE CLASSIFICATION OF THE OUT-OF-BAG SAMPLES.

| type | burnt | unburnt | class error |
|---|---|---|---|
| unburnt | 17687 | 368 | 0.02 |
| burnt | 703 | 4944 | 0.12 |

Variable importance estimate for the training data can be seen in figure 1.Variable importance, determined by the mean accuracy decrease, showed that the most important variables were surface temperature, GLC2000 land-cover class, GEMI monthly difference and surface temperature monthly difference and GEMI. The less important variables were the albedo and albedo monthly difference.

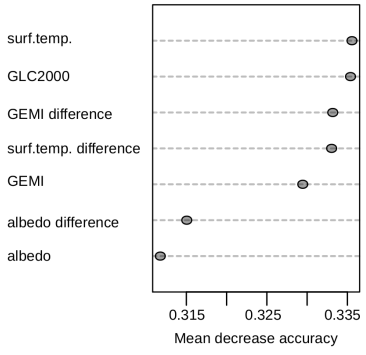


Fig. 1. Random Forest algorithm evaluation for variable importance as result of a random permutation of the values in the out-of-bag samples.

TABLE V
GLOBAL BURNED AREA PRODUCTS USED FOR GLOBAL AND REGIONAL AVERAGE COMPARISON WITH THE LBAP-PAL PRODUCT.

| Product | Sensor | Satellite | Spatial Resolution | Time-frame | Website |
|---|---|---|---|---|---|
| GBA2000 | VGT | SPOT-VEGETATION | 1km | 2000 | http://bioval.jrc.ec.europa.eu/products/burnt_areas_gba2000/global2000.php |
| GFEDv2 | ATSR and MODIS | ENVISAT, TERRA and AQUA | 0.5 degree | 1997-2006 | http://daac.ornl.gov/VEGETATION/guides/global_fire_emissions_v2.html |
| MCD45 | MODIS | TERRA and AQUA | 500m | 2001-2009 | http://modis-fire.umd.edu/Burned_Area_Products.html |

### *B. Burned Area Classification*

The LBAP-PAL annual estimates of global burned area showed considerable variability. On average, considering the full 19-year dataset, a total of $1.4Mkm^2$ burned every year. This value rises to $1.9Mkm^2$ when not considering the incomplete years of 1981 and 1994. Although no statistical significant trend exists, the annual time series showed a rising trend from 1981 onward until 1990 reaching the maximum, followed by a quick decrease to an averaged $1.4Mkm^2$ until 1999 (fig.2). The highest and lowest global burned area values were recorded on 1990 and 1988 with values of 1.90 and 1.04 $Mkm^2$, respectively.

The monthly series for the eight study regions were also characterised by annual variations characteristic of each region fire regime (fig..3). The North America region, with an average amount of 20,400$km^2$, represents only 1.5% of the global burned area. The monthly time series shows a peaking August and lower values for the rest of the fire season months (fig.3a). Year 1986 and 1999 recorded the higher values and 1985 and 1992 the lower values. The fire season can start in July and end in October, but most of the burn detection occurs in August (fig.4a). In July, fire normally occurs in the Canadian province of Quebec and in some small parts in the boreal forest belt (fig.5). In August, fires are mainly located around the boreal belt and the remaining season fires are localised in an area between the Idaho and Montana US states and the Canadian provinces of Alberta and British Columbia. Small, scattered fires were also detected throughout the study region but the only off season fires were detected in the US Florida State during April. On average, BF is one but there are some exceptions, with pixels that burned twice or three times during the study period (fig.6). Most of the detected burned areas were dominated ($>$60%) by the TNE land-cover class and some minor occurrences were observed in the TBE and the Mosaic Tree Cover classes (M) (fig.7a). Regarding the land-cover distribution of the entire study region, fire tends to select TNE, M class and avoid the remaining ones.

In the South American region, the average burned area is 54,800$km^2$ representing 3.9% of the global extent. Large inter-annual differences are highlighted, not by a particular month, but by an increase during the entire season. Year 1992 records the lowest values and year 1993 the largest values of area burned (fig.3b). The annual burned area time series reveals no significant trend, but form an oscillating pattern (not shown). This region is characterised by year-round fire activity, divided into two main fire seasons. The first, larger in terms of areal extent (fig.4b), occurs from August to October, in the Amazon deforestation-arc, over the Brazilian state of Mato Grosso and extending south to the Paraguay and east to the Atlantic coast (fig.5). The other season runs from January to March over the Venezuela-Colombia savanna, in the Argentinian Neuquen province and some burned surfaces in December over the Brazilian state of Roraima. The results show that the most frequent burned land cover classes are the TBE, HRB and the CM, which amount to 65% of the area burned in this region (fig.7b). Of these, only the TBE has a higher areal percentage than burned percentage. The HRB and CM have higher percentages of burned area than region area. An interesting result is that the TBDC land-cover class accounts for 10% of the area burned but is only present in 5% of the continent. Most pixels in the south American region burn only once, with exceptions noted for the HRB class, where values can reach three times (fig.6).

For the Northern Africa study region, the mean area burned was 0.76$km^2$ representing 54,8% of the total global area. Annual time-series showed no significant trend with the higher recorded year in 1990 and the lowest in 1985 (fig.3c). Burned activity is considered very regular; the fire season starts in October in the Sahel at the higher latitudes and burns continuously expanding further south until March (fig.4c, fig.5). The TBDO and the SCD classes record the higher percentages, totalling more than 57%, of the burned area (fig.7c). The other land-cover classes, like the some types of mosaics (MSG and M), HRB, CM and TBDC, are also present but are less representative. When compared to the region total area extent, both the TBDO and SCD are the least representative. High BF values are easily recognised, located over the Sudan-Central African Republic border, characterised by the SCD land cover class (fig.6). The average BF for this region is three times but values can reach a maximum of 15 times.

The Southern Africa region is characterised by an average of 316,100$km^2$ of burned area representing 21,4% of the global extent. The larger detected values correspond to years 1985, 1989 and 1990 and the lowest years are 1988 and 1992 (fig.3d). Although the region exhibits large variability, it displays no significant trend (not shown). Fire season can be quite long ranging from June through September, between Angola and Democratic Republic of Congo, and from September to November on the eastern part of the region, affecting countries from Tanzania to South Africa, Zambia, Zimbabwe and Madagascar (fig.5d, fig.4). There are also some minor detections in the Cape province of South Africa during December through March. Most of the burned area occurs in the TBDO class (35%) followed by the SCD, TBDC, HRB, CM and finally the TBE (fig.7d). Compared to the corresponding regional percentages, the TBDO and TBE show the larger differences, the TBDO extent being considerable lower and the TBE higher. Most of the detected areas have an average BF values of two times (fig.6), but for all land covers, minor exceptions of pixels with values above 10 were observed.

In the North Asia study region, an average of 70,000$km^2$

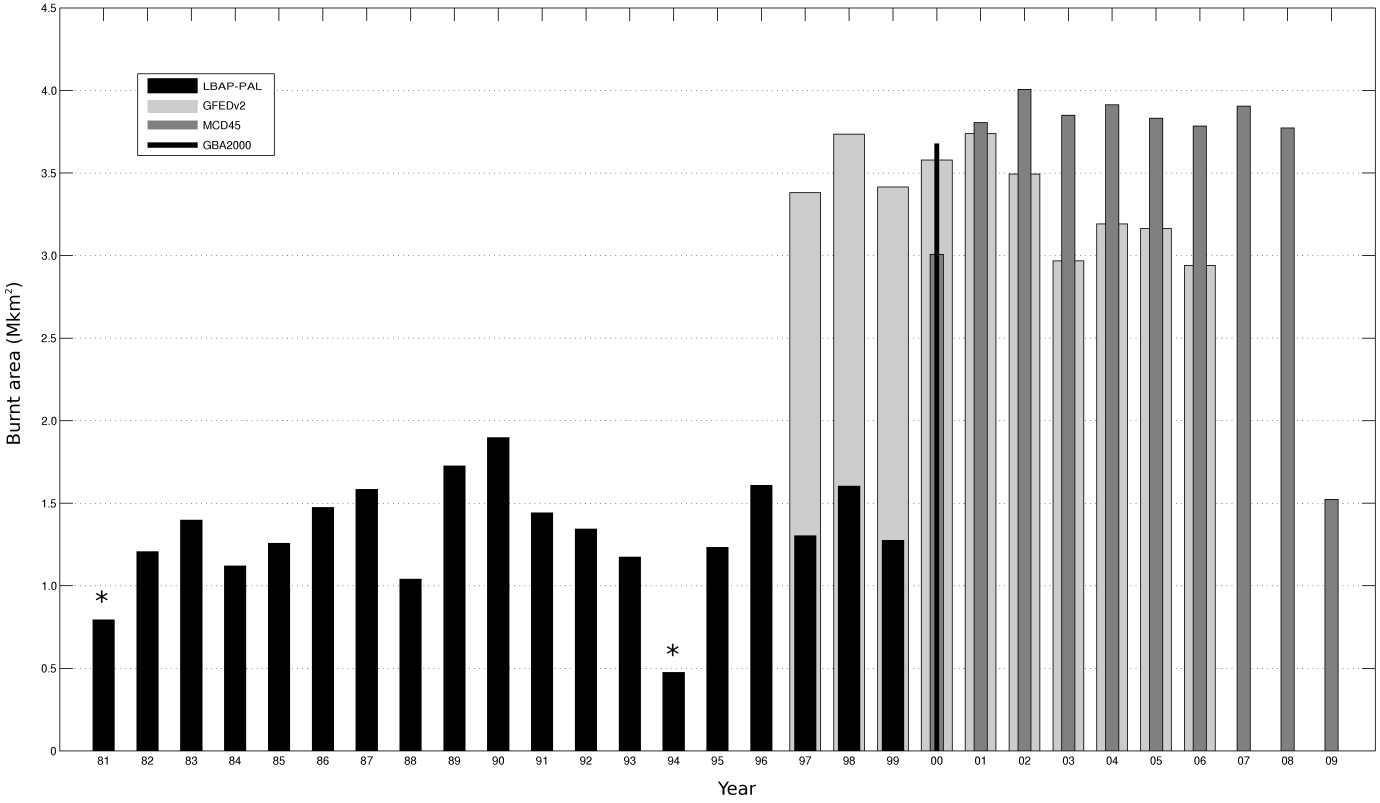


Fig. 2. Global annual burned area estimates for the LBAP-PAL, GFEDv2, GBA2000 and MCD45, covering the period from 1981 to 2009. LBAP-PAL incomplete years are marked by $*$.

burned annually, which represent 5% of the average detected global burned area. Years 1987 and 1996 record the larger annual burned area and years 1985 and 1992 the lower values. During the full study period no significant trend was recorded (fig.3e). Fire seasonality displays two distinctive periods (fig.4e). From April to June, burned areas were detected over the lower latitudes along the Mongolia-China border, and in central Asia, from July to September extending to the higher latitudes in eastern Russia (fig.5). There were also some detections in August and September in central Asia, north of the Caucasus region. The TND and CM land cover classes represent areas with high burnt percentages, followed by the SCD and HRB classes which in total account for 66% of the burned area. In comparison to the region extent, the TND, SHSS and HRB land-cover classes reveal the larger differences, i.e., the TND is significantly less represented in the region and highly represented in burned extent and, both SHSS and HRB are least represented in the burned extent than in the region areal extent (fig.7e). Most of the region burned only once, but some minor exceptions were detected over the HC and SCD classes (fig.6).

The South Asia study area is characterized by an average of 70,000$km^2$ burned annually, representing 4.7% of the global burned extent. Annual amounts showed a significant increasing trend, as determined by the Mann-Kendall test. The years of 1989 and 1993 represent the larger extents and 1983 and 1992 the smaller extents (fig.3f). The results also show year-round burn activity with major events occurring in January-February over Southeast Asia, in Thailand, Kampuchea and Vietnam, and from March to April in Central and North India, Myanmar and Malaysia (fig.4f, fig.5). Small areas were also detected over Indonesia, in Sumatra and Borneo, from July to November, and in southern China and west India in October-December. Burned land-cover is mainly characterized by CM, TBDC and TBE representing 64% of the burned area. The remaining burned areas are on SCD, SCE and MCTCN land-covers (fig.7f). Compared to the region areal extent, the TBDC shows the larger difference, which indicates the preference to burn more that the other classes. Most of the area burned for this region showed BF values below two times (84%), and exceptions are mostly noted in India and Kampuchea where values can reach as high as seven times (fig.6).

For the Australia study region, the average annual burned area was 100,000$km^2$, which represents 7% of the average global burned area. The annual time-series does not show any significant trend and years 1983, 1989 1990 and 1996 record the highest values and 1991 and 1992 the lowest values (fig.3g). Fire season is year round, with the maximum areal extent recorded in October (fig.4g). From July to November burning occurs in the northern latitudes, over Kimberley in Western Australia, Arnhem Land in the Northern Territories, Cape York Peninsula in Queensland and extending south to New South Wales over the Great Dividing Range. November through May fires occur over the south tip of Western Australia and mainly in January and February over Victoria State and April-May in Tasmania (fig.5). The dominant burned land-

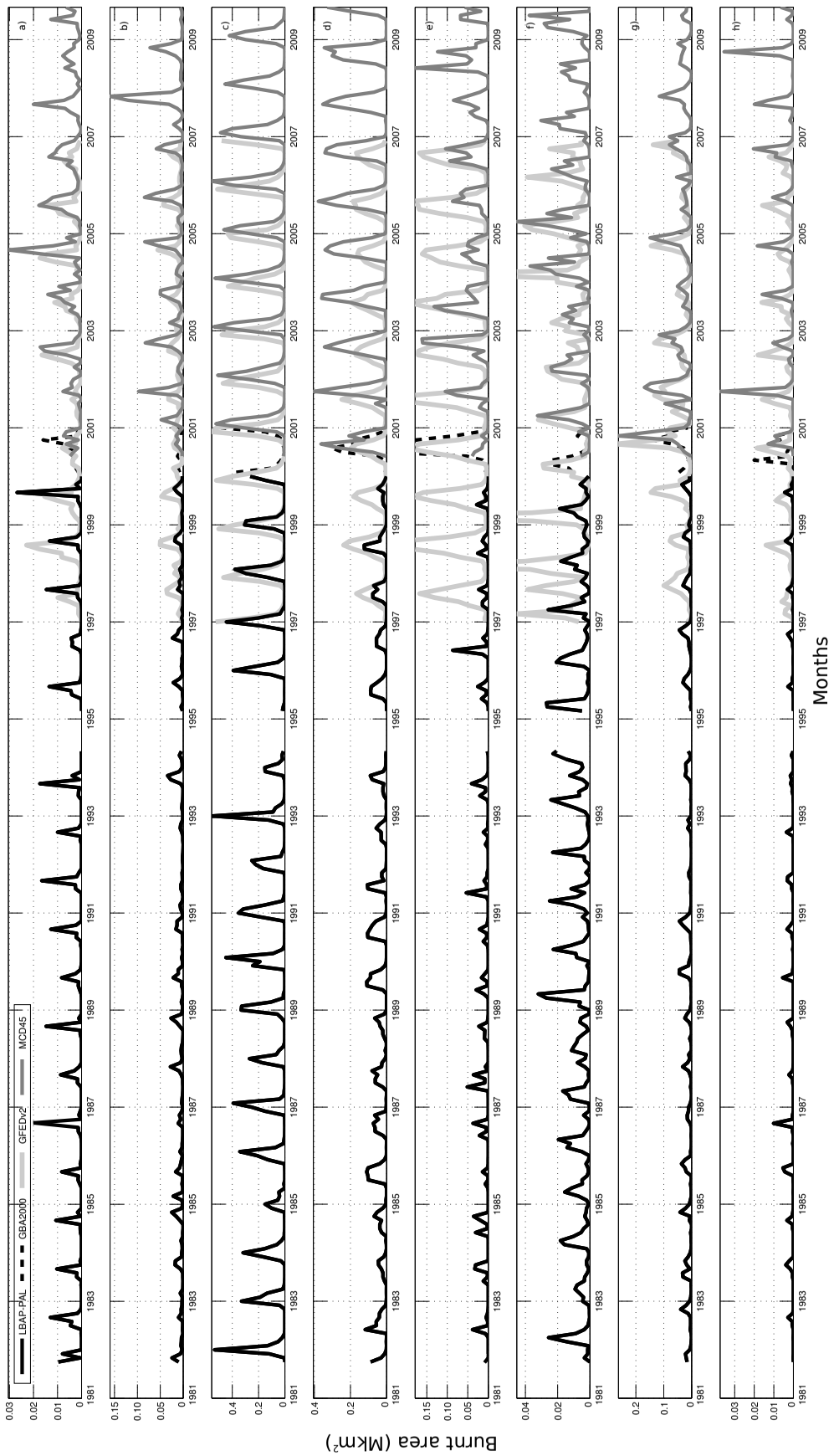


Fig. 3. Burned area monthly time-series for the a) North America, b) South America, c) North Africa, d) Southern Africa, e) North Asia, f) South Asia, g) Australia and h) Europe study region for the LBAP-PAL, GFEDv2, GBA2000 and MCD45 global burned area products.

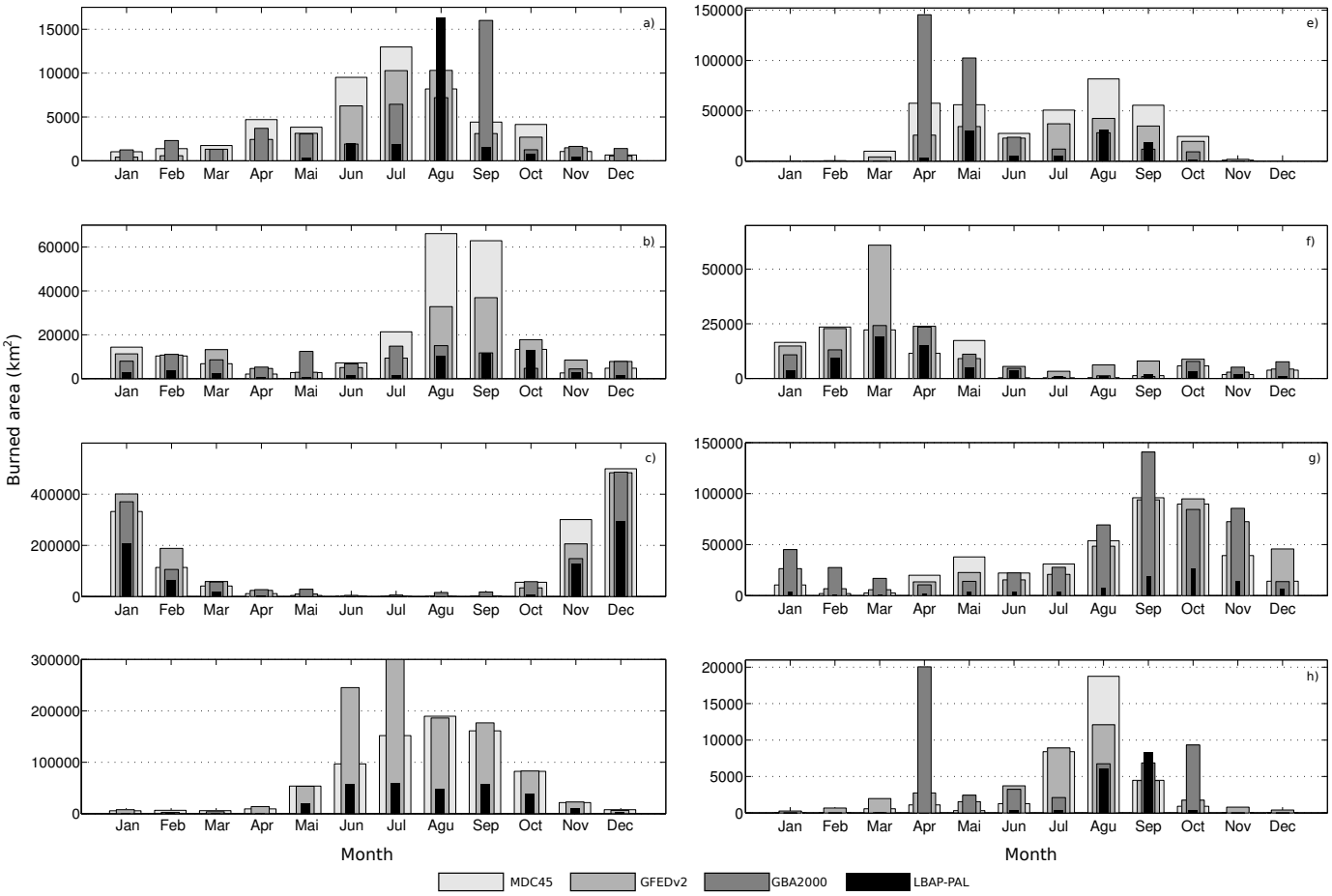


Fig. 4. Monthy averaged burned area for the a) North America, b) South America, c) North Africa, d) Southern Africa, e) North Asia, f) South Asia, g) Australia and h) Europe study region for the LBAP-PAL, GFEDv2, GBA2000 and MCD45 global burned area products.

covers for this region are the SCD, TBDO, TBE and HRB classes, which correspond to 93% of the total area burned. For all, except the HRB burned area percentage is higher than the corresponding region areal extent (fig.7g). More than half of the fires (60%) have BF values of one time except in the north where values can reach six times (fig.6).

The European study region shows the smallest contribution to the global burned area amounts (0.5%), totalling an average of only $6000km^2$ were no significant annual trend was detected. The years 1986 and 1985 represent the larger extents of burned area and 1987 the lowest (fig.3h). Fire season is relatively short, with most of the burning activity occurring in August and September (fig.4h). Burned areas were detected in the Iberia Peninsula between August and October, on the southern European countries, Ukraine and near the northern shores of Morocco in August, and in western Russia during September (fig.5). Burned land-cover was characterised by TBDO and SCD (49%), with minor contributions of the TBDC, M and CM classes (fig.7h). Regional extents showed that, although dominated by CM class, it is the TBDO class that reveals the largest difference with the burned area percentage. All burned areas burned only once, with some exceptions in parts of the Iberia peninsula where BF values reach three times (fig.6).

### C. Accuracy Assesment

*1) Annual comparison:* For Europe, the 15 years of comparable data in the Portuguese database shows a correlation of 0.75 and a mean 15% overestimation error (fig.8a). The less accurate years are 1986, 1987 and 1989 with underestimation and years 1996, 1997 and 1999 with overestimation. For Portugal the LBAP-PAL successfully detects years of large burned areas. For Spain, the ten year comparison, resulted in a 0.28 correlation coefficient and a mean 32% overestimation error. There is large overestimation ($>$50%) for the years 1993, 1996 and 1999 and large underestimation ($>$50%) for the years 1992, 1994 and 1995 (fig.8b). The spatially aggregated southern Europe countries, with only 9 years for comparison, showed to be dominated by underestimation with a mean 50% underestimation error and a correlation coefficient of 0.36 (fig.8c). LBAP-PAL shows fails to detect large burned area years, like 1992, 1992 and 1994. For North America, the comparison with the USA National interagency forest service statistics, covering the full 19 year period, highlights the LBAP-PAL limitations in detecting seasons with large burned areas (fig.8d). It fails to detect annual amounts above $20{,}000km^2$ but it appears to follow the annual tendency. The mean detection error is -26% and the correlation coefficient is 0.27. For Canada (fig.8e), similar results revealed a ten-

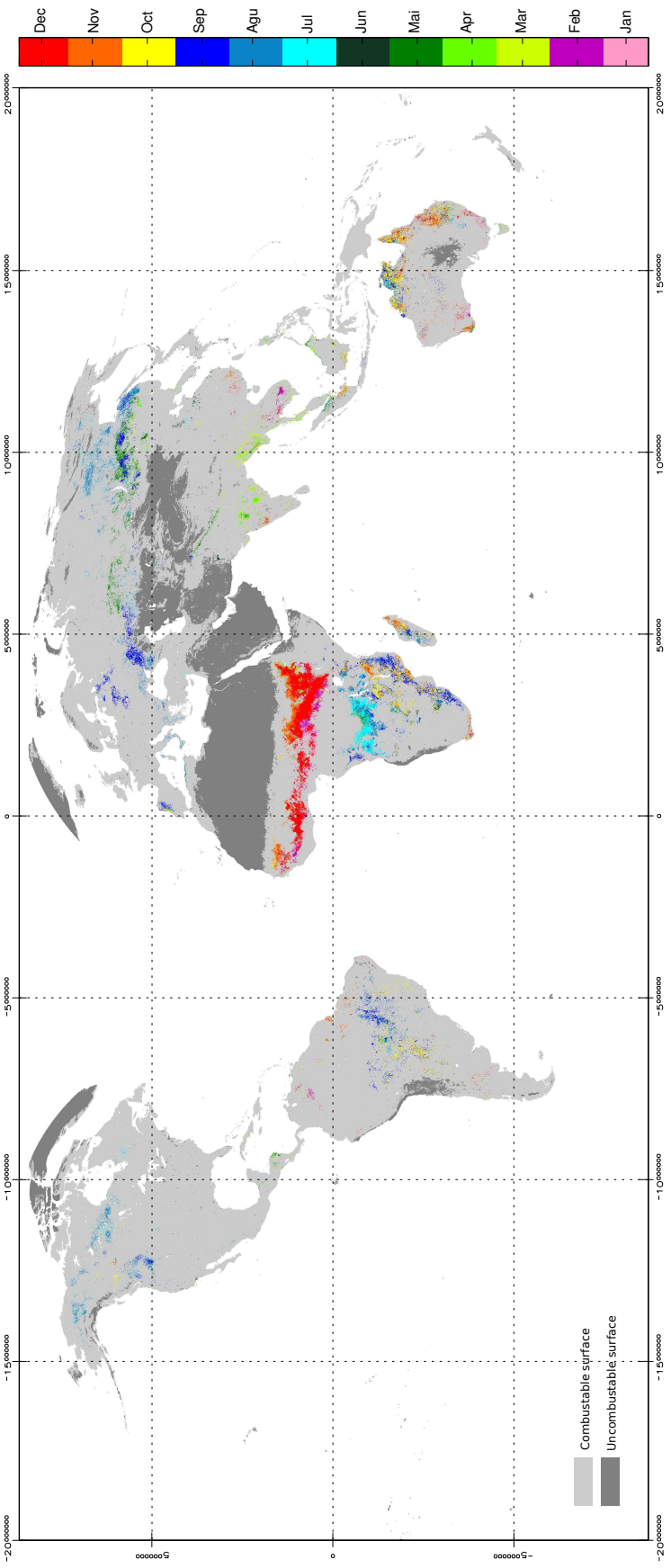


Fig. 5. Month of the highest number of burnt detections derived from the LBAP-PAL product, covering the period from 1981 to 2009.

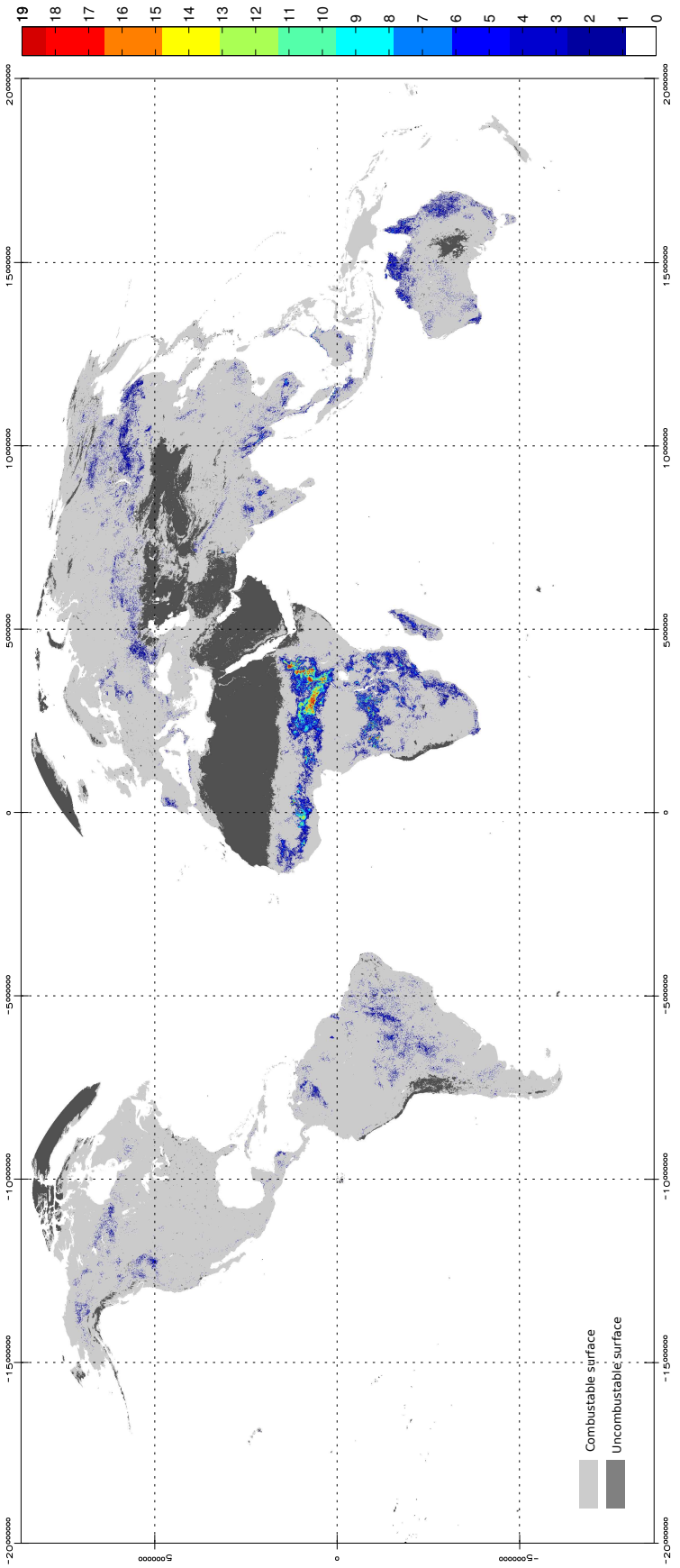


Fig. 6. Number of detections a pixel was classified as burned by the LBAP-PAL product during the period from 1981 to 2009.

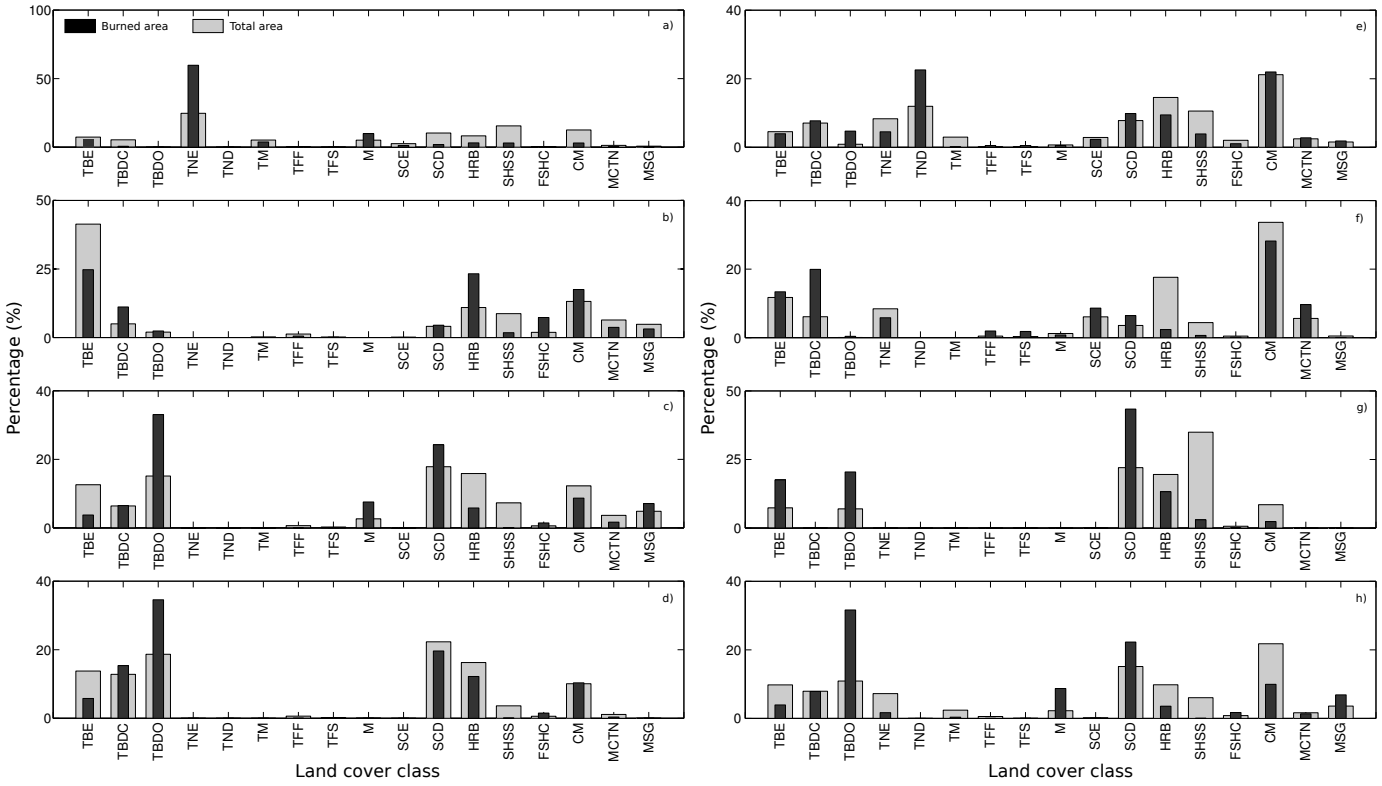


Fig. 7. Land cover class distribuition for the a) North America, b) South America, c) North Africa, d) Southern Africa, e) North Asia, f) South Asia, g) Australia and h) Europe study region for the LBAP-PAL, GFEDv2, GBA2000 and MCD45 global burned area products.

dency for underestimation in years when burned area exceeds 15,000$km^2$. The correlation coefficient is 0.19 and there is a mean underestimation of 14% error. The larger underestimation is mainly contributed by years 1989, 1995 and 1998. In South America, for Chile and Argentina (fig.8f,g), the LABP-PAL shows similar results by underestimating years with large burned areas amounts. In spite of these limitations, the LBAP-PAL follows the annual tendency, with overestimation exceptions for the year 1997. Average detection error is -45% and -41% and correlations were 0.48 and 0.78, for Chile and Argentina, respectively. For Asia, in Russia and the former USSR (fig.8h), the 14 years comparison with the LBAP-PAL shows contradicting results. Prior to 1991, there is large overestimation, and afterwards underestimation predominates. This resulted in an average overestimation error of 250% and a low correlation of 0.01. For Mongolia (fig.8i), the correlation is higher reaching 0.8 with an average underestimation error of -43%. After 1996, statistics show higher values that are supported by the LBAP-PAL results and overestimation only happens for years 1981, 1983 and 1995.

*2) Spatial comparison:* Comparison between the three remote sensing products and the LBAP-PAL product exhibit distinctive relations between the northern hemisphere products (North America and Russia) and the southern hemisphere product (Australia). For North America (fig.9a), the LBAP-PAL product fails to detect the higher burnt cell proportions, resulting in underestimation. Misdectecions, composed of undetected cells proportion by the LBAP-PAL, account for 83% of the data. Of these, 90% have burned proportions less than 0.1 in the less coarser resolution product. Overestimation also occurs and 85% of the cases are below the 0.2 burned proportion of the coarser resolution product. Considering only LBAP-PAL burned cells with burnt proportions above zero, for the period between 1989 and 1999 excluding 1994, correlation values range between 0.30 (1990) and 0.74 (1997) resulting an average value of 0.39. Similar results are obtained in the comparison between the LBAP-PAL and Russia product cell proportions (fig.9b). Underestimation affects not only the lower proportion cells, where misdetection account for 87% of the data, and 90% fall below the 0.1 coarser resolution cell proportion, but low accurate detections were also shown for cells with higher burned proportion, occurring only during the year 1998. Again, overestimation only affects the partially low burned cells, where 87% of the cases are below the 0.2 coarser resolution burnt proportion. The averaged correlation coefficient is 0.17 with the highest value of 0.28 recorded for year 1996. For the Australia, burnt cell comparison results differ (fig.9c). Not only is the correlation coefficient higher (0.4) but overestimation is almost non existent ($<$2.4%) and LBAP-PAL shows higher ability in detecting burning thoroughly different burnt cells porportions. Although underestimation is always present along the full range of cell proportions, complete miss-detections account for less than 72% of the number of cells, of which 42% and 60% are below 0.1 and 0.2 cell proportion, respectively. The rare cases of overestimation are dominated (85%) by burnt cell proportions below 0.2.

*3) Global products estimate comparison:* The LBAP-PAL estimates show some similarities with the other three global

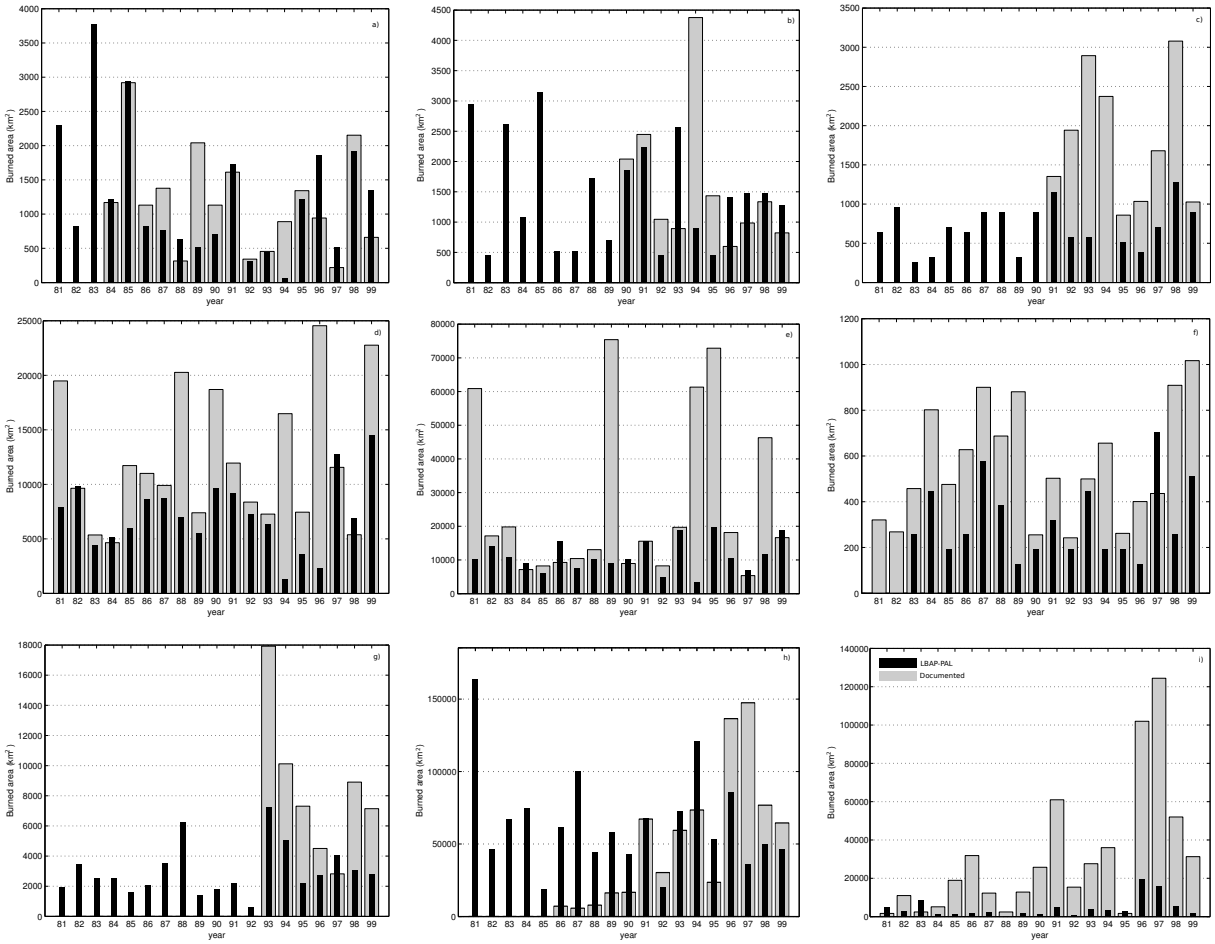


Fig. 8. Annual burned area estimates for a) Portugal, b) Spain, c) Southern Europe, d) USA, e) Canada, f) Chile, g) Argentina, h) Russia and i) Mongolia.

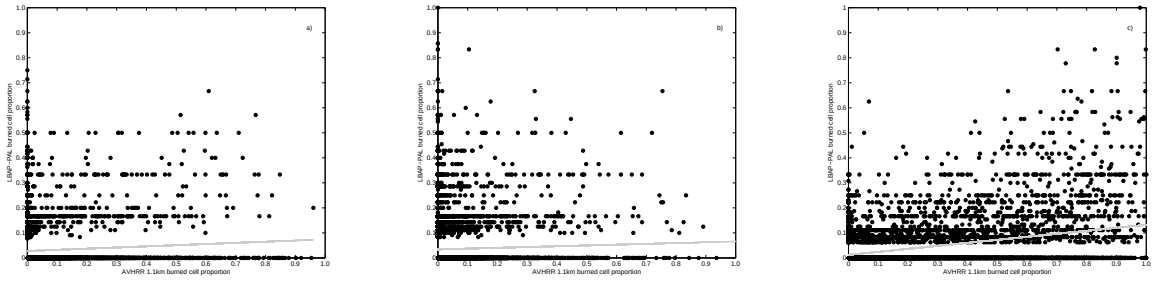


Fig. 9. Spatial comparison of burned cell proportion between the LBAP-PAL and a) North America, b) Russia and c) Australia burned area products.

burned area products. On average, global the LABAP-PAL estimates revealed to be -57.85%, -61.69% and -63.63% than the GFEDv2, GBA2000 and MCD45 products, respectively (Table VII). Using the same geographical region extents (Table II), the aggregated estimates vary with region and product. The smaller differences are of -45% with the GFEDv2 product for the North American region and -42% and 37% with the GBA2000 and MCD45 South Asia region. On the other hand, the larger differences are -84%, -87.6% and -82.46%, with the GFEDv2, GBA000 and MCD45 products for the European study region.

The averaged spatial distribution of each product estimates shows interesting results. Both the LBAP-PAL and the GFEDv2 product show a larger differences between the African northern hemisphere and southern hemisphere, where the northern region assumes the larger areal extent of 54.76% for the LBAP-PAL and 42.68% for the GFEDv2. For GBA2000 and the MCD45 products, both African hemispheric region show similar areal extents, 30.21% and 36.49% for the GBA000 and 33.26% and 35.59% for MCD45.

The comparison between the LBAP-PAL and the re-sampled MCD45 product (MCD45re) showed that LBAP-PAL detects almost twice as much as the MCD45re. The larger differences ($>$1000%) were observed for both the two African and the

TABLE VII
GLOBAL BURNED AREA PRODUCTS AREAL ESTIMATES, REGIONAL BURNED FRACTIONS AND CORRESPONDING LBAP-PAL RELATIVE FRACTION (PALF)

| | **LBAP-PAL** | | **GFEDv2** | | | **GBA2000** | | | **MCD45** | | | **MCD45re** | | |
|---|---|---|---|---|---|---|---|---|---|---|---|---|---|---|
| Study region | ($Mkm^2$) | (%) | ($Mkm^2$) | (%) | PALf | ($Mkm^2$) | (%) | PALf | ($Mkm^2$) | (%) | PALf | ($Mkm^2$) | (%) | PALf |
| North America | 0.0201 | 1.44 | 0.0426 | 1.29 | -52.82 | 0.0475 | 1.31 | -57.68 | 0.0536 | 1.40 | -62.51 | 0.0137 | 1.86 | 46.72 |
| South America | 0.0548 | 3.94 | 0.1607 | 4.87 | -65.90 | 0.1103 | 3.04 | -50.32 | 0.2145 | 5.61 | -74.45 | 0.0184 | 2.50 | 197.83 |
| Southern Africa | 0.3163 | 22.73 | 0.7887 | 23.89 | -59.90 | 1.0974 | 30.21 | -71.18 | 1.2724 | 33.26 | -75.14 | 0.0204 | 2.77 | 1450.49 |
| Northern Africa | 0.7621 | 54.76 | 1.4094 | 42.68 | -45.93 | 1.3254 | 36.49 | -42.50 | 1.3616 | 35.59 | -44.03 | 0.0338 | 4.59 | 2154.73 |
| North Asia | 0.0694 | 4.99 | 0.2238 | 6.78 | -68.99 | 0.3328 | 9.16 | -79.15 | 0.3645 | 9.53 | -80.96 | 0.1036 | 14.07 | -33.01 |
| South Asia | 0.0658 | 4.73 | 0.1704 | 5.16 | -61.38 | 0.1104 | 3.04 | -40.40 | 0.1047 | 2.74 | -37.15 | 0.0044 | 0.60 | 1395.45 |
| Australia | 0.0969 | 6.96 | 0.4670 | 14.14 | -79.25 | 0.5581 | 15.36 | -82.64 | 0.4188 | 10.95 | -76.86 | 0.5294 | 71.91 | -81.70 |
| Europe | 0.0063 | 0.45 | 0.0394 | 1.19 | -84.01 | 0.0508 | 1.40 | -87.60 | 0.0359 | 0.94 | -82.46 | 0.0125 | 1.70 | -49.6 |
| **Global** | **1.3917** | | **3.302** | | **-57.85** | **3.6327** | | **-61.69** | **3.8261** | | **-63.63** | **0.7362** | | |

south Asia regions and underestimation for the north Asia, Australia and European regions. In comparison with the other burned area products, regional burned proportions for the MCD45re is totally dominated by the Australian region.

## V. DISCUSSION AND CONCLUDING REMARKS

With considerably small overall error, the random forest classification performed well at capturing key combinations of spectral changes related to burning. Variable importance, dictated by of the RF classifier, highlights the powerful tool of using land-cover as a discriminator factor. It can be argued that the land cover map used, the GLC2000, corresponds to a later date than the studied period, and land cover changes during the full period are not contemplated. Although true, the spatial aggregation into 8km pixels can smooth these differences, and only changes above $32km^2$ (half the 8km pixel) might lead to land cover classification error. As for multi-year global burned area maps, global multi-year land cover maps are non existent. At a global scale, land-cover changes are known to be attributed to agriculture or deforestation practices. These normally affect the tropical forest or the mid latitudes where fires have small dimensions. Nevertheless, the results show that not only is the land-cover class setting the vegetation GEMI range, but change can also be observed. Inclusion of a probabilistic fire climatology to revise the burned classification probabilities helped to reduce false alarms. This was achieved by scaling the detections with the climatological-like fire season probabilities and not by restricting the area under revision. Annual global burned area showed variability that is hard to confirm due to lack of comparable records. The last 3 years of the LBAP-PAL, 1997 to 1999, coincide with the variation observed by the GFEDv2, but the small period is not enough to extrapolate the validity of the observed variation for the previous period. Severe ENSO years, which are know to cause exceptional burning activity, do not stand out. This clearly indicates a lack of detection that, in part, can be attributed to thick smoke released by tropical forest burning under ENSO influence, like the tropical forest of the Amazon and Indonesia and Boreal forests of the Siberian Far East. Land-cover class differences, between each regional burnt area percentage and the regional total combustible percentages, suggests human influence in the form of deforestation and agricultural fires. For North America, Australia and Europe regions, fire incidence in CM land-cover is much lower than for the both Asian, African and South American regions. This indicates differences in the use of fire as an agricultural tool. The remarkable difference observed for the TBDC class, in South America, South Asia and Southern Africa is suggestive of tropical deforestation fires. Burned area extents depend on many factors, but annual variability is mostly associated with climate variability, since land cover and demographic dynamics tend to have slower trends. Severe meteorological conditions stressing vegetation will favour fire ignition situations and increase fire intensity and severity, contributing to higher burned area extents. These environmental conditions depend, directly or indirectly, on climate and its variability. Based on this, regions that exhibit high annual burned area variability can be considered to have higher correlation with climate variability, whereas regions with low annual variability depend less on climate or have lower climatic variability. Our results allowed to differentiate between regimes where annual variability is high and regimes where it is low. The North African region shows regular annual results, with high burned area extents and low inter-annual variability. This result can imply low climatic variability. On the other hand, in North America and North Asia, climate can have a higher influence leading to higher annual variability. The LBAP-PAL is characterised by large underestimation of regional and global burned area. These results were expected and in part attributed by the low PAL data coarse resolution and re-sampling scheme [77]. The high level of misdetections found in the spatial burned area product comparisons is linked to the PAL's re-sampling procedure that represents an 8km x 8km area, using only four 1.1km pixels out of the possible 57, representing only 7% of the information. This low data sampling rate, easily leads to underestimation of the full range of fire scars sizes, overestimating small scars and miss detecting the smaller scars. In [77], the authors highlighted this feature and showed that fires below 100ha are more difficult to detect with coarser resolution products like the AVHRR, GAC and especially the PAL product. The same study also shows that fires above 10,000ha represent more than half the area affected. Comparing with the 6,400ha of a PAL pixel, the detection achieved with the LBAP-PAL is considered a good result. Contribuiting to underestimation is also the GAC to PAL format procedure based on the the maximum NDVI pixel selection, out of the four possible pixels. This feature resembles the maximum NDVI compositing algorithm, which increases the probability of burned area underestimation for grasslands and shrub lands.

The PAL re-sampling scheme applied to the MODIS burned area product, applied in a simple form, showed that data re-sampling can have a severe effect on the outcome of burned area products. The spatial analysis with other burned area products suggest that this scheme can have a higher impact

on the higher latitudes by underestimation and overestimating small proportions of fires and misdetecting a large number of the smaller fires. For the tropics, due to the size of the scars, errors are dominated by underestimation. The severe underestimation found on the LBAP-PAL for the Australia window can be attributed to the 30 day compositing period. At theses latitudes, not only is vegetation already dry leading to a lower decrease in the albedo and GEMI, but is followed by a rapid increase as the char and charcoal is removed by wind revealing a bright soil underneath. As mentioned in part one of this study, the selected time period for compositing can be large causing the pre burnt dry or green vegetation to be replaced by a post burn bright soil.

Underestimation is not only a by-product of the re-sampling procedure. The classification algorithm can also be ineffective at detecting fire scars, under certain conditions. The spectral data available from the AVHRR lack the necessary information to detect scars under dense smoke. This could be addressed using the reflective component of channel 3 ($3.7\mu m$) data. Unfortunately, channel 3 saturates easily during the daily orbital passes and no orbital drift filtering was possible, which precludes its use. The LBAP-PAL provides 19 years of data, from July 1981 to December 1999, global monthly maps of burnt areas. The product is characterised by the large underestimations which makes it improper for areal extent analysis and pyrogenic emission estimation, and for research of low frequency severe fire-climate events, namely the ENSO events. Nevertheless, the product can be a valuable tool for characterising fire regimes, for low frequency climate-fire relation analysis and for comparison to future global burned area products covering the same period. This paper highlights the disadvantage of using remote sensed imagery products that suffered drastic spatial re-sampling. For future burned area mapping, based on the Long Term Data Record AVHRR product (LTDR); although with improved calibration corrections, one must be aware that, its data was derived not only from LAC but from GAC imagery.

## ACKNOWLEDGMENTS

The authors would like to thank the Portuguese Science Foundation for the financial sponsorship of Bernardo Mota through PhD grant (SFRH/BD/25119/2005) and the contribution made by all the different datasets used in this study.

## REFERENCES

[1] M. Andreaae, "Biomass burning- its history, use, and distribution and its impact on environmental quality and global climate," *Global biomass burning- Atmospheric, climatic, and biospheric implications(A 92-37626 15-42). Cambridge, MA, MIT Press, 1991*, 1991.

[2] A. Ito and J. E. Penner, "Global estimates of biomass burning emissions based on satellite imagery for the year 2000," *J. Geophys. Res.-Atmos.*, vol. 109, no. D14, p. 18, 2004.

[3] J. Pereira and M. Santos, "Fire risk and burned area mapping in portugal," Ministrio da Agricultura, DEsenvolvimento Rural e Pescas, Tech. Rep., 2003.

[4] P. M. Barbosa, J. M. Gregoire, and J. M. C. Pereira, "An algorithm for extracting burned areas from time series of AVHRR GAC data applied at a continental scale," *Remote Sensing of Environment*, vol. 69, no. 3, pp. 253–263, 1999.

[5] D. Stroppiana, J. M. Grgoire, and J. M. C. Pereira, "The use of SPOT VEGETATION data in a classification tree approach for burnt area mapping in australian savanna," *International journal of remote sensing*, vol. 24, no. 10, p. 21312151, 2003.

[6] J. M. Grgoire, K. Tansey, and J. M. N. Silva, "The GBA2000 initiative: Developing a global burnt area database from SPOT-VEGETATION imagery," *International Journal of Remote Sensing*, vol. 24, no. 6, pp. 1369–1376, 2003.

[7] S. Plummer, O. Arino, F. Fierens, G. Borstlap, J. Chen, G. Dedieu, F. Ranera, and M. Simon, "The GLOBCARBON initiative: multi-sensor estimation of global biophysical products for global terrestrial carbon studies," in *ENVISAT-ERS Symposium Proceedings, Salzburg, Austria*, 2004, p. 610.

[8] S. Plummer, O. Arino, M. Simon, and W. Steffen, "Establishing a earth observation product service for the terrestrial carbon community: The GLOBCARBON initiative," *Mitigation and adaptation strategies for global change*, vol. 11, no. 1, pp. 97–111, 2006.

[9] K. Tansey, J. M. Grgoire, E. Binaghi, L. Boschetti, P. A. Brivio, D. Ershov, S. Flasse, R. Fraser, D. Graetz, and M. Maggi, "A global inventory of burned areas at 1 km resolution for the year 2000 derived from SPOT VEGETATION data," *Climatic Change*, vol. 67, no. 2, pp. 345–377, 2004.

[10] K. Tansey, J. M. Grgoire, D. Stroppiana, A. Sousa, J. Silva, J. M. C. Pereira, L. Boschetti, M. Maggi, P. A. Brivio, and R. Fraser, "Vegetation burning in the year 2000: Global burned area estimates from SPOT VEGETATION data," *Journal of Geophysical Research*, vol. 109, no. D14, p. D14S03, 2004.

[11] D. P. Roy, Y. Jin, P. E. Lewis, and C. O. Justice, "Prototyping a global algorithm for systematic fire-affected area mapping using MODIS time series data," *Remote Sensing of Environment*, vol. 97, no. 2, pp. 137–162, 2005.

[12] D. P. Roy, L. Boschetti, C. O. Justice, and J. Ju, "The collection 5 MODIS burned area product–Global evaluation by comparison with the MODIS active fire product," *Remote Sensing of Environment*, vol. 112, no. 9, pp. 3690–3707, 2008.

[13] D. P. Roy, P. E. Lewis, and C. O. Justice, "Burned area mapping using multi-temporal moderate spatial resolution data–a bi-directional reflectance model-based expectation approach," *Remote Sensing of Environment*, vol. 83, no. 1-2, pp. 263–286, 2002.

[14] K. Tansey, J. M. Gregoire, J. M. C. Pereira, P. Defourny, R. Leigh, J. F. Pekel, A. Barros, J. Silva, E. van Bogaert, and E. Bartholome, "L3JRC-A global, multi-year (2000-2007) burnt area product (1 km resolution and daily time steps)," in *Remote Sensing and Photogrammetry Society Annual Conference*, 2007, pp. 11–14.

[15] K. Tansey, J. M. Grgoire, P. Defourny, R. Leigh, J. F. Pekel, E. van Bogaert, and E. Bartholom, "A new, global, multi-annual (2000-2007) burnt area product at 1 km resolution," *Geophys. Res. Lett*, vol. 35, no. 1, 2008.

[16] A. J. L. Harris, "Towards automated fire monitoring from space: semi-automated mapping of the january 1994 new south wales wildfires using AVHRR data," *Int. J. Wildland Fire*, vol. 6, no. 3, pp. 107–116, 1996.

[17] Z. Li and L. Giglio, "A review of AVHRR-based fire detection algorithms," in *Forest fire monitoring and mapping: a component of global observation of forest cover. Report of a workshop*, 1999, p. 35.

[18] G. G. Gutman, "On the use of long-term global data of land reflectances and vegetation indices derived from the advanced very high resolution radiometer," *Journal of Geophysical Research*, vol. 104, no. 6, p. 62416255, 1999.

[19] J. Pinzon, M. E. Brown, and C. J. Tucker, "Satellite time series correction of orbital drift artifacts using empirical mode decomposition," *Hilbert-Huang Transform: Introduction and Applications*, p. 167186, 2004.

[20] C. J. Tucker, J. E. Pinzn, M. E. Brown, D. A. Slayback, E. W. Pak, R. Mahoney, E. F. Vermote, and N. E. Saleous, "An extended AVHRR 8-km NDVI dataset compatible with MODIS and SPOT vegetation NDVI data," *International Journal of Remote Sensing*, vol. 26, no. 20, pp. 4485–4498, 2005.

[21] K. B. Kidwell, "Global vegetation index users guide," *US Department of Commerce/National Oceanic and Atmospheric Administration/National Environmental Satellite Data and Information Service/National Climatic Data Center/Satellite Data Services Division*, 1990.

[22] B. N. Holben, "Characteristics of maximum-value composite images from temporal AVHRR data," *International Journal of Remote Sensing*, vol. 7, no. 11, pp. 1417–1434, 1986.

[23] P. Frederiksen, S. Langaas, and M. Mbaye, "NOAA-AVHRR and GIS-based monitoring of fire activity in senegal: A provisional methodology and potential applications," *Ecological studies: analysis and synthesis (USA)*, 1990.

[24] S. Langaas, "Temporal and spatial distribution of savanna fires in senegal and the gambia, west africa, 1989-90, derived from multi-temporal AVHRR night images." *Int. J. Wildl. Fire.*, vol. 2, no. 1, pp. 21–36, 1992.

[25] P. M. Smith, S. N. V. Kalluri, S. D. Prince, and R. DeFries, "The NOAA/NASA pathfinder AVHRR 8-km land data set," *PE & RS-Photogrammetric Engineering & Remote Sensing*, vol. 63, no. 1, p. 12, 1997.

[26] M. E. James and S. N. V. Kalluri, "The pathfinder AVHRR land data set: an improved coarse resolution data set for terrestrial monitoring," *International Journal of Remote Sensing*, vol. 15, no. 17, pp. 3347–3363, 1994.

[27] P. A. Agbu and M. E. James, "The NOAA/NASA pathfinder AVHRR land data set users manual," *Goddard Distributed Active Archive Center, NASA, Goddard Space Flight Center, Greenbelt*, 1994.

[28] P. M. Barbosa, C. Carmona-Moreno, and J. M. Gregoire, "The use of the NASA-GAC pathfinder global data set for the extraction of burned areas." in *28 International Symposium on Remote Sensing of Environment, Cape Town, South Africa*, 2000.

[29] C. Carmona-Moreno, A. Belward, P. Caperan, A. Hartley, J. P. Malingreau, M. Antonovskiy, V. Buchshtaber, and V. Pivovarov, "Global fire calendar probability maps from the analysis of global burned surfaces time series (1982-1999)." in *28 International Symposium on Remote Sensing of Environment, Cape Town, South Africa*.

[30] C. Carmona-Moreno, A. Belward, J. P. Malingreau, A. Hartley, M. Garcia-Alegre, M. Antonovskiy, V. Buchshtaber, and V. Pivovarov, "Characterizing interannual variations in global fire calendar using data from earth observing satellites," *Global Change Biology*, vol. 11, no. 9, pp. 1537–1555, 2005.

[31] H. Eva, "Preliminary evaluation of the global burnt area product GBA82-99 V0. a database for characterising global fire activity for the period 1982-1999," Joint Research Center, Institute for Enviroment and Sustainability, Ispra, Italy., Tech. Rep., 2004.

[32] A. C. R. Gleason, S. D. Prince, S. J. Goetz, and J. Small, "Effects of orbital drift on land surface temperature measured by AVHRR thermal sensors," *Remote Sensing of Environment*, vol. 79, no. 2-3, pp. 147–165, 2002.

[33] A. Hartley, M. Garcia-Alegre, and M. Antonovskiy, "Characterizing interannual variations in global fire calendar using data from earth observing satellites," *Global Change Biology*, vol. 11, pp. 1537–1555, 2005.

[34] Y. Julien, J. A. Sobrino, and W. Verhoef, "Changes in land surface temperatures and NDVI values over europe between 1982 and 1999," *Remote Sensing of Environment*, vol. 103, no. 1, pp. 43–55, 2006.

[35] M. Jin and R. E. Dickinson, "Interpolation of surface radiative temperature measured from polar orbiting satellites to a diurnal cycle. i-without clouds," *Journal of Geophysical Research*, vol. 104, no. D2, pp. 2105–2116, 1999.

[36] M. Jin and R. E. Treadon, "Correcting the orbit drift effect on AVHRR land surface skin temperature measurements," *International Journal of Remote Sensing*, vol. 24, no. 22, pp. 4543–4558, 2003.

[37] M. Deng, L. Di, I. Raytheon, and M. D. Lanham, "Solar zenith angle correction of global NDVI time-series from AVHRR," in *IEEE 2001 International Geoscience and Remote Sensing Symposium, 2001. IGARSS'01*, vol. 4, 2001.

[38] S. O. Los, G. J. Collatz, P. J. Sellers, C. M. Malmstrm, N. H. Pollack, R. S. DeFries, L. Bounoua, M. T. Parris, C. J. Tucker, and D. A. Dazlich, "A global 9-yr biophysical land surface dataset from NOAA AVHRR data," *Journal of Hydrometeorology*, vol. 1, no. 2, pp. 183–199, 2000.

[39] J. Pinzon, M. E. Brown, and C. J. Tucker, "EMD correction of orbital drift artifacts in satellite data stream," *The HilbertHuang transform and its applications*, pp. 167–183, 2005.

[40] L. Breiman, "Random forests," *Machine learning*, vol. 45, no. 1, pp. 5–32, 2001.

[41] R. W. Saunders, "The determination of broad band surface albedo from AVHRR visible and near-infrared radiances," *International Journal of Remote Sensing*, vol. 11, no. 1, pp. 49–67, 1990.

[42] B. Pinty and M. M. Verstraete, "GEMI: a non-linear index to monitor global vegetation from satellites," *Plant Ecology*, vol. 101, no. 1, pp. 15–20, 1992.

[43] S. D. Prince, "Satellite remote sensing of primary production: comparison of results for sahelian grasslands 1981-1988," *International Journal of Remote Sensing*, vol. 12, no. 6, pp. 1301–1311, 1991.

[44] A. M. O. Sousa, J. M. C. Pereira, and J. M. N. Silva, "Evaluating the performance of multitemporal image compositing algorithms for burned area analysis," *International Journal of Remote Sensing*, vol. 24, no. 6, pp. 1219–1236, 2003.

[45] A. Cabral, M. Vasconcelos, J. M. C. Pereira, E. Bartholome, and P. Mayaux, "Multi-temporal compositing approaches for SPOT-4 VEGETATION," *International Journal of Remote Sensing*, vol. 24, no. 16, pp. 3343–3350, 2003.

[46] N. E. Huang, Z. Shen, S. R. Long, M. C. Wu, H. H. Shih, Q. Zheng, N. C. Yen, C. C. Tung, and H. H. Liu, "The empirical mode decomposition and the hilbert spectrum for nonlinear and non-stationary time series analysis," *Proceedings: Mathematical, Physical and Engineering Sciences*, vol. 454, no. 1971, pp. 903–995, 1998.

[47] N. E. Huang, Z. Shen, and S. R. Long, "A New View of Nonlinear Water Waves: the hilbert spectrum 1," *Annual Review of Fluid Mechanics*, vol. 31, no. 1, pp. 417–457, 1999.

[48] D. R. Steinwand, "Mapping raster imagery to the interrupted goode homolosine projection," *International journal of remote sensing(Print)*, vol. 15, no. 17, pp. 3463–3471, 1994.

[49] D. R. Steinwand, J. A. Hutchinson, and J. P. Snyder, "Map projections for global and continental data sets and an analysis of pixel distortion caused by reprojection," *Photogrammetric Engineering and Remote Sensing*, vol. 61, no. 12, pp. 1487–1497, 1995.

[50] E. Bartholome and A. S. Belward, "GLC2000: a new approach to global land cover mapping from earth observation data," *International Journal of Remote Sensing*, vol. 26, no. 9, pp. 1959–1977, 2005.

[51] O. Arino and J. Rosaz, "1997 and 1998 world atsr fire atlas using ers-2 atsr-2 data," in *Proc. Joint Fire Sci. Conf.* Boise, ID, 1999, pp. 177–182.

[52] B. W. Mota, J. M. C. Pereira, D. Oom, M. J. P. Vasconcelos, and M. Schultz, "Screening the ESA ATSR-2 world fire atlas (1997-2002)," *Atmos. Chem. Phys.*, vol. 6, pp. 1409–1424, 2006.

[53] R. H. Fraser, Z. Li, and J. Cihlar, "Hotspot and NDVI differencing synergy (HANDS)-A new technique for burned area mapping over boreal forest," *Remote Sensing of Environment*, vol. 74, no. 3, pp. 362–376, 2000.

[54] E. S. Kasischke, N. H. F. French, P. Harrell, N. Christensen, J. N. L, S. Ustin, and D. Barry, "Monitoring of wildfires in boreal forests using large area AVHRR NDVI composite image data," *Remote Sensing of Environment*, vol. 45, no. 1, pp. 61–71, 1993.

[55] J. Kucera, Y. Yasuoka, and D. G. Dye, "Creating a forest fire database for the far east of asia using NOAA/AVHRR observation," *International Journal of Remote Sensing*, vol. 26, no. 11, pp. 2423–2439, 2005.

[56] J. M. C. Pereira, A. C. L. Sa, A. M. O. Sousa, J. M. N. Silva, T. N. Santos, and J. M. B. Carreiras, "Spectral characterisation and discrimination of burnt areas," *Remote sensing of large wildfires in the European Mediterranean Basin*, p. 123138, 1999.

[57] D. P. Roy, "Multi-temporal active-fire based burn scar detection algorithm," *International Journal of Remote Sensing*, vol. 20, no. 5, pp. 1031–1038, 1999.

[58] E. Chuvieco, M. P. Martin, and A. Palacios, "Assessment of different spectral indices in the red-near-infrared spectral domain for burned land discrimination," *International Journal of Remote Sensing*, vol. 23, no. 23, pp. 5103–5110, 2002.

[59] E. Chuvieco, P. Englefield, A. P. Trishchenko, and Y. Luo, "Generation of long time series of burn area maps of the boreal forest from NOAA-AVHRR composite data," *Remote Sensing of Environment*, vol. 112, no. 5, pp. 2381–2396, 2008.

[60] A. T. Vafeidis and N. A. Drake, "A two-step method for estimating the extent of burnt areas with the use of coarse-resolution data," *International Journal of Remote Sensing*, vol. 26, no. 11, pp. 2441–2459, 2005.

[61] M. P. Martin and E. Chuvieco, "Mapping and evaluation of burned land from multitemporal analysis of AVHRR NDVI images," *EARSeL Advances in Remote Sensing*, vol. 4, pp. 7–13, 1995.

[62] J. M. C. Pereira, "A comparative evaluation of NOAA/AVHRR vegetation indexes forburned surface detection and mapping," *IEEE Transactions on Geoscience and Remote Sensing*, vol. 37, no. 1 Part 1, pp. 217–226, 1999.

[63] J. M. N. Silva, J. M. C. Pereira, A. I. Cabral, A. C. L. S, M. J. P. Vasconcelos, B. Mota, and J. M. Grgoire, "An estimate of the area burned in southern africa during the 2000 dry season using SPOT-VEGETATION satellite data," *Journal of Geophysical Research-Atmospheres*, vol. 108, no. D13, p. 8498, 2003.

[64] M. Prasad A, R. Iverson L, and A. Liaw, "Newer classification and regression tree techniques: bagging and random forests for ecological prediction," *Ecosystems*, vol. 9, pp. 181–199, 2006.

[65] O. Gislason P, A. Benediktsson J, and R. Sveinsson J, "Random forests for land cover classification," *Pattern Recognition Letters*, vol. 27, pp. 294–300, 2006.

[66] S. Archibald, D. P. Roy, W. van Wilgen B, and R. J. Scholes, "What limits fire?: An examination of drivers of burnt area in southern africa," *Global Change Biology*, vol. 15, pp. 613–630, 2009.
[67] A. Liaw and M. Wiener, "Classification and regression by randomForest," *R news*, vol. 2, no. 3, p. 1822, 2002.
[68] J. Pereira and R. Itami, "Gis-based habitat modeling using logistic multiple regression- a study of the mt. graham red squirrel," *Photogrammetric Engineering and Remote Sensing*, vol. 57, no. 11, pp. 1475–1486, 1991.
[69] A. H. Strahler, "The use of prior probabilities in maximum likelihood classification of remotely sensed data," *Remote Sensing of Environment*, vol. 10, no. 2, pp. 135–163, 1980.
[70] M. G. Kendall, "Rank correlation measures," *Charles Griffin, London*, vol. 202, 1975.
[71] J. Goldammer, "of book: Fra global forest fire assessment 1990-2000," 2001.
[72] A. I. Sukhinin, N. H. F. French, E. S. Kasischke, J. H. Hewson, A. J. Soja, I. A. Csiszar, E. J. Hyer, T. Loboda, S. G. Conrad, and V. I. Romasko, "AVHRR-based mapping of fires in russia: New products for fire management and carbon cycle studies," *Remote Sensing of Environment*, vol. 93, no. 4, pp. 546–564, 2004.
[73] R. Pu, Z. Li, P. Gong, I. Csiszar, R. Fraser, W. M. Hao, S. Kondragunta, and F. Weng, "Development and analysis of a 12-year daily 1-km forest fire dataset across north america from NOAA/AVHRR data," *Remote Sensing of Environment*, vol. 108, no. 2, pp. 198–208, 2007.
[74] B. J. Stocks, J. A. Mason, J. B. Todd, E. M. Bosch, B. M. Wotton, B. D. Amiro, M. D. Flannigan, K. G. Hirsch, K. A. Logan, and D. L. Martell, "Large forest fires in canada, 19591997," *Journal of Geophysical Research*, vol. 107, no. D1, p. 8149, 2002.
[75] R. Congalton, "A review of assessing the accuracy of classifications of remotely sensed data," *Remote sensing of environment*, vol. 37, no. 1, pp. 35–46, 1991.
[76] G. R. V. der Werf, J. T. Randerson, L. Giglio, G. J. Collatz, P. S. Kasibhatla, and A. F. A. Jr, "Interannual variability of global biomass burning emissions from 1997 to 2004," *Atmospheric Chemistry and Physics Discussions*, vol. 6, no. 2, pp. 3175–3226, 2006.
[77] B. Mota, J. M. C. Pereira, and A. Sousa, "Classification accuracy limits induced by burned area spatial patterns: a global, multi-sensor analysis." *Remote Sens. Environ.*, to be submited.

**Bernardo Mota** received the undergraduate degree in geosciences-metreology and oceanography in 2000 from the Faculdade de Ciências at the Universidade de Lisboa, Portugal, and is presently finishing is Ph.D. Degree in forestry engineering at the Instituto Superior de Agronomia, Universidade Técnica de Lisboa, Lisbon, Portugal. He is a researcher with the Departmant of Forestry, Instituto Superior de Agronomia, Universidade Técnica de Lisboa, and his current research interests include the development of remote sensing algorithms for burned area mapping, climate and biomass burning relations, feedbacks and trends.

**Ricardo Machado Trigo** received the undergraduate degree in Atmospheric Sciences in 1992 from the Faculty of Sciences, Universidade de Lisboa, Lisbon, Portugal, and a Ph.D. Degree in Climatology in 2000 from the University of East Anglia, Norwich, UK. He is a senior researcher and Climate Change group leader at the Instituto Dom Luiz, Faculty of Sciences, Universidade de Lisboa. His current research interests include climate change scenarios over the Mediterranean basin and impact studies of weather driven natural hazards such as extreme precipitation, floods, droughts, landslides, heatwaves and wildfires. In 2008 he was awarded with the International Journal of Climatology prize endorsed by the Royal Meteorological Society, UK.

**José M.C. Pereira** received the undergraduate degree in forestry in 1983 from the Instituto Superior de Agronomia, Universidade Técnica de Lisboa, Lisbon, Portugal, and a Ph.D. Degree in renewable natural resources studies in 1989 from the University of Arizona, Tucson. He is an associate Professor with the Departmant of Forestry, Instituto Superior de Agronomia, Universidade Técnica de Lisboa, teaching courses in vegetation fires, forest ecology and remote sensing. His current research interests include the geographical ecology of wildfires in southern Europe and the development of remote sensing algorithms for burned area mapping at regional and global scales.

.